2013-05-14

Insights into the Functional Link between MtHsp40:MtHsp70 Network and Mitochondrial Homeostasis

Lee, Byoung Chun

UNIVERSITY OF CALGARY

Insights into the Functional Link between MtHsp40:MtHsp70 Network

and

Mitochondrial Homeostasis

by

Byoung Chun Lee

A THESIS

SUBMITTED TO THE FACULTY OF GRATDUATE STUDIES

IN PARTIAL FULFILMENT OF THE REQUIREMENTS FOR THE

DEGREE OF DOCTOR OF PHILOSOPHY

DEPARTMENT OF BIOCHEMISTRY AND MOLECULAR BIOLOGY

CALGARY, ALBERTA

MAY, 2013

Abstract

Mitochondrial apoptosis, morphology and function can be modulated by the activity of mitochondrial chaperones including mtHsp40 and mtHsp70. We found that both overexpression and depletion of mtHsp40 reversibly changed mitochondrial morphology from tubular network to fragmented puncta, in a process known as mitochondrial fragmentation, which was not coupled with apoptosis. Using domain deletion mutant constructs, we determined that mitochondrial targeting sequence (MTS) and DnaJ domain of mtHsp40 were required for mitochondrial fragmentation. Both inhibition and loss of mtHsp70 also caused mitochondrial fragmentation. Ectopic expression of mtHsp70, with the exception of substrate binding domain-deletion mutant, did not affect mitochondrial morphology. These data suggest that the stoichiometric ratio between mtHsp40 and mtHsp70 determines mitochondrial morphology independently of apoptosis. Mitochondrial fragmentation resulting from the imbalance between mtHsp40 and mtHsp70 was dependent on DRP1 level, but mitochondrial translocation of DRP1 was not detected in fragmented mitochondria. In addition, OPA1 short-isoform highly accumulated in fragmented mitochondria, suggesting that ratio between mtHsp40 and mtHsp70 is a determinant of OPA1 cleavage, which in turn determines mitochondrial morphology. Imbalance between mtHsp40 and mtHsp70 led to dramatic crista remodeling which enhances cancer cell sensitivity to drug-induced apoptosis, and lowered both ATP production and oxygen consumption rate in fragmented mitochondria, which resulted in cell-growth retardation. Collectively, we propose that perturbations of mtHsp40:mtHsp70 network might reduce their own activity, which causes OPA1 cleavage and mitochondrial fragmentation depending on DRP1, leading to mitochondrial innermembrane remodeling, indicating the apoptosis-independent coupling between mitochondrial homeostasis and mtHsp40:mtHsp70 network.

Acknowledgements

Thank you to all previous and current members of the Kim lab that I have had great privilege to work with and to learn a great deal from. All your technical advice, guidance, and the scientific discussions that we have had are deeply appreciated. A special thank you to Dr. Adam Elwi for being such a great co-worker and friend. You have provided me with amazing memories and experiences. I would like to thank Diane Trinh for correcting and editing this thesis. You are one of the most excellent writers that I have ever met.

Thank you to my supervisor, Dr. Sung-Woo Kim, co-supervisor, Dr. Randal Johnston, and to those who served on my supervisory committee, Dr. Karl Riabowol and Dr. Janice Braun. Their advice and support has guided me throughout my PhD's thesis and has taught me to begin to think more like a scientist, and their warm words have encouraged me to get back up at the disappointing moments. I would also like to thank Dr. David Hansen and Dr. David Chan for serving on my examination committee, and collaborators in South Korea, Dr. Yeong-Yeol Yang and Dr. Seok-Hun Yoon for providing lactate analysis.

Finally, I would like to thank my family in South Korea who have supported and encouraged me. My daughter, Juyeon has cheered for me with kisses and smile, and my son, Daniel has encouraged me with big hugs. My wife, Soonmi has been there for me while I have had ups and downs and my good days and bad, who have been so confident in my success. It is thanks to your support that I can succeed in this five year journey.

Table of Contents

List of Tables

List of Figures and Illustrations

List of Symbols, Abbreviation and Nomenclature

-/-	null
%	percentage
m-AAA	mitochondrial ATPases Associated with diverse cellular Activities
AD	Alzheimer's Disease
ADOA	autosomal dominant optic atrophy
ADP	adenosine diphosphate
AMPK	AMP-activated protein kinase
ATP	adenosine triphosphate
ATPase	ATP synthase
Aβ	beta amyloid
Bak	Bcl-2 homologous antagonist killer
Bax	Bcl-2-associated X protein
bp	base pairs
BSA	bovine serum albumin
℃	degrees Celsius
Ca^{2+}	calcium ion
CaMK1α	calcium/calmodulin-dependent protein kinase 1 alpha
CCCP	carbonyl cyanide m-chlorophenyl hydrazone
CDK1	cyclin-dependent kinase 1
cDNA	complementary DNA
cm	centimeter
CMT2A	Charcot-Marie-Tooth Neuropathy Type 2A
CMV	cytomegalovirus
CO_2	carbon dioxide
Co-IP	co-immunoprecipitation
COX 1	cytochrome *c* oxidase subunit I
COX IV	cyclooxygenase IV
CTD	C-terminal domain
C-terminus	carboxy-terminus
Cys-rich	Cysteine-rich
DAPI	4',6-diamidino-2-phenylindole
ddH_2O	double distilled water
DFX	Desferrioxamine Mesylate
DMEM	Dulbecco's Modified Eagle Media
DMSO	dimethyl sulfoxide
DNA	deoxyribonucleis acid
dNTP	deoxyrionucleotide triphosphate
DOX	doxycycline

Drp1	Dynamin-Related Protein 1
DsRed2	Discosoma sp. red fluorescent protein 2
DTT	dithiothreitol
E. coli	Escherichia coli
ECAR	extracellular acidification rate
EDTA	ethylenediaminetetraacetate
EEVD	Glu-Glu-Val-Asp
EGTA	ethyleneglycoltetraacetate
ES	embryonic stem cells
FACS	Fluorescence Activated Cell Sorting
FAD	flavin adenosine diphosphate
FBS	fetal bovine serum
FCCP	trifluorocarbonylcyanide phenylhydrazone
Fis1	fission 1
FMN	flavinmononucleotide
g	gram
G/F	glycine/phenylalanine
GAPDH	glyceraldehyde 3-phosphate dehydrogenase
GFP	green fluorescent protein
GTP	guanosine triphosphate
GTPase	GTP hydrolase
h	hour
HBSS	Hanks' Balanced Salt solution
HEK293	human embryonic kidney 293
Hep1	HSP70 escort protein 1
HPD	Histidine-Proline-Aspartic acid
HRP	horseradish peroxidase
Hs68	human foreskin fibroblast 68
HSC	heat shock cognate
HSF1	heat shock factor 1
Hsp	heat shock protein
hTid1	human tumorous imaginal disc 1
HTT	huntingtin
IgG	immunoglobulin G
INF2	inverted formin 2
J Protein	DnaJ domain-containing protein
kb	kilobases
kDa	kilodalton
KOH	potassium hydroxide
L	Litre
l(2)Tid	lethal(2) tumorous imaginal discs

LacZ	beta galgatosidase
LB	Luria-Bertani
MAD	Multiwavelength Anomalous Dispersion
MAPL	mitochondrial-anchored protein ligase
MEF	mouse embryonic fibroblasts
µg	microgram
µl	microliter
µM	micromolar
µs	microsecond
Mff	mitochondrial fission factor
Mfn1	Mitofusin 1
Mfn2	Mitofusin 2
$MgCl_2$	magnesium chloride
MIM	mitochondrial innermembrane
MitoGFP	mitochondrial-targeted GFP
MitoRFP	mitochondrial-targeted RFP
ml	mililitre
mM	milimolar
MOM	mitochondrial outermembrane
MOPS	3-(N-morpholino)propanesulfonic acid,
MPP	matrix processing peptidase
mRNA	messenger RNA
mtDNA	mitochondrial DNA
mtHsp40	mitochondrial Hsp40
mtHsp70	mitochondrial Hsp70
mTid1	mouse Tid1
MTS	mitochondrial targeting sequence
$NAD^{+/}NADH$	nicotinamide adenine dinucleotide
$NADP^{+}/NADPH$	nicotinamide adenine dinucleotide phosphate
NEF	nucleotide exchange factor
ng	nanogram
nm	nanometer
NO	nitric oxide
NP40	nonidet-40
N-terminus	amino-terminus
OCR	oxygen consumption rate
Opa1	Optic atrophy 1
$Opa1_L$	long isoform of Opa1
$Opa1_S$	short isoform of Opa1
Opti-MEM	Modified Eagle's Minimum Essential Media

OXPHOS	oxidative phosphorylation
PAM	translocase-associated motor
PARL	presenilins-associated rhomboid-like
PBS	phosphate-buffered saline
PBST	phosphate-buffered saline Tween20
PCR	polymerase chain reaction
PD	Parkinson's Disease
PFA	paraformaldehyde
PGC-1α	peroxisome-proliferator-activated receptor gamma co-activator alpha
PINK1	PTEN induced putative kinase 1
PKA	protein kinase A
PNK	polynucleotide kinase
Polga	DNA polymerase gamma
PVDF	polyvinylidene fluoride
qPCR	quantitative PCR
RNA	ribonucleic acid
RNAi	RNA interference
ROS	reactive oxygen species
SBD	substrate binding domain
SDS	sodium dodecylsulfate
SDS-PAGE	sodium dodecyl sulfate poly acrylamide gel electrophoresis
shRNA	short hairpin RNA
siRNA	short interference RNA
SNARE	N-ethylmaleimide-sensitive fusion protein attachment receptors
TCA	tricarboxylic acid
TEM	transmission electron microscopy
TetR	tetracycline repressor
Tid1	Tumor Imaginal Disc 1
$Tid1_L$	long isoform of Tid1
$Tid1_S$	intermediate isoform of Tid1
TIM	translocase of innermembrane
TMRM	tetramethylrhodamine methyl and ethyl esters
TPR	tetratricopeptide repeat
UPS	ubiquitin proteosome system
v/v	volume / volume
wt	wildtype
$\Delta\psi m$	mitochondrial membrane potential

CHAPTER ONE: INTRODUCTION

1.1 General Background

Mitochondria perform diverse and critical function by supplying energy (ATP) and electrons (NADH and $FADH_2$), synthesizing numerous intermediates which are components of biosynthetic pathways of amino acids, lipids, heme or Fe-S molecules, *etc* and also contributing to cellular stress responses such as autophagy and apoptosis[1]. The macro- and micro-structure of mitochondria are linked to their function. The external structure of mitochondria is tightly regulated through activities of mitochondrial fission and fusion, and is closely integrated with oxidative phosphorylaton (OXPHOS), mitochondrial DNA (mtDNA) replication, mitochondrial motility and quality control of mitochondria[1-3]. More about regulation of mitochondrial external morphology and its effects on mitochondrial homeostasis will be described in **Section 1.2**. The innermembrane of mitochondria is highly folded and penetrated into the matrix, forming the typical crista structure, which is thought to increase the charge density of intermembrane space of mitochondria resulting in the enhancement of ATP production via OXPHOS[1,2].

It is not surprising that mitochondrial dysfunction is associated with a myriad of diseases such as neurodegenerative and metabolic disorders, cardiomyopathies, obesity, ageing and cancers (Table 1). The most common nuclear mutations associated with mitochondrial diseases are found in PolgA, a gene encoding mitochondrial DNA polymerase γ, result in mtDNA loss and eventually manifest epilepsy or ataxia-neuropathy syndrome[1,4]. Compared with mutations in nuclear-encoded mitochondrial genes, mtDNA mutations produce variable phenotypes due to the multiple copy number of mitochondrial genome in mammalian cells. For example, for the T89993C/G mutation of mtDNA, defective in ATPase subunit 6, whereas a low mutant load causes pigment retinopathy, ataxia and neuropathy, a high mutant load such as maternally inherited mutation causes Leigh syndrome[1,5]. Mitochondrial tRNA and rRNA mutations also result in multiple diseases such as myoclonic epilepsy and ragged red fiber (MERRF), the mitochondrial encephalomyopathy, and stroke-like episodes (MELAS) syndromes, *etc*[6]. Studies show that many cancers reprogram mitochondrial metabolism to survive harsh environments such as hypoxia and starvation resulting in bulky growth of tumors[1,7]. Since Otto Warburg observed over 70 years ago that cancer cells highly activate glycolysis in the presence of oxygen, which he termed ‘aerobic glycolysis’, researchers found a lot of mutations altering metabolism in

Table 1. Examples of Mitochondrial Diseases

Diseases	Major Genetic Alterations		Symptoms
	Gene Name	Encoded Products	
Mitochondrial DNA (Maternally inherited)			
Diabetes mellitus and deafness (DAD)	MT-TL1	tRNA leucine 1	Diabetes Deafness
Neuropathy, ataxia, and retinitis pigmentosa (NARP)	ATP6	ATP synthase subunit 6	Neuropathy Ataxia Dementia
Myoclonic epilepsy with ragged red fibers (MERRF)	MT-TK	tRNA lysine	Epilepsy Short stature Hearing loss Lactic acidosis
Mitochondrial encephalomyopathy, lactic acidosis and stroke-like episodes (MELAS)	ND1, ND5 MT-TH, MT-TL1, MT-TV	NADH dehydrogenase tRNAs	Muscle weakness Pain Headaches Seizures Altered consciousness Vision loss
Leber's hereditary optic neuropathy (LHON)	ND4, ND1 and ND6 PolgA	Complex 1 of OXPHOS DNA polymerase γ	Visual loss Eye disorder Multiple sclerosis-type syndrome
Nuclear DNA			
Mitochondrial neurogastrointestinal encephalopathy syndrome (MNGIE)	TYMP	Thymidine phosphorylase	Neuropathy Gastrointestinal pseudo-obstruction
Leigh's disease	Subunit of OXPHOS complexes, PDHC, SURF1	OXPHOS complexes Pyruvate dehydrogenase complex Surfet locus protein 1	Seizures Dementia Ventilatory failure
Neurodegeneration	PARK6 PARK2 PARK7	PINK1 Parkin DJ-1	Parkinsonism

many cancers; for example, upregulation of pyruvate kinase M2 (PKM2) and phosphofructokinase/fructose-2, 6-bisphosphatase B3 (PFKFB3) and inactivation of pyruvate dehydrogenase (PDH) leading to enhanced glycolysis and ablated carbon flux into mitochondria[8]. In addition, mutations in isocitrate dehydrogenase 1 (IDH1, cytosol) or 2 (IDH2, mitochondria) decrease mitochondrial TCA cycle and accumulate an oncometabolite, 2-hyroxyglutarate (2HG), which leads to hypermethylation of cancer genomes[9]. Furthermore, cancer mitochondria activate alternative pathways to provide cancer cells with energy and anabolic intermediates, one of which is reductive metabolism of glutamine. Glutamine metabolizing genes including glutaminase (GLS1) and glutamate dehydrogenase (GLDH) are upregulated in many cancers[8,10]

Mitochondrial membrane structure also changes in cancers. For example, many cancers downregulate proapoptotic proteins such as Bcl-2-associated X (BAX) and Bcl-2-antagonist/killer (BAK) or upregulate antiapoptotic proteins such as BCL-2, BCL-XL and MCL1, which inhibits formation of mitochondrial outermembrane permeabilization pore (MOMP) leading to resistance to apoptotic cell death[11,12]. Recent findings show that permeability transition pore complex (PTPC) in cancer mitochondria is scarcely open due to oncoprotein binding such as TRAP, which inhibits necrotic cell death of cancer cells[13]. It is therefore obvious that mitochondrial homeostasis of function and structure is critical in regulating cell death and health.
Heat Shock Proteins (HSPs, also known as chaperones) are one of the most common proteins and play central roles in protein homeostasis. Upon exit from ribosomes, proteins meet the aqueous cytosol which is highly crowded with 300-400 g/L of proteins[14,15]. Whereas small proteins fold very rapidly for less than microseconds (μs), larger proteins can take up to several hours for proper folding[16,17]. Proteins trafficked to organelles such as mitochondria take even longer[18-20]. During folding and trafficking, proteins face numerous challenges: degradation and/or aggregation[21-23]. Misfolded or aggregated proteins often become potential risks to cells due to their toxicity[24-26]. Thus, in order to maintain proteostasis and avoid potential dangers of toxic protein aggregates, both prokaryotes and eukaryotes evolve guardians of proteome, which are molecular chaperones (also called heat shock proteins, HSPs)[27]. For historical reasons, the term HSP is used even if many chaperones are not responsive to heat-shock. Under cellular stresses such as heat-shock, proteins become more prone to aggregation. Cells thus induce HSPs mediating protein folding/refolding, protein assembly, protein deaggregation, and degradation by delivering protein aggregates to Ubiquitin-Proteosome System (UPS) to maintain proteostasis.

HSPs consist of several main classes: (1) HSP70/HSP40 system, (2) HSP90 system, (3) HSP60/HSP10 (chaperonins), and (4) small HSPs (Table 2)[28-31]. HSP70s are ubiquitous molecular chaperons that are involved in a myriad of biological processes: preventing newly synthesized protein from aggregating, deaggregating aggregated protein, helping protein trafficking and/or transmembrane transport of protein, protecting cells from thermal or oxidative stress, participating in degradation of damaged or defective protein, and directly inhibiting apoptosis[29,30]. HSP70s never work alone, but as a team with HSP40 and nucleotide exchange factors (NEFs). More details about HSP70/HSP40 system will be described in **Section 1.3**. Major HSPs except HSP70/HSP40 were summarized in Table 2. HSP90s are the most abundant HSPs, almost 1% of total cellular protein, and known to bind more than 200 proteins such as protein kinases and transcription factors that are essential for cell signaling and adaptive response(s) to stress[13,32]. To accomplish chaperonic function, HSP90s form the dynamic complex with HSP70 and co-chaperones. ER HSP90 homolog, glucose-regulated protein 94 (GRP94) is essential for the maturation and secretion of insulin-like growth factors (IGFs), and mitochondrial homolog, whereas tumor necrosis factor receptor-associated protein 1 (TRAP1) protects mitochondria from oxidative stress[32]. Interestingly, many cancers upreglate HSP90s to protect an array of mutated and/or upregulated oncoproteins from misfolding and degradation. Thus, HSP90 has been recognized as a promising target for cancer treatment[33]. Mammalian equivalents of bacterial chaperonin GroEL include HSP60/HSP10 (mitochondria) and TRiC (cytosol). These proteins form a large complex and participate in the protein folding and assembly in specific cellular compartments. While HSP60 interacts with multiple client proteins including mtHsp70, Survivin, TP53, α3β1 integrin, cell surface receptors such as CD14, CD40 and Toll-like-receptors (TLRs), only a few proteins such as the cytoskeletal proteins actin and tubulin have been reported to require the TRiC complex[29,34]. Small HSPs are least conserved members of HSPs and have a low molecular weight of between 14-45 kDa with most in the 20 kDa range. In humans, ten small HSPs are identified, and termed the HSP27 family. HSP27s may promiscuously bind and then present unfolded proteins to other ATP-dependent HSPs (for example HSP60, HSP70 or HSP90). The best studied HSP27, α-crystallin is abundant in eye lens and prevents protein aggregation resulting from light damage[35]. As HSPs are involved in myriad of biological processes, dysfunction of HSPs is obviously associated with numerous diseases, examples of which are summarized in Table 3. In this study, we focus on HSP70/HSP40 system,

Table 2. Major Heat Shock Proteins

Name	Synonyms	Function/Structure
HSP60/HSP10 Family		
CCT2	TCP1β, CCTB, CCT β	Component of TRiC
CCT3	CCTG, CCTγ, TRIC5, TCP1γ	Component of TRiC
CCT4	CCTδ, SRB	Component of TRiC
CCT5	CCTE, CCTε, TCP1ε	Component of TRiC; upregulated in TP53-mutated tumors
CCT6A	CCT6, CCTζ, HTR3, TCPζ, TCP20, MoDP-2, TTCP20, CCT ζ,CCT-ζ1, TCP1-ζ	Component of TRiC
CCT6B	CCT- ζ2, TCP1-ζ2	Component of TRiC
CCT7	HIV-1 Nef interacting protein (Nip7-1), TCP1-η, Cctη, CCT-η	Component of TRiC
TCP1	CCT1, CCTα, TCP1α	TRiC
HSP10	CPN10, GroES, HSPE1	Interaction with HSP60
HSP60	HspD1, CPN60, GroEL, Hsp65, SPG13, HuCHA60	Mitochondrial protein folding and assembly
HSP90s		
AHA1	Activator of HSP90	Stimulates ATPase activity of HSP90
GRP94	HSP90B1, Gp96	ER; protein folding and assembly
HSP90A	HSP90AA1, HSP86, HSP89	Cytosol; protein folding and assembly
HSP90A	HSP90AA2	Cytosol; induced by temperature
HSP90b	HSP90AB1	Cytosol; protein folding and assembly
TRAP1	HSP75	Mitochondria; binding PTPC
HOP	STIP1, STI1	Golgi; binding HSP70 and HSP90
P23	TEBP, PGE Synthase 3	Binding telomerase
P50	CDC37	Binding HSP90
Small HSPs		
Crystallin, αA	CRYAA, CRYA1, HSPB4	Specific to the lens
Crystallin, αB	CRYAB, CRYA2, HSPB5	Elevated in neurological diseases

Name	Synonyms	Function/Structure
Small HSPs		
Crystallin, βA1	CRYBA1	Acidic group of β crystallins, forms aggregates; mutated in zonular cataract with sutural opacities
Crystallin, βA2	CRYBA2	Acidic group of β crystallins
Crystallin, βA4	CRYBA4	Mutations linked to cataractogenesis
Crystallin, βB1	CRYBB1	Basic group of β crystallins
Crystallin, βB2	CRYBB2	Mutated in type 2 cerulean cataracts
Crystallin, βB3	CRYBB3	Basic group of β crystallins
Crystallin, γA	CRYGA, CRYG1, CRYG5	Part of γ-crystallin gene cluster
Crystallin, γB	CRYGB, CRYG2	Part of γ-crystallin gene cluster
Crystallin, γC	CRYGC, CRYG3, CCL	Part of γ-crystallin gene cluster
Crystallin, γD	CRYGD, CRYG4, CCP, PCC, CACA, CCA3	Part of γ-crystallin gene cluster
Crystallin, γN	CRYGN	β/ γ-hybrid crystalline
Crystallin, γS	CRYGS, CRYG8	The most significant γ-crystallin in adult eye lens tissue
HSP22-8	H11, E2IG1, HSP22, HSPB8	CMT-2L; hereditary motor neuropathy type II
HSP22-1	HSP27, HSP25, HSPB1	CMT-2F; hereditary motor neuropathy type
HSP22-2	HSPB2, MKBP	Associates with DMPK
HSP22-3	HSPB3, HSPL27	Inhibitor of actin polymerization
α-crystallin-related, B6	HSPB6, HSP20	Structural component of eye lens
α-crystallin-related, B9	HSPB9, CT51	

in particular, mitochondrial HSP70 and HSP40, one member of Hsp40s or HSP70s.

Our laboratory has studied the roles of mtHsp40, a human homolog of the *Drosophila melanogaster* tumor suppressor gene lethal(2) tumorous imaginal discs (l(2)tid), as a tumor suppressor. As it has been reported in 1995 that the l(2)tid gene in homozygotes causes malignant growth of the imaginal discs in Drosophila, the gene has been proposed as a tumor suppressor. In addition, the l(2)tid gene shows the significant homology of DnaJ-related proteins of bacteria and yeast, indicating that the l(2)tid gene is one member of HSP40 (J proteins)[36]. Since it was known in 1998 that mtHsp40, a mammalian homolog of l(2)tid, interacts with human papillomavirus type 16 E7 oncoprotein, a majority of groups including us began investigation of its tumor suppressor function[37]. For example, Syken *et al* demonstrated that expression of $mtHsp40_L$ enhances apoptosis induced by the DNA-damaging agent mitomycin c and tumor necrosis factor alpha (TNF-α), which is DnaJ domain-dependent, and that depletion of mtHsp40 renders multiple cancer cell lines resistant to apoptosis induced by an array of proapoptotic stimuli such as cisplatin, TNF-α, cycloheximide and mitomycin c[38,39]. Our laboratory has found that mtHsp40 interacts with and translocates TP53 to mitochondria, resulting in enhanced mitochondria-associated apoptosis induced by apoptosis-inducing stimuli including DNA-damaging agents and hypoxia, suggesting that facilitating effects of mtHsp40 on apoptotic cell death may involve TP53 translocation to mitochondria[40]. Although plenty of reports have demonstrated that mtHsp40 positively affects apoptosis, the mechanisms how it facilitates apoptosis remain elusive. In addition, little is known about the roles of mtHsp40 as a mitochondrial co-chaperone of mtHsp70 in mitochondrial homeostasis of morphology, function and apoptosis.

In this study, we thus aim to investigate the roles of mtHsp40 as a mitochondrial co-chaperone of mtHsp70 in mitochondrial structure, function and apoptosis, and ultimately provide insights into the functional link between mtHsp40:mtHsp70 network and mitochondrial homeostasis.

1.2 Mitochondrial Homeostasis of Morphology and Its Link to Mitochondrial Function and Apoptosis

Mitochondrial morphology is diverse among cell and tissue types and dynamic through constant fusion and fission processes (collectively termed “mitochondrial dynamics”). For example, fibroblasts and neurons show the typical interconnected network via the balance

Table 3. HSPs-Associated Diseases

Chaperon Family	Associated Diseases	Altered Chaperones
Chaperonin	Lactic academia, hereditary spastic paraplegia	HSP60
HSP40	Huntington's Disease, Parkinson's Disease	HDJ1/2, Auxilin
HSP70	Alzheimer's Disease, Multiple Sclerosis, Parkinson's Disease, Schizoprenia, *etc*	HSC70, HSP70, HSP110, mtHSP70
HSP90	Prostate cancers, Melanomas, Leukaemias, Non-small-cell lung cancer	HSP90, GRP94
Small HSP	William's syndrome, Cataract, Multiple Sclerosis, CMT, Hereditary motor neuropathies	α-Crystallin, HSP27

between these two processes[41]. These two events are also important in maintaining the pool of functional mitochondria. Key components of fusion and fission have now been identified, and molecular mechanisms regulating these complex processes have been revealed. Recently, mitochondrial dynamics has been recognized as cs haso important in maintaining the ps critical roles in mitochondrial quality control and cell viability[41]. Increasing evidence demonstrate that defects in mitochondrial dynamics result in a list of degenerative disorders such as neuropathy and neurodegeneration[48], indicating that mitochondrial morphology is directly linked to mitochondrial function and apoptosis.

1.2.1 Mechanisms of Mitochondrial Fusion

Since it was revealed in the 1980s that mitochondria build the interconnected and tubular network[42], evidence on mitochondrial fusion machinery and mechanisms have accumulated in the past two decades. In general, membrane fusion including mitochondrial membrane is a complex process mediated by membrane-anchored protein complexes: for instance, soluble N-ethylmaleimide-sensitive fusion protein attachment receptors (SNAREs) in intracellular membrane fusion events[43]. The first mediator of mitochondrial fusion was discovered in Drosophila, *fzo*[44]. It is highly conserved in other metazoans such as yeast (Fzo) and mammals (MFNs)[45]. Later, it was found that MFNs are large dynamin-like GTPases that have distinct domain structures (Fig 1A): (1) a GTPase domain with a long helix-loop-helix and a long four-helix bundle; (2) two transmembrane helices resembling a hydrophobic paddle that is involved in membrane spanning; and (3) tetratricopeptide repeat motif (TPR) that mediates oligomerization[46-48]. These domain structures suggest that MFN1/2 is located at mitochondrial outermembrane (MOM) and is directly involved in MOM fusion. Mgm1, the yeast homolog of OPA1, is also a dynamin-related GTPase that is required for mitochondrial innermembrane (MIM) fusion[49]. It contains an N-terminal MTS that is cleaved by matrix processing peptidase (MPP) following mitochondrial import, indicating that Mgm1 is located in MIM or intermebrane space (IS)[50]. Mgm1 also has a distinct domain structure, which is more complex than MFN1/2: (1) MTS; (2) MPP processing site; (3) transmembrane domain; (4) alternative processing sites; (5) GTPase domain; (6) middle helical domain and (7) GTPase effector domain (Fig 1A)[48,51]. Opa1 mRNA contains eight splice variants, and two cleavage sites (S1 and S2). On their own, long and short OPA1 isoforms are inactive for membrane fusion, whereas they are functionally active

Figure 1. Mitochondrial Fusion.

(A) Top panel is a domain model of MFN1/2, showing the conserved N-terminal GTPase domain following heptad repeats which mediate homo- or hetero-dimer formation at MOM, and the transmembrane domain which is integrated into MOM. OPA1 contains a typical N-terminal MTS and MPP cleavage site following transmembrane region which mediates its integration into MIM, two alternative processing sites (S1 & S2), GTPase domain and GTPase effector domain followed by middle domain (Ref 41). (B) Bottom panel briefly illustrates two step processes of mitochondrial fusion. MFN2 homotypically interacts *in trans* across two mitochondria and facilitates MOM fusion, possibly by binding to and forming clusters at mitochondrial tips. Following MOM fusion, OPA1 mediates MIM fusion depending on GTP hydrolysis, resulting in matrix contents mix (Ref 48).

1A

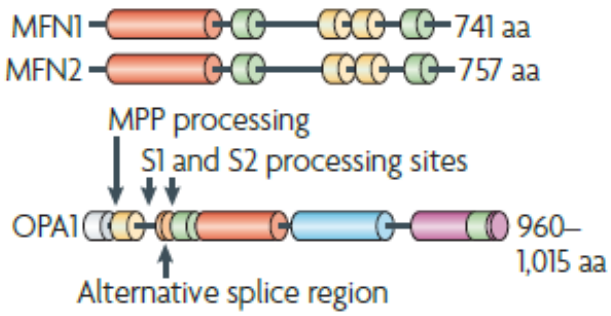
MFN1
741 aa
MFN2
757 aa
MPP processing
S1 and S2 processing sites
OPA1
960–
1,015 aa
Alternative splice region

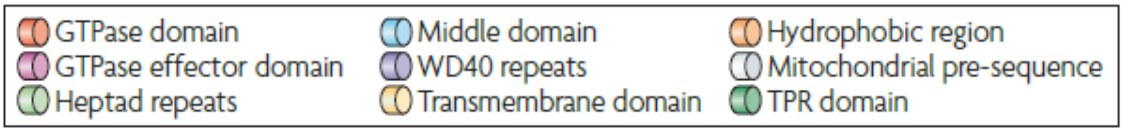
GTPase domain
GTPase effector domain
Heptad repeats
Middle domain
WD40 repeats
Transmembrane domain
Hydrophobic region
Mitochondrial pre-sequence
TPR domain

1B

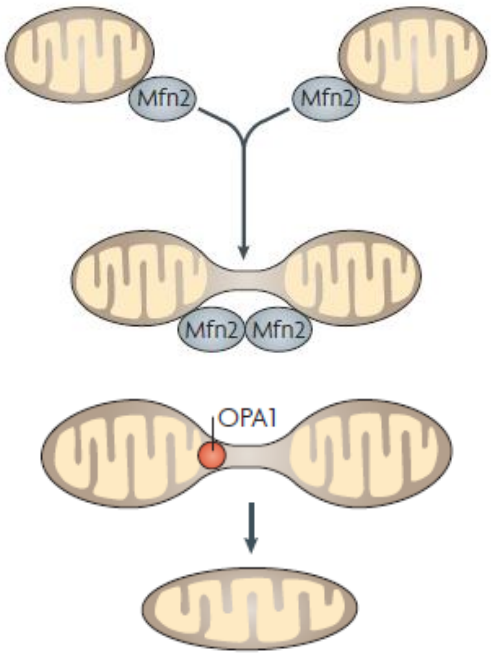
Mfn2
Mfn2
Mfn2
Mfn2
OPA1

when coexpressed. Recently, several mitochondrial proteases were identified in alternative processing of OPA1 at S1 or S2, resulting in the mix of $OPA1_L$ and $OPA1_S$ or $OPA1_S$ accumulation[52,53]. Those processing peptidases include the rhomboid-related protease presenilins-associated rhomboid-like (PARL)[54], i-AAA proteases (e.g. YME1L)[52,53,55,56], and an innermembrane peptidase OMA1[56,57].

Brief molecular pathways of mitochondrial fusion are as follows: (1) the key components of mitochondrial fusion, MFN1/2 and OPA1, are constitutively expressed and located at MOM and MIM; (2) As two mitochondria approach and kiss each other, they are constantly tethered through the C-terminal heptad repeats of MFN1/2 to form an intermolecular anti-parallel coiled coil; (3) Following formation of coiled coil between MFN1 and/or MFN2, GTPases provide energy for membrane fusion following GTP hydrolysis[48,58], (4) after the completion of MOM fusion, OPA1 mediates MIM tethering and fusion by following similar steps with MFN1/2 (Fig 1B)[59]. Under normal condition, MOM fusion is coordinated with MIM fusion, but MOM can operate separately from MIM fusion in some cases[60]. Some evidences demonstrate that under OPA1 depletion or inactivation, overall mitochondrial fusion is impaired with normal MFN1/2 activity[56,57], suggesting that molecule(s) coordinating activities of MFN1/2 and OPA1 may coordinate MOM and MIM fusion events[60,61].

1.2.2 Mechanism of Mitochondrial Fission

Dynamin, a GTPase, has long been known to mediate endocytosis by remodeling plasma membrane structure[62]. Following GTP hydrolysis, assembled Dynamin drives the fission of underlying tubular membrane[63]. Likewise, mitochondrial fission is mainly mediated by a large GTPase, Dynamin-Related Protein 1 (DRP1)[48], and its deletion resulted in highly interconnected mitochondrial network[63,64]. DRP1 is soluble and constitutively expressed in the cytosol. It has four functional domains: (1) N-terminal GTPase domain; (2) middle domain with a helix; (3) GTPase effector domain (4) heptad repeats (Fig 2A)[62,66]. As DRP1 does not possess an MTS and transmembrane domain, it interacts with other mitochondrial partners to allow for its recruitment to MOM. Two proteins, mitochondrial fission 1 (Fis1) and mitochondrial division protein 1 (Mdv1, no known in human homolog) have been first identified to recruit the cytosolic DRP1 to the MOM in yeast[67,68]. Following mitochondrial localization, DRP1 forms oligomeric spiral complexes with a belt-like shape (diameter of ~ 100 nm) at the MOM constriction sites by

interacting with each other through their N-terminal heptad repeats[68,69]. Finally, GTP-bound DRP1 oligomers undergo GTP hydrolysis, which provides energy required for its Dynamin-like action in membrane budding pathways leading to eventual mitochondrial division (Fig 2B)[62,70]. Although it was apparent that hFIS1 recruits the cytosolic DRP1 to MOM, increasing evidence showed that hFIS1 overexpression or depletion did not affect mitochondrial dynamics at a significant level, suggesting that additional pathway for DRP1 recruitment may exist[71]. Mitochondrial fission factor (MFF) can be a possible candidate for the alternative mitochondrial fission proteins. Otera *et al* demonstrated that MFF overexpression enhances DRP1 translocation and results in mitochondrial fragmentation, suggesting that MFF is critical for mitochondrial fission[72].

1.2.3 Roles of Mitochondrial Dynamics on Functional Homeostasis of Mitochondria

Mitochondria tightly control fusion and fission events to maintain their homeostatic morphology. Interestingly, mitochondria are responsive to mitochondrial stresses such as membrane potential loss (me_m) and then modulate fusion and fission[73]. As key regulators of fusion and fission are constitutively expressed, mitochondria contain mechanisms to regulate activities of key components. Studies demonstrated that MFN1/2 were ubiquitinated via PINK1/PARKIN axis in the presence of a membrane uncoupler, carbonyl cyanide-m-chlorophenylhydrazone (CCCP), resulting in reduced MFN1/2 level and ultimate mitochondrial fragmentation[74,75,242]. OPA1 cleavage also regulates mitochondrial fusion responding to mitochondrial damage. Whereas balanced long and short OPA1 isoforms are necessary for MIM fusion leading to interconnected tubular mitochondria, cells undergoing apoptosis or showing lower membrane potential or ATP levels accumulate $OPA1_S$ resulting in fragmented mitochondria[52,54,55,76]. These data together suggest that inducible cleavage of OPA1 and/or MFN1/2 decrease in dysfunctional mitochondria attenuate mitochondrial fusion leading to mitochondrial fragmentation in a DRP1-dependent manner, which ultimately induces mitophagy-dependent clearance of dysfunctional mitochondria to maintain functional network of mitochondria[56].

Lastly, DRP1, a major regulator of mitochondrial fission, is posttanslationally modified for its translocation to mitochondria by various methods: for example, MARCH5 associates with and ubiquitinates DRP1[77] and mitochondrial-anchored protein ligase (MAPL) sumoylates DRP1[78]. MARCH5 or MAPL depletion lowers mitochondrial fission leading to highly elongated

Figure 2. Mitochondrial Fission.

(A) Domain structure of a major regulator of mitochondrial fission; DRP1 has the GTPase domain at the N-terminus, heptad repeats and GTPase effector domain followed by middle domain. (B) Brief mechanism of fission; DRP1 is mainly found in the cytosol and cycles in and out of contact with MOM, possibly by interacting with mitochondrial fission proteins such as hFIS1 and MFF. Following activation such as phosphorylation and dephosphorylation, DRP1 is recruited to MOM, forms homo-oligomers at the scission sites and divides mitochondria following GTP hydrolysis (Refs 41,48).

2A

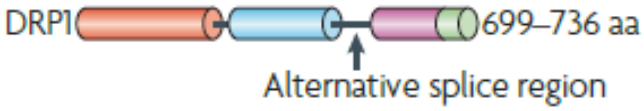
DRP1
699–736 aa
Alternative splice region

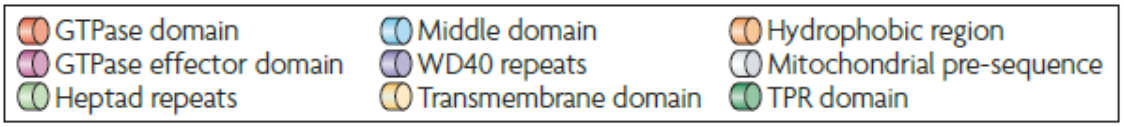
GTPase domain
GTPase effector domain
Heptad repeats
Middle domain
WD40 repeats
Transmembrane domain
Hydrophobic region
Mitochondrial pre-sequence
TPR domain

2B

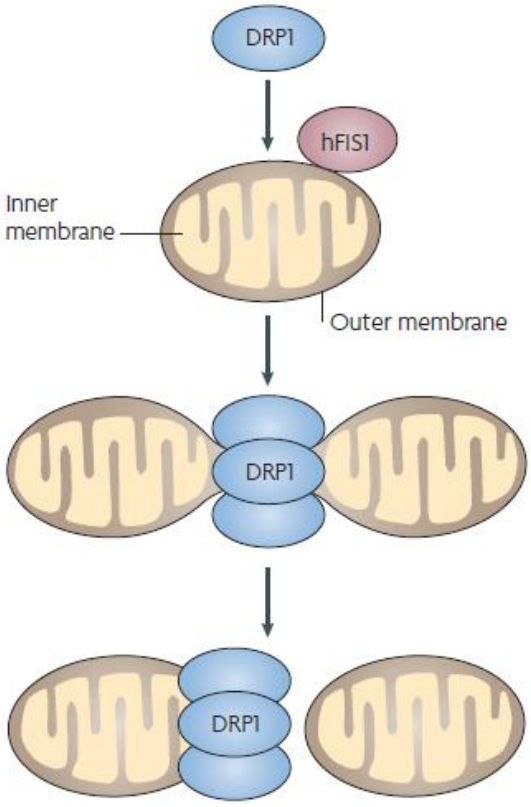
DRP1
hFIS1
Inner membrane
Outer membrane
DRP1
DRP1

mitochondrial network. Furthermore, DRP1 activity is regulated by reversible phosphorylation with three different kinases/phosphatases: cyclin-dependent kinase 1 (CDK1)[79], cAMP-dependent protein kinase A (PKA)[80] and Ca2+/calmodulin-dependent protein kinase 1in-dependen[81,82]. Following phosphatase activation, DRP1 is dephosphorylated and translocated to MOM leading to mitochondrial fragmentation[82]. Increasing evidence showed that cellular stresses often caused both DRP1 activation and OPA1 cleavage simultaneously resulting in mitochondrial fragmentation. In addition, recent findings demonstrated that mitochondria are highly fragmented at ER tubule contact sites, which is dependent on actin polymerization through ER-localized inverted formin 2 (INF2)[83,84]. Taken together, in mammalian cells, mitochondria develop multiple regulatory factors/pathways and communicate with other organelles such as ER to modulate their fusion and fission events, resulting in homeostasis of their morphology and function.

1.2.4 Relevance of Mitochondrial Dynamics in Physiology

Mitochondrial proteins and mtDNA are almost always exposed to harmful environments including ROS, irradiation, toxic chemicals and protein aggregates. Paradoxically, damaged mitochondria recover by sharing contents with healthy mitochondrial network through fusion, and they are also removed by autophagy (″mitophagy″, autophagy specific to mitochondria) following separation from functional network to avoid the catastrophe of whole mitochondria[48]. Here, we describe physiological relevance of mitochondrial homeostasis of morphology in several perspectives.

Cell cycle control and development. Mitochondria must be inherited during cell division. For mitochondrial inheritance, it is known that mitochondria are amplified during interphase, completely fragmented, and set apart during cytokinesis[85]. Current arguing findings show that DRP1 deletion in mouse embryonic fibroblasts did not affect cytokinesis, although Drp1-knockout mice were embryonic lethal[86]. In addition, disruption of fusion through OPA1 deletion in mouse models led to mitochondrial dysfunction and heteroplasmy rise followed by mitochondrial nucleoid loss in forebrain and cerebellum, but mice were not embryonic lethal[87,88]. These data imply that mitochondrial fission and fusion processes are critical in cell cycle control and mammalian brain development.

Mitochondrial distribution. Obviously, large and elongated cells such as neurons

require mitochondrial distribution to supply energy throughout their extended dendrites. Drp1-knockout mice showed severe abnormalities in the forebrain and the cerebellum, and mitochondrial accumulation in the cell body of neurons[86]. Intriguingly, Mfn2-knockout mice also failed to distribute mitochondria to the long branched neurites[88]. These data suggest that both fusion and fission are critical for mitochondrial distribution.

1.2.5 Possible Link between Mitochondrial Dynamics and Apoptosis.

It has been well studied that upon MOM permeabilization by oligomerized BAX/BAK following proapoptotic stimuli, cytochromce *c* and other proapoptotic proteins are released into the cytosol from mitochondria, which triggers the apoptotic caspase cascade reactions[89]. Interestingly, current findings demonstrated that cytochrome *c* release involves mitochondrial fragmentation through direct DRP1 interaction with BAX/BAK at MOM during apoptosis[90]. DRP1 deficiency attenuates cytochrome *c* release and caspase-3/PARP cleavage[91]. Conversely, Brooks *et al* argued that during apoptosis, BAK dissociates from MFN2 and associates with MFN1 leading to mitochondrial fragmentation[92], implying a crosstalk between apoptosis and mitochondrial fragmentation via the direct interaction between proapoptotic facilitators such as BAX/BAK and mitochondrial dynamics regulators such as DRP1/MFN1/MFN2[92,93]. In addition, Chen *et al* found markedly higher apoptosis in MFN2-null cerebella and OPA1 deletion mice[88]. Ishihara *et al* reported that DRP1 is required for cytochrome *c* release and caspase activation during apoptosis, although mitochondrial outer membrane permeabilization occurrs independent of DRP1[86]. In spite that many issues still remain controversial and further work is required to elucidate the mechanisms connecting cytochrome *c* release and mitochondrial fragmentation, we believe a direct link between mitochondrial morphology and apoptosis.

1.2.6 Defects of Mitochondrial Dynamics in Diseases

Defects in mitochondrial fusion and fission from mouse models mainly led to neuronal disorders, which is consistent with the facts that neurons are sensitive to mitochondrial dysfunction and impairment of mitochondrial distribution[48]. Genetic mutations in MFN2 causes a particular neuropathy, Charcot-Marie-Tooth disease type 2a (CMT2A), resulting in progressive distal sensory and motor neuron impairments caused by degeneration of long peripheral nerves[94]. In addition, OPA1 mutations were discovered in autosomal dominant optic atrophy (ADOA), the

most common childhood blindness resulting from degeneration of retinal ganglion cells[95,96]. Together, mitochondrial homeostasis of morphology is closely coupled with mitochondrial function and apoptosis.

1.3 HSP40:HSP70 System

1.3.1 Structure and Classification

1.3.1.1 J proteins (also known as HSP40s)

All J proteins contain a highly conserved DnaJ domain, which is named after *Escherichia coli* DnaJ protein, but other amino acid sequences except DnaJ domain are very diverse among members[30,97,98]. Although the molecular weights of J protein members are varied, they have often been referred to as HSP40s for historical reasons. We refer to J proteins as HSP40s in this study. As of 2010, forty-one HSP40s have been identified in humans, and these have been classically grouped into three classes (A, B and C) according to their domain structures (Table 4)[30,99-101]. Briefly, class A HSP40s have the N-terminal DnaJ domain, followed by Gly and Phe-rich domain and C-terminal domains that are known as the client-binding and dimerization domain (Fig 3A). Class B members include DnaJ and Gly-Phe rich domains, and other HSP40s are designated as class C. It must be noted that this classification does not relate to their cellular and biochemical functions.

DnaJ domain. A His-Pro-Asp tripeptide (HPD) motif is typically conserved in the DnaJ domain. This HPD motif is a crucial linker between helix I, II and helix III, IV, through which HSP40 interacts with HSP70 and stimulates ATPase activity of HSP70s[102-105]. One amino acid change His to Gln (HQ mutation) in the HPD motif has been discovered to abolish the interaction between HSP40 and HSP70 and its activity to stimulate ATP hydrolysis (Fig 3B)[106-108].

Gly-Phe rich domain. Besides functioning as a linker between the DnaJ domain and C-terminal domains, its function is questionable, and its requirement for co- chaperone function is flexible[109,110].

C-terminal domain (CTD). This domain is structurally diverse and has low sequence similarity among the various HSP40s, and composed of two domains, CTD I and CTD II. CTD I has four repeats of the CxxCxGxG type zinc fingers and a hydrophobic pocket forming a client protein binding site[111-113]. CTD II is an extension of CTD I, but has no identified motifs except a

Table 4. Human J Proteins (HSP40s)

Gene name	Function	Synonyms
Promiscous client binding		
DNAJA1	Protein folding, androgen receptor signaling, heat-inducible	DJ2, NEDD7
DNAJA2/A4	Protein folding, heat-inducible	DJ3; DJ4
DNAJA3	Protein folding, positive regulation of apoptosis, mtDNA replication, mitochondrial	Tid1, hTid1
DNAJB1	Protein folding	Sis1, Hsp40
DNAJB4, B5	Protein folding	DJB4; Hsc40
DNAJB11	ER protein folding, mRNA modification	DJ-9, ABBP2
DNAJB9	ER protein folding	MDG1
DNAJB2a, 2b	Protein folding, negative regulation of protein ubiquitination	HSJ1
DNAJB6a, 6b	Protein folding, intermediate filament organization	DJ-4, MSJ1
DNAJB8	Protein folding	DJ-6
DNAJB7	Protein folding	DJ-5
DNAJB12a, 12b	Protein folding	DJ-10
DNAJB14a, 14b	Unclear	
DNAJC18	Unclear	
Selective client binding		
DNAJC21	Unclear	DNAJA5
DNAJC24	Unclear	DPH4
DNAJC5, 5b, 5g	Regulating K^+/Na^+ channel, synaptic transmission	CSPα
DNAJC20	Iron-sulfur cluster assembly, mitochondrial	HSC20, Jac1
DNAJC17	Unclear	
DNAJC10	ER protein folding	JPDI
DNAJC16	Unclear	
DNAJC6	Protein folding, cellular membrane organization	DJC6
DNAJC26	Cell cycle regulation	
DNAJC27	Small GTPase signaling, mitochondrial	RBJ
DNAJC3	Negative regulation of protein kinase, ER	p58
DNAJC7	Protein folding	DJ11
DNAJC29	Mutated in ARSACS	ARSACS
DNAJC14	Protein folding	HDJ3
DNAJC22	Unclear	
Client binding is unclear		
DNAJB13	Protein folding	Tsarg
DNAJB3	Unclear	HCG3
DNAJC13	Unclear	RME8

Client binding is unclear		
DNAJC28	Unclear	
DNAJC9	Protein folding	HDJC9
DNAJC8	RNA splicing	SPF31
DNAJC25	Unclear	
No client binding		
DNAJC23	Protein targeting to membrane	SEC63L
DNAJC1	Translation regulation	HTJ1
DNAJC2	DNA replication and chromatin modification	ZRF1
DNAJC15	Unclear	MCJ
DNAJC12	Unclear	JDP1
DNAJC19	Protein targeting to mitochondria, mitochondrial innermembrane, interacting with mtHsp70	TIM14
DNAJC30	Unclear	
DNAJC4	Unclear	HSPF2

* J proteins employed in this study were boxed in pink.

Figure 3. Domain Structure of HSP40s

(A) HSP40 structure consists of a list of distinct domains: the DnaJ domain with HPD motif, G/F-rich domain, C-terminal domain I with zinc finger repeats, C-terminal domain II with or without Cys-rich domain, and dimerization domain. (B) DnaJ domain contains four α-helices and His-Pro-Asp (HPD) tripeptide motif between helix II and III which is critical for the interaction of HSP40s with HSP70s and stimulates ATPase activity of HSP70s. (C) Dimerized client binding domains of yeast Ydj1 form a pocket with zinc finger repeat, CTD I and CTD II (Ref 30).

3A

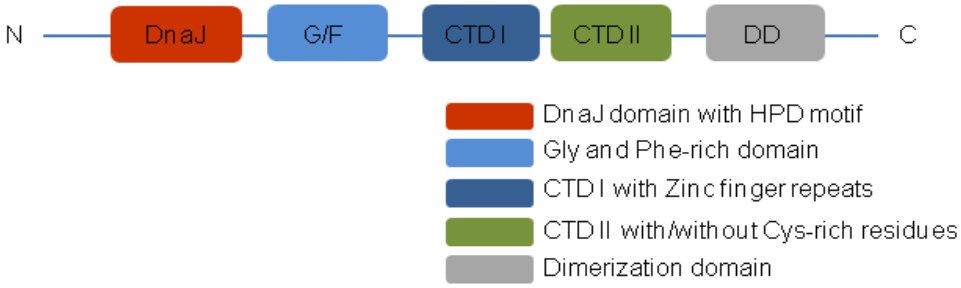
N
DnaJ
G/F
CTD I
CTD II
DD
C
DnaJ domain with HPD motif
Gly and Phe-rich domain
CTD I with Zinc finger repeats
CTD II with/without Cys-rich residues
Dimerization domain

3B

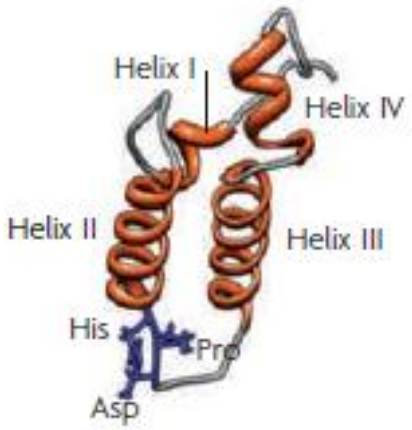
Helix I
Helix IV
Helix II
Helix III
His
Pro
Asp

3C

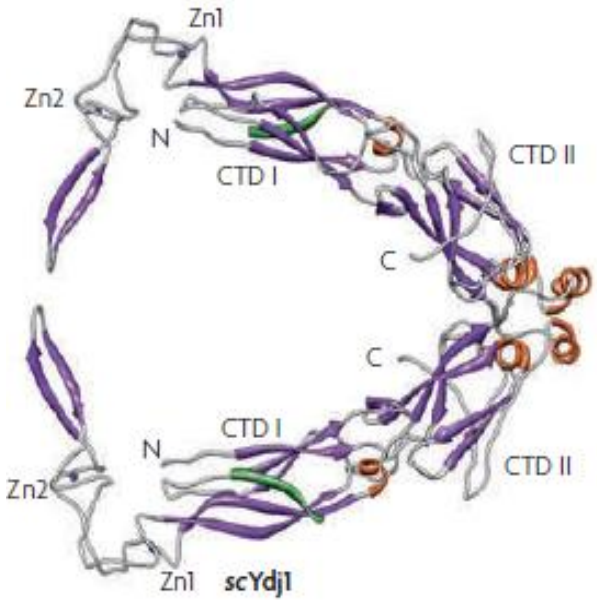
Zn1
Zn2
N
CTD I
CTD II
C
C
CTD I
N
CTD II
Zn2
Zn1
scYdj1

Cys-rich domain[114,115]. Mutants lacking CTDs in yeast HSP40s, Ydj1 and Sis1 are not viable, indicating that the client binding ability of these domains is required for cell viability *in vivo* (Fig 3C)[114,116].

Dimerization domain (DD). The extreme C-terminus is required for forming homo-dimers, which increases client binding affinity[117,118]. The crystal structure of this domain was first determined by Wu *et al* in yeast Ydj1 using the MAD method. The C-terminus of one monomer forms a nding affinityility of thpeat, CTD I and CTD II (lix I, II and helix III, IVstructures [119].

1.3.1.2 HSP70s

As shown in Table 5, eleven HSP70s have been discovered in humans by 2010. Unlike the diversity of HSP40 functions and structures, most HSP70s mediate protein (re)folding or deaggregation. All key domains except the subcellular localization signal sequences are well conserved in most HSP70s except HSPA12 and HSPA14: ATPase domain and C-terminal domain consisting of substrate binding domain (SBD) and Lid domain (Fig 4A)[27,30,120,121].

ATPase domain. The 40 kDa ATPase domain consists of two lobes: helix IA and IB in lobe I, and helix IIA and IIB in lobe II. In the interface between subdomain IIA and IIB, there is a cleft that is important in ATP-binding (Fig 4B)[122,123]. C-terminal helix 8, helix 9, and rface between subdomain IIA and Inucleotide exchange factor (NEF) recognition[124]. Freeman *et al* identified the regulatory motif of ATPase activity in HSP70 by mapping the C-terminal boundary between the ATPase domain and substrate binding domain, Glu-Glu-Val-Asp (EEVD) motif which is well conserved in all cytosolic HSP70s[125]. Interestingly, HSP70 ATPase activity has been reported to be regulated by EEVD motifs in the extreme C-terminal Lid domain and, not by the ATPase domain[124,125].

Substrate binding domain (SBD) and Lid domain. The 25 kDa C-terminal SBD binds to five hydrophobic amino acid residues of substrate proteins exposed externally[126]. The crystal structure of the SBD demonstrated that the α-helical Lid domain and at the α-helical SBD dobic amino acid residues [127]. The α-helical Lid domain located at the extreme C-terminus increases the stability of substrate-bound HSP70 complex, but has no contact with substrates. In addition, the Lid-forming helix B has three different states of conformation, providing HSP70s with the flexibility of substrate-binding or a broad spectrum of substrate-specificity. Through a channel

Table 5. Yeast and Human HSP70s

Yeast	Human		
Gene name		Function	Synonyms
Ssa1-4; Ssb1,2	HSPA1	Protein folding, protein ubiquitination, heat-inducible	HSP70
	HSPA2	Protein folding	HSP72
	HSPA6	Protein folding	HSp70B'
	HSPA7	Protein folding, protein modification	HSP70B
	HSPA8	Protein folding, neurotransmitter secretion, mRNA processing and membrane organization, constitutive	HSC70
Kar2	HSPA5	Protein folding, ER stress	GRP78
Ssc1; Ssq1; Emc10	HSPA9	Protein folding, negative regulation of apoptosis, p53 interaction, mitochondrial	GRP75, Mortalin, mtHsp70
	HSPA12A, B	Unclear	
Ssz1	HSPA14	Protein folding	HSP70L1

* Mitochondrial HSP70 was boxed in pink.

Figure 4. Domain Structure of HSP70s

(A) HSP70s have well conserved domains among other members: ATPase domain critical for binding to HSP40s and NEFs, peptide binding domain (SBD) and LID domain. (B) ATPase domain structure consists of 4 subdomains: IA, IB, IIA & IIB. Helix 8, helix 9 and β-sheet E in IIB are involved in NEF binding. Yellow stick represents ADP (Ref 124). (C) The structure of ADP-bound HSP70 (close form). A hydrophobic linker connects the ATPase domain and peptide-binding domain. ATP binding to ATPase domain stretches LID domain out of substrate binding domain (open form) (Ref 30).

4A

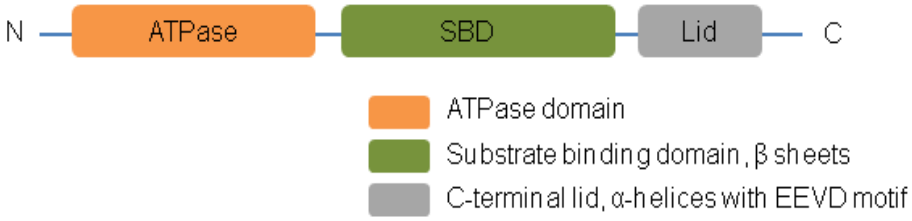
N
ATPase
SBD
Lid
C
ATPase domain
Substrate binding domain, β sheets
C-terminal lid, α-helices with EEVD motif

4B

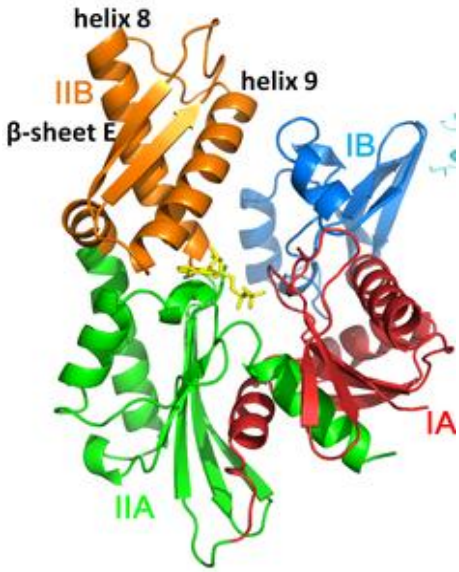
helix 8
IIB
helix 9
β-sheet E
IB
IA
IIA

4C

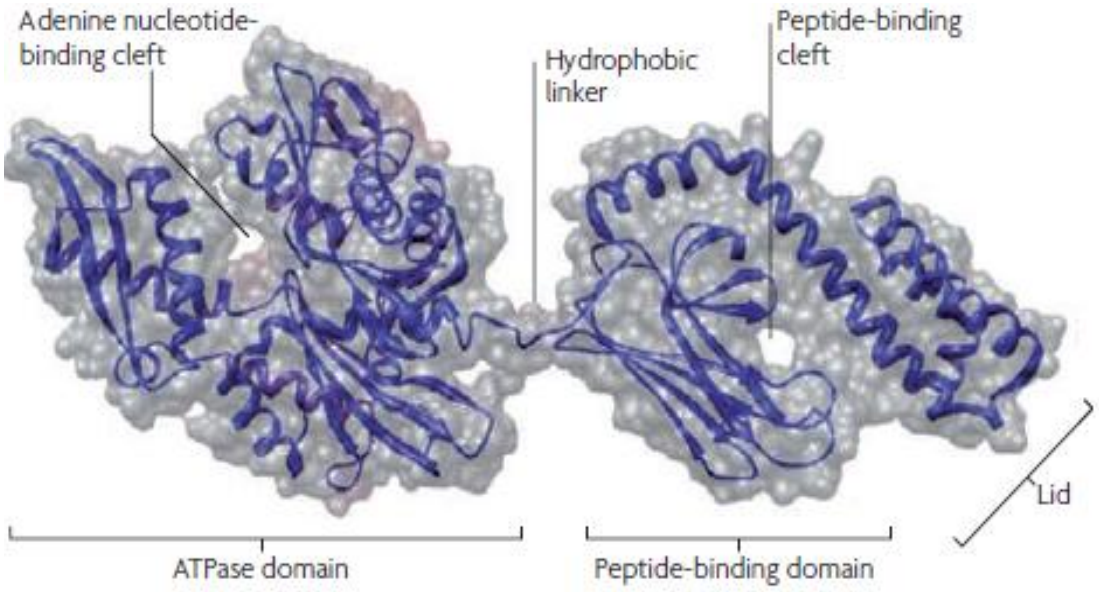
Adenine nucleotide-binding cleft
Hydrophobic linker
Peptide-binding cleft
Lid
ATPase domain
Peptide-binding domain

stretched by loops of the client binding domains of yeast Ydj1 form a pocket4C)[128-130]. EEVD motifs in the C-terminal Lid domain regulate the ATPase activity of the N-terminal ATPase domain.

1.3.2 Mode of HSP40:HSP70 Network

Looking at the domain structures of HSP40s and HSP70s, it is first of note that the DnaJ domain or ATPase domain alone may be sufficient for some cellular roles. In other words, HSP40s and HSP70s lacking SBD can function without substrate binding[30]. HSP70s always function as a team with HSP40s and NEFs. Unfolded or misfolded proteins with hydrophobic amino acid residues exposed externally are first delivered to ATP-bound HSP70 by co-chaperones like HSP40s containing the C-terminal client binding domain. As ATP-bound HSP70s has a low affinity to substrates, HSP40s accelerate ATP-bound HSP70s interaction with substrates[114,131-134]. During this step, the HPD motif of DnaJ domain mediates HSP40 interaction with ATP-bound HSP70 through the ATPase domain of HSP70[106-108]. Upon formation of HSP40-substrate-ATP-HSP70 complexes, the DnaJ domain of HSP40 triggers ATP hydrolysis, followed by its conformational change to substrate-ADP-HSP70 which has a high substrate affinity to substrates, resulting in the release of HSP40 and closing of the Lid domain[135-139]. Next, ADP replacement by ATP is catalyzed by NEFs and ATP binding causes opening of the α-helical Lid domain, leading to dissociation of substrate, ATP-HSP70 and NEF. Open ATP-bound HSP70 and NEF are recycled for further substrate binding as HSP40 (Fig 5)[140,141]. Accumulating *in vitro* evidence using recombinant proteins of HSP40 and HSP70 showed that HSP70 chaperonic activity reached the maximal activity at a critical concentration of HSP40, and HSP40 protein alone could be served as a substrate of HSP70, which could reduce HSP70 chaperonic activity for other substrates[142,143]. Hageman and Kampinga proposed (unpublished observations) that HSP40 overexpression above the optimal ratio of HSP40:HSP70 could reduce the folding capacities of HSP70 in cells, respectively[30]. Those data suggest that the HSP40:HSP70 chaperonic network may function *in vivo* at a stoichiometric ratio. However, this proposal of *in vivo* HSP40:HSP70 stoichiometry needs to be tested.

1.3.3 Chaperone Dysfunction and Diseases

As described in Table 3, a number of diseases including cancers and CNS defects are

Figure 5. A Proposed Mode of HSP40:HSP70 Chaperonic Network.

(1) HSP40 recognizes and tightly binds a client polypeptide through CTD I and CTD II followed by its interaction with ATP-bound HSP70. (2) A client polypeptide interacts transiently with "open" ATP-bound HSP70. (3) ATP hydrolysis is stimulated by DnaJ domain of HSP40, which causes a conformational change of mtHsp70 leading to tight binding of mtHsp70 to the client polypeptide ("closed"). (4) HSP40 is released from the complex. (5) NEF recognizes ADP-bound HSP70 and replaces ADP by ATP, which triggers the opening of LID domain. (6) ATP-bound HSP70 and the client polypeptide are dissociated. Until the client polypeptide is folded properly, it undergoes this folding / refolding cycle.

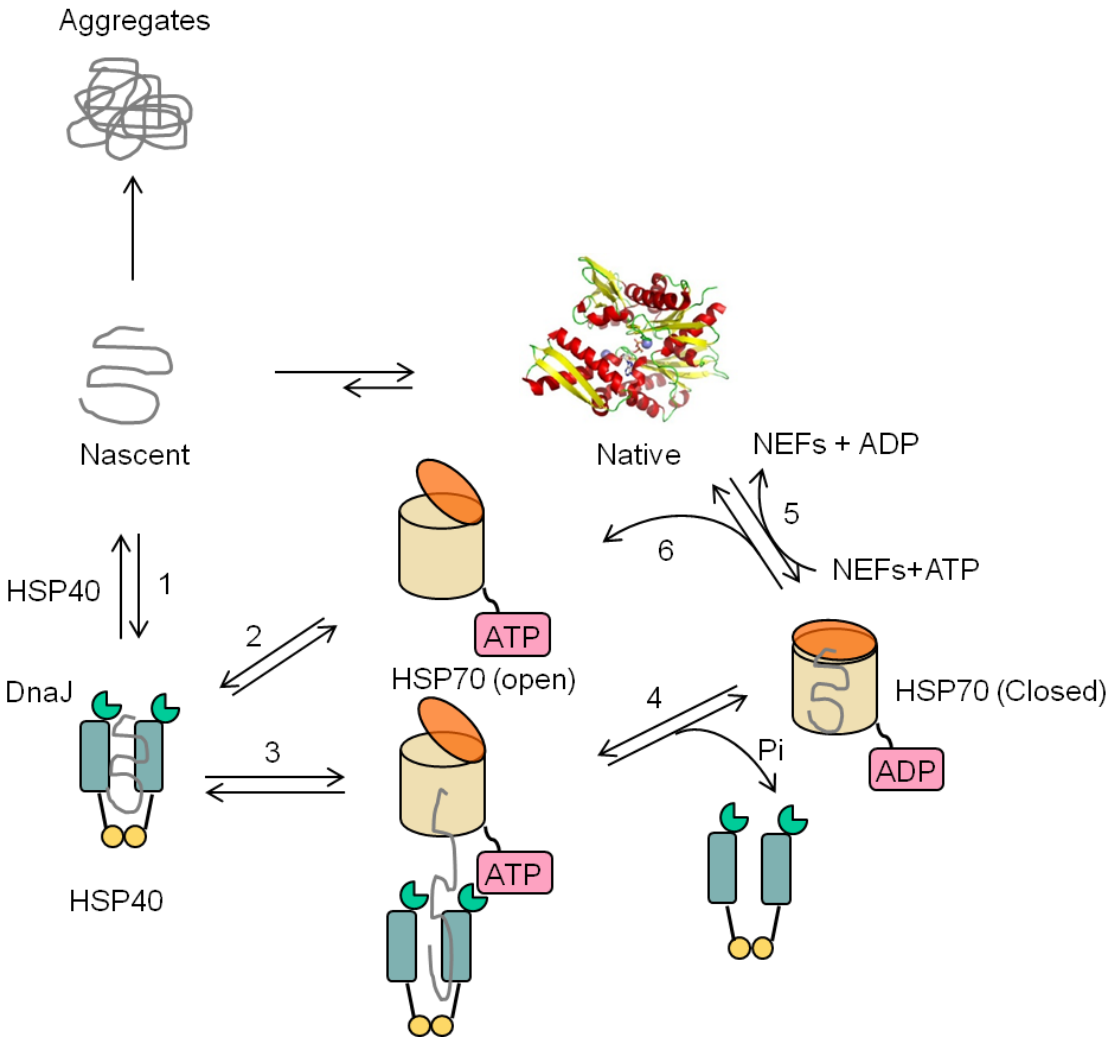
Aggregates
Nascent
Native
NEFs + ADP
5
6
NEFs+ATP
HSP40
1
2
DnaJ
ATP
HSP70 (open)
HSP70 (Closed)
4
3
Pi
ADP
HSP40
ATP

associated with chaperone dysfunction or deregulation[24-26]. Tokuriki and Tawfik reported an interesting finding that *E. coli* chaperonin (GroEL/GroES) overexpression stabilized mutant proteins, leading to higher genetic variation and protein evolution[144]. In many cancers, it has long been reported that gain-of function mutations or upregulation of chaperones including HSP40, HSC70 and HSP90, accumulate and stabilize mutated or upregulated oncogenes and stimulate cell survival[145-147]. Conversely, loss-of function of chaperones or downregulation of chaperones were often found in genetic disorders and neurodegenerative diseases such as Alzheimer′s Disease (AD) and Parkinson's Disease (PD)[25,148]. For instance, as aging occurs, patients often fail to activate chaperones in a response to deposits of protein aggregates, which insults devastating effects on cell life; for example, misfolded aggregates of insoluble heat-stable devastating effects on cell life; for exampdeposited in neurons, resulting in neuronal death and ultimately causing neurodegeneration[149,150]. In an attempt to reactivate chaperones in these loss-of-function diseases and to reduce aggregated protein deposits, activating heat-shock factor 1 (HSF1) or HSP70 was tested and its efficacy has already been demonstrated[151,152].

Taken together, organisms regulate the chaperonic activity of HSP40:HSP70 network to maintain proteostasis and cell viability responding protein-related stresses.

1.4 Mitochondrial Heat Shock Protein 40 (mtHsp40 or Tid1)

Mitochondrial heat shock protein 40 (mtHsp40, also called h-Tid1 or Tid1) is the homolog of the yeast Mdj1 and the Droshophila Tid56 tumor suppressor[36]. Since it has been reported that mtHsp40 modulates apoptosis in cancer cell lines, a majority of studies on mtHsp40 (or Tid1) focused on its functions as a tumor suppressor[37-39,153-155]. For example, signaling pathways and apoptosis in a response to mtHsp40 overexpression or deletion were investigated in cells or *in vivo*. Conversely, its roles for mitochondrial proteostasis and functions did not gain the attention from researchers, and most results related with its chaperonic functions came from the yeast homolog Mdj1.

1.4.1 MtHsp40 Isoforms

The human mtHsp40 gene encodes for three splice variants of mtHsp40 mRNA based on mRNA sequence analysis. The longest isoform, mtHsp40$_L$ (43 kDa), includes all eleven exons,

and the intermediate isoform, mtHsp40$_I$ lacks 34 amino acids (447-480, 40 kDa) resulting from splicing between exons ten and eleven[156]. There also exists a shorter isoform, mtHsp40$_S$ lacking exon 5 (50 amino acids, 38 kDa); however, this isoform is hard to detect (Fig 6)[156]. In this study, since we detected only two isoforms, mtHsp40$_L$ and mtHsp40$_I$, we designated mtHsp40$_I$ as mtHsp40$_S$.

1.4.2 MtHsp40 Expression and Subcellular Localization

Even though it has been classified as one of heat shock protein 40s, mtHsp40 is not heat-inducible, but constitutively expressed. In a majority of tissues, transcripts of both mtHsp40$_L$ and mtHsp40$_S$ were highly detected; however, expression level was dependent on tissue types, metabolic states and developmental stages[156]. For instance, the highest mtHsp40 levels were found in liver and skeletal muscle[157]. Even though many proteins were reported to interact with mtHsp40 in multiple intracellular compartments including the cytosol[158-160], plasma membrane[161] and mitochondria (Table 6)[162], endogenous mtHsp40 has been found mainly in mitochondria[158]. In particular, Syken *et al* demonstrated that both isoforms of mtHsp40 are localized in the mitochondrial matrix[38].

1.4.3 MtHsp40 Structural Domains

Although mtHsp40 crystal structure has not been identified yet, primary amino acid sequences indicated that mtHsp40 belongs to the DnaJA family, and it contains their five distinct structural domains: mitochondrial targeting sequence (MTS), DnaJ domain, Gly/Phe-rich domain, C-terminal domains (CTDs), and putative dimerization domain (DD) (Fig 7). Human and mouse mtHsp40s have a sequence similarity of 87.5% in MTS, 95% in DnaJ domain, and 92% in CTDs[38,159]. MtHsp40 MTS contains both the mitochondria targeting (MAARCS) and processing (LRPGV) sequences[38,153]. Following import to mitochondria, the pre-sequence is cleaved off in the matrix by a certain matrix processing peptidase (MPP)[160]. Unprocessed mtHsp40 is not detectable under normal condition, suggesting that transport of endogenous mtHsp40 is highly efficient. Other domains of mtHsp40 are well conserved between different members of Type A HSP40s (Fig 3). Its CTD 1 has zinc finger motifs and CTD II has a Cys-rich motif[163].

1.4.4 Roles for MtHsp40 in Cell Physiology

Figure 6. Genetic and Domain Structure of MtHsp40.

(A) Genomic organization of mtHsp40 and the exon structure of its three splice variants. Long isoform (mtHsp40$_L$, 480 amino acids) consists of 11 exons, intermediate isoform (mtHsp40$_I$, 453 amino acids) is deficient in exon 11, and short isoform lacks exon 5 (mtHsp40$_S$, 427 amino acids) (156). (B) Domain structure of mtHsp40: N-terminal mitochondrial-targeting sequence (MTS) and processing site by MPPs, DnaJ domain with HPD motif, G/F rich domain, C-terminal domain I with zinc finger repeats, C-terminal domain II with Cys-rich domain and putative dimerization domain.

6A

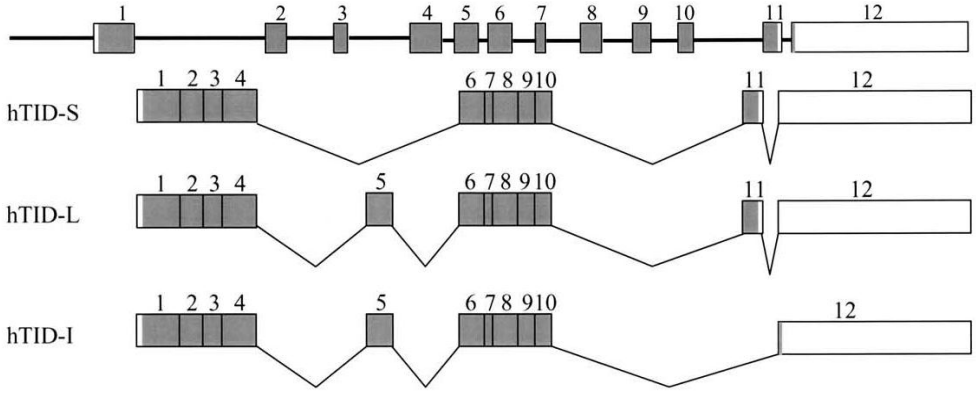
1 2 3 4 5 6 7 8 9 10 11 12
hTID-S
1 2 3 4 6 7 8 9 10 11 12
hTID-L
1 2 3 4 5 6 7 8 9 10 11 12
hTID-I
1 2 3 4 5 6 7 8 9 10 12

6B

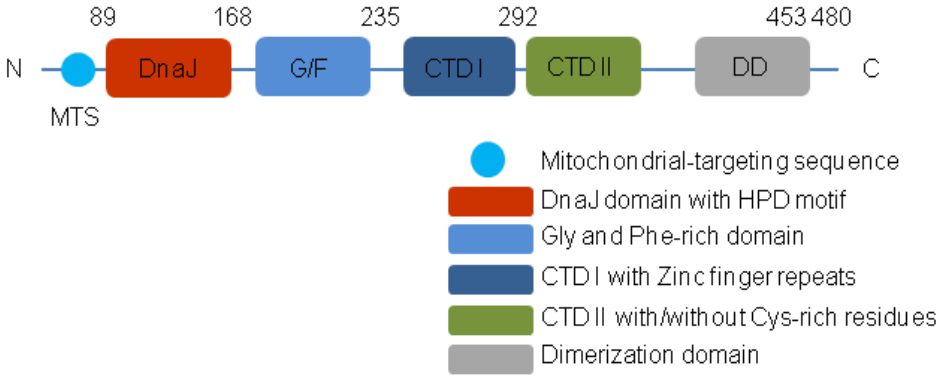
89
168
235
292
453 480
N
DnaJ
G/F
CTD I
CTD II
DD
C
MTS
Mitochondrial-targeting sequence
DnaJ domain with HPD motif
Gly and Phe-rich domain
CTD I with Zinc finger repeats
CTD II with/without Cys-rich residues
Dimerization domain

Table 6. MtHsp40-Interacting Proteins

Name	Compartment	Related Functions	Refs
HPV16 E7	Cytosol	Viral oncoprotein	
Tax	Cytosol	Viral	
HSV1 UL9	Cytosol	Viral	
HBV	Cytosol	Viral	
EBV	Cytosol	Viral	
BARF	Cytosol	Viral	
Patched	Plasma membrane	Sonic Hedgehog (SHH) signaling	
ErbB-2	Plasma membrane	RTK signaling	
EGFR	Plasma membrane	RTK signaling	
Trk	Plasma membrane	RTK signaling	
MET	Cytosol	RTK signaling	
pVHL	Cytosol	HIF1α signaling	
IFN-γR2	Cytosol	JAK/STAT signaling	
IKK	Cytosol	NF-κB signaling	
RasGAP	Plasma membrane / cytosol	Ras signaling	
Smad	Cytosol	TGFβ signaling	
APC	Cytosol	Wnt signaling	
MuSK	Cytosol	Agrin signaling	
TP53	Cytosol(?)	Apoptosis	
CHIP	Cytosol	Protein stability	
mtHsp70	Mitochondria	Protein folding and import	
PolgA	Mitochondria	mtDNA replication	
CRIF	Mitochondria	mt mRNA translation	

It has been reported that mtHsp40 null mice died in the early embryonic stage, indicating that mtHsp40 plays an important role in embryogenesis[163]. To address its function during embryogenesis, Lo *et al.* generated a conditional knockout mouse model of mtHsp40. They found that mouse embryos were lethal between the E4.5 to E7.5 stage, suggesting that mtHsp40 is required for early stages of development[163]. Their unpublished observations demonstrated that brain-specific knockout mouse models of mtHsp40 also died shortly after their birth, indicating that mtHsp40 is also critical for brain development. Hayashi *et al* studied the effects of heart-specific mtHsp40 deletion on heart organogenesis and function. They found that embryos were lethal between the E4.5 to E7.5 stage, suggesting that mtHsp40 is required for early stages of development[163]. Their unpublished observations demonstrated that brain-specific knockout mouse model of mtHsp40 also died shortly after their birth, indicating that mtHsp40 is also critical for brain development. Hayashi *et al* studied the effects of heart-specific mtHsp40 deletion on heart organogenesis and function. They found that mice with heart-specific deletion of mtHsp40 died before the 10 week of age after birth, and showed typical features of heart failure and cardiomyocyte degeneration[162]. In addition, they found that mtHsp40 physically interacts with PolgA, and mtHsp40 deletion caused defects in mtDNA replication, leading to mtDNA loss in cardiomyocytes[162]. Overall, mtHsp40 plays important roles in functional homeostasis of mitochondria during embryonic development, which is not consistent with a Drosophila homolog, TID56, of which deletion causes the tumorous growth of imaginal discs[36].

1.4.5. Relevance of MtHsp40 in Cancers and Apoptosis

Since its discovery, mtHsp40 was soon reported to play a causal role in cancer-related responses including senescence, apoptosis and migration. Kim *et al* found that mtHsp40 depletion by small interfering (si)RNA both in breast cancer cell lines and xenograft models resulted in increased migration, demonstrating that cancer migration and metastasis can be inhibited in the presence of mtHsp40[154,164]. This effect was due to elevated production and secretion of Interleukin (IL)-8, which is modulated by NF-κB transcriptional activity. MtHsp40 seemed to negatively regulate NF-κB, which possibly modulates IL-8 levels[164]. Recently, accumulating data show that mtHsp40 expression level is negatively associated with tumor stages, survival or recurrence in Human Head and Neck Squamous Cell Carcinomas (HNSCC) and breast cancers[155,165,166].

It is also known that mtHsp40 plays a general role in apoptosis as an important apoptotic regulator. Multiple reports showed that its overexpression enhances apoptosis and its deletion causes resistance to proapoptotic stresses[38,153]. Syken *et al* demonstrated an opposing effect on apoptosis between mtHsp40$_L$ and mtHsp40$_S$. While mtHsp40$_L$ demonstrated pro-apoptotic, mtHsp40$_S$ showed anti-apoptotic activities[38]. In glioma cells such as SF767 which interestingly harbors a 52kDa mtHsp40 variant, ectopic expression of mtHsp40$_S$, was able to sensitize this cell line to apoptosis[153]. Taken together, it is well established that mtHsp40 plays roles in apoptosis leading to inhibition of cancer cell proliferation and metastasis; however, it remains questionable how mitochondrial matrix HSP40 (mtHsp40) can modulate apoptosis.

1.5 Mitochondrial Heat Shock Protein 70 (mtHsp70 or Mortalin)

Wadhwa and Kaul identified a 66-kDa protein (named as ix HSP4in″) in the cytosol which was expressed differentially between mortal MEFs and immortal MN48-1 (a derivative of NIH313) cells using differential proteome analysis, and later identified a member of HSP70 family by employing cell fusion of MEFs and MN48-1 cells[167,168]. When they first discovered Mortalin, they reported two variants, mot-1 and mot-2 and two amino acid variation between mot-1 and mot-2[167,168]. MOT-1 was perinucleic and MOT-2 was mainly cytosolic. MOT-2 was later known as mtHsp70. Enhanced MOT-2 induced cellular senescence in NIH 3T3 cells[169,170]. Since mtHsp70 has been reported to induce immortality in fibroblasts in the early 1990s, researchers have focused on mtHsp70 function in cancers. More recently, it has been reported that mtHsp70 is inactivated in neurodegenerative diseases like Parkinson Disease[171,172]. Since then, its function as a mitochondrial chaperone has gained the attractions from researchers. Here, we briefly review mtHsp70 as follows.

1.5.1 Expression and Subcellular Localization

Although it was initially isolated from the cytosol and reported to interact with numerous cytosolic proteins such as TP53, mtHsp70 is mainly expressed in mitochondria[173,174]. Like mtHsp40, mtHsp70 is constitutively expressed, not heat-inducible and detectable in a majority of organs. In rat, brain, heart, and skeletal muscle produce the highest level of mtHsp70, followed by lung, liver, and kidney. Testis and spleen are the least[175-176].

1.5.2 Structural Domains

The crystal structure of mtHsp70 has not been identified so far. Human mtHsp70 has a high amino acid similarity with other organisms: *E. coli* DnaK (51%) and Yeast Ssc1 (65%)[177]. It is 679 amino acids long, and its molecular weight is 74 kDa. Its primary amino acid sequences showed that mtHsp70 conserves all important domains with other human HSP70s except MTS (Fig 4)[177]: MTS, ATPase domain, SBD and C-terminal Lid domain[174]. Premature mtHsp70 contains a 46 amino acid-long MTS followed by cleavage site, and is processed in the mitochondrial matrix by matrix processing proteases(s) (MPPs)[174]. Unprocessed form of mtHsp70 is not detectable under physiological condition.

1.5.3 Roles of MtHsp70 in Cancers

Since initially discovered in the cytosol by Wadhwa *et al*, mtHsp70 has been reported to interact with the tumor suppressor TP53 in the cytosol. Surprisingly, TP53-mtHsp70 interaction resulted in attenuation of TP53 transactivity and cytoplasmic sequestration of TP53[178,179]. Later, Iosefson *et al* supported this finding by identifying additional interaction regions of C-terminal domain of TP53[180]. More recently, several groups have investigated the crystal structure of TP53-mtHsp70 complexes to clarify their physical interaction[180]. MtHsp70 is upregulated in multiple cancers such as brain tumors, colorectal adenocarcinomas, hepatocellular carcinomas, breast cancers, and leukemias[181-187]. Several groups have tested the potential of inhibiting mtHsp70 activity as a novel cancer therapy by using RNAi or small molecules such as MKT-077, an mtHsp70 inhibitor, and the efficacy has been reported[184,188-191].

1.5.4 Relevance of MtHsp70 in Neurodegeneration

Ssc1, the yeast homolog of *E. coli* DnaK and human mtHsp70, has been well studied regarding its dual biochemical functions in mitochondria: protein folding/refolding and protein import. First, its mutants defective in ATPase activity or substrate binding led to loss of mitochondrial DNA and thermotolerance defects, suggesting that Ssc1 is critical for mitochondrial functions and stress responses[192-194]. Liu *et al* used the luciferase protein as an Ssc1 substrate to study the biochemical function of Ssc1 and molecular mechanisms of Ssc1-mediated protein folding/refolding *in vitro*, and they provided numerous results showing that Ssc1 is a mitochondrial member of HSP70[195]. They also reported important partners including a

mitochondrial NEF, Mge1 (not identified yet in humans) and a co-chaperone, Mdj1 (mtHsp40 in human)[196-200]. Interestingly, Ssc1 required another DnaJ protein, Hep1 (HSP70 escort protein 1) that stimulates ATPase activity of Ssc1 and also prevents protein aggregation similarly to Mdj1. Hep1 interaction with Ssc1 was regulated by the C-terminal helical Lid region of Ssc1[201]. However, the Hep1 interaction at the ATPase domain of Ssc1 was mutually exclusive with Mdj1 for triggering conformational change of Ssc1[202]. The physiological function of Hep1 is still unknown. In humans, Hep1 is still not identified.

Since yeast Ssc1 was reported to function as a mitochondrial HSP70, it was soon revealed by Voos *et al* that it interacted reversibly with TIM44, a component of TIM23 complex that mediates protein import. These data suggested that Ssc1 also plays a role in import of nuclear genome-encoded mitochondrial proteins, and proposed a controversial model of Ssc1 action: (1) ATP-independent physical trapping of preproteins and (2) ATP-dependent pulling preproteins into matrix[203-205]. Furthermore, they proposed molecular mechanisms of preprotein import by Ssc1 as follows: (1) TIM44 interacts with Ssc1 in a ATP-dependent manner[206]; (2) Ssc1 substrate-binding domain determines the interaction of Ssc1 ATPase domain with TIM44[207,208]; (3) TIM44 does not stimulate Ssc1 ATPase activity, and PAM18, another known mitochondrial J protein localized to the mitochondrial inner-membrane stimulates ATP hydrolysis during protein import[209]; (4) PAM16 and PAM18 form a hetero-dimer and interact with TIM44 in the TIM23 translocase complex and PAM17 is also involved in this process[210-212]. Fig 7 briefly describes protein complexes involved in matrix protein import in Yeast. Although most understanding of mitochondrial protein import mechanisms came from yeast models, yet the high conservation between yeast and human HSP40/HSP70 merits applying those findings to the human mtHsp70 and mitochondrial protein import machinery[191].

As mtHsp70 is essential for protein folding and import, it has been proposed that mtHsp70 deficiency may cause many disorders. Specifically, a quantitative proteomic approach done by Jin *et al* demonstrated that mtHsp70 is substantially decreased in PD patients, and manipulation of mtHsp70 levels in dopaminergic neurons resulted in significant changes in the sensitivity to PD pathology[213,214]. Later, Burbulla *et al* found mutations in the ATPase domain and the substrate binding domain that caused increased reactive oxygen species (ROS) and reduced mitochondrial membrane potential ($\Delta\psi_m$) leading to alterations of mitochondrial network, which supports its importance in neurodegeneration and PD[191,215,216]. Intriguingly,

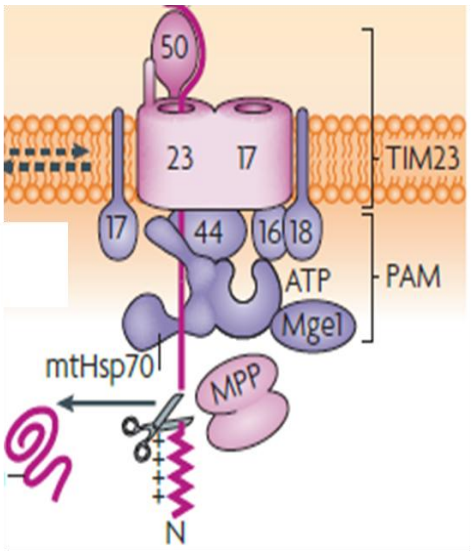

Figure 7. Mitochondrial Protein Import Machinery.

For mitochondrial protein import into the MIM or matrix, two MIM complexes including TIM23 and TIM17 are integrated into the MIM and the import motor complex is anchored at the matrix surface of MIM. MtHsp70, a component of import motor, interacts with TIM44, an MIM anchor. Following preprotein entrance through the import channel(s), TIM23, mtHsp70 interacts with and pull preproteins into the matrix dependent on ATP hydrolysis catalyzed by PAM16/PAM18, followed by the MTS cleavage by certain MPP(s) in the matrix (212).

another recent finding demonstrated that mtHsp70 mutations (P506S) enhanced interaction with J-protein cochaperones, resulting in mitochondrial dysfunction including compromised growth, impairment in protein import, reduced functional mitochondria, mtDNA loss, respiration decrease, and oxidative stress increase[216]. These data indicate that mtHsp70 plays critical roles in mitochondrial protein folding/refolding and import, which determine mitochondrial morphology and function.

1.6 Rationale, Scientific Question, Hypothesis, and Aims

It is known that mtHsp40 facilitates apoptosis responding to proapoptotic stimuli. Our laboratory has found that mtHsp40 collaborates with mtHsp70 in the cytosol to physically interact with and translocate TP53 to mitochondria, leading to mitochondria-associated apoptosis in the presence of proapoptotic stimuli[40].

Notably, mtHsp70 is known to have opposing effects on apoptosis: upregulated mtHsp70 in many cancers also interacts with TP53 in the cytoplasm, but inhibits the transcriptional activity of TP53 causing resistance to proapoptotic agents[178,179]. Thus, we come up with a scientific question to address in this study: what roles do mtHsp40 and mtHsp70 network play in apoptotic cell death and/or cell life in cancers?

As described in Section 1.2, mitochondrial morphology is somehow linked to mitochondrial outer membrane permeabilization (MOMP) and/or apoptosis through direct or indirect cross-talks between apoptotic effectors and mitochondrial fusion/fission proteins on MOM: for example, (1) a mitochondrial fission GTPase, DRP1, positively affects apoptosis[91]; (2) oligomerized BAK interacts with MFN1 and MFN2 involved in MOM fusion, resulting in mitochondrial fragmentation during apoptosis[92,93]; (3) apoptosis requires a certain form of OPA1-dependent crista remodeling by BAX/BAK, but independent of cytochrome *c* release[54]. Together, we could propose that mitochondrial fragmentation is structurally coupled with apoptosis.

Our preliminary observations showed that ectopic expression of mtHsp40 in MCF7 breast cancer cells caused mitochondrial fragmentation in the both absence and presence of proapoptotic stimuli (data not shown). In addition, TP53 expression itself did not affect mitochondrial morphology (data not shown). These data suggest that mtHsp40 triggers mitochondrial fragmentation irrespective of TP53 status.

In order to address the above scientific question, we put the above rationale together into

the following hypothesis (Fig 8): the perturbations of mtHsp40:mtHsp70 network result in mitochondrial fragmentation by modulating mitochondrial fusion and/or fission molecules or independently of these modulators, which possibly induces apoptotic cell death and negatively affects cell life in cancers.

In order to test this hypothesis, we have fulfilled the following specific aims: (1) exploring the roles of mtHsp40 and mtHsp70 in mitochondrial morphology and apoptosis in multiple cell types (wildtype or mutant p53); (2) studying roles of major proteins associated with mitochondrial fusion and fission processes during mitochondrial fragmentation and apoptosis induced by altering the ratio between mtHsp40 and mtHsp70; (3) investigating the roles of mtHsp40 and mtHsp70 in mitochondrial homeostasis of functions and cell growth. To address the above hypothesis and specific aims, this study has consisted of three individual story has rationales, results, discussion and future directions, which are then summarized into one comprehensive model.

Figure 8. Rationales and Hypothesis

(1) It is known that mtHsp70 interacts with TP53 in the cytoplasm of cancer cells, which inhibits TP53 nuclear transport and its tumor suppressor activity leading to resistance to proapoptotic drugs. (2) Our laboratory found that mtHsp40 also interacts with TP53 in the cytosol and mediates TP53 translocation to the mitochondria, which facilitates cytochrome *c* release and intrinsic apoptosis pathway. (3) Current debating reports demonstrate that mitochondria undergoing apoptosis modulates mitochondrial dynamics machinery such as DRP1 and MFN1/2, leading to mitochondrial fragmentation. In a few mouse models, defects in mitochondrial fusion cause mitochondrial fragmentation, resulting in apoptosis; (4) We preliminarily observed that ectopic expression of mtHsp40 resulted in mitochondrial fragmentation in breast cancer cells. We therefore hypothesize that altering mtHsp40:mtHsp70 network modulates mitochondrial fusion and/or fission processes, leading to mitochondrial fragmentation and apoptosis.

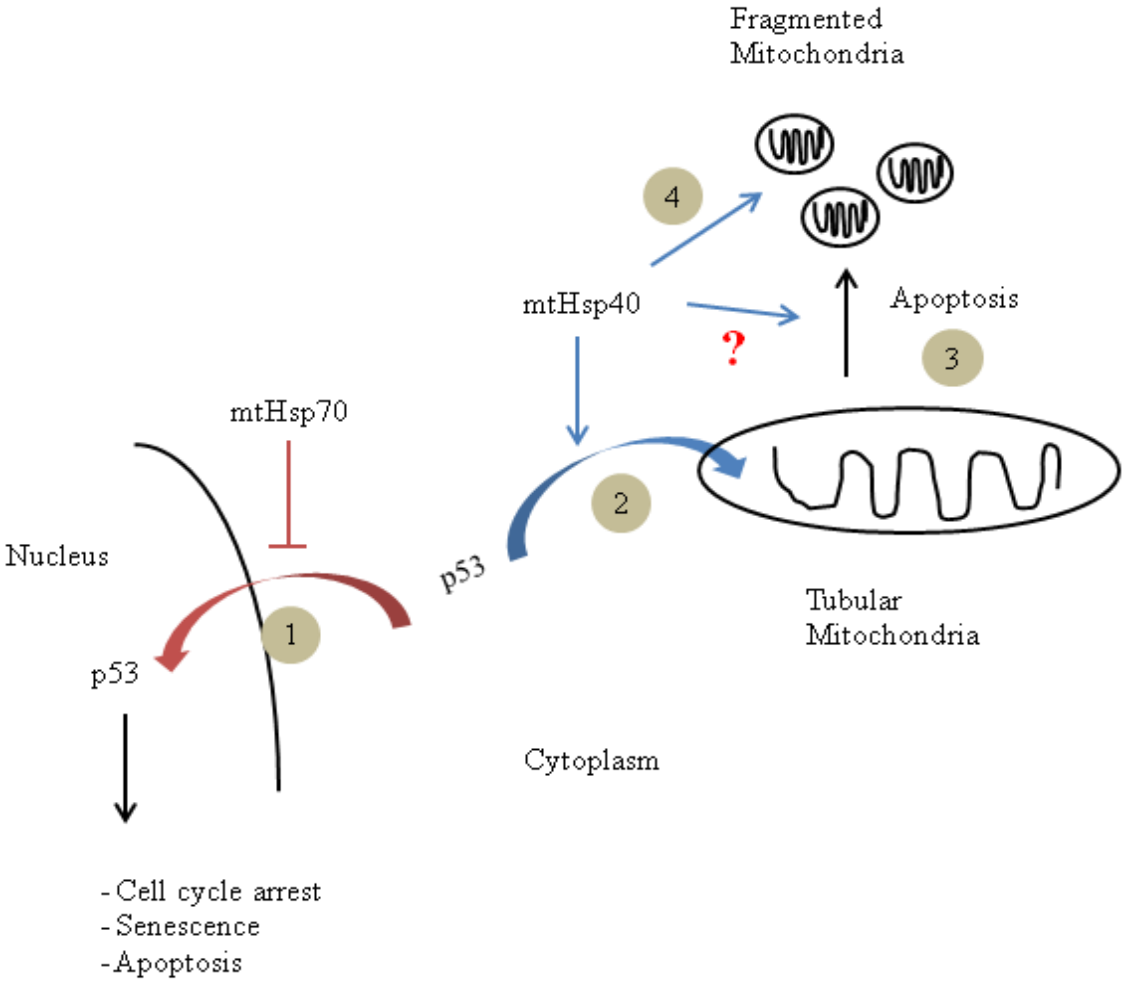
Fragmented
Mitochondria
4
mtHsp40
?
Apoptosis
3
mtHsp70
2
Nucleus
p53
1
Tubular
Mitochondria
p53
Cytoplasm
- Cell cycle arrest
- Senescence
- Apoptosis

CHAPTER TWO: MATERIALS AND METHODS

2.1 Cell Culture

Normal human skin fibroblast Hs68 cells and the neuroblastoma cell line SK-N-SH were from Senger, D. (University of Calgary), glioblastoma cell lines (U87 & U251) were from Forsyth, P. (University of Calgary), human cervical carcinoma cell line HeLa and human embryonic kidney cell line HEK293-TetR stably expressing tetracycline repressor gene were from Kurz, E. (University of Calgary). Cells were cultured in high-glucose Dulbecco's modified eagle medium (DMEM; Invitrogen) supplemented with 10 % fetal bovine serum (FBS) in a humidified atmosphere containing 5 % CO_2 at 37 ℃, with bi-daily or weekly sub-culture using Trypsin-EDTA detachment (0.05 % Trypsin, 2 mM EDTA; Invitrogen).

For cryopreservation of cells, trypsinized cells were stored in FBS containing 10% sterile Dimethyl Sulfoxide (DMSO; Sigma) in 1 ml aliquots (one approximately 90% confluent 15-cm plate to three cryopreservation vials). Cells were frozen overnight at -80 ℃, and then transferred to liquid nitrogen for long term storage. For the same batch of experiments, the same cell passage was utilized. When cells were thawed, cells were warmed up in a 37 ℃ water bath, then transferred to plates containing pre-warmed media supplemented with 10 % FBS, and incubated at 37 ℃ for cell attachment to the plates. The following day, media was replaced with new media to remove DMSO.

2.2 Mammalian Expression Plasmids

2.2.1 Mitochondrial-Targeted GFP (mitoGFP) or - DsRed2 (mitoRFP)

Mitochondrial-targeted variant of Discosoma sp. Red Fluorescent Protein (DsRed2; mitoRFP) or Enhanced Green Fluorescent Protein (EGFP; mitoGFP) were cloned by inserting the MTS of cyclooxygenase IV (COX IV) in frame with pDsRed2-N1 or pEGFP-N1 (Clontech) by the annealing and ligating the *NheI* and *BamHI* site-flanked oligonucleotides (COX VI-MTS-Forward and COX VI-MTS-Reverse, Table 7) into pDsRed2-N1 or pEGFP-N1. Briefly, oligonucleotide dried pellets (synthesized by Core DNA Services, University of Calgary) were dissolved in ultrapure water up to 0.05 µM, and 1 µl of each forward and reverse primer transferred to 48 µl annealing buffer (100 mM potassium acetate, 30 mM HEPES-KOH pH 7.4, 2 mM magnesium acetate). The primer mix was denatured at 95 ℃ for 5 minutes, annealed at

Table 7. List of Primers for the Generation of Mitochondrial-Targeted DsRed2 and EGFP

Primer name	Restriction sites	Primer sequences
COX VI-MTS-Forward	*Nhe1/BamH1*	CTAGCATGTCCGTCCTGACGCCGCTGCTGCTGCGGGG CTTGACAGGCTCGGCCCGGCGGCTCCCAGTGCCGCGC GCCAAGATCCATTCGTTGGGG
COX VI-MTS-Reverse		GATCCCCCAACGAATGGATCTTGGCGCGCGGCACTGG GAGCCGCCGGGCCGAGCCTGTCAAGCCCCGCAGCAG CAGCGGCGTCAGGACGGACATG
MitoRFP – Forward	*HindIII/XhoI* (40℃, 1762bp)	AAAGCTTTAGTTATTAATAGTAATCAA
MitoRFP - Reverse		ACTCGAGCACTCAACCCTATCTCGGTC
pRS-Forward	None (55℃, ~2.3kb)	CCCTTGAACCTCCTCGTTCGACC
pRS-Reverse		GAGACGTGCTACTTCCATTTGTC

* Restriction enzyme sites were underlined.

70 ℃ for 10 minutes and cooled in ice until used or stored at -20 ℃. To phosphorylate oligos, 2 µl of annealed oligos were added to T4 polynucleotide kinase (PNK; NEB Biolabs) buffer containing 0.1 mM ATP, and 1 µl of T4 PNK was added. After incubation at 37 ℃ for 30 minutes, the reaction mixture was incubated at 70 ℃ for 10 minutes to inactivate T4 PNK. Two-µl of phosphorylated oligos were mixed with 100 ng of gel-purified pDsRed2-N1 or pEGFP-N1 plasmid digested with *NheI* and *BamHI* and total volume was adjusted to 5 µl or 10 µl with ultrapure water. The DNA mix was heat-denatured at 65 ℃ for 10 minutes in a PCR machine (Eppendorf), and chilled in ice for 5 minutes. Five-µl or 10 µl of 2x Ligase Buffer and 1 µl of DNA Ligase (Roche) were added, and incubated at 15 ℃ overnight. Two-µl of ligation mixture was transformed into 25 µl One Shot TOP10 cells (Invitrogen) using the heat-shock method, and bacterial cells were plated onto Luria-Bertani (LB; Invitrogen) agar plates supplemented with 50 µg/ml Kanamycin (Invitrogen). Ten Kanamycin-resistant colonies were cultured in 5 ml LB broth overnight at 37 ℃ on a shaker at 200 rpm, and plasmid DNA was purified using the QIAprep miniprep kit (Qiagen) following manufacturer's protocol. Restriction digestion using *NheI* and *BamHI* restriction enzymes (Invitrogen) and DNA sequencing (University of Calgary DNA Sequencing Laboratory) using primers against CMV promoters in pDsRed2-N1 and pEGFP-N1 confirmed successful insertion of mitoRFP and mitoGFP.

To generate retroviral expression construct for mitoRFP and mitoGFP, mitoRFP or mitoGFP sequences were PCR-amplified from pDsRed2-MTS-N1 or pEGFP-MTS-N1 plasmid using the primers (MitoRFP-Forward and MitoRFP-Reverse) described in Table 7. Ten-ng of pDsRed2-MTS-N1 or pEGFP-MTS-N1 was amplified using the Expand Long Template PCR System (Roche) utilizing Buffer I. The cycling conditions for PCR amplification were as follows: 95 ℃ for 5 minutes; 30 cycles at 95 ℃ for 30 seconds, 45 ℃ for 30 seconds, and 72 ℃ for 2 minutes; extension at 72 ℃ for 10 minutes. PCR products of the correct size were purified following 1 % agarose gel electrophoresis using the Qiagen Gel Extraction Kit according to manufacturer's protocol. The Expand Long PCR enzyme is a mixture of *Taq* DNA polymerase and *Tgo* DNA polymerase, and thus decreases the mutation rate and generates deoxyadenosine (dA) overhangs allowing for TOPO TA cloning. One hundred-ng of purified PCR product was cloned into the pCR2.1-TOPO vector using the TOPO TA Cloning Kit (Invitrogen) and then 2 µl of reaction mix was transformed into 25 µl of One Shot TOP10 cells following manufacturer's protocol and plated onto LB agar plates supplemented with 50 µg/ml Kanamycin. Kanamycin-

resistant colonies were identified by colony PCR using M13 primers included in the pCR2.1-TOPO TA Cloning Kit (Invitrogen). Positive clones were cultured in 5 ml LB broth overnight at 37 ℃ on a shaker at 200 rpm, and plasmid DNA was purified using the Qiagen QIAprep Miniprep Kit following manufacturer's protocol. Restriction digestion using *HindIII* and *XhoI* restriction enzymes (Invitrogen) and DNA sequencing (University of Calgary DNA Sequencing Laboratory) using M13 primers confirmed the successful insertion of mitoRFP and mitoGFP.

In order to insert mitoRFP or mitoGFP into the pRetroSuper vector (pRS; Origene), pRS vector and positive inserts from pCR2.1-TOPO were digested by using *HindIII* and *XhoI* restriction enzymes and purified by gel extraction using the Qiagen Gel Extraction Kit. The pRS vector and gel-extracted mitoRFP or mitoGFP were ligated using the Rapid DNA Ligation Kit (Roche) following the manufacturer's protocol. Briefly, 100 ng of the gel-extracted pRS vector and 100 ng of mitoRFP or mitoGFP insert were mixed to a total 5 µl of reaction and incubated at 65 ℃ for 10 minutes then placed on ice for 5 minutes. Five-µl of 2x T4 DNA Ligation Buffer and 1 µl of T4 DNA Ligase were added to the DNA mix and incubated overnight at 15 ℃ in a PCR machine. Two-µl of the ligation mix was transformed into 25 µl of One Shot TOP10 cells and plated onto LB agar plates supplemented with 100 µg/ml Ampicillin. Positive colonies were determined by colony PCR using pRS-forward and pRS-reverse primers (Table 7), and plasmid DNA was purified using the Qiagen QIAprep Miniprep Kit. One-µg of plasmid DNA was digested by 1 µl (or 10 units) of *HindIII* and *XhoI* restriction enzymes and DNA sequencing was performed to confirm positive clones.

Amplification of plasmid DNA was performed by transforming 10 ng of plasmid DNA into chemically competent TOP10 cells (Invitrogen), and cells were cultured in 100 ml LB broth with desired antibiotics. Plasmid DNA was purified using the Qiagen Midiprep Kit following manufacturer's protocol.

2.2.2 MtHsp40 Domain Deletion Mutants

Full length and various domain deletion mutants of mtHsp40 were cloned into *XbaI* and *HindIII* restriction sites of the pRK5 mammalian expression vector (BD Biosciences). To construct these mutants, mtHsp40 cDNA was PCR-amplified from pCI-mtHsp40$_L^{wt}$ plasmid using the primers described in Table 8. PCR amplification, TOPO TA cloning, and ligation were performed as described above. pCI-mtHsp40$_S^{wt}$ was used as a template to PCR-amplify

mtHsp40$_S^{wt}$ and pCI-mtHsp40$_L^{HQ}$ was used for PCR-amplification of mtHsp40$_L^{HQ}$. In addition, C-terminal FLAG-tagged mtHsp40 deletion mutants or full length were also generated by using primers described in Table 8. PCR amplification, TOPO TA cloning, and ligation were performed as described above. A summary of the mtHsp40 mammalian expression constructs can be found in Table 9.

2.2.3 Doxycycline-Inducible MtHsp40 Mammalian Expression Construct

In order to clone GFP or mtHsp40$_L$ into the *HindIII* and *XbaI* restriction sites of pcDNA4/TO/myc-His-A gifted by Kurz, E. (University of Calgary), 10 ng of pRK5-mtHsp40$_L^{WT}$ was PCR-amplified using the primers; 5' – AAAGCTTCTAGTTTCCAGTGGATCT – 3' (Forward), and 5' – ATCTAGATGAGGTAAACATTTTCTTAAG – 3' (Reverse). PCR conditions were as follows; 95 ℃ for 5 minutes; 30 cycles at 95 ℃ for 30 seconds, 50 ℃ for 30 seconds, and 72 ℃ for 1.5 minutes; extension at 72 ℃ for 10 minutes. PCR products of ~ 1443 bp were gel-extracted using the Qiagen Gel Extraction Kit following manufacturer's protocol. PCR amplification and TOPO TA cloning were performed as described in **Section 2.2.1**. Positive colonies were determined by colony PCR and DNA sequencing utilizing the above primers. Next, ten-µg of positive clone DNA and pcDNA4/TO/myc-His-A vector were incubated with the *HindIII* and *XbaI* restriction enzymes and were gel-extracted using the Qiagen Gel Extraction Kit following manufacturer's protocol. Ligation and transformation were performed as described in **Section 2.2.1**.

2.2.4 MtHsp70 Domain Deletion Mutants

Full length and various domain deletion mutants of mtHsp70 were cloned into *XbaI* and *HindIII* restriction sites of the pRK5 mammalian expression vector (BD Biosciences). To construct these mutants, mtHsp70 cDNA was PCR-amplified from pCMV6-AC-mtHsp70^{wt} plasmid (SC320242; Origene) using the primers described in Table 10. PCR amplification, TOPO TA cloning, and ligation were performed as describe in **Section 2.2.1**. In addition, C-terminal FLAG-tagged mtHsp40 deletion mutants or full length were generated by using primers described in Table 10. PCR amplification, TOPO TA cloning, and ligation were performed as described in **Section 2.2.1**. A summary of the mtHsp70 mammalian expression constructs can be found in Table 11.

Table 8. List of Primers for the Generation of MtHsp40 Mammalian Expression Constructs

Constructs	Anneal Temp.	Restriction sites	Forward Primer/Reverse Primer
$MtHsp40_{L}$(1-480)	50 °C	*XbaI/HindIII*	ATCTAGACTAGTTTCCAGTGGATCT AAGCTTTGAGGTAAACATTTTCTTAAG
$MtHsp40_{\Delta MTS}$(89-480)	50 °C	*XbaI/HindIII*	ATCTAGAATGTTGGCCAAAGAAGAT AAGCTTTGAGGTAAACATTTTCTTAAG
$MtHsp40_{L}$(H121Q)	50 °C	*XbaI/HindIII*	ATCTAGACTAGTTTCCAGTGGATCT AAGCTTTGAGGTAAACATTTTCTTAAG
$MtHsp40_{S}$(1-453)	50 °C	*XbaI/HindIII*	ATCTAGACTAGTTTCCAGTGGATCT AAGCTTTGAGGTAAACATTTTCTTAAG
$MtHsp40_{\Delta CT}$(1-292)	55 °C	*XbaI/HindIII*	ATCTAGACTAGTTTCCAGTGGATCT AAAGCTTCTAGCAGACCACACAGGG
$MtHsp40_{\Delta CT}$(1-235)	55 °C	*XbaI/HindIII*	ATCTAGACTAGTTTCCAGTGGATCT AAAGCTTCTACGTGTCCATGATGTTCAC
$MtHsp40_{\Delta CT}$(1-168)	60 °C	*XbaI/HindIII*	ATCTAGACTAGTTTCCAGTGGATCT AAAGCTTCTAGCCGCTGGCCCCAGGATC
$MtHsp40_{L}$(1-480)	50 °C	*XbaI/HindIII*	ATCTAGACTAGTTTCCAGTGGATCT AAGCTTCTACTTGTCGTCATCGTCTTTGTAG TCTGAGG*T*AAACATTTTCTTAAG
$MtHsp40_{\Delta MTS}$(89-480)	50 °C	*XbaI/HindIII*	ATCTAGAATGTTGGCCAAAGAAGAT AAGCTTCTACTTGTCGTCATCGTCTTTGTAG TCTGAGGTAAACATTTTCTTAAG
$MtHsp40_{L}$(H121Q)	50 °C	*XbaI/HindIII*	ATCTAGACTAGTTTCCAGTGGATCT AAGCTTCTACTTGTCGTCATCGTCTTTGTAG TCTGAGGTAAACATTTTCTTAAG
$MtHsp40_{\Delta CT}$(1-292)	55 °C	*XbaI/HindIII*	ATCTAGACTAGTTTCCAGTGGATCT AAGCTTCTACTTGTCGTCATCGTCTTTGTAG TCGCAGACCACACAGGGCGATAT
$MtHsp40_{\Delta CT}$(1-168)	60 °C	*XbaI/HindIII*	ATCTAGACTAGTTTCCAGTGGATCT AAGCTTCTACTTGTCGTCATCGTCTTTGTAG TCGCCGCTGGCCCCAGGATC

* Restriction enzyme sites were underlined.
* FLAG-tag (DYKDDDDK) sequences were boxed in yellow.

Table 9. Summary of MtHsp40 Mammalian Expression Constructs

Constructs	Insert Size (bp)	No of Amino Acids	Domains
$MtHsp40_{L}$(1-480)	1443	480	All, long isoform
$MtHsp40_{\Delta MTS}$(89-480)	1179	392	DnaJ, CTD I & CTD II, DD
$MtHsp40_{L}$(H121Q)	1443	480	All; DnaJ (H121Q)
$MtHsp40_{S}$(1-453)	1362	453	All, short isoform
$MtHsp40_{\Delta CT}$(1-292)	876	292	MTS, DnaJ, CTD I
$MtHsp40_{\Delta CT}$(1-235)	706	235	MTS, DnaJ, truncated CTD I
$MtHsp40_{\Delta CT}$(1-168)	505	168	MTS, DnaJ

Table 10. List of Primers for the Generation of MtHsp70 Mammalian Expression Constructs

Constructs	Anneal Temp.	Restriction sites	Forward Primer/Reverse Primer
$MtHsp70_{FL}$ (1-679)	55 ℃	*BamHI/HindIII*	GGATCCATGATAAGTGCCAGCCGAGCT
			AAGCTTTTACTGTTTTTCCTCCTTTT
$MtHsp70_{\Delta MTS}$ (57-679)	55 ℃	*BamHI/HindIII*	GGATCCATGATAAGTGCCAGCCGAGCT
			AAGCTTTTACTGTTTTTCCTCCTTTT
MtHsp70 $_{\Delta ATPase}$	60 ℃	*BamHI/XbaI*	GGATCCATGATAAGTGCCAGCCGAGCT
			TCTAGACATAACTGCCACGCAGGA
	55 ℃	*XbaI/HindIII*	TCTAGAAGCTGCCATTCAGGGAGGT
			AAGCTTTTACTGTTTTTCCTCCTTTT
$MtHsp70_{\Delta CT}$ (1-434)	58 ℃	*BamHI/HindIII*	GGATCCATGATAAGTGCCAGCCGAGCT
			AAGCTTTTAATCCGTGACATCGCCGGCCAA
$MtHsp70_{FL}$ (1-679)	55 ℃	*BamHI/HindIII*	GGATCCATGATAAGTGCCAGCCGAGCT
			AAGCTTCTACTTGTCGTCATCGTCTTTGTA
			GTCATCCGTGACATCGCCGGCCAA
$MtHsp70_{\Delta MTS}$ (57-679)	55 ℃	*BamHI/HindIII*	GGATCCATGATAAGTGCCAGCCGAGCT
			AAGCTTCTACTTGTCGTCATCGTCTTTGTA
			GTCATCCGTGACATCGCCGGCCAA
MtHsp70 $_{\Delta ATPase}$	60 ℃	*BamHI/XbaI*	GGATCCATGATAAGTGCCAGCCGAGCT
			TCTAGACATAACTGCCACGCAGGA
	55 ℃	*XbaI/HindIII*	TCTAGAAGCTGCCATTCAGGGAGGT
			AAGCTTCTACTTGTCGTCATCGTCTTTGTA
			GTCATCCGTGACATCGCCGGCCAA
$MtHsp70_{\Delta CT}$ (1-434)	58 ℃	*BamHI/HindIII*	GGATCCATGATAAGTGCCAGCCGAGCT
			AAGCTTCTACTTGTCGTCATCGTCTTTGTA
			GTCATCCGTGACATCGCCGGCCAA

* Restriction enzyme sites were underlined.
* FLAG-tag (DYKDDDDK) sequences were boxed in yellow.

Table 11. Summary of mtHsp70 Mammalian Expression Constructs

Constructs	Insert Size (bp)	No of Amino Acids	Domains
$MtHsp70_{FL}$ (1-678)	2037	678	All
$MtHsp70_{\Delta MTS}$ (57-678)	1866	622	ATPase, SBD, LID
$MtHsp70_{\Delta ATPase}$	903	301	MTS, SBD, LID
$MtHsp70_{\Delta CT}$ (1-434)	1302	434	MTS, ATPase

2.2.5 iZEG-human MtHsp40$_L$ Construct

In order to clone mtHsp40$_L$ into the *XhoI* restriction sites of iZEG plasmid (Miami Mice Research Corp), 10 ng of pRK5-mtHsp40$_L^{WT}$ was PCR-amplified using the primers described in Table 12. PCR conditions were as follows; 95 ℃ for 5 minutes; 30 cycles at 95 ℃ for 30 seconds, 50 ℃ for 30 seconds, and 72 ℃ for 1.5 minutes; extension at 72 ℃ for 10 minutes. PCR products of ~ 1443 bp were gel-extracted using the Qiagen Gel Extraction Kit following manufacturer's protocol. PCR amplification and TOPO TA cloning were performed as described in **Section 2.2.1**. Next, ten-μg of iZEG plasmid DNA and positive TOPO clones were incubated with the *XhoI* restriction enzyme and were gel-extracted using the Qiagen Gel Extraction Kit following manufacturer's protocol. Following dephosphorylation of gel-extracted iZEG plasmid using rAPid Alkaline Phosphatase (Roche), ligation and transformation were performed as described in **Section 2.2.1**.

2.2.6 Mitochondrial-Targeted Luciferase Plasmid

Cytomegalovirus (CMV) promoter was first cloned into the *KpnI* and *NheI* sites of pGL3-enhancer vector to generate pGL3-CMV, and the MTS of mtHsp70 was cloned into the *NheI* and *NcoI* restriction sites of the pGL3-CMV vector. Briefly, ten-ng of pDsRed2-N1 plasmid was amplified using the Expand Long Template PCR System utilizing Buffer I using primers; 5' – GGTACCCCCCTGATTCTGTGGATAACCGTA – 3' (Forward) and 5' – GCTAGCGGATCTGACGGTTCACTA – 3' (Reverse). PCR conditions were as follows; 95 ℃ for 5 minutes; 30 cycles at 95 ℃ for 30 seconds, 55 ℃ for 30 seconds, and 72 ℃ for 1 minute; extension at 72 ℃ for 10 minutes. PCR products of ~ 600 bp were gel-extracted using the Qiagen Gel Extraction Kit following manufacturer's protocol. PCR amplification and TOPO TA cloning were performed as described at **Section 2.2.1**. Positive colonies were determined by colony PCR and DNA sequencing utilizing the above primers. Next, ten-μg of positive plasmid DNA and pGL3-enhancer vector were incubated with the *KpnI* and *NheI* restriction enzymes and were gel-extracted using the Qiagen Gel Extraction Kit following manufacturer's protocol. Ligation and transformation were performed as described in **Section 2.2.1**. To clone mtHsp70 MTS into the *NheI* and *NcoI* sites of pGL3-CMV, pCMV6-AC- mtHsp70^{wt} plasmid was PCR-amplified by using the primers; 5' – GCTAGCATGATAAGTGCCAGCCGAGCT – 3' (Forward), and 5' – CCATGGCAAGTCGCTCACCATCTGCTG – 3' (Reverse). PCR conditions were as

Table 12. List of Primers for Generation of iZEG-hmtHsp40L Construct and Genotyping PCR

Target	Restriction sites	Sequence
mtHsp40$_L$ (1443bp)	*XhoI/XhoI*	ACTCGAGCTAGTTTCCAGTGGATCT
		ACTCGAGTGAGGTAAACATTTTCTTAAG
LacZ (389bp)	60 ℃	GTTGCAGTGCACGGCAGATACACTTGCTGA
		GCCACTGGTGTGGGCCATAATTCAATTCGC
Cre (408bp)	60 ℃	GCATTACCGGTCGATGCAACGAGTGATGAG
		GAGTGAACGAACCTGGTCGAAATCAGTGCG
Mouse Actin (390bp)	50 ℃	GAGACCTTCAACACCCCAGC
		ACCCAAGAAGGAAGGCTGGA

* Restriction enzyme sites were underlined.

* Genotyping primers were referred to Washington University in St. Louis Mouse Genetics Core (http://mgc.wustl.edu/Protocols/PCR

follows; 95 ℃ for 5 minutes; 30 cycles at 95 ℃ for 30 seconds, 55 ℃ for 30 seconds, and 72 ℃ for 30 seconds; extension at 72 ℃ for 10 minutes. PCR products of ~ 300 bp were gel-extracted using the Qiagen Gel Extraction Kit following manufacturer's protocol. PCR amplification and TOPO TA cloning were performed as described in **Section 2.2.1**. Positive colonies were determined by colony PCR and were confirmed by DNA sequencing utilizing the above primers. Next, ten-μg of positive plasmid and pGL3-CMV plasmid DNA were incubated with the *NheI* and *NcoI* restriction enzymes and were gel-extracted using the Qiagen Gel Extraction Kit following manufacturer's protocol. Ligation and transformation were performed as described in **Section 2.2.1**.

2.2.7 Other Constructs

We were also kindly gifted constructs by several researchers as follows; (1) pCxNeo-mouse mtHsp70 by Kaul, S. C. (AIST, Tsukuba, Japan); (2) DRP1-YFP and DRP1(K38A) by Youle, R. J. (NINDS, NIH, MD, USA); (3) MFN11-Myc, MFN2-Myc and OPA1 by Chan, D. (Caltech, CA, USA); (4) MFF-Flag by Otera, H. (Kyushu University, Japan); (5) OMA1-HA by Bliek, A. (UCLA, CA, USA).

2.3. Transient Transfections

2.3.1 Mammalian Constructs

Cells were seeded in 6-well cell culture plates or 10-cm cell culture dishes one day prior for 50 % (HEK293 cells) or 80 % confluence (the other cells) on the day of transfection. Five-μl (6-well plate) or 15 μl (10-cm dish) of Lipofectamine2000 (Invitrogen) was mixed with 100 μl (6-well plate) or 500 μl (10-cm dish) of DMEM supplemented with 10 % FBS and incubated at room temperature for 5 minutes. Indicated amount of plasmid DNA was mixed with 100 μl (6-well plate) or 500 μl (10-cm dish) of DMEM supplemented with 10 % FBS and incubated at room temperature for 5 minutes simultaneously. Next, DNA and Lipofectamine2000 were mixed and incubated at room temperature for another 20 minutes. In the meantime, old growth media was replaced with 1 ml (6-well plate) or 4 ml (10-cm dish) of fresh DMEM supplemented with 10 % FBS. Lipofectamine2000/DNA/media mix was added to the cells drop wise. Six to 12 hours post-transfection, media was replaced with 2 ml (6-well plate) or 10 ml (10-cm dish) of fresh DMEM + 10 % FBS. Transfection efficiency was measured by fluorescence as indicated.

2.3.2 Small Interfering RNAs (siRNAs)

Cells were seeded in 6-well cell culture plates or 10-cm cell culture dishes one day prior for 50 % on the day of transfection. Five-µl (6-well plate) or 20 µl (10-cm dish) of Lipofectamine RNAiMAX (Invitrogen) was mixed with 100 µl (6-well plate) or 500 µl (10-cm dish) of Opti-MEM only without FBS and incubated at room temperature for 5 minutes. Ten or 100 µM of siRNAs (Table 13) were mixed with 100 µl (6-well plate) or 500 µl (10-cm dish) of Opti-MEM only and incubated at room temperature for 5 minutes simultaneously. Next, siRNAs and Lipofectamine RNAiMAX were mixed and were incubated at room temperature for another 20 minutes. In the meantime, old growth media was replaced with 1 ml (6-well plate) or 4 ml (10-cm dish) of fresh Opti-MEM only. Lipofectamine RNAiMAX/siRNAs/media mix was added to the cells drop wise. Twelve hours post-transfection, media was replaced with 2 ml (6-well plate) or 10 ml (10-cm dish) of fresh DMEM + 10 % FBS, and incubated for at least 48 hours to obtain significant suppression of target gene expression.

2.4 Establishing Stable Cell Lines

2.4.1 HeLa-MitoRFP or 293-TetR-MitoRFP Cells

To produce retrovirus containing pRS-mitoRFP, HEK293T-ampho cells were grown up to 50 % confluence at the day of transfection in 10-cm cell culture dishes with DMEM with 10 % FBS. Five-µg of pRS-mitoRFP plasmid DNA constructed in **Section 2.2.1** was transfected into HEK293T-ampho cells using Lipofectamine2000 following manufacturer's protocol as described above. Twelve-hour post-transfection, fresh DMEM + 5 % FBS was added up to 10 ml. In the meantime, HeLa cells or 293-TetR cells were seeded ~ 50 % (HeLa) or ~ 30 % (293-TetR) confluence in a 10-cm cell culture dish and grown overnight. One day post-transfection, media of pRS-MitoRFP-transfected HEK293T-ampho cells was collected and filtered using 0.45-µm syringe filters (BD Biosciences). Media of HeLa and 293-TetR cells was replaced with filtered retrovirus-containing media and 8 µg/ml of polybrene (Sigma) was added onto the cells. Following 24-hour incubation, media was replaced with fresh DMEM + 10 % FBS and cells were incubated up to 90 % confluence for another two days. Cells were then treated with 2 µg/ml of Puromycin (Invitrogen) for at least one week. Once colonies were formed, they were trypsinized, diluted, seeded onto 48-well cell culture plates, and grown under Puromycin-treatment. Several clones were selected based on growth and mitoRFP expression, amplified, and

Table 13. List of Oligonucleotides of shRNAi or siRNA

Target	Restriction sites	Sequence
Scramble	BamH1/HindIII	GATCCCCAATTCTCCGAACGTGTCACGTTTCAAGAGAACGTGACACGTTCGGAGAATTTTTTGGAAA
		AGCTTTTCCAAAAAAATTCTCCGAACGTGTCACGTTCTCTTGAAACGTGACACGTTCGGAGAATTGGG
mHsp40	BamH1/HindIII	GATCCCCCAGCTACGGCTACGGAGACTTCAAGAGAGTCTCCGTAGCCGTAGCTGTTTTTGGAAA
		AGCTTTTCCAAAAACAGCTACGGCTACGGAGACTCTCTTGAAGTCTCCGTAGCCGTAGCTGGGG
mHsp70	BamH1/HindIII	GATCCCCGCACATTGTGAAGGAGTTCAACTCGAGTTGAACTCCTTCACAATGTGCTTTTTTGGAAA
		AGCTTTTCCAAAAAAGCACATTGTGAAGGAGTTCAACTCGAGTTGAACTCCTTCACAATGTGCGGG
Drp1	BamH1/HindIII	GATCCCCTCCGTGATGAGTATGCTTTTTCAAGAGAAAAGCATACTCATCACGGATTTTTTGGAAA
		AGCTTTTCCAAAAATCCGTGATGAGTATGCTTTTCTCTTGAAAAAGCATACTCATCACGGAGGG
SiRNAs	Scramble	AATTCTCCGAACGTGTCACGT
	mtHsp40	CCGGATTAACAGCTACGGCTA
	mtHsp70	AATTGTATTCTCCGAGTCAGA
	Drp1	CAGGAGCCAGCTAGATATTAA

* Restriction enzyme sites were underlined.
* Targeting sequences were boxed in blue.
* Loop sequences were boxed in yellow.

stored as a frozen stock at -80 ℃ or in liquid nitrogen.

2.4.2 293-TetR-mitoRFP-MtHsp40$_L$ Cells

293-TetR-mitoRFP cells were seeded up to 30 % - 50 % confluence one day prior transfection, and were transfected with 5 μg of pcDNA4/TO/mtHsp40$_L$ plasmid generated as described in Section **2.2.3** using Lipofectamine2000 as described in Section **2.3.1.** Following 24-hour incubation, media was replaced with fresh DMEM + 10 % FBS and cells were incubated up to 90 % confluence for one more day. Cells were then treated with a combination of 1 μg/ml of Puromycin (Invitrogen), 100 μg/ml Blasticidin (Invitrogen), and 100 μg/ml Zeocin (Invivogen) for at least one week. Once colonies were formed, they were trypsinized, diluted, seeded onto 48-well cell culture plates, and grown with a combination of Puromycin/Blasticidin/Zeocin. Several clones were selected based on growth, amplified, and stored as a frozen stock at -80 ℃ or in liquid nitrogen.

2.5 Infection of Adenoviral Constructs

Cells were seeded onto 6-well cell culture plates and grown for the confluence of 50 % (mitochondrial imaging) or 90 % (Western blot) on the day of infection. Growth media was replaced with 1 ml of DMEM supplemented with 5 % FBS. One or 2 μl of pAdTrack-CMV adenoviral construct containing EGFP as a reporter was added to the cells. Twelve hours following infection, 1 ml of DMEM supplemented with 5 % FBS was added to the infected cells, and cells were grown as indicated.

2.6 Doxycycline-Inducing MtHsp40$_L$

293-TetR-mitoRFP-EGFP or 293-TetR-mitoRFP-mtHsp40$_L$ cells were seeded and grown on 6-well tissue culture plates up to 50 % for imaging or 70 % of confluence for Western blots, and at the following day, media was replaced with fresh media supplemented with the indicated concentration of Doxycycline (DOX; Sigma) and incubated for the indicated time.

2.7 Luciferase Reporter Assays

Cells were seeded in 10-cm cell culture dishes and grown to 90 % confluence on the day of transfection as described in **Section 2.2.5**, in addition to the pGL3-CMV-Mito constructs, 5 μg

of pRK5 or pRK5-mtHsp40$_L$ plasmid DNA was co-transfected. Twenty four hours following transfection, cells were trypsinized, resuspended in 500 µl of PBS, and treated with heat shock at the indicated temperature for the indicated time using a heat block. Following heat-shock, cells were incubated at 37 ℃ or room temperature for the indicated time for recovery. Upon centrifugation, cells were lysed with 100 µl of 1x Passive Lysis Buffer (PLB) and stored on ice. One hundred-µl of Luciferase Assay Reagent (Promega) was dispensed into white opaque 96-well flat bottom plates (Falcon) in triplicates and 20 µl of cell lysates were added. Upon shaking gently for 5 seconds, the luminescence was measured using GloMAX® Luminometer (Promega). Data was background-subtracted and fold increase was measured based on the activity of control-transfected cells.

2.8 Subcellular Fractionation

Two different methods were utilized including Qiagen QProteome Mitochondria Isolation Kit and centrifugation-based mitochondrial isolation: (1) Qiagen QProteome Mitochondria Isolation Kit is based on the buffer formulation. Briefly, cells were trypsinized, washed with ice-cold PBS, and incubated with 1 ml of the Lysis Buffer at 4 ℃ for 10 minutes with shaking. Following centrifugation, the cytosolic fraction (supernatant) was collected, and the cell pellet was further incubated with 1 ml of the Disruption Buffer and completely disrupted by using a blunt-ended needle and a syringe. Following 20 strokes and centrifugation, the supernatant was carefully transferred to a fresh tube and the mitochondrial pellet was collected following another centrifugation. (2) Frezza *et al* reported a centrifugation-based protocol of mitochondrial isolation as follows[218]. Cells were harvested using a cell scraper, washed with PBS, and resuspended in Mitochondria Isolation Buffer (10 ml of 0.1MTris–MOPS, pH 7.4, 1 ml of 0.1 M EGTA/Tris, 20 ml of 1M sucrose in 100 ml). Cells were homogenized using a Teflon pestle, and centrifuged at 600 g for 10 minutes at 4 ℃. Next, the supernatant was collected, transferred to a fresh tube, and centrifuged further at 7000 g for 10 minutes at 4 ℃. Supernatant was stored at -80 ℃ for the cytosol fraction, and the homogenate was resuspended in Mitochondria Isolation Buffer and repeated with the same centrifugation. Lastly, the mitochondrial pellet was resuspended in Mitochondria Storage Buffer, and stored at -80 ℃. Equal proportions of cytosol and mitochondrial fraction were loaded on 10 % SDS-PAGE gels, and the purity of each fraction was determined by Western blot analysis using anti-β-Tubulin and

anti-Tom20 or –mtHsp70 antibodies for the cytosolic and the mitochondrial fractions, respectively.

2.9 Protein Aggregation and Silver Staining

Cells in 10-cm cell culture dishes were transfected with pRK5-mtHsp40$_L$ (5 µg) or treated with DOX (100 ng/ml for 24 hours) to overexpress mtHsp40$_L$. Twenty four hours following transfection or DOX-treatment, cells were harvested, washed with ice-cold PBS, and subjected to mitochondrial isolation following the above protocols. Mitochondria (1 mg/ml) were resuspended in the Mitochondria Lysis Buffer (25 mM Tris-HCl pH7.4, 300 mM NaCl, 5 mM EDTA, protease inhibitors), and an equal volume of Mitochondria Lysis Buffer containing either SDS (4%) or NP-40 (2, 1, 0.4 or 0.2%) was added to each mitochondria[243]. Mitochondria were further incubated on ice for 10 minutes, and centrifuged at 20,000g for 10 minutes at 4°C to pellet insoluble aggregates. Insoluble aggregates were resuspended in the protein sample buffer (1 % SDS, 10 mM Dithiothreitol, 20 % Glycerol, 0.2 M Tris-HCl pH 6.8, 0.05 % Bromophenol Blue), and separated on 10 % SDS-PAGE for silver staining. Following SDS-PAGE, gels were incubated with milli-Q water with shaking for 30 minutes. After water was discarded, gels were incubated in Fixing Solution (50% Ethanol, 10% glacial acetic acid) with shaking for 10 minutes, and then Fixing Solution was replaced with Rinse Solution (50% Ethanol) with shaking for 5 minutes. Next, the Rinse Solution was replaced with Sensitizer (0.02% Sodium Thiosulphate; Sigma) with shaking for 2 minutes, and Sensitizer was discarded. Gels were washed with milli-Q water with shaking for 2 minutes, and were stained with cold Staining Solution (0.1% Silver Nitrate; Sigma) with shaking for 20 minutes. Following rinsing with milli-Q water, gels were incubated in Developer (2% Sodium Carbonate, 200 ul (37% v/v) Formaldehyde, 20 ml Sensitizer) with shaking for from 1 minute until bands were visible. To stop developing, gels were incubated in Stop Solution (1% Acetic acid) with shaking for at least 5 minutes. All the steps of silver staining were performed at room temperature.

2.10 Protein Quantification and Western Blots

Cells were washed with ice-cold PBS, lysed with 200 µl (6-well) or 500 µl (10-cm) of ice-cold RIPA buffer (20 mM Tris-Cl pH7.4, 150 mM NaCl, 0.5 % [v/v] NP-40, 1 % Sodium deoxycholate, 0.2 % SDS and protease inhibitor cocktail [Mini Complete, Roche]), scraped into

suspension, and transferred to 1.5 ml Eppendorf tubes. Cell debris was discarded after centrifugation. Protein was quantified using the Bradford Reagent (Roche) on SpectraMax M2 spectrophotometer (Molecular Devices) with bovine serum albumin (BSA, Sigma) as a standard. Twenty to 50-µg of cell lysates were mixed with 5x protein sample buffer and boiled at 95 ℃ for 5 minutes. Following centrifugation, samples were subjected to 10 % - 12 % sodium dodecyl sulfate polyacrylamide gel electrophoresis (SDS-PAGE) for approximately 1.5 hours at 100 volts, transferred to Nitrocellulose (Bio-Rad) or polyvinylidene difluoride (PVDF) membrane (PALL) for 2 hours at 40 mA, blocked with 5 % skim milk (EMD Biosciences) in PBS with 0.05 % Tween-20 (PBST), and incubated with primary antibody diluted 1:500 – 1:20000 in 5 % skim milk in PBST overnight at 4 ℃ or for two hours at room temperature. Next, membranes were washed three times with PBST, incubated with secondary antibody diluted 1:5000 in 5 % skim milk in PBST for two hours at room temperature, and washed three times with PBST. Protein bands were detected using horse-radish-peroxidase (HRP) conjugated enhanced chemiluminescence (Perkin Elmer Life Sciences) and X-ray film (Pierce).

The primary antibodies used were as follows: mtHsp40$_{L/S}$ (RS-11; Santa Cruz; 1:5000), mtHsp70 (MA3-028; Thermo Scientific; 1:20000), β-Tubulin (H-235; Santa Cruz; 1:5000), TOM20 (F-10, Santa Cruz; 1:500), DRP1 (611738; BD Transduction; 1:2000), OPA1 (612606; BD Transduction; 1:5000), Cytochrome c (556432; BD Pharmingen; 1:1000), FLAG (F3165 or F7425; Sigma; 1:5000), MYC (R950-25; Invitrogen; 1:5000), HA (house-made; 1:5000), and DsRed2 (29; Santa Cruz; 1:1000). The secondary antibodies were as follows: goat anti-mouse IgG-HRP (sd-2005; Santa Cruz), goat anti-rabbit IgG-HRP (sc-2004; Santa Cruz), and goat-anti rat IgG-HRP (sc-2006; Santa Cruz). Data was quantified using the Image J software with normalization to a background and fold-change was measured based on control samples.

2.11 Co-Immunoprecipitation (Co-IP)

Two different conditions were tested in this study: high and low stringency. (1) High stringent conditions; cells in three 10-cm or one 15-cm cell culture dish was trypsinized, washed with ice-cold PBS, and lysed with non-denaturing lysis buffer (20 mM Tris-HCl pH 7.5, 137 mM NaCl, 1 % Nonidet P-40, 2 mM EDTA, and protease inhibitor cocktail). Following centrifugation, protein (supernatant) was quantified using the Bradford Reagent (Bio-Rad) on the SpectraMax M2 spectrophotometer with BSA as a standard. Up to 1 mg of total protein lysate was incubated

with Protein A-Sepharose (Sigma) beads at 4 ℃ for 30 minutes to remove bead-binding proteins, and Protein A-Sepharose beads were discarded following centrifugation. Protein supernatant was incubated with 1 - 5 µg of normal IgG (Santa Cruz) or primary antibody overnight at 4 ℃ with rotating, and Protein A-Sepharose beads was added to the antibody/protein mix and incubated for 2 hours at 4 ℃ with rotating. Protein A-Sepharose bead/antibody/protein complex was collected by centrifuging, and washed three times with non-denaturing lysis buffer. Lastly, Protein A-Sepharose bead/antibody/protein complex was dissolved in 50 µl of 2x protein sample buffer, boiled at 95 ℃ for 5 minutes, and whole cell extracts, IgG control and Co-IP samples were then subjected to Western blot analysis as described above. (2) Low stringent condition; typsinized cells were lysed with low detergent non-denaturing lysis buffer (20 mM Tris-HCl pH 7.5, 137 mM NaCl, 0.1 % Nonidet P-40, 2 mM EDTA, and protease inhibitor cocktail) or PBS, and subjected to sonication. Following centrifugation, protein (supernatant) was quantified by using the Bradford Reagent (Bio-Rad) on the SpectraMax M2 spectrophotometer with BSA as a standard. Up to 1 mg of total protein lysate was incubated with Protein A-Sepharose (Sigma) beads at 4 ℃ for 30 minutes to remove beads-binding proteins, and Protein A-Sepharose beads were discarded following centrifugation. Protein supernatant was incubated with 1 - 5 µg of normal IgG (Santa Cruz) or primary antibody for 4 hours at 4 ℃ with rotating, and Protein A-Sepharose beads was added to the antibody/protein mix and incubated for 1 hour at 4 ℃ with rotating, and washed three times with ice-cold PBS. Lastly, Protein A-Sepharose bead/antibody/protein complex was dissolved in 50 µl of 2x protein sample buffer, boiled at 95 ℃ for 5 minutes, and whole cell extracts, IgG control and Co-IP samples were then subjected to Western blot analysis as described above.

2.12 Immunofluorescence and Imaging

Cells were seeded onto 22 mm x 22 mm cover slips (VWR) up to 30 % - 50 % confluence one day prior to experiments. Following treatment, transfection or infection as indicated, cells were directly incubated in ice-cold 4 % paraformaldehyde in PBS solution (PFA; Sigma) at 4 ℃ for from 1 hour to overnight to fix. Fixed cells were washed three times with PBS for 5 minutes at room temperature, blocked and permeabilized with 3 % BSA and 0.2 % Triton X-100 in PBS at 4 ℃ for 1 hour, and incubated with primary antibody at 1:100 - 1:2000 dilution in 3 % BSA and 0.1 % Triton X-100 at 4 ℃ overnight or at room temperature for 2 hours. Cells

were washed three times with PBS, and incubated with Alexa-Fluor-488 or Alexa-Fluor-568 anti-mouse, -rabbit, or –rat secondary antibodies (Invitrogen) at 1:1000 dilution in 3 % BSA and 0.1 % Triton X-100 for 1 hour at room temperature. Cells were washed three times with PBS and cover slips were mounted using anti-fade with 4',6-diamino-2-phenylindole (DAPI; Invitrogen). Images were captured by Fluorescence microscopy using the Zeiss Axiovert fluorescence microscope in the presence of Apoptome (Carl Zeiss).

2.13 Live Cell Imaging

Cells were seeded on 22 mm x 22 mm cover slips one day prior to infection for 30 % – 50 % confluence. Cells were infected as described in **Section 2.5**. Six hours post-infection, cells were mounted into 1-well Chamlide CMS magnetic chambers (Quorum Technologies) and placed into Chamlide TC Environment Adaptor maintaining 37 ℃ humidified atmosphere with 5 % CO_2 and mounted onto an Axiovert fluorescence microscope. Media was replaced with fresh DMEM + 10 % FBS. Following 1 hour-cell stabilizing, images were taken every 20 minute for 18 hours with z-stack. All images were processed using the Velocity software (PerkinElmer) to make a video file. *This experiment was performed by Chris Meijndert.

To observe mitochondrial motility, cells were seeded on 35-mm glass bottom dishes (MatTek) one day prior to infection for 30 % – 50 % confluence. Cells were infected as described in **Section 2.5**. Twenty four-hours post-infection, a dish was mounted into 1-well Chamlide CMS magnetic chambers (Quorum Technologies) and placed into Chamlide TC Environment Adaptor maintaining 37 ℃ humidified atmosphere with 5% CO_2 and mounted onto an Axiovert fluorescence microscope for visualization. Media was replaced with fresh DMEM + 10 % FBS. Following 1 hour-cell stabilizing, Images were taken every 2 seconds for 15 minutes. All images were taken with one focal plane, and sharpened using the AxioVision Software (Carl Zeiss).

2.14 Genomic DNA Isolation

Confluent cells in 6-well cell culture plates were washed twice with ice-cold PBS and subjected to GenElute Mammalian Genomic DNA Purification Kit (Sigma) following manufacturer's protocol. Briefly, cells were pelleted and resuspended in 200 µl of Resuspension Buffer. Two hundred-µl of Lysis Buffer and 20 µl of Proteinase K (Invitrogen) were added to the

cells, and cells were incubated at 70 ℃ for 10 minutes. Two hundred-µl of absolute ethanol was added and mixed. The samples were loaded into the spin column, and washed twice with 500 µl of Wash Buffer and the gDNA was eluted with 200 µl of ultrapure water. The purity and amount of gDNA was analyzed using the NanoVue Spectrophotometer (GE Healthcare).

2. 15 Quantitative PCR

Using gDNAs isolated above, Real Time PCR was performed to compare mitochondrial DNA amount following modified Grewal's protocol. The PCR condition was as follows: one hundred-ng of gDNA, 1x *Tag* PCR buffer with 1.5 mM $MgCl_2$, 250 µM dNTP mixture, 0.1x SyberGreen (Molecular Probes), 0.1 µM each primer, and 0.15 µl of *Taq* polymerase (Invitrogen). Primers were as follows: 5' – GTAACCCGTTGAACCCCATT – 3' (16S rRNA; Forward); 5' – CCATCCAATCGGTAGTAGCG – 3' (16S rRNA; Reverse); 5' – ACCCTAGACCAAACCTACGCCAAA – 3' (Cytochrome *c* oxidase 1; Forward); 5' – TAGGCCGAGAAAGTGTTGTGGGAA – 3' (Cytochrome *c* oxidase 1; Reverse). The cycling conditions for PCR amplification was as follows: 95 ℃ for 5 minutes; 40 cycles at 95 ℃ for 15 seconds, 60 ℃ for 15 seconds, 68 ℃ for 30 seconds. Samples were run in triplicates using white opaque PCR tubes with flat lids (Bio-Rad) on the StepOnePlus Real-Time PCR System (ABI Biosystems) and analyzed by the StepOne Software v2.2. Data was background-subtracted and normalized to a control.

2.16 Cell Counting and Tryphan Blue Exclusion Assay

Cells were trypsinized in 6-well cell culture plates, 10 ul of cell was mixed with 10 ul of Tryphan Blue reagent (Bio-Rad), and 10 µl of Cell-Tryphan Blue mix was loaded into disposable chamber slides (Bio-Rad), and slides were inserted into TC10 Automated Cell Counter (Bio-Rad). Tryphan blue-stained or -excluded cells were counted automatically.

2.17 Cell Viability Assay using Alamar Blue

Following infection or transfection, two thousand-cells were seeded onto 96-well cell culture plates in triplicates one day prior to Alamar Blue assay, and were grown overnight. Ten-ul of AlamarBlue reagent (Invitrogen) was added to each well with 90 ul of fresh DMEM + 10 % FBS. Plates were incubated in a CO_2 incubator and read every 4 hours up to 12 hours on the

SpectraMAX M2 Spectrophotometer at a wavelength of 595 nm (emission) and 540 nm (excitation). Each value was background-subtracted and control-normalized.

2.18 Fluorescence Activated Cell Sorting (FACS) for TMRM, MitoSOX Red and MitoTracker Green Staining

To compare mitochondrial membrane potential, mitochondrial ROS levels or mitochondrial contents, cells were seeded and grown onto 6-well cell culture plates one day prior to staining. Media was replaced with 1 uM tetramethyl rhodamine methy ester (TMRM; molecular probes) with 1 uM cyclosporine H (Enzo Life Sciences), 5 uM MitoSOX Red (Invitrogen) or 1 mM MitoTrackerGreen (Invitrogen) in Hank's Buffered Salt Solution (HBSS; Invitrogen) at 37 ℃ for 30 minutes. Cells were trypsinized, washed with PBS, and then resuspended in 300 ul of HBSS into 15 ml Falcon tubes, and analyzed by the BD LSR II (BD Biosciences) at the University of Calgary Flow Cytometry Core Facility. * MitoSOX Red staining was performed by Adam Elwi.

2.19 ATP Analysis

In order to measure intracellular ATP levels, luciferase-associated ATP assay was performed by using Adenosine 5-triphosphate (ATP) Bioluminescent Somatic Cell Assay Kit (Sigma) following manufacturer's protocol. Briefly, 10^5 cells were trypsinized, washed twice with ice-cold PBS, and resuspended in PBS. One hundred-ul of 1x Somatic Cell ATP Releasing Reagent was mixed with 50 ul of ultrapure water in a fresh vial. Fifty-ul of cell samples was added to 1x Somatic Cell ATP Releasing Reagent, mixed, and 100 ul of the sample-Somatic Cell ATP Releasing Reagent was immediately transferred to a white opaque 96-well flat bottom plates in triplicates. Luminescence was measured as described in **Section 2.7**. *This experiment was performed by Shin Kim.

2.20 Measurement of Oxygen Consumption Rate (OCR) and Extracellular Acidification Rate (ECAR)

Oxygen consumption rate (OCR) and extracellular acidification rate (ECAR) were measured using the Seahorse XF24 Extracellular Flux Analyzer (Seahorse Bioscience) to analyze the activity of OXPHOS. This device uses a disposable sensor cartridge which is embedded with

fluorescence-based optical biosensors (oxygen and protons) that allows for simultaneous extracellular real-time measurements of intact cells. First, the optimum number of cells and FCCP concentration needed were determined. Next, the mitochondrial function assay used sequential injection of oligomycin (1ug/ml; Enzo Life Sciences), FCCP (0.5uM; Sigma), and rotenone (1uM; Sigma) to define the mitochondrial function parameters such as basal level of oxygen consumption and the maximal respiration capacity. All assays were conducted using a seeding density of 40000 cells/well and the cells were switched to assay media, that is the unbuffered DMEM supplemented with specified metabolic substrates (10mM sodium pyruvate and 10mM glucose), 1 hr prior to the beginning of the assay and incubated without CO2 at 37 ℃. Transfection efficiency is visualized directly by fluorescence microscopy for qualitative analysis. Values were normalized to the total cell numbers per well after the completion of the XF assay by the DAPI staining. Data were acquired from three replicate plates per cell line. Average values of OCR and ECAR from cells transfected with mtHsp40 or mtHsp40 siRNA were compared with untransfected control cells (vector only or scramble RNA). *This experiment was performed by Yonghee Ahn.

2.21 Transmission Electron Microscopy (TEM)

In order to observe mitochondrial microstructure, the Transmission Electron Microscopy was performed. Cells were cultured onto 6-well cell culture plates, and were infected or transfected as described in **Sections 2.3 & 2.7**. Following transfection or infection, cells were fixed with 2.5 % glutaraldehyde (v/v) in phosphate buffer pH 7.0 at room temperature for 30 minutes. Further sample processing including postfixation, dehydration and resin embedding was performed by University of Calgary Microscopy and Imaging Facility. Intracellular structures were visualized using the Hitachi H-7650, a 120 kV Transmission Electron Microscope. Images were taken at 4000 or 10000 magnification.

2.22 Generation of Cre-Inducing mtHsp40$_L$ Mouse Model and Mating

For pronuclear injection, iZEG-hmtHsp40$_L$ construct was isolated using Qiagen Plasmid Midiprep kits following manufacturer's protocol. Ten-µg of plasmid was linearized with *NotI* restriction enzyme and subjected to gel extraction using Qiagen Gel Extraction kit. Next, linearized DNA was pronuclear-injected into C57BL6 fertilized eggs, which were transferred to

pseudopregnant mice by Transgenic Services Centre for Mouse Genomics (University of Calgary). In order to generate transgenic mouse model brain-specifically expressing hmtHsp40$_L$, iZEG-hmtHsp40$_L$ mice were mated with CamK.Cre mice expressing Cre-recombinase mainly in brain (gifted by Minh Dang Nguyen, University of Calgary, or purchased from JAX Lab).

2.23 Genotyping PCR

Ears were incubated in 100 µl of lysis buffer (KCl, 1.15 g; 1 M Tris-Cl pH 8.3, 2.0ml; 1M $MgCl_2$, 0.4 ml; Gelatin, 20 mg; Nonidet P-40, 900 µl; Tween-20, 900 µl; 0.5 ml of Proteinase K (10 mg/ml, Invitrogen) in 200 ml of ultrapure water) at 55 ℃ overnight. Following centrifugation, the supernatant containing genomic DNA was transferred to a fresh 1.5 ml eppendorf tube, and stored at 4 ℃. The Genotyping PCR condition was as follows: 1 µl of gDNA, 1x *Tag* PCR buffer with 17.5 mM $MgCl_2$, 250 µM dNTP mixture, 0.1 µM each primer, and 0.15 µl of *Taq* polymerase (Invitrogen) in total 20 µl reaction. Primers were described in Table 12. The cycling conditions for PCR amplification was as follows: 95 ℃ for 5 minutes; 30 (for actin) or 35 cycles (for lacZ and cre) at 95 ℃ for 30 seconds, 50 ℃ or 60 ℃ for 30 seconds, 72 ℃ for 30 seconds; extension at 72 ℃ for 10 minutes. PCR products were analyzed on 1.5 % agarose gel electrophoresis.

CHAPTER THREE: IMBALANCE OF MTHSP40 AND MTHSP70 CAUSES MITOCHONDRIAL FRAGMENTATION INDEPENDENTLY OF APOPTOSIS

3.1 Preliminary Findings and Rationales

To date, studies have shown that mitochondrial fragmentation is an early event before caspase activation and membrane blebbing during apoptosis. For example, Karbowski *et al* found that this process occurs either just in prior or simultaneously to cytochrome *c* release, as fragmented mitochondria seemingly retain cytochrome *c*. During early stages of apoptosis, cytochrome *c* is retained in fragmented mitochondria. Progressively later stages of apoptosis show some portion of fragmented mitochondria with cytochrome *c* visible in the cytosol, and mitochondrial cytochrome *c* becomes undetectable at the completing stage of apoptosis[219], suggesting that mitochondrial morphology is closely coupled with apoptosis. It is of note that although mitochondrial fragmentation is associated with apoptosis, it also occurs in absence of apoptosis, such as that which occurs under mitochondrial membrane potential loss ($\Delta\psi m$)[73].

Our previous findings clearly demonstrated that ectopic expression of mtHsp40 sensitizes cancer cells to apoptotic stimuli[40]. Our preliminary results apparently showed that mtHsp40 overexpression in a breast cancer cell line MCF7 induced mitochondrial morphology change in both absence and presence of proapoptotic conditions such as hypoxia and DNA damage. We also noticed that mtHsp40-knockout MEF showed mitochondrial fragmentation with no treatments[163], which led us propose that altered expression level of mtHsp40 may promote apoptosis by modulating mitochondrial morphology.

It is recently known that mtHsp70 mutations defective in ATP hydrolysis or substrate binding activity result in mitochondrial fragmentation leading to neuronal cell death[215]. Iosefen *et al* found that *in vitro* disaggregation activity of Ssc1, yeast homolog of mtHsp70, is dependent on the concentration of Mdj1, yeast homolog of mtHsp40[143]. Later, Iosefen *et al* reported their *in vitro* findings that upon further increase in Mdj1 over its optimal concentration, the deaggregation activity decreases[143]. In addition, Hageman and Kampinga mentioned their unpublished findings in a review article that raising HSP40 levels in cells reduced protein refolding activity of HSP70s in the absence of concomitant increase of HSP70 levels[30]; however, it is not experimentally proved *in vivo*. In addition, it is not known that mitochondrial morphology is closely linked to mitochondrial chaperonic network, in particular, the

stoichiometric ratio between mtHsp40 and mtHsp70.

Thus, we wish to determine the effects of ratio between mtHsp40 and mtHsp70 on mitochondrial morphology, and elucidate whether apoptosis is functionally or mechanistically coupled with mitochondrial fragmentation caused by mtHsp40:mtHsp70 imbalance.

3.2 Apoptosis-independent Mitochondrial Fragmentation Caused by Ectopic Expression of MtHsp40 in MCF7 and U87 Cells

To determine whether mitochondrial fragmentation caused by ectopic expression of mtHsp40 is coupled with apoptosis, we examined the effects of mtHsp40 overexpression on mitochondrial morphology and apoptotic cell death. Whereas MCF7 mitochondria were tubular and well distributed, U87 mitochondria were slightly fragmented with no treatments (data not shown). Both mitochondria are fragmented in more than 50 % of GFP-positive cells both breast cancer MCF7 and glioma U87 expressing mtHsp40 (Fig 9A). However, significant portion of TUNEL-positive cells were not detectable in either cell line (Fig 9B). We found no significant increase of cytochromce *c* release in fragmented mitochondria compared with control MCF7 or U87 cells (data not shown), suggesting that mtHsp40 overexpression induced mitochondrial fragmentation independently of apoptosis.

3.3 Generation of HeLa-mitoRFP and MCF7-mitoRFP Cells

In order to monitor the mitochondrial morphology and apoptosis on real-time, we established MCF7 and HeLa cell lines stably expressing mitochondrial-targeted fluorescent protein. We first generated the pDsRed2-MTS-N1 plasmid carrying the DsRed2 gene, N-terminal fused with MTS of a mitochondrial innermembrane protein, cytochromce *c* oxidase IV. Using this construct, we established two cell lines MCF7-mitoRFP and HeLa-mitoRFP. Immunofluorescence results showed that MitoRFP protein well co-localized with mtHsp70 in both MCF7-mitoRFP and HeLa-mitoRFP cell lines, and we could not detect the cytosolic RFP, suggesting that MitoRFP protein was well targeted to mitochondria (Fig 10A). Mitochondrial localization of MitoRFP was confirmed by subcellular fractionation experiments, and was analyzed with Western blots using each fraction markers; mtHsp70 (mitochondria) and β-Tubulin (cytosol) to check purity of each fraction. RFP protein was mainly located in the cytosol,

Figure 9. Effects of Ectopic Expression of mtHsp40 on Apoptosis and Mitochondrial Morphology in MCF7 and U87 cells

MCF7 and U87 cells were adenoviral-infected by either Ad-GFP or Ad-mtHsp40 as indicated for 48 hours. Cells were stained with 1 μM MitoTracker Green, a mitochondria-specific dye for 30 min (A). TdT-mediated dUTP nick end labeling (TUNEL) assays were performed by counting over 100 cells to measure apoptotic cells (B). Bars indicate + SEM, and the data represent three independent experiments. ** means $p < 0.01$.

9A

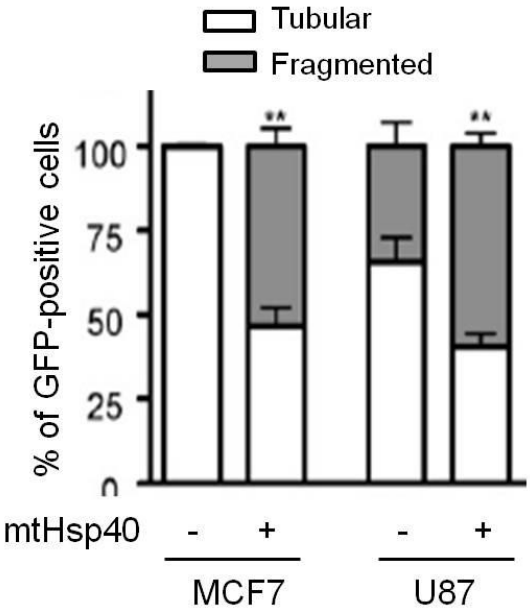
Tubular
Fragmented
% of GFP-positive cells
100
75
50
25
0
**
**
mtHsp40
-
+
-
+
MCF7
U87

9B

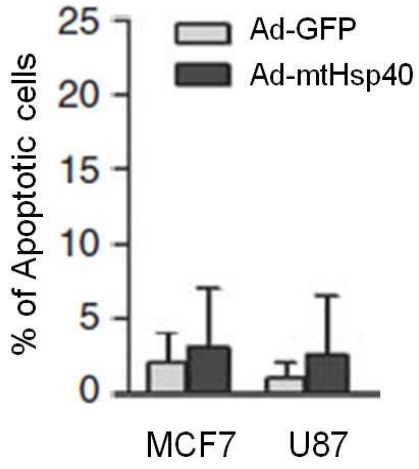
25
20
15
10
5
0
% of Apoptotic cells
Ad-GFP
Ad-mtHsp40
MCF7
U87

Figure 10. Determination of MitoRFP Localization of MCF7-MitoRFP and HeLa-MitoRFP Cells

(A) MitoRFP construct was transfected into MCF7 and HeLa cells by Lipofectamine2000 for 24 hours. Cells were fixed with 4 % PFA, and stained for mtHsp70/AF488 goat anti-mouse IgG to determine the co-localization of MitoRFP with mitochondria. MitoRFP was visualized as red (568 nm) and mtHsp70 as green (488 nm). (B) Subcellular fractions from the cells as described in (A) were separated by biochemical fractionation (WCE = whole cell extract; Cyto = cytosolic; Mito = mitochondrial fraction) followed by immunoblotting. Purity of the fractions was determined by Western blots with anti-mtHsp70 (mitochondrial) and β-Tubulin (cytosolic).

10A

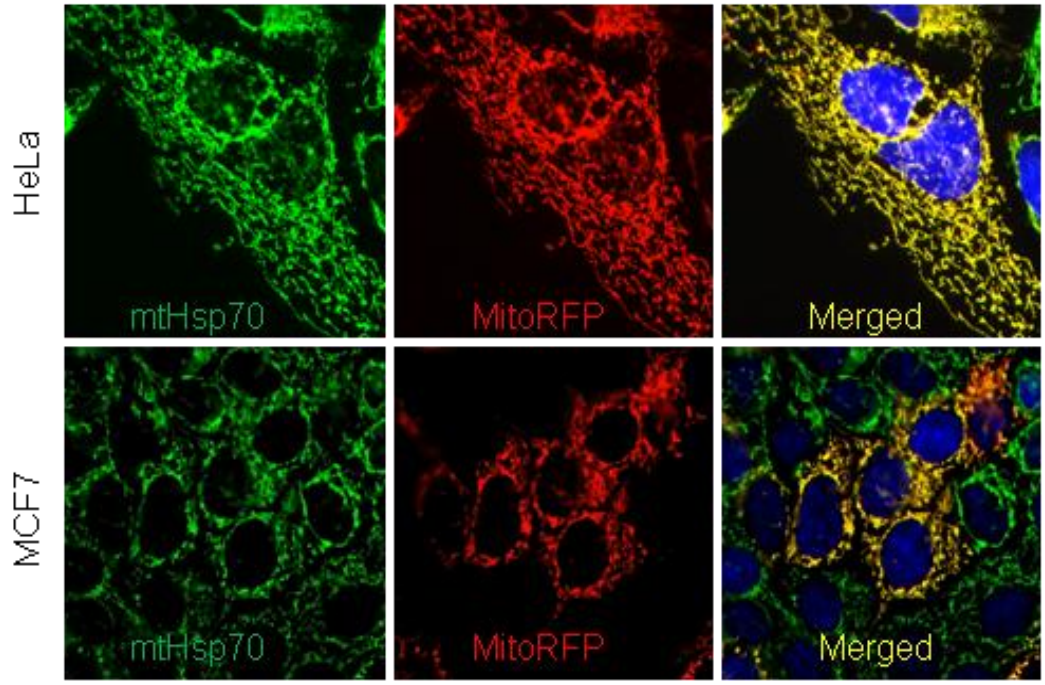
HeLa
MCF7
mtHsp70
MitoRFP
Merged
mtHsp70
MitoRFP
Merged

10B

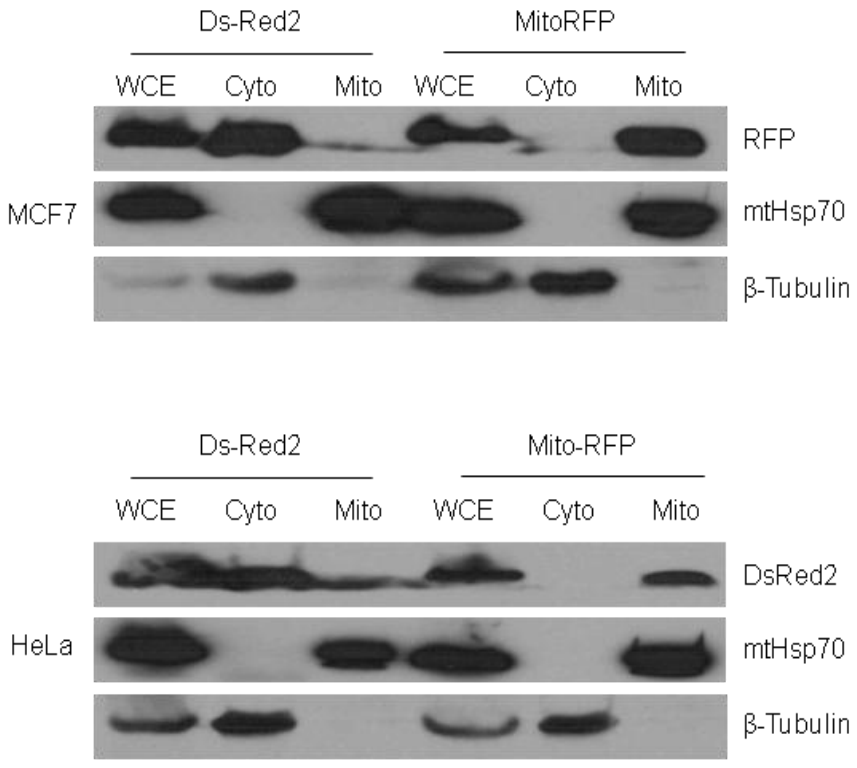
Ds-Red2
MitoRFP
WCE
Cyto
Mito
WCE
Cyto
Mito
RFP
MCF7
mtHsp70
β-Tubulin
Ds-Red2
Mito-RFP
WCE
Cyto
Mito
WCE
Cyto
Mito
DsRed2
HeLa
mtHsp70
β-Tubulin

although it also was detectable in the mitochondrial fraction of both cell lines. Conversely, MitoRFP proteins were mostly detected in the mitochondria, but not in the cytosol (Fig 10B), showing that MitoRFP proteins are specifically expressed in mitochondria.

3.4 Enhanced Apoptosis in Fragmented Mitochondria Caused by Ectopic Expression of MtHsp40 in HeLa, Hs68 and SK-N-SH cells

In order to confirm our findings from MCF7 and U87 cells, we observed mitochondrial morphology and apoptosis in HeLa-mitoRFP cells ectopically expressing mtHsp40. HeLa-mitoRFP cells were first infected with 2 μl of either Ad-GFP as a control or Ad-mtHsp40$_L$ for 48 hours, and treated with cisplatin, an alkylating agent as indicated. In both Ad-GFP- and Ad-mtHsp40$_L$ - infected cells, GFP-positive cells were > 90 % of total cells. While Ad-GFP-infection did not affect the levels of either long or short mtHsp40 isoform, only mtHsp40$_L$ was highly expressed in Ad-mtHsp40$_L$-infected cells. The unprocessed mtHsp40$_L$ also accumulated but mtHsp40$_S$ level did not change (Fig 11A). Ad-GFP-infected control cells showed the tubular network of mitochondria, and their mitochondria were well distributed throughout the cells. Conversely, mtHsp40$_L$-overexpressed cells showed completely fragmented puncta of mitochondria, and were perinuclear (Fig 11B). To quantify cells with fragmented mitochondria, we observed counted than 100 GFP-positive cells and quantified cells showing homogenous mitochondrial morphology as shown in Fig 11B. GFP-positive cells > 80 % showed fragmented mitochondria in the presence of mtHsp40$_L$ overepxression, whereas control cells showed fragmented mitochondria in less than 5 % of GFP-positive cells (Fig 11C). Cells with unclear or mixed morphology of mitochondria were excluded. The effects of mtHsp40$_L$ overexpression on cytochrome *c* release were also tested in HeLa. In control cells, mitochondria were tubular and cytochrome *c* mostly localized in mitochondria in the absence of cisplatin, whereas mitochondria were fragmented in most cells and cytochrome *c* was released into the cytosol from 35 % of cells in the presence of cisplatin. In mtHsp40$_L$-overexpressed cells, mitochondria were mostly fragmented and retained cytochrome *c* without cisplatin, whereas they extensively released cytochrome *c* into the cytosol from 80 % cells in the presence of cisplatin, suggesting that ectopic expression of mtHsp40$_L$ itself does not trigger apoptosis, but enhances apoptosis sensing proapoptotic stresses. *Adam Elwi performed the work.

Figure 11. Effects of Ectopic Expression of MtHsp40 using Adenoviral Constructs on Apoptosis and Mitochondrial Morphology in HeLa Cells

(A) HeLa-mitoRFP cells were adenoviral-infected by Ad-GFP or Ad-mtHsp40$_L$ as indicated for 48 hours. Proteins were analyzed by Western blots using the indicated primary antibodies. Up = unprocessed form. (B) Cells were fixed using 4 % PFA, and MitoRFP was visualized by fluorescence microscopy (568 nm, red). White stars indicate GFP-positive (virus-infected, green) cells. White boxes were zoomed in. White bar means 10 μm. (C) To quantify mitochondrial fragmentation, more than 100 GFP-positive cells were counted, and cells showing unclear or mixed mitochondrial morphology were not included. ***$P < 0.001$ denotes significant difference from the control group. Bars mean + S.E.M, n = 6. (D) Cells described in (A) were treated with either DMSO or 2 μM Cisplatin in a combination with 20 μM Z-VAD-FMK for 12 hours, and immunostained using anti-cytochrome *c* antibodies/AF633. White stars indicate infected cells, white arrows, apoptotic cells and white bars, 10 μm. (E) Among more than 100 cells, cells showing complete release of cytochorome *c* were counted. Bars mean + S.E.M, n = 2.

11A

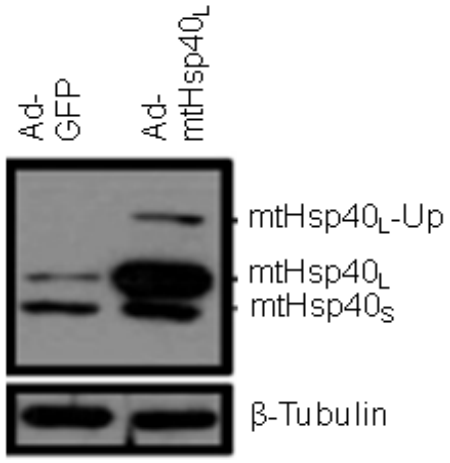
Ad-GFP
Ad-mtHsp40L
mtHsp40L-Up
mtHsp40L
mtHsp40S
β-Tubulin

11B

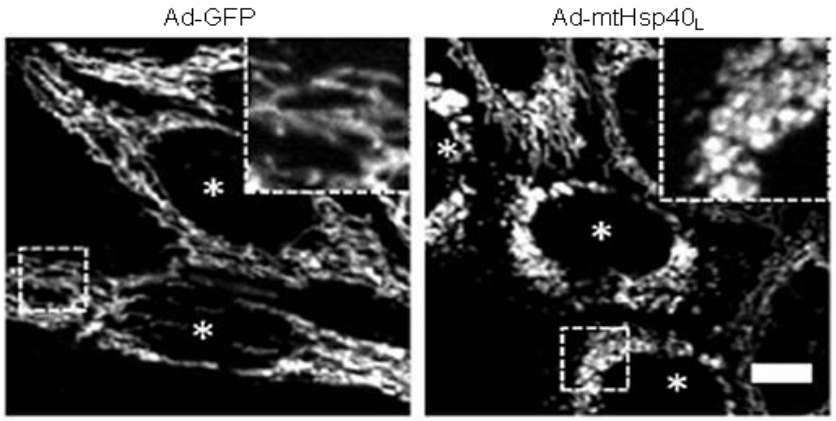
Ad-GFP
Ad-mtHsp40L

11C

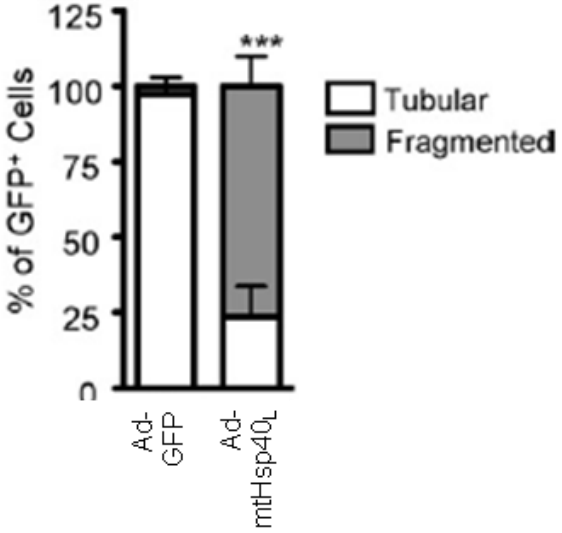
125
100
75
50
25
0
% of GFP+ Cells
***
Tubular
Fragmented
Ad-GFP
Ad-mtHsp40L

11D

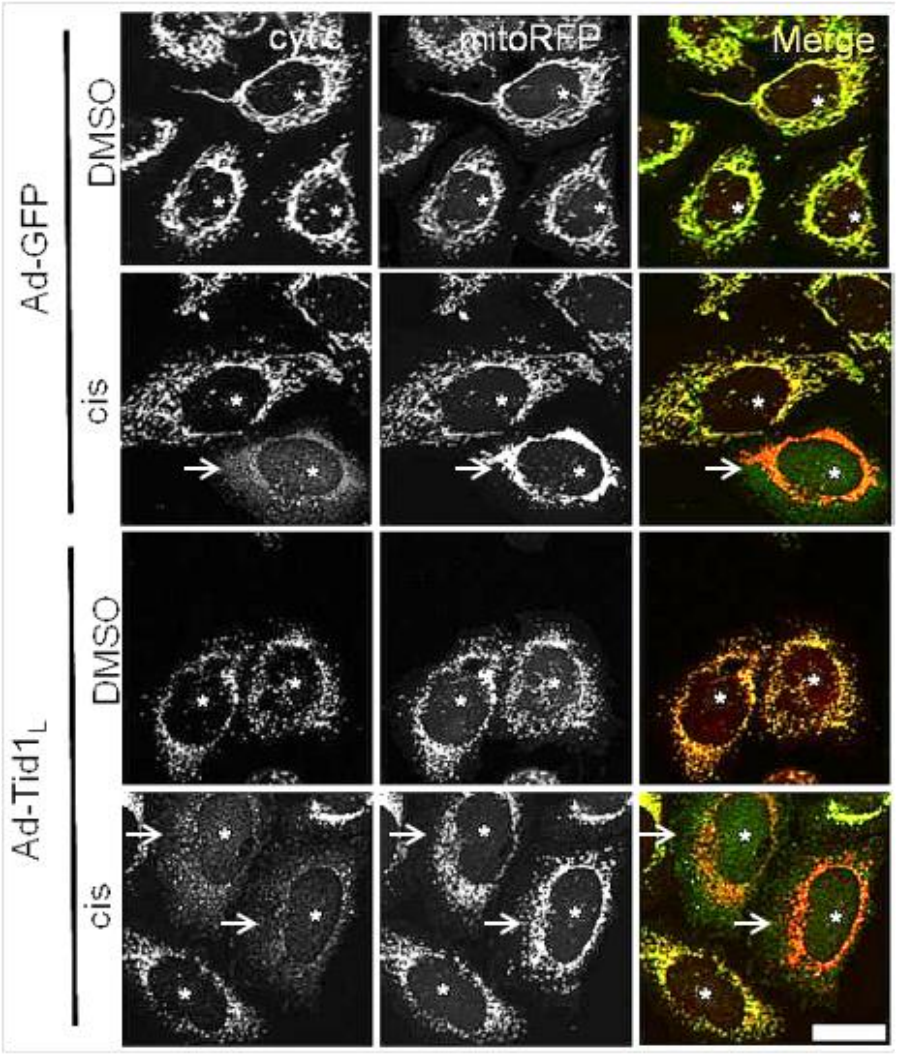
cyt c
mitoRFP
Merge
Ad-GFP
DMSO
cis
Ad-Tid1L
DMSO
cis

11E

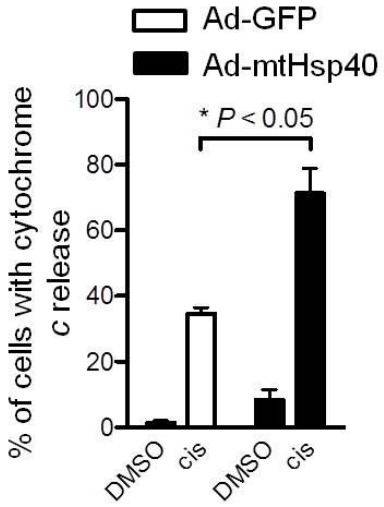
Ad-GFP
Ad-mtHsp40
* P < 0.05
% of cells with cytochrome c release
100
80
60
40
20
0
DMSO
cis
DMSO
cis

In order to test whether effects of mtHsp40 overexpression on mitochondrial morphology and apoptosis are general, we included human primary skin fibroblast Hs68 and neuroblastoma SK-N-SH. Hs68 showed lower infection efficiency than cancer cell lines such as HeLa and SK-N-SH cells. As expected, immunoblotting results showed that both Hs68 and SK-N-SH cells highly expressed mtHsp40$_L$, but the unprocessed form of mtHsp40$_L$ accumulated in only SK-N-SH cells, not in Hs68 cells; however, mtHsp40$_S$ or mtHsp70 protein levels were not affected (Fig 12A). Hs68 cells developed highly elongated tubular network and SK-N-SH cells showed heterogeneous mitochondrial morphology. Irrespective of original morphology of mitochondria, ectopic expression of mtHsp40$_L$ resulted in fragmented mitochondria in both cell lines (Fig 12B), and the percentage of cells showing fragmented mitochondria was various between two cell lines (Fig 12C); however, consistently with MCF7, U87 and HeLa, significant cytochrome *c* release was not detected in fragmented mitochondria from either cell line (data not shown). To rule out the possible effects of adenoviruses on mitochondrial morphology or apoptosis, we constructed the C-terminal Flag-tagged mtHsp40$_L$ in a mammalian expression vector and introduced it into HeLa-mitoRFP cells for 24 hours. Similarly, following transfection of the mammalian construct, mtHsp40$_L$-Flag was highly expressed and unprocessed form accumulated, but did not affect mtHsp40$_S$ or mtHsp70 level (Fig 13A). Overexpressed mtHsp40$_L$-Flag well localized at mitochondria and resulted in fragmented mitochondria (Fig 13B), but did not affect cytochrome *c* release (data not shown). In order to monitor mitochondrial morphology on Real-Time and determine how fast mitochondrial fragmentation occurs, we performed the live cell imaging using HeLa-mtoRFP cells infected by either Ad-GFP or Ad-mtHsp40$_L$. We started imaging 7 hours following infection, and took z-stack images. Since both Ad-GFP and Ad-mtHsp40$_L$ expressed GFP as a infection marker, we took two-colored images, green for GFP and red for MitoRFP. In some cells, we could detect GFP approximately 10 hours following viral infection indicating mtHsp40$_L$ expression. Mitochondrial morphology started to change around 12 hours following viral infection, and was completed within 3 hours (Fig 14).
*This experiment was performed by Chris Meijndert.

3.5 Level of MtHsp40 as a Determinant of Mitochondrial Morphology

The above results suggest that level of mtHsp40 may determine mitochondrial morphology, but not affect apoptosis. Thus, we first determined the range of Ad-mtHsp40$_L$

Figure 12. Effects of Ectopic Expression of MtHsp40 on Mitochondrial Morphology in Hs68 and SK-N-SH cells

(A) Both Hs68 and SK-S-SH cell lines were adenoviral-infected by either Ad-GFP or Ad-mtHsp40$_L$ as indicated for 48 hours, and were analyzed by Western blots using the indicated primary antibodies. Up = unprocessed form. (B) Cells were fixed using 4 % PFA, and MitoRFP was analyzed by fluorescence microscopy (568 nm). White stars indicate GFP-positive cells, and white bar, 10 μm. White boxes were zoomed in. (C) More than 100 GFP-positive cells were counted. We quantified only cells with clear mitochondrial morphology, but did not include cells showing unclear or mixed mitochondria. ***P < 0.001 and **P < 0.01 denote significant difference from the corresponding control group. Bars mean + S.E.M, n = 3.

12A

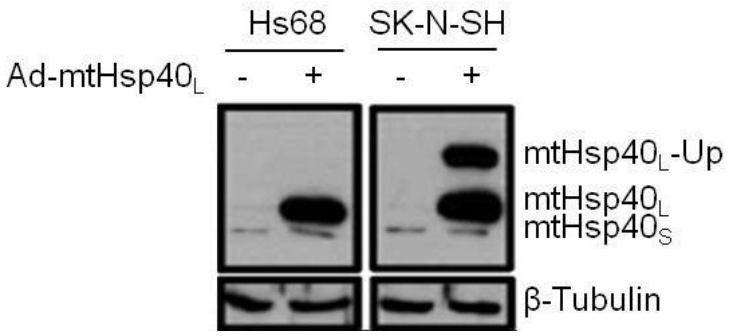

12B

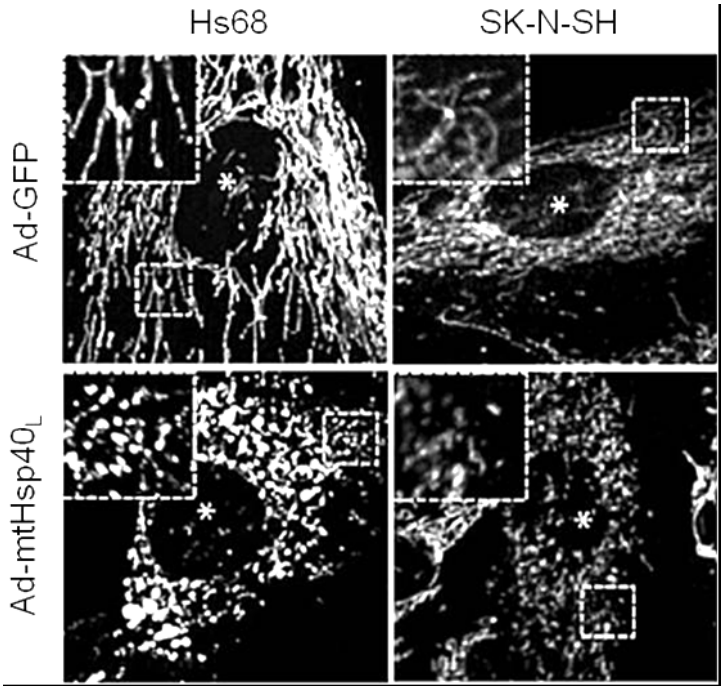

Figure 12C

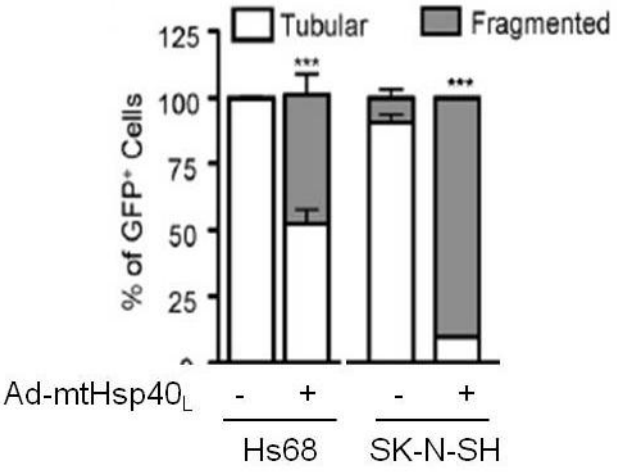

Figure 13. Determination of Effects of MtHsp40 Overexpression Using Mammalian Expression Construct on Mitochondrial Morphology

(A) HeLa-mitoRFP cells were transfected with pRK5-mtHsp40$_L$-Flag expressing C-terminal Flag tagged mtHsp40$_L$ using Lipofectamine2000 for 24 hours. Cells were analyzed by Western blots using the indicated primary antibodies. Up = unprocessed form. (B) Cells were fixed using 4 % PFA, and stained by anti-Flag/AF488 goat anti-Mouse IgG. MitoRFP was visualized as red (568 nm) and Flag as green (488 nm). White stars indicate untransfected cells, and white bar, 10 μm.

13A

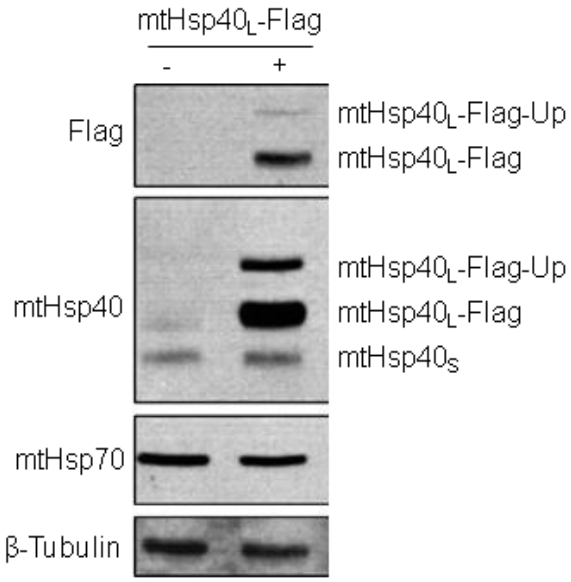
mtHsp40L-Flag
-
+
Flag
mtHsp40L-Flag-Up
mtHsp40L-Flag
mtHsp40
mtHsp40L-Flag-Up
mtHsp40L-Flag
mtHsp40S
mtHsp70
β-Tubulin

13B

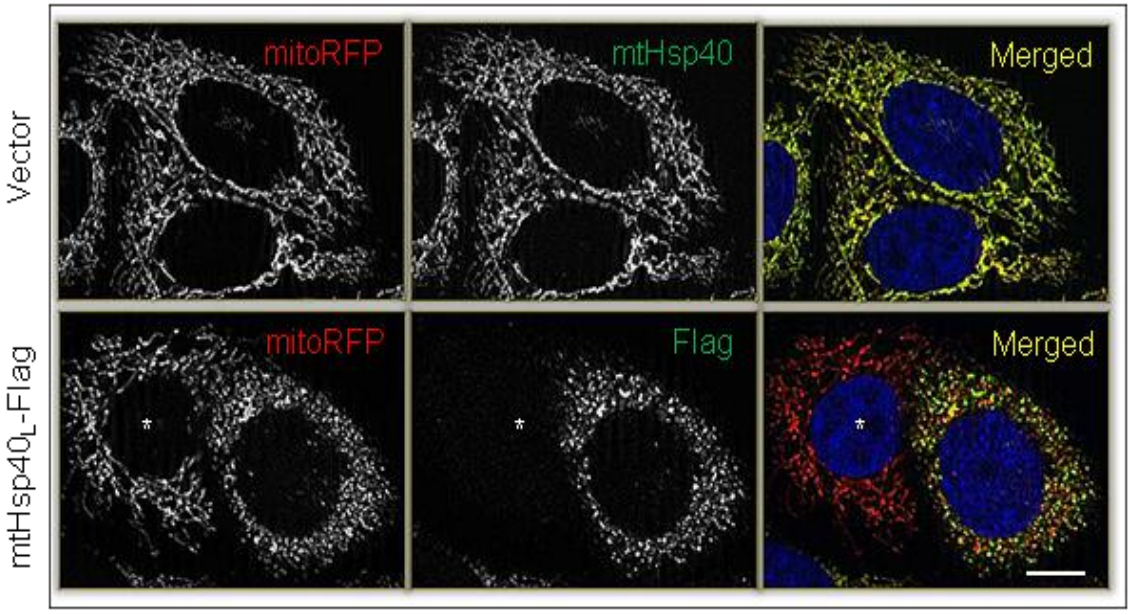
Vector
mtHsp40L-Flag
mitoRFP
mtHsp40
Merged
mitoRFP
Flag
Merged

Figure 14. Real-Time Effects of Ectopic Expression of MtHsp40 on Mitochondrial Morphology

HeLa-mitoRFP cells were adenoviral-infected by Ad-GFP or Ad-mtHsp40$_L$ as indicated. Following seven-hour infection, real-time imaging was performed by taking images with 488 nm and 568 nm channels in the presence of z-stack every 30 minute for 18 hours. A zoomed-in cell showed that mitochondria first broke apart and then became highly compact followed by localization surrounding the nucleus. White stars indicate infected cells, and white bars, 5 μm.

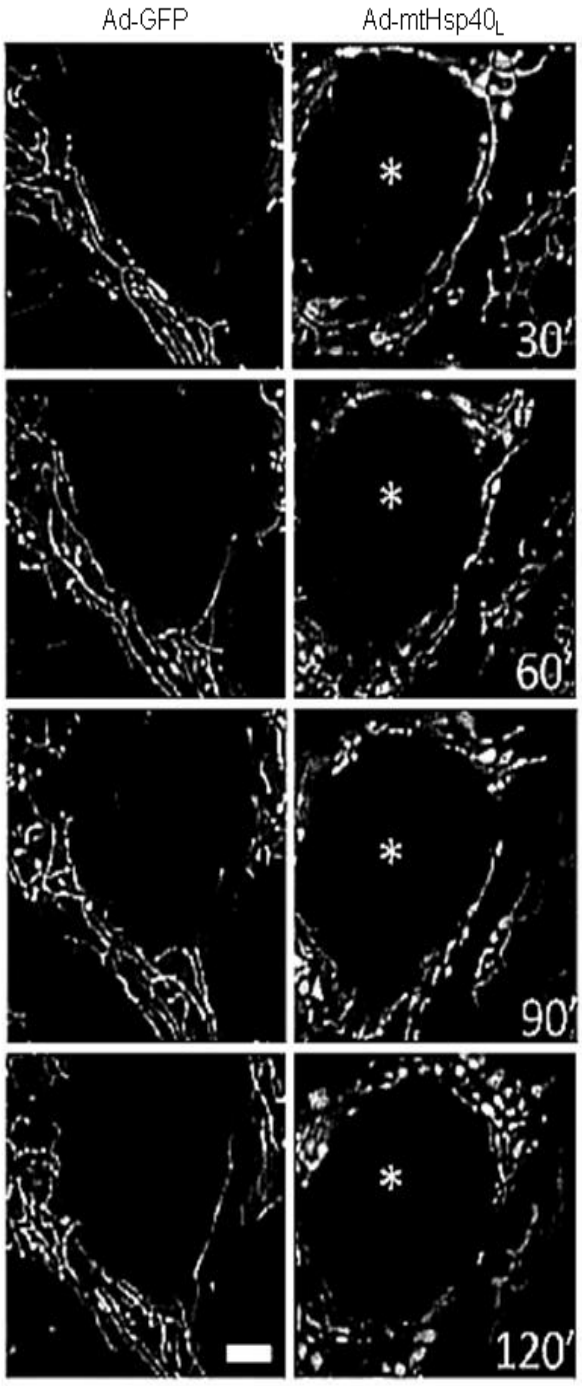
Ad-GFP
Ad-mtHsp40L
30′
60′
90′
120′

adenovirus which caused mitochondrial fragmentation. We infected HeLa-mitoRFP cells with a range of Ad-GFP or Ad-mtHsp40$_L$ for 24 hours, and analyzed mtHsp40$_L$ protein levels and mitochondrial morphology. MtHsp40$_L$ protein levels correlated with the viral amount, and unprocessed MtHsp40$_L$ protein bands became detectable with at least 1.0 μl of Ad-mtHsp40$_L$ (Fig 15A). We assumed that mtHsp40$_L$ protein levels may be correlated with mitochondrial morphology change, but our data demonstrated that there was a threshold of mtHsp40$_L$ level required for mitochondrial fragmentation. Most of mitochondria in > 80 % cells were fragmented with as low as 0.5 μl of Ad-mtHsp40$_L$, and more viruses than 0.5 μl did not induce further mitochondrial fragmentation (Fig 15B). Twenty-percent of cells expressing very strong GFP showed mitochondrial fragmentation with 0.25 μl of viruses, indicating that cells were still not infected homogeneously with adenoviruses.

In order to accomplish homogenous overexpression of mtHsp40$_L$, we attempted to generate DOX-inducible mtHsp40$_L$ system from HeLa and HEK293 cells, and succeeded in only HEK293 cell line, which we named HEK293-TetR-mitoRFP-mtHsp40$_L$. When cells were treated with 100 ng/ml Doxycycline for 24 hours, mtHsp40$_L$ was highly induced, but no unprocessed isoform or no change in mtHsp70 level was detectable (Fig 16A). Consistently, most of mitochondria in more than 80 % of cells changed in morphology from the tubular network to fragmented puncta (Fig 16B & 16C). In order to determine the level of mtHsp40$_L$ triggering mitochondrial fragmentation, cells were treated with a gradient of DOX for 24 hours. Five-ng/ml of DOX increased mtHsp40$_L$ 33-fold over control, but did not affect the levels of either mtHsp40$_S$ or mtHsp70. No unprocessed mtHsp40$_L$ was detectable with any concentration of DOX in HEK293 cells (Fig 17A). We quantified cells showing mitochondrial fragmentation as described in Fig 16B, and found that more than 80 % of cells showed fragmented mitochondria (Fig 17B). DOX doses higher than 5 ng/ml had no further effects on mitochondrial morphology, suggesting that mtHsp40 level should be regulated within a certain range to maintain mitochondrial morphology.

3.6 Reversibility of Mitochondrial Morphology Change

Under physiological condition, mitochondrial morphology is known reversibly dynamic in a response to cellular stresses[68]. Therefore, we next tested whether mtHsp40-induced mitochondrial fragmentation was reversible. After HEK293-TetR-mtRFP-mtHsp40$_L$ cells were

Figure 15. Effects of Different Amount of Adenoviral mtHsp40$_L$ Constructs on Mitochondrial Morphology

HeLa-mitoRFP cells were infected with a gradient of adenovirus (2 µl, 1 µl, 0.5 µl, & 0.2 µl), Ad-GFP or Ad-mtHsp40$_L$ as indicated for 48 hours. (a) Proteins were analyzed by Western blots using the indicated primary antibodies. Up = unprocessed form. (b) Cells described above were fixed using 4 % PFA, and mitochondria were visualized using fluorescence microscopy (568 nm). We quantified GFP-positive cells showing homogeneous tubular or fragmented mitochondria by counting more than 100 cells. Bars mean + S.E.M., n = 3.

15A

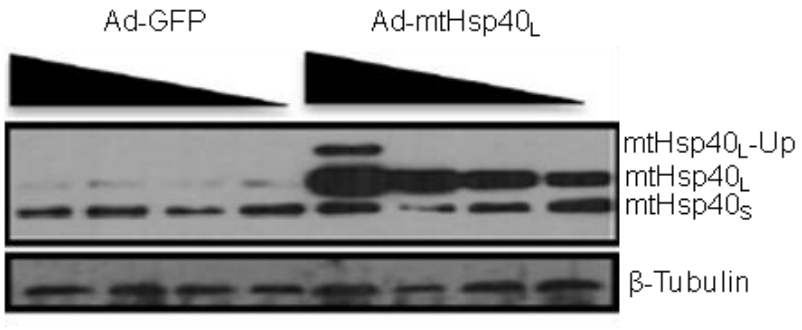
Ad-GFP
Ad-mtHsp40L
mtHsp40L-Up
mtHsp40L
mtHsp40S
β-Tubulin

15B

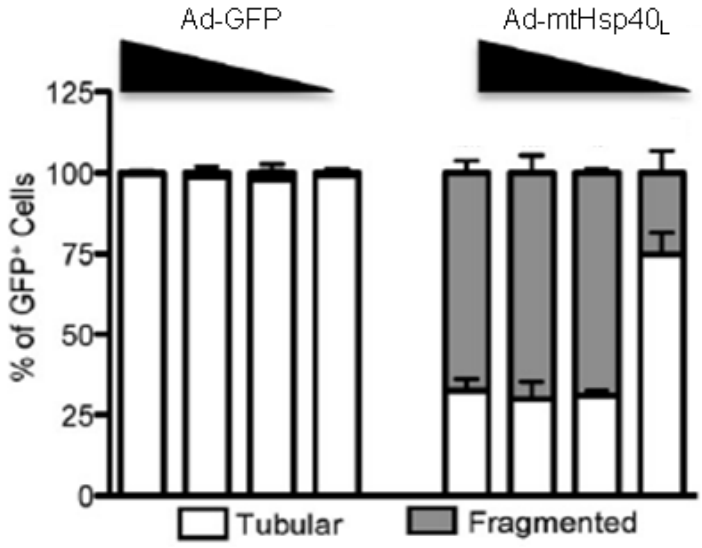
Ad-GFP
Ad-mtHsp40L
125
100
75
50
25
0
% of GFP+ Cells
Tubular
Fragmented

Figure 16. Effects of Doxycycline-Induction of MtHsp40 on Mitochondrial Morphology in HEK293 Cells

(A) HEK293-MitoRFP-TetR-GFP or –mtHsp40$_L$ cells were treated with Doxycycline (100ng/ml) for 24 hours. Cells were analyzed by Western blots using the indicated primary antibodies. (B) Cells described above were fixed using 4 % PFA, and stained by mtHsp40/AF488 goat anti-mouse IgG antibody. White boxes were zoomed in, and white bars, 10 µl. (C) Cells showing fragmented mitochondria were quantified out of more than 100 cells. Bars mean + S.E.M, n = 3.

16A

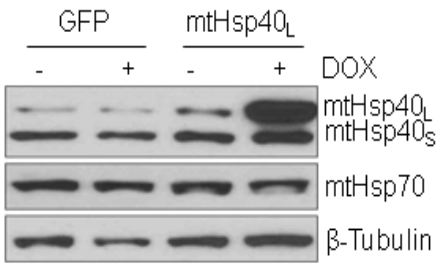
GFP
mtHsp40L
- + - + DOX
mtHsp40L
mtHsp40S
mtHsp70
β-Tubulin

16B

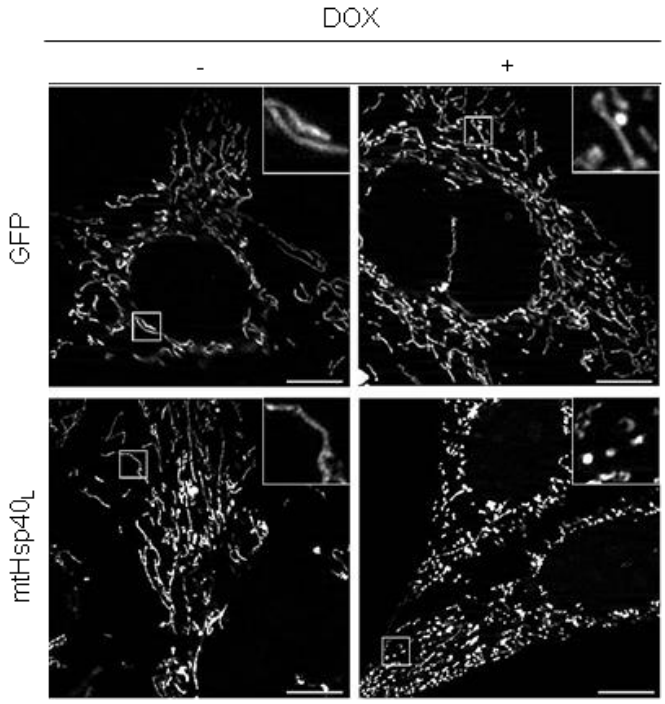
DOX
- +
GFP
mtHsp40L

16C

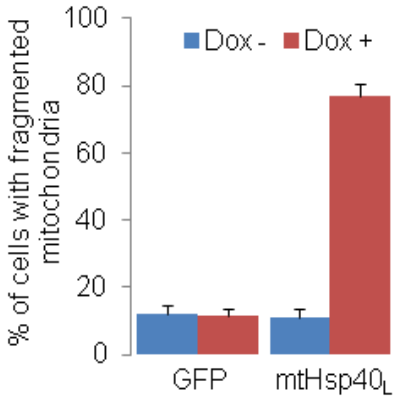
% of cells with fragmented mitochondria
100
80
60
40
20
0
Dox -
Dox +
GFP
mtHsp40L

Figure 17. Determination of Level of MtHsp40 Causing Mitochondrial Fragmentation by DOX-Inducing MtHsp40

(A) HEK293-MitoRFP-TetR-mtHsp40$_L$ cells were treated with a gradient (0, 0.5, 1.0, 2.0, 5.0 & 10.0 ng/ml) of DOX as indicated for 24 hours, and were analyzed by Western blots using the indicated primary antibodies. The relative band intensity of mtHsp40$_L$ to control was quantified using the Image J software. Each sample was normalized with the β-Tubulin band intensity. (B) Cells were fixed using 4 % PFA, and stained by anti-mtHsp40 antibody / AF488. MitoRFP was visualized by fluorescence microscopy (568 nm). Cells showing homogenous fragmented mitochondria as shown in Fig 16B were quantified out of more than 100 cells. Bars mean + S.E.M, n = 3.

17A

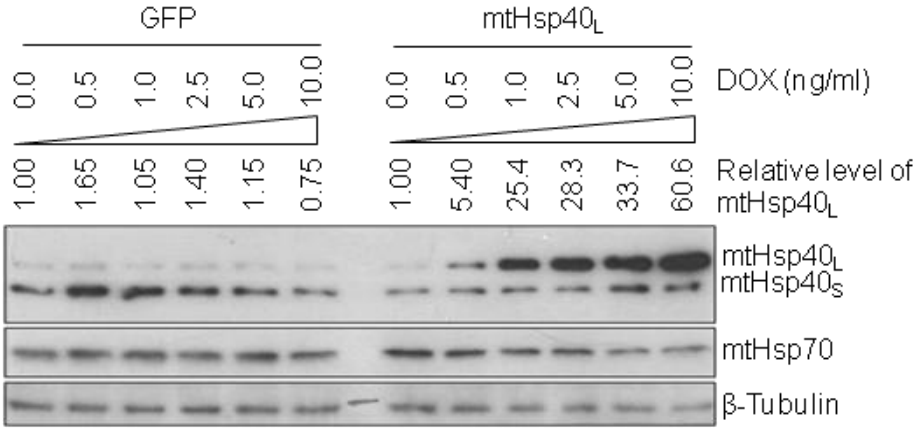
GFP
mtHsp40L
0.0
0.5
1.0
2.5
5.0
10.0
DOX (ng/ml)
1.00
1.65
1.05
1.40
1.15
0.75
1.00
5.40
25.4
28.3
33.7
60.6
Relative level of mtHsp40L
mtHsp40L
mtHsp40S
mtHsp70
β-Tubulin

17B

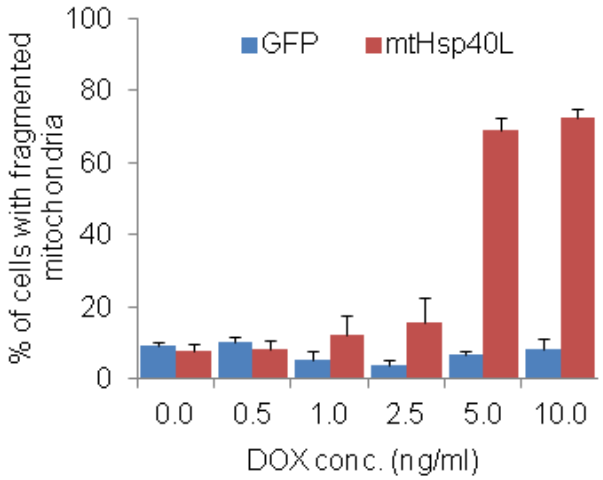
100
80
60
40
20
0
GFP
mtHsp40L
% of cells with fragmented mitochondria
0.0
0.5
1.0
2.5
5.0
10.0
DOX conc. (ng/ml)

treated with 10 ng/ml DOX for 24 hours and mitochondrial fragmentation was confirmed, DOX was then washed away. Within two days following DOX removal, mtHsp40$_L$ level returned to the control level (Fig 18A) and fragmented mitochondria were restored to the tubular network three days following DOX-removal (Fig 18B & 18C).

It is still possible that cells showing tubular network may become dominant against cells with fragmented mitochondria following DOX-treatment, which may lead to the dominance of tubular mitochondria. Thus, five days following DOX-removal, we treated those cells with DOX again, and analyzed mtHsp40$_L$ protein levels and mitochondrial morphology. The level of mtHsp40$_L$ expression was still highly induced (Fig 18A), and mitochondrial fragmentation trend was very similar to the initial DOX-treatment (Fig 18B & 18C). In other words, cycles of treatment and removal of DOX resulted in cyclical increases and decreases in mtHsp40 protein levels and concomitant cycles of mitochondrial fragmentation. These data clearly demonstrated that cyclical changes in the levels of mtHsp40$_L$ triggered reversible mitochondrial fragmentation, indicating that mitochondrial morphology change is reversible with mtHsp40 levels.

3.7 Effects of MtHsp40 Loss on Mitochondrial Morphology

Considering mtHsp40 is a mitochondrial cochaperone of mtHsp70, we presumed that mtHsp40 may affect numerous events and pathways in mitochondria, which may include mitochondrial fragmentation. Thus, we constructed a plasmid, pRS-shmtHsp40 expressing shRNAs against mtHsp40, and introduced it into HeLa-mitoRFP cells (Table 13). Three days following transfection, mtHsp40 protein level decreased at a significant level (Fig 19A), but the mitochondrial morphology did not change, which was not consistent with the results of mtHsp40 knockout MEFs (Fig 19B). As Lo *et al* showed fragmented mitochondria from mtHsp40 knockout in MEFs[163], we attempted to reproduce their results by deleting mtHsp40 using siRNAs purchased from Qiagen (Table 13). We observed mitochondrial morphology at three or six days following transfection of siRNAs, and six days following transfection, we could see mitochondrial fragmentation (Fig 20B & 20C), and mtHsp40 protein was hardly detected (Fig 20A & 20B). However, we could not see any significant mitochondrial fragmentation at three days post-transfection, suggesting that mtHsp40 itself as a cochaperone may not have dominant effects on mitochondrial morphology.

Figure 18. Determination of Reversibility of Mitochondrial Fragmentation Caused by DOX-Inducing MtHsp40

(A) HEK293-MitoRFP-TetR-mtHsp40$_L$ cells were treated with DOX (10 ng/ml) for 24 hours. Following DOX-treatment, cells were washed with PBS and grown in the absence of DOX for further five days. Cells were subjected to one more cycle of treating/washing with DOX. After 2 cycles of treating/washing with DOX, cells were lastly treated with DOX (10 ng/ml) for 24 hours. Cells at each time point were analyzed by Western blots using the indicated primary antibodies. (B) Cells described above were fixed using 4 % PFA, and stained by mtHsp40 / AF488 goat anti-mouse IgG. Cells showing fragmented mitochondria were quantified by counting more than 100 cells. Cells with mixed and unclear mitochondria were excluded. Arrows indicate DOX-treatment and bars + S.E.M., n = 2. (C) Representative mitochondria at each time point as indicated were shown. White bar means 10 μl.

18A

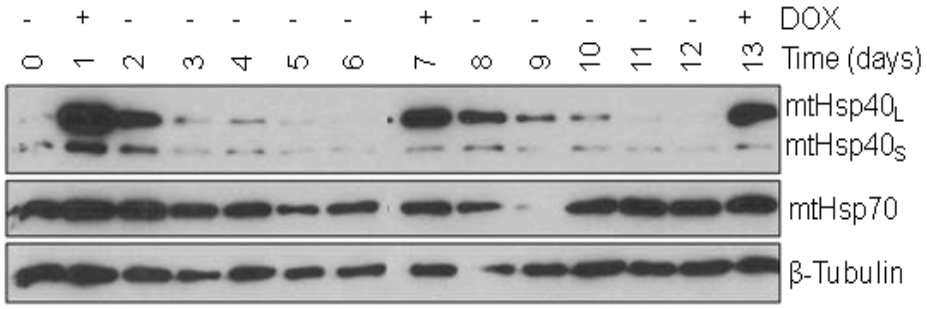
- + - - - - - + - - - - - + DOX
0 1 2 3 4 5 6 7 8 9 10 11 12 13 Time (days)
mtHsp40L
mtHsp40S
mtHsp70
β-Tubulin

18B

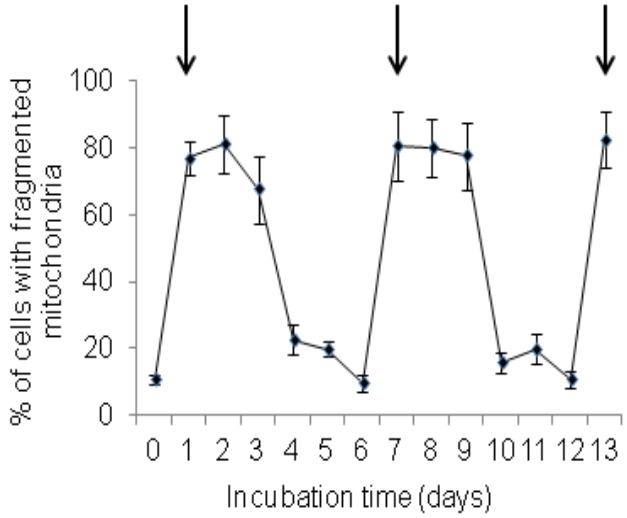
% of cells with fragmented mitochondria
100
80
60
40
20
0
0 1 2 3 4 5 6 7 8 9 10 11 12 13
Incubation time (days)

18C

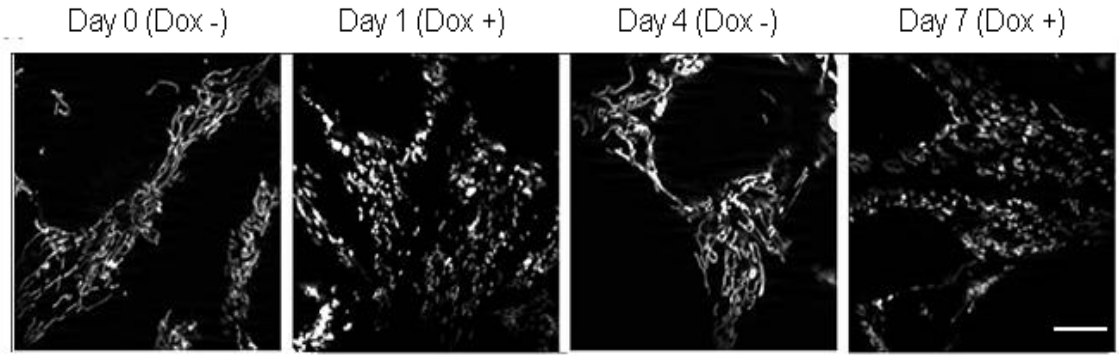
Day 0 (Dox -)
Day 1 (Dox +)
Day 4 (Dox -)
Day 7 (Dox +)

Figure 19. Effects of MtHsp40 Deletion Using Mammalian Expression Vector Based-shRNA on Mitochondrial Morphology

(A) HeLa-mitoRFP cells were transfected with pRS-GFP-shScramble or –shmtHsp40 constructs expressing short hairpin sequences against Scramble or mtHsp40 and GFP as a transfection marker using Lipofectamine2000 for 3 days, and were analyzed by Western blots using the indicated primary antibodies. (B) Cells transfected above were fixed using 4 % PFA and analyzed by fluorescence microscopy. White stars indicate GFP-positive transfected cells. MitoRFP was visualized at 568 nm and GFP at 488 nm. White bars, 5 μm

19A

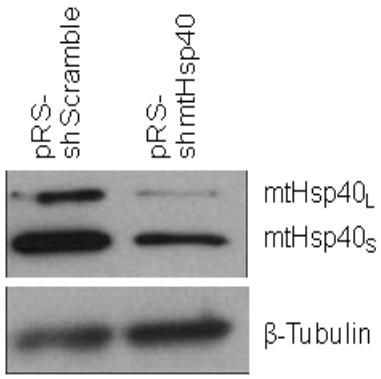

19B

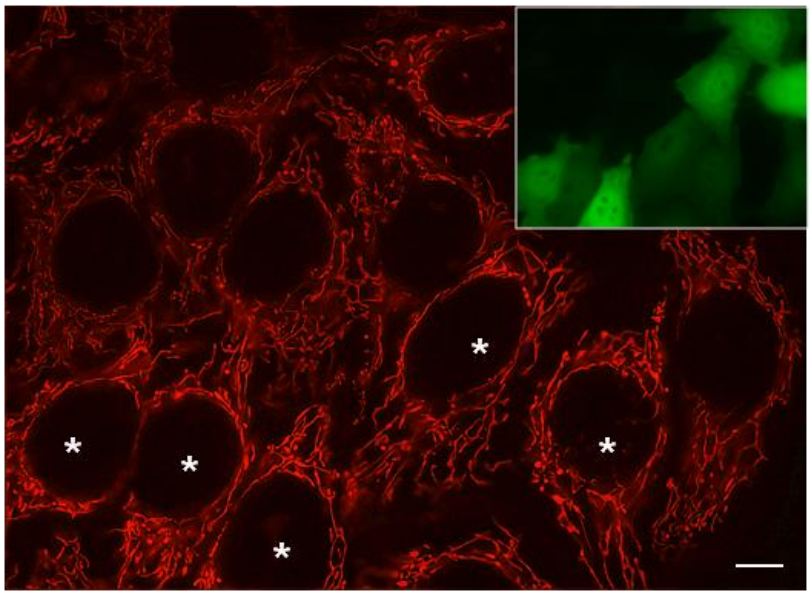

Figure 20. Effects of Deletion of MtHsp40 Using siRNAs on Mitochondrial Morphology

(A) HeLa-mitoRFP cells were transfected with 100 μM of siRNAs as indicated using Lipofectamine RNAiMAX for 6 days, and were analyzed by Western blots using the indicated primary antibodies. (B) Cells were fixed using 4 % PFA and stained by mtHsp40 / AF488 goat anti-mouse IgG. Mitochondrial morphology was analyzed by fluorescence microscopy (red; 568 nm). White bar means 10 μm. (C) Cells with fragmented mitochondria were quantified by counting more than 100 cells. Bars mean + S.E.M, n = 3.

20A

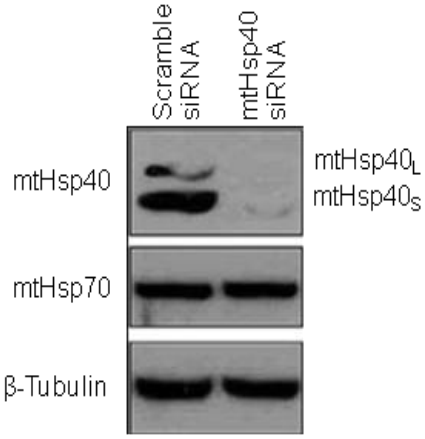
Scramble siRNA
mtHsp40 siRNA
mtHsp40
mtHsp70
β-Tubulin
mtHsp40L
mtHsp40S

20B

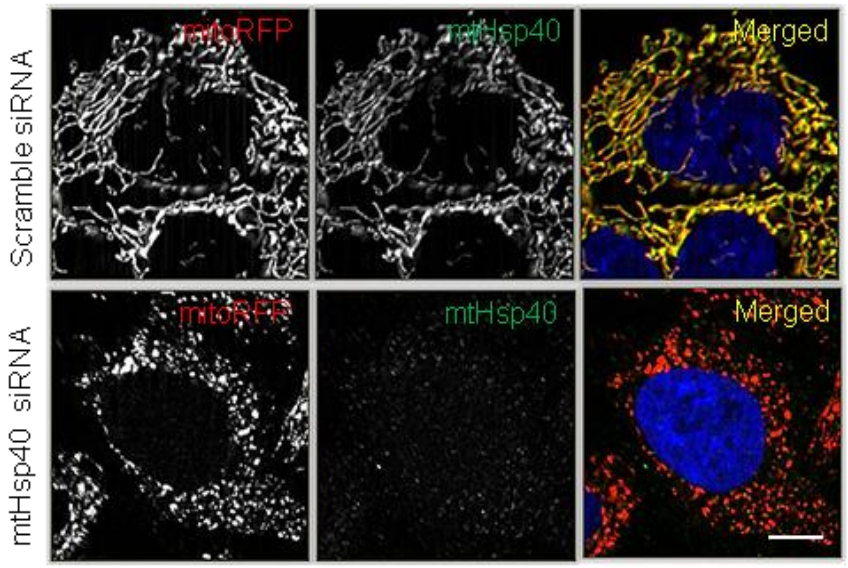
Scramble siRNA
mtHsp40 siRNA
mtoRFP
mtHsp40
Merged

20C

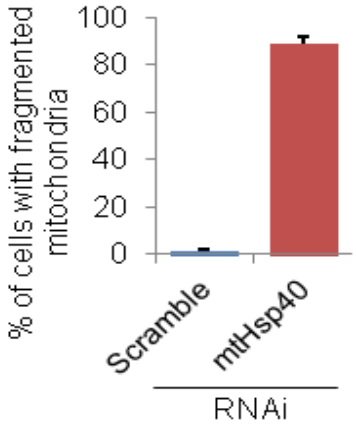
% of cells with fragmented mitochondria
100
80
60
40
20
0
Scramble
mtHsp40
RNAi

3.8 Identification of MtHsp40 Domains Required for Mitochondrial Morphology Change

Our data in this study clearly demonstrated that ectopic expression of mtHsp40 induced mitochondrial fragmentation but mtHsp40 loss did not, which led us to propose that mtHsp40 may associate some other factors or pathways to induce mitochondrial fragmentation. To address this, we thus attempted to determine the important domains of mtHsp40 required for mitochondrial fragmentation. We first generated a number of mtHsp40 domain deletion mutants (Fig 6B & Fig 21A) with different systems as follows: (1) intact mtHsp40$_L$-based mammalian expression vector system; (2) C-terminal Flag-tagged mtHsp40$_L$-based mammalian expression vector system; (3) intact mtHsp40$_S$-based adenoviral expression system. Overall, the results were very similar among three systems, and therefore, representative data were shown here.

Construction of all domain deletion mutants were as follows: (1) full-length of long isoform, mtHsp40$_L$ (1-480); (2) long isoform lacking MTS, mtHsp40$_{L\Delta MTS}$ (89-480); (3) long isoform with a mutation in the HPD motif of DnaJ domain, mtHsp40$_L$ (H121Q); (4) full-length of short isoform, mtHsp40$_S$ (1-453); (5) Cys-rich domain and DD-lacking, mtHsp40$_{\Delta CT}$ (1-292); (6) CTD II and DD-lacking, mtHsp40 (1-235); (7) MTS and DnaJ domain, mtHsp40 (1-168) (Fig 21A). All the mutants were highly expressed compared with control, and did not affect endogenous mtHsp40$_L$ or mtHsp40$_S$. Whereas MTS-containing wildtype and mutants showed the accumulation of unprocessed forms, and MTS-lacking mutants did not. MtHsp40$_L$ (H121Q) level was slightly less compared with other mutants, and mtHsp40$_{\Delta CT}$ (1-292) mutant produced a couple of unidentified bands. Most of mutant protein levels, except MtHsp40$_L$ (H121Q), were similarly overexpressed (Fig 21B). Constructs containing MTS well colocalized with MitoRFP, indicating that they were well targeted to mitochondria. Conversely, mtHsp40$_{L\Delta MTS}$ mutants formed puncta in the cytosol. In addition, the green fluorescence intensity was relatively less compared with other mutants, suggesting that mtHsp40$_{L\Delta MTS}$ protein may be retained in the cytosol and aggregated following degradation. Surprisingly, mtHsp40$_L$ (1-480), mtHsp40$_S$ (1-453), mtHsp40$_{\Delta CT}$ (1-292), mtHsp40 (1-235) and mtHsp40 (1-168) mutants that contain the MTS and DnaJ domain localized well to mitochondria, and resulted in mitochondrial fragmentation (Fig 21C). MtHsp40 (1-168) mutant contains only the MTS and DnaJ domain, thus, following MTS-cleavage by MPP in the matrix, only DnaJ domain (80 amino acids) is supposed to accumulate in the matrix. Our results indicate that only the MTS and DnaJ domain of mtHsp40 are required for mitochondrial fragmentation.

The mtHsp40$_L$ H121Q mutant also well localized at mitochondria. However, it did not cause mitochondrial fragmentation as significantly as the other mutants (Fig 21D). Since its protein level was relatively low (Fig 21B), we repeated separately the ectopic expression of this mutant, and confirmed the similar protein level with mtHsp40$_L$. However, we could not still detect mitochondrial fragmentation (data not shown). In addition, this mutant showed somewhat a different staining pattern at mitochondria. They were distributed throughout the mitochondria, but formed puncta (Fig 21C). These data suggest that a mutation inactivating DnaJ domain of mtHsp40 may affect its interaction with mtHsp70, resulted in attenuated mitochondrial fragmentation.

When mtHsp40 was ectopically expressed in multiple cell lines, the unprocessed form of mtHsp40 was detected, led us hypothesize that ectopically expressed cytosolic DnaJ proteins may affect the mitochondrial morphology. To this hypothesis, we expected that mtHsp40$_{L\Delta MTS}$ mutant overepxression may provide us some answers, but highly expressed mtHsp40$_{L\Delta MTS}$ mutant were apparently aggregated in the cytosol. Thus, we instead tested the effects of ectopic expression of cytosolic DnaJA proteins on mitochondrial morphology. We transfected HeLa-mitoRFP cells with four DnaJA family members fused with GFP, DnaJA1-GFP, DnaJA2-GFP, DnaJA3-GFP (mtHsp40$_L$-GFP), and DnaJA4-GFP for 24 hours. Proteins were analyzed by Western blot and mitochondria were visualized with the fluorescence microscopy. Three cytosolic DnaJA proteins N-terminal fused with GFP were highly expressed compared with DnaJA3 (mtHsp40) (Fig 22A). While all cytosolic DnaJAs were well distributed throughout the cytosol but not aggregated like mtHsp40$_{L\Delta MTS}$, DnaJA3 was located in mitochondria. Lower expressed DnaJA3 induced mitochondrial fragmentation in most GFP-positive cells, whereas cytosolic DnaJAs did not affect mitochondrial morphology (Fig 22B).

Next, we also tested a small mitochondrial J protein, DnaJC20, a homolog of yeast Jac1. DnaJC20 is known to play a certain role in the iron-cluster biosynthesis in the mitochondria[198,199]. However, DnaJC20 interaction with mtHsp70 has not been reported. As DnaJC20 is a mitochondrial J protein, it was well expressed in mitochondria (Fig 22C), but its overexpression did not change mitochondrial morphology (Fig 22D). These data suggest that mitochondrial-located DnaJ domain of mtHsp40 sufficiently induces mitochondrial fragmentation, and its chaperonic partner may be important in this event.

Figure 21. Determination of Domains of MtHsp40 Required for Mitochondrial Fragmentation

(A) Schematic diagram of pRK5-mtHsp40 wildtype or domain deletion mutants. (B) HeLa-mitoRFP cells were transfected with wildtype or different mutant pRK5-mtHsp40 constructs using Lipofectamine2000 for 24 hours, and immunoblotting was performed using the indicated primary antibodies. Up means unprocessed forms and black stars indicate unidentified bands. (C) Cells described above were fixed using 4 % PFA and stained by mtHsp40 / AF488 goat anti-mouse IgG. MitoRFP was visualized as red (568 nm) and mtHsp40 as green (488 nm) by fluorescence microscopy. (D) Cells showing fragmented mitochondria were quantified by counting more than 100 cells. **P < 0.01 and ***P < 0.001 denote significant difference from control, ## 0.01 < P < 0.05 denotes difference from control. Bars mean + S.E.M., n = 3.

21A

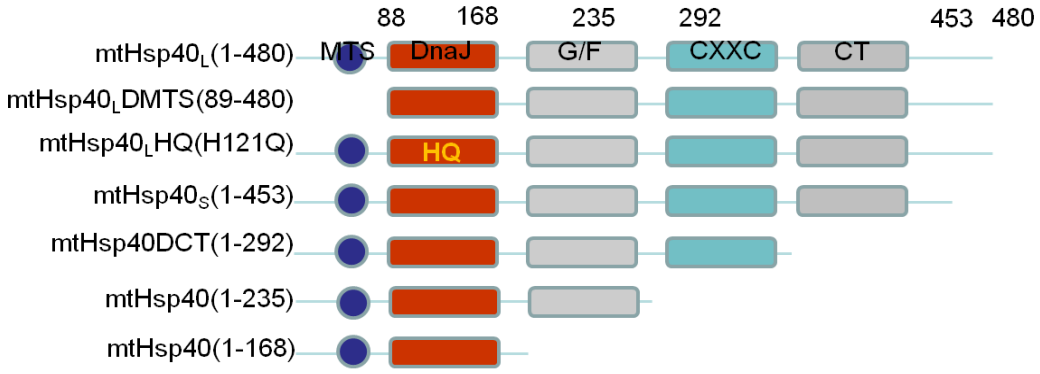
88
168
235
292
453
480
mtHsp40L(1-480)
MTS
DnaJ
G/F
CXXC
CT
mtHsp40LDMTS(89-480)
mtHsp40LHQ(H121Q)
HQ
mtHsp40S(1-453)
mtHsp40DCT(1-292)
mtHsp40(1-235)
mtHsp40(1-168)

21B

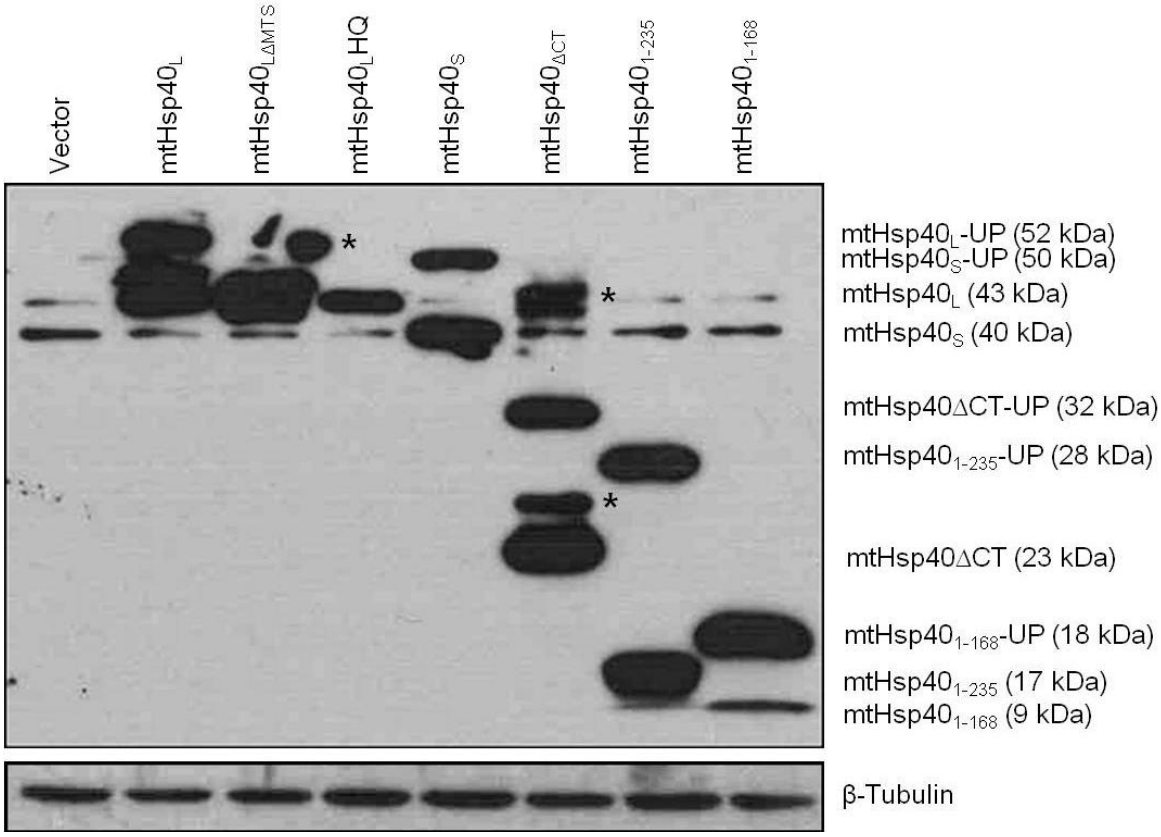
Vector
mtHsp40L
mtHsp40LΔMTS
mtHsp40LHQ
mtHsp40S
mtHsp40ΔCT
mtHsp401-235
mtHsp401-168
*
*
*
mtHsp40L-UP (52 kDa)
mtHsp40S-UP (50 kDa)
mtHsp40L (43 kDa)
mtHsp40S (40 kDa)
mtHsp40ΔCT-UP (32 kDa)
mtHsp401-235-UP (28 kDa)
mtHsp40ΔCT (23 kDa)
mtHsp401-168-UP (18 kDa)
mtHsp401-235 (17 kDa)
mtHsp401-168 (9 kDa)
β-Tubulin

21C

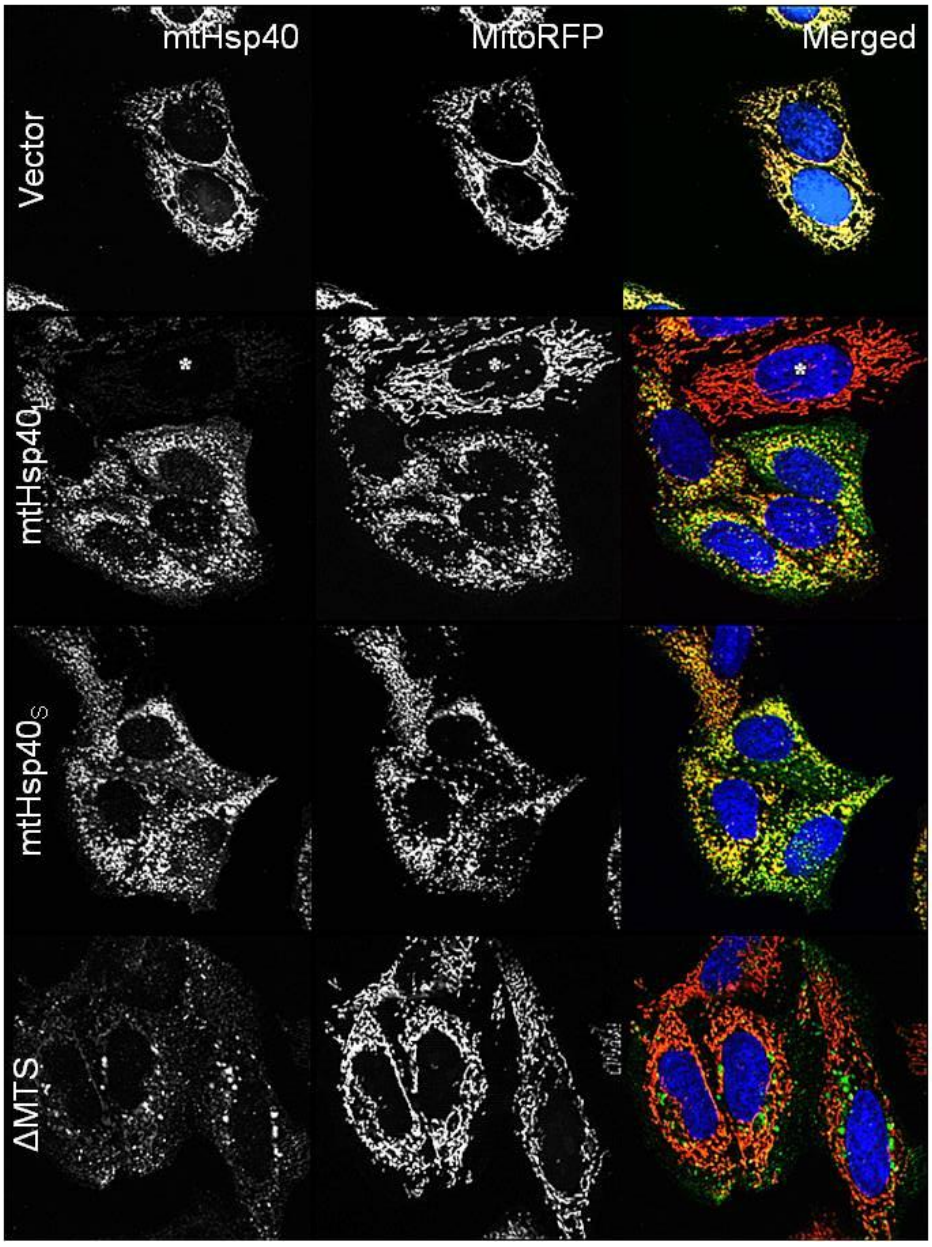

21C (Continued)

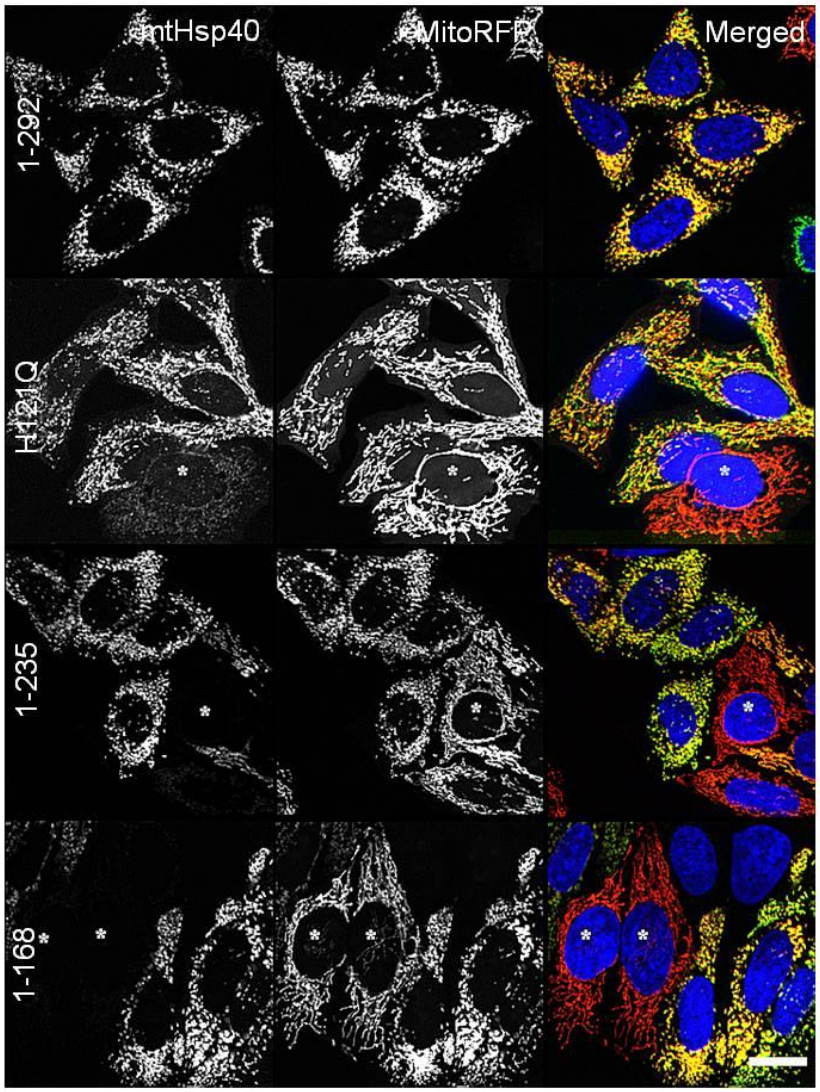

21D

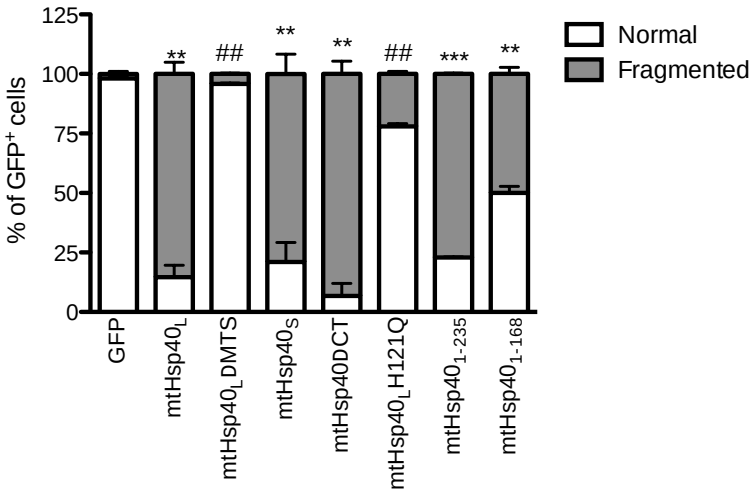

Figure 22. Effects of Ectopic Expression Other DnaJ Proteins on Mitochondrial Fragmentation

(A) Wildtype GFP-DnaJA1, GFP-DnaJA2, DnaJA3-GFP and GFP-DnaJA4 were introduced into HeLa-mitoRFP cells using Lipofectamine2000 reagent for 24 hours, and cells were analyzed by Western blots using the indicated primary antibodies. (B) Cells were fixed using 4 % PFA, and MitoRFP was visualized by florescence microscopy (568 nm). White bar means 10 μm. (C) HeLa-mitoRFP cells were transfected by wildtype DnaJC20-Myc construct encoding C-terminal Myc-tagged DnaJC20, a homolog of Yeast Jac1 using Lipofectamine2000 reagent for 24 hours, and analyzed by Western blots using the indicated primary antibodies. (D) Cells were fixed using 4 % PFA, and were stained by Myc / AF488 goat anti-mouse IgG. MitoRFP was visualized as red (568 nm) and Myc as green (488 nm) by fluorescence microscopy. White bar indicates 10 μm, n = 1.

22A

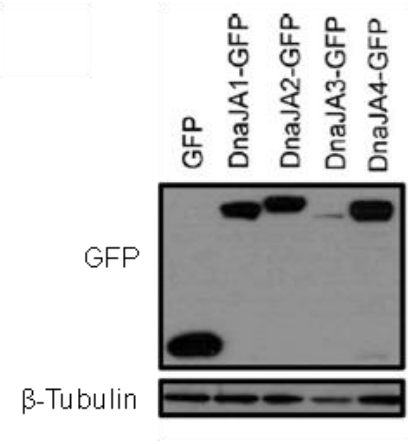

22C

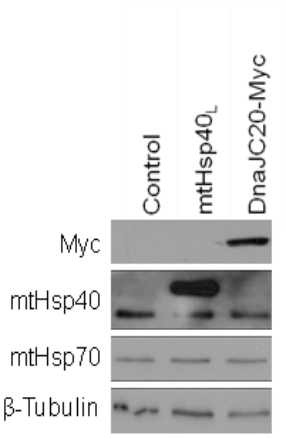

22B

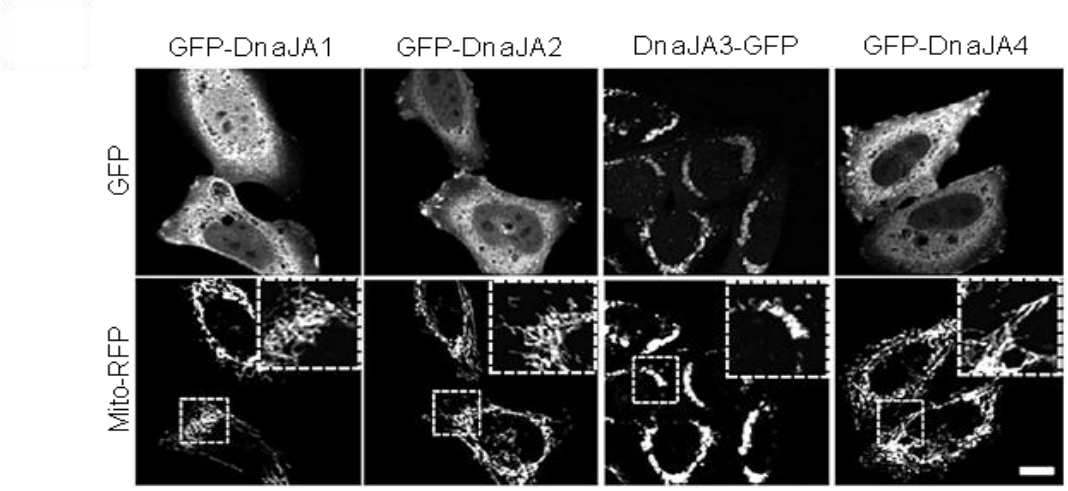

22D

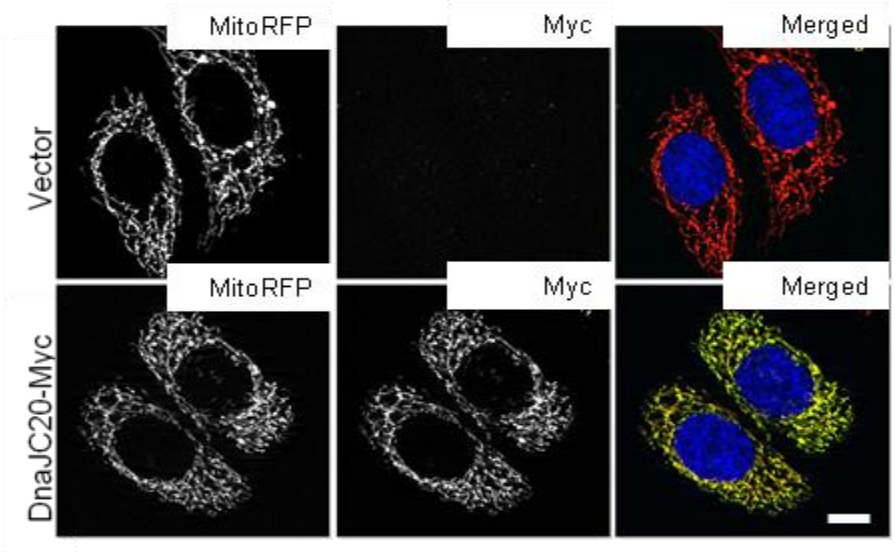

Taken together, our data led us propose that ectopically expressed mitochondrial DnaJ domain of mtHsp40 is sufficient to trigger mitochondrial fragmentation by inhibiting the mtHsp70 activity, respectively.

3.9 Effects of MtHsp70 Knockdown on Mitochondrial Morphology and Apoptosis

In addition to our findings showing the possibility of the involvement of mtHsp70 in this mitochondrial fragmentation, it has also been known that mtHsp70 dysfunction causes mitochondrial fragmentation[139]. We thus suppressed mtHsp70 using siRNAs for two days to investigate the effects of mtHsp70 on mitochondrial morphology (Table 13). As mtHsp70 have dual activities, mitochondrial protein import and folding, mtHsp40 level may be affected by mtHsp70 knockdown; however, mtHsp40 was not affected, although mtHsp70 protein level was decreased by mtHsp70 RNAi for two days (Fig 23A). As expected, depletion of mtHsp70 caused a dramatic change in mitochondrial morphology in most cells, which was consistent with the previous reports (Fig 23B & 23C)[215], suggesting that depletion of mtHsp70 decreases folding activity of mtHsp70 leading to mitochondrial fragmentation. Following cisplatin-treatment, whereas 40 % of cells released cytochrome *c* into the cytosol, cells with fragmented mitochondria in the presence of mtHsp70 RNAi showed cytochrome *c* release in 95 % of cells. Together, similarly with ectopic expression of mtHsp40, depletion of mtHsp70 caused mitochondrial fragmentation independently of apoptosis, which facilitates apoptosis.

3.10 Effets of Ectopic Expression of MtHsp70 on Mitochondrial Morphology

Based on preliminary findings, we proposed that ectopically expressed mtHsp40 not bound to clients may inhibit the chaperonic activity of ATP-bound mtHsp70 by masking ATPase domain of mtHsp70, suggesting that ATP-bound mtHsp70 may interact with ectopically expressed mtHsp40. To test this, we transfected HeLa-mitoRFP cells with a range of C-terminal Flag-tagged mtHsp70 construct. One day following transfection, we analyzed mtHsp70-Flag protein levels and mitochondrial morphology. MtHsp70-Flag proteins accumulated at a detectable level with 50 ng of plasmid, and was highly expressed with $\geq$ 0.1 μg of plasmid. Unprocessed form of mtHsp70-Flag was detectable with $\geq$ 0.5 μg of plasmid, but mtHsp40 level was not affected (Fig 24A). Unexpectedly, mitochondrial morphology was not affected by any levels of mtHsp70 (Fig 24B). These data provided us some speculations: (1) ectopically

Figure 23. Effects of Loss of MtHsp70 on Mitochondrial Fragmentation

(A) HeLa-mitoRFP cells were transfected with 10 μM of Scramble or mtHsp70 siRNAs as indicated using Lipofectamine RNAiMAX for two days, and were analyzed by Western blots using the indicated primary antibodies. (B) Cells were fixed using 4 % PFA, and stained mtHsp70 / AF488 goat anti-mtHsp70 antibodies. MitoRFP was visualized by fluorescence microscopy (red; 568 nm). Regions in white boxes were zoomed in. White bars mean 10 μm. (C) Cells showing fragmented mitochondria were quantified by counting more than 100 cells. Bars mean + S.E.M., n = 5. Cells described in (A) were treated with either DMSO or 2 μM Cisplatin in a combination with 20 μM Z-VAD-FMK for 12 hours, and immunostained using anti-cytochrome *c* antibodies (D). White stars indicate infected cells, white arrows, apoptotic cells and white bars, 10 μm. (E) Among more than 100 cells, cells showing complete release of cytochorome *c* were counted. Bars mean + S.E.M, n = 2.

23A

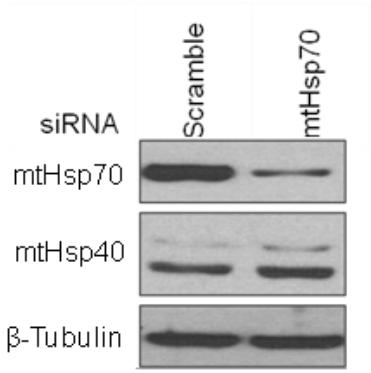
siRNA
Scramble
mtHsp70
mtHsp70
mtHsp40
β-Tubulin

23B

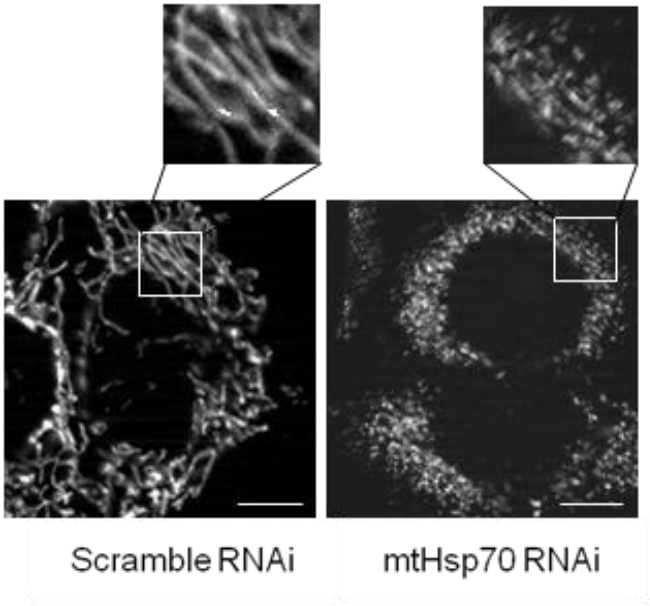
Scramble RNAi
mtHsp70 RNAi

23C

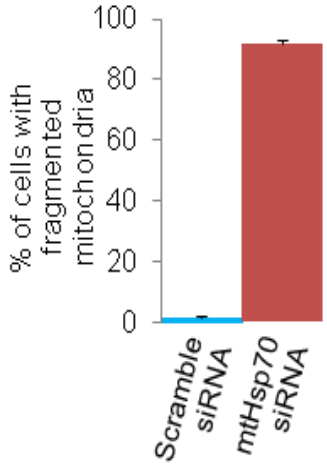
% of cells with fragmented mitochondria
100
80
60
40
20
0
Scramble siRNA
mtHsp70 siRNA

23D

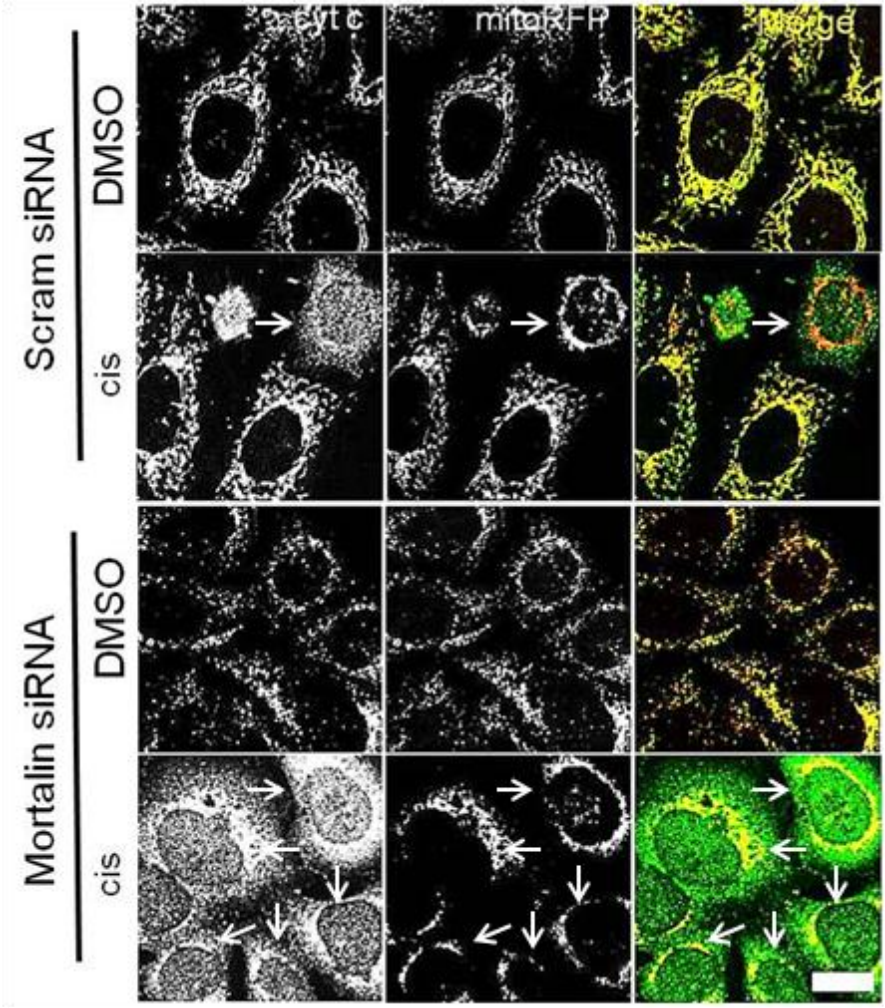
cyt c
mitoRFP
Merge
Scram siRNA
DMSO
cis
Mortalin siRNA
DMSO
cis

23E

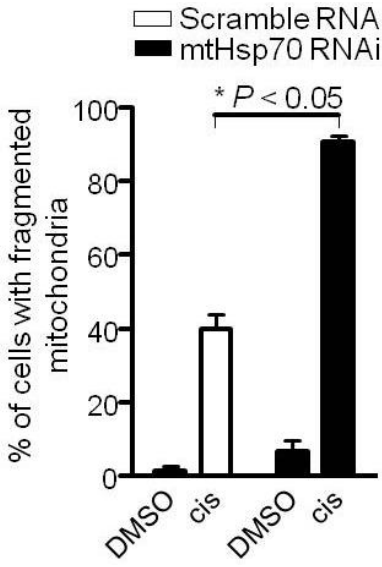
Scramble RNAi
mtHsp70 RNAi
* P < 0.05
% of cells with fragmented mitochondria
100
80
60
40
20
0
DMSO
cis
DMSO
cis

Figure 24. Effects of Ectopic Expression of Different Amount of mtHsp70 on Mitochondrial Morphology

(A) HeLa-mitoRFP cells were transfected with a range (0, 50 ng, 100 ng, 200 ng, 500 ng & 1000 ng) of pRK5-mtHsp70-Flag expressing C-terminal Flag-tagged mtHsp70 using Lipofectamine2000 for 24 hours, and were analyzed by Western blots using the indicated primary antibodies. Up = unprocessed form. (B) Cells showing fragmented mitochondria were quantified by counting more than 100 Flag-positive cells, n = 1.

24A

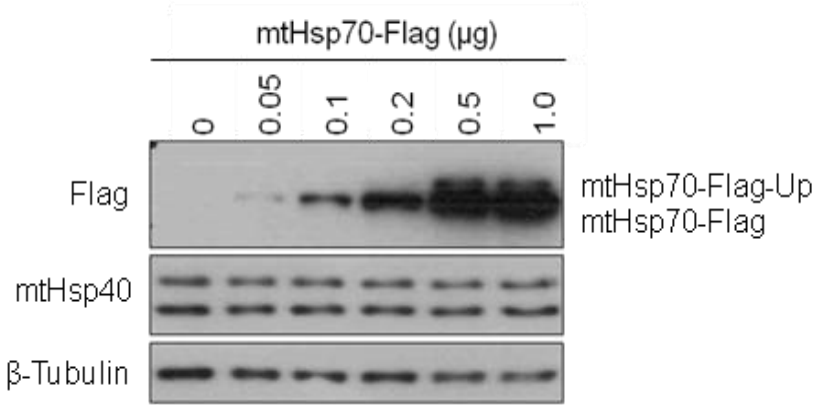
mtHsp70-Flag (μg)
0
0.05
0.1
0.2
0.5
1.0
Flag
mtHsp70-Flag-Up
mtHsp70-Flag
mtHsp40
β-Tubulin

24B

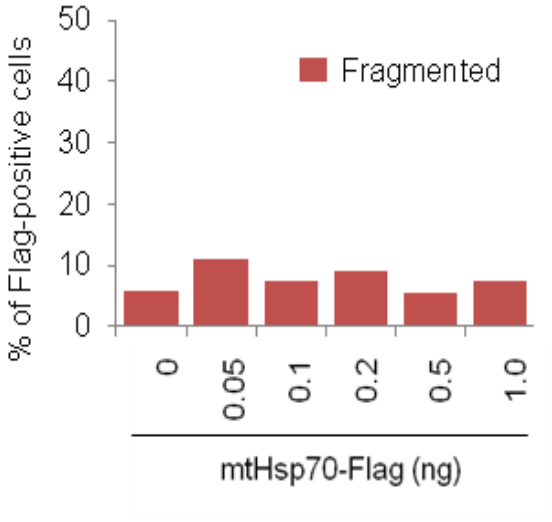
% of Flag-positive cells
50
40
30
20
10
0
Fragmented
0
0.05
0.1
0.2
0.5
1.0
mtHsp70-Flag (ng)

expressed mtHsp70 does not bind mtHsp40 or (2) its interaction with mtHsp40 has no significant impact on mitochondrial morphology.

3.11 Effects of MtHsp70 Domain Deletion Mutants on Mitochondrial Morphology

In order to test the effects of mtHsp70 domains on mitochondrial morphology, we first generated C-terminal Flag-tagged mtHsp70 domain deletion mutants as described in Fig 25A: (1) full length, mtHsp70 (1-679); (2) MTS-lacking mutant, mtHsp70 (58-679); (3) ATPase-lacking mutant, mtHsp70$_{\Delta ATPase}$; (4) SBD & LID-lacking mutant, mtHsp40 (1-434). Unfortunately, we could not generate a mutant lacking the SBD or LID domain alone. All constructs were highly expressed and MTS-containing mutants showed unprocessed forms, indicating that those were expressed over the capability of mitochondrial protein import, but did not affect mtHsp40 levels (Fig 25B). Full-length mtHsp70 and ATPase domain-lacking mutant localized at the mitochondria, but did not affect mitochondrial morphology. An MTS-lacking mutant was retained in and spread throughout the cytosol, and mitochondria were tubular. Interestingly, the SBD and LID-lacking mutant showed mitochondrial fragmentation in ~ 40 % of Flag-positive cells (Fig 25C). Compared with ectopic expression of mtHsp40, the tendency of mitochondrial fragmentation was relatively less with mtHsp70 (1-434) overexpression (Fig 25D). Together, we could propose that ectopically expressed mtHsp70 may bind substrate-bound mtHsp40 more preferentially than mtHsp40 alone. In other words, ATP-bound mtHsp70 has higher affinity to substrate-bound mtHsp40 than mtHsp40 alone. Thus, in case of overexpression of full-length mtHsp70, excess ATP-bound mtHsp70 interacts with substrate-bound mtHsp40 complex, and then undergoes a normal chaperonic cycle. Overexpressed ATP-bound mHsp70 (1-435) mutant can also bind the substrate-mtHsp40 complex and form an mtHsp40-substrate-mtHsp70 complex, but it does not proceed further for protein folding due to the lack of the SBD and LID domain, which may lead to mitochondrial fragmentation.

3.12 Impinge of Combined Expression of MtHsp40 and MtHsp70 on Mitochondrial Morphology

To test whether mitochondrial fragmentation caused by ectopic expression of mtHsp40 is directly linked to mtHsp70 level, we transfected HeLa cells with a range of mtHsp40$_L$-Flag in the absence or presence of mtHsp70 (expressing RFP as a transfection marker). One-day following

Figure 25. Determination of mtHsp70 Domains affecting Mitochondrial Morphology.

(A) Schematic diagram of pRK5-mtHsp70-Flag wildtype or domain deletion mutants. (B) HeLa-mitoRFP cells were transfected with wildtype or different mutant pRK5-mtHsp70-Flag constructs by Lipofectamine2000 reagent for 24 hours, and immunoblotting was performed using the indicated primary antibodies. Arrows mean unprocessed forms. (C) Cells described above were fixed using 4 % PFA, and stained by Flag / AF488 goat anti-mouse IgG. MitoRFP was visualized as red (568 nm) and Flag as green (488 nm) by fluorescence microscopy. (D) Cells showing fragmented mitochondria were quantified by counting more than 100 cells. *$P < 0.05$ denotes significant difference from control, and #$0.05 < P$ denotes no significant difference from control. Bars means + S.E.M., $n = 3$.

25A

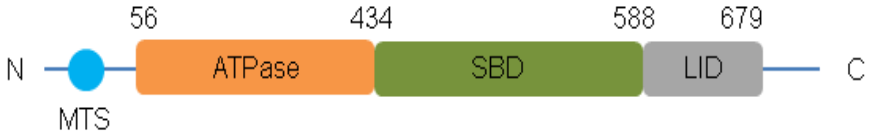

25B

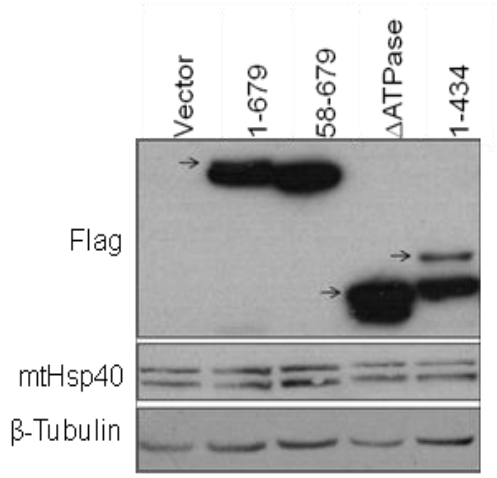

25D

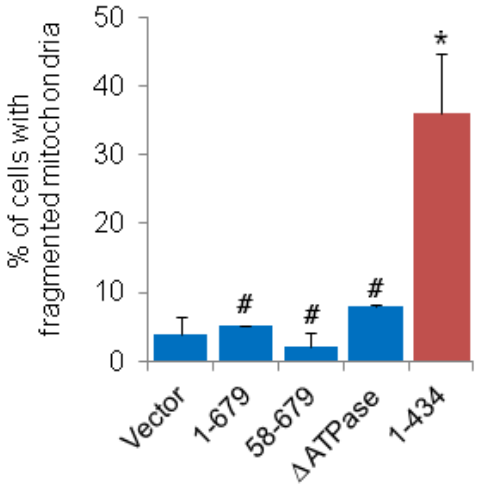

25D

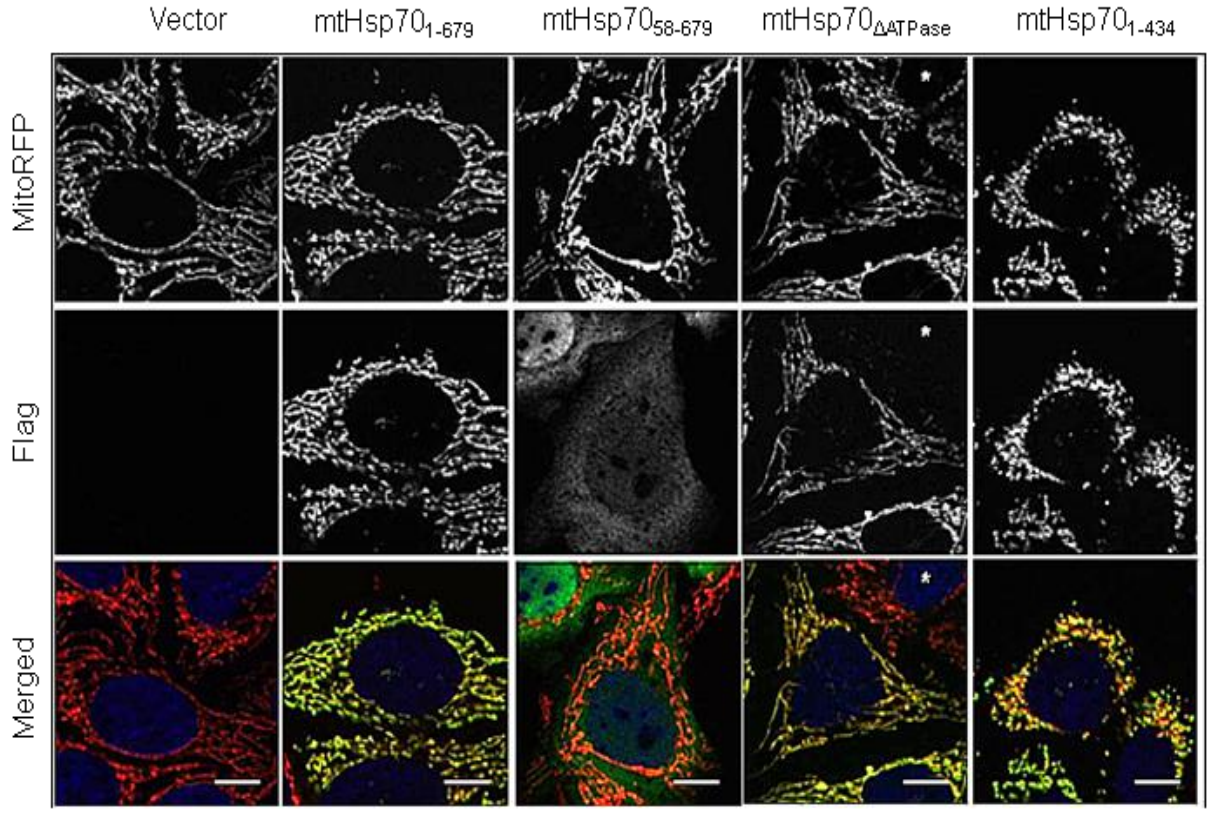

transfection, we focused on the mitochondria of RFP-positive cells. Significant overexpression was detectable at ≥ 15 ng of mtHsp40$_L$-Flag both in the absence and presence of mtHsp70 overexpression. Unprocessed form of mtHsp40$_L$-Flag was also detected, but bands were not shown in this figure (Fig 26A). Whereas detectable levels of mtHsp40$_L$-Flag resulted in mitochondrial fragmentation in more than 80 % of cells in the absence of mtHsp70 overexpression, the presence of mtHsp70 overexpression reduced cells showing mitochondrial fragmentation up to 40 % (Fig 26B), suggesting that levels of mtHsp40 and mtHsp70 together determine the mitochondrial morphology.

3.13 Effects of MtHsp40 Overexpression on MtHsp40:MtHsp70 Interaction

To determine whether physical interaction between endogenous mtHsp40 and mtHsp70 is affected by ectopic expression of mtHsp40, we performed co-immunoprecipitation (Co-IP) using anti-Flag or -mtHsp70 antibodies. We first tested two different conditions including low and high stringency. We first overexpressed the long-isoform of mtHsp40 by treating HEK293-TetR-mitoRFP-mtHsp40$_L$ with DOX for 24 hours, and then Co-IP was performed. Under a high stringent condition, mtHsp40 was not co-immunoprecipitated using anti-mtHsp70 antibodies (Fig 27A). Thus, we reduced the detergent amount to 0.1 % NP-40 and washed Protein-A Sepharose Beads with PBS instead of lysis buffer containing 1 % NP-40 according to Susan Lees-Miller's protocol. MtHsp40 was successfully pulled down by anti-mtHsp70 antibody, but was not detectable in the IgG control. Under the ectopic expression of mtHsp40$_L$, mtHsp40$_L$ was well co-immunoprecipitated with anti-mtHsp70 antibody. Interestingly, it was apparent that ectopic expression of mtHsp40$_L$ abolished the pull-down of endogenous mtHsp40$_S$ (Fig 27B), suggesting that ectopically expressed mtHsp40$_L$ may block endogenous mtHsp40$_S$ interaction with mtHsp70. This experiment was performed once, and thus needs to be repeated.

3.14 Effects of Ectopic Expression of MtHsp40 on Mitochondrial-Targeted Luciferase Refolding

In addition to mtHsp40-mtHsp70 interaction experiments, we considered the direct evidence showing that mtHsp70 activity in protein folding or refolding might be inhibited in fragmented mitochondria caused by mtHsp40 overexpression. Most *in vitro* studies on the chaperonic activity of mtHsp40 and mtHsp70 involve the use of enzymes such as luciferase or

Figure 26. Effects of a Combination of MtHsp40 and MtHsp70 on Mitochondrial Morphology

(A) HeLa cells were transfected with a range of pRK5-mtHsp40$_L$-Flag constructs in the absence or presence of pRK5-RFP-mtHsp70 expressing wildtype mtHsp70 and RFP as a transfection marker using Lipofectamine2000 for 24 hours, and were analyzed by Western blots using the indicated primary antibodies. (B) Cells were fixed using 4 % PFA, and stained by Flag/AF488 goat anti-mouse IgG. Mitochondria were visualized fluorescence microscopy (Flag; 488 nm). Cells showing fragmented mitochondria were quantified by counting more than 100 RFP-positive and Flag-positive cells, n = 1.

Figure 26A

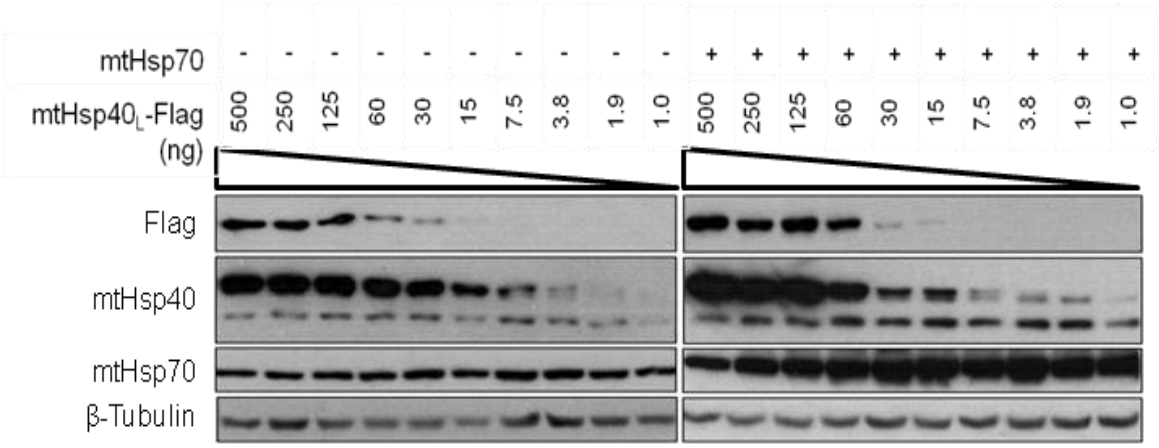

26B

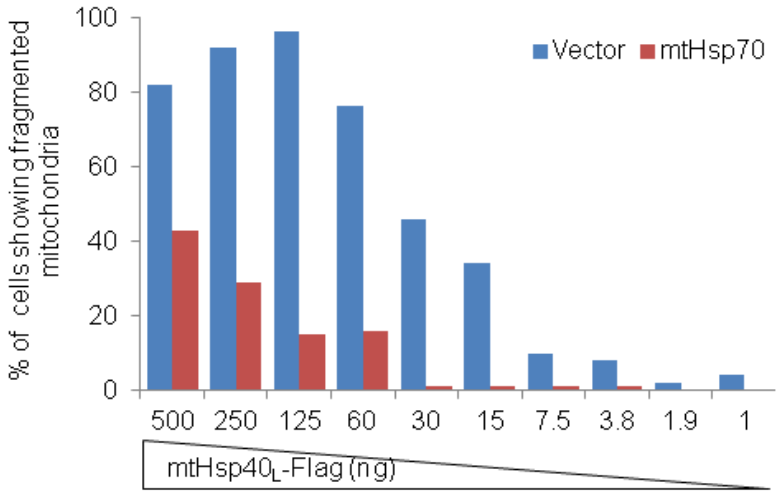

Figure 27. Effects of Ectopic Expression of MtHsp40 on Endogenous MtHsp40$_S$ Interaction with MtHsp70

(A) HEK293-MitoRFP-TetR-mtHsp40$_L$ cells were grown for 24 hours in the absence or presence of DOX (100 ng/ml). Cell lysates were prepared using lysis buffer containing 1 % NP40, and subjected to immunoprecipitation (IP) using anti-mtHsp70 antibodies. IP was performed by employing high stringent condition, and Co-IP samples were analyzed by Western blots using the indicated primary antibodies. (B) Cells described in (A) were subjected to sonication in PBS, and IP was performed using the lysate by employing low stringent protocol. Co-IP samples were analyzed by Western blots using the indicated primary antibodies.

27A

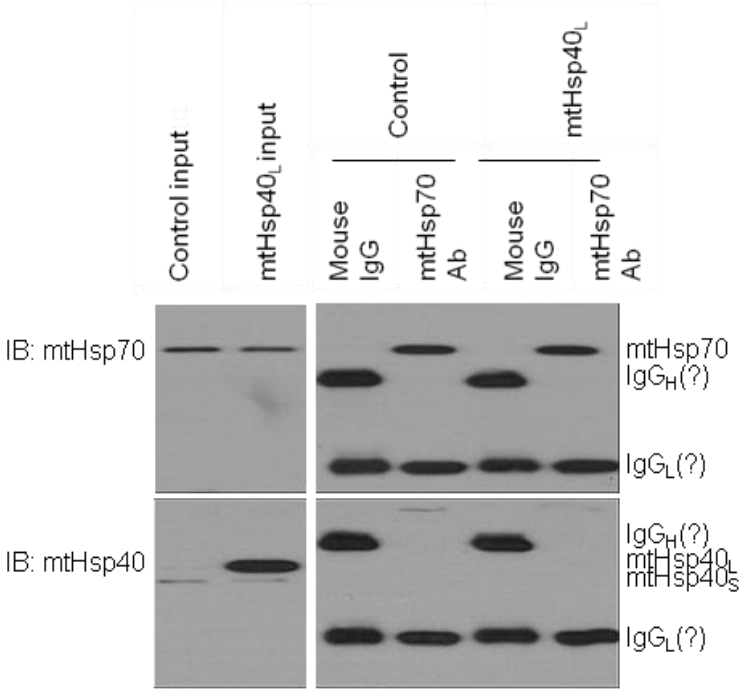
Control input
mtHsp40L input
Control
mtHsp40L
Mouse IgG
mtHsp70 Ab
Mouse IgG
mtHsp70 Ab
IB: mtHsp70
IB: mtHsp40
mtHsp70
IgGH(?)
IgGL(?)
IgGH(?)
mtHsp40L
mtHsp40S
IgGL(?)

27B

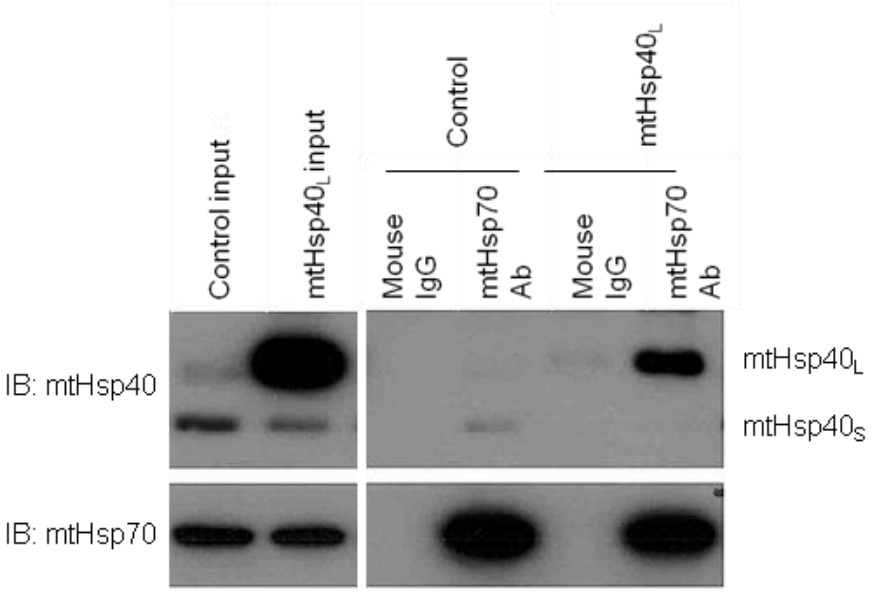
Control input
mtHsp40L input
Control
mtHsp40L
Mouse IgG
mtHsp70 Ab
Mouse IgG
mtHsp70 Ab
IB: mtHsp40
IB: mtHsp70
mtHsp40L
mtHsp40S

GADH (Glyceraldehyde dehydrogenase), because those enzymes are easily denatured and efficient to analyze its activity. Thus, we generated a mitochondrial-targeted luciferase to test the effects of mtHsp40 or mtHsp70 on the luciferase activity in mitochondria. We first constructed a cytosolic luciferase by fusing CMV promoter and firefly luciferase gene in pGL3-enhancer mammalian vector, and next inserted the MTS of mtHsp70 in between the CMV promoter and luciferase gene resulting in the luciferase fused with MTS on its N-terminus (Fig 28A). To test whether those constructs were expressed in specific organelles, we co-transfected HeLa-mitoRFP cells with Cyto-Luc and Mito-Luc in the absence or presence of $mtHsp40_L$ construct. One day following transfection, cells were analyzed by Western blot and immunofluorescence microscopy. Both Cyto-Luc and Mito-Luc were expressed at a significant level, but did not affect mtHsp40 or mtHsp70 level (Fig 28C). Next, the cytosolic and mitochondrial fractions were isolated, and were subjected to the luciferase assay. As expected, Cyto-Luc showed luciferase activity mainly in the cytosol, but was not detectable in mitochondria. Mito-Luc was expressed at a very similar level in both the cytosol and mitochondria. To confirm this result, we performed immunostaining using anti-Luciferase antibodies, and found its mixed localization: some cells showed mitochondrial luciferase and others cytosolic luciferase (Fig 28D). These data suggest that Mito-Luc may be targeted to mitochondria; however, its targeting efficiency is pretty low, which results in both cytosolic and mitochondrial luciferase. Although we attempted to reduce the cytosolic luciferase by optimizing the DNA amount of pGL3-MitoLuc construct, it was not successful to lower the level of cytosolic luciferase. Thus, as an alternative method, we isolated each cell compartment including the cytosol and mitochondria following the transfection of pGL3-MitoLuc, and gave each compartment a heat-shock, and analyzed the luciferase activity during recovery. We first checked the heat-shock response to confirm our heat-shock condition. Upon heat-shock, heat-shock proteins such as HSP70 and HSP90 were induced promptly, but mtHsp40 or mtHsp70 did not respond to heat-shock, which was consistent with previous findings showing that mtHsp40 and mtHsp70 were not induced by heat-shock (Fig 29A). In the meantime, luciferase activity was analyzed with each time point of recovery as indicated. Although results were not consistent, mtHsp40 overexpression was likely to negatively affect luciferase recovery in fragmented mitochondria (Fig 29B). These experiment needs to be repeated.

Figure 28. Generation of Mitochondrial-Targeted Luciferase Construct

(A) Schematic diagram of pGL3-Cyto-Luc (cytosolic luciferase) and pGL3-Mito-Luc (mitochondrial luciferase). (B) HeLa-mitoRFP cells were transfected with pGL3-Cyto-Luc or pGL3-Mito-Luc for 24 hours, and analyzed by Western blots using the indicated primary antibodies. Up = unprocessed form. (C) Subcellular fractions were isolated from cell lysates of (B) using QProteome Mitochondria Isolation kit and luciferase activity assay were performed using Promega Luciferase assay kit. WCE = whole cell extract; Cyt = cytosol; Mit = mitochondria. (D) Cells described in (B) were fixed using 4 % PFA, and stained with Luc / AF488 goat anti-rabbit IgG.

28A

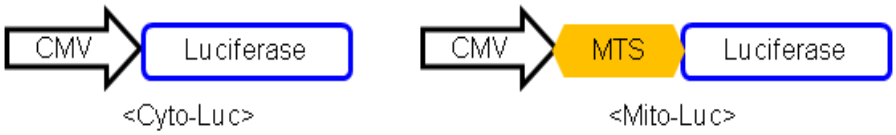

28B

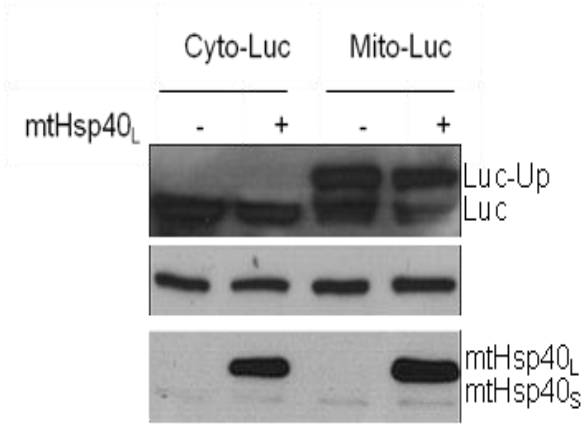

Figure 28C

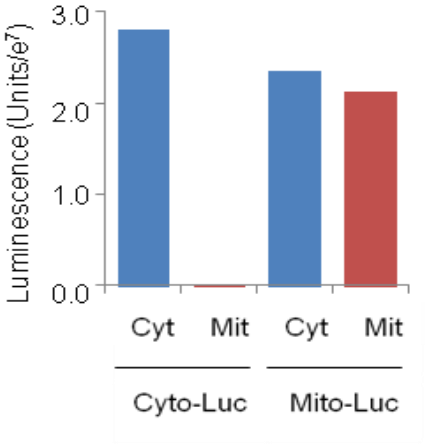

28D

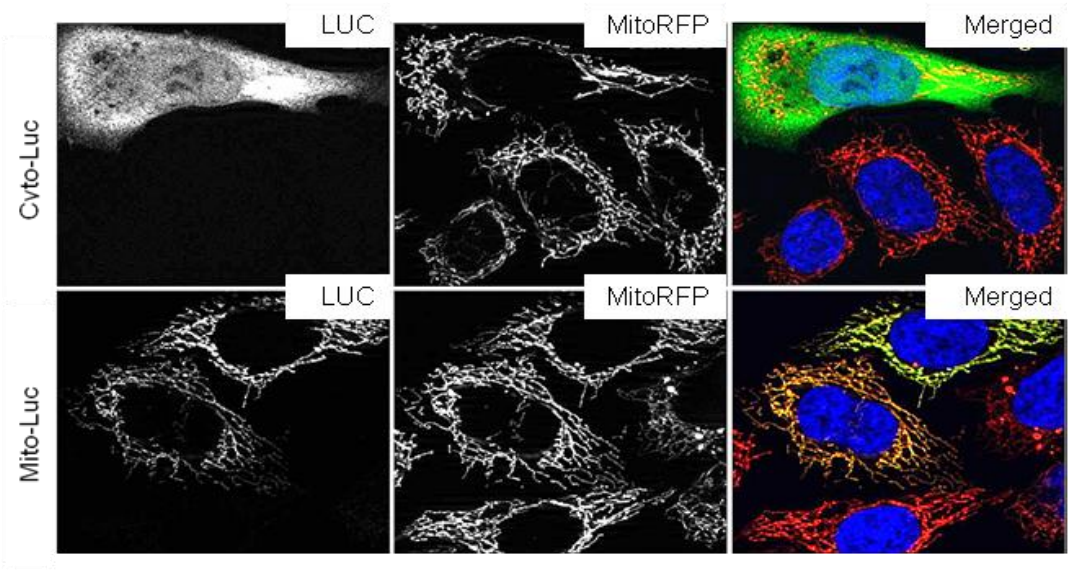

Figure 29. Effects of MtHsp40 Overexpression on Luciferase Refolding

(A) HeLa-mitoRFP cells were transfected with pGL3-Cyto-Luc or -Mito-Luc in the absence or presence of $mtHsp40_L$ for 24 hours, and subjected to mitochondria isolation, followed by heat shock at 42 ℃ for one minute. Later, mitochondria were further incubated at 37 ℃ for indicated time for recovery, and analyzed by Western blots using the indicated primary antibodies, and were subjected to the luciferase assay (B).

29A

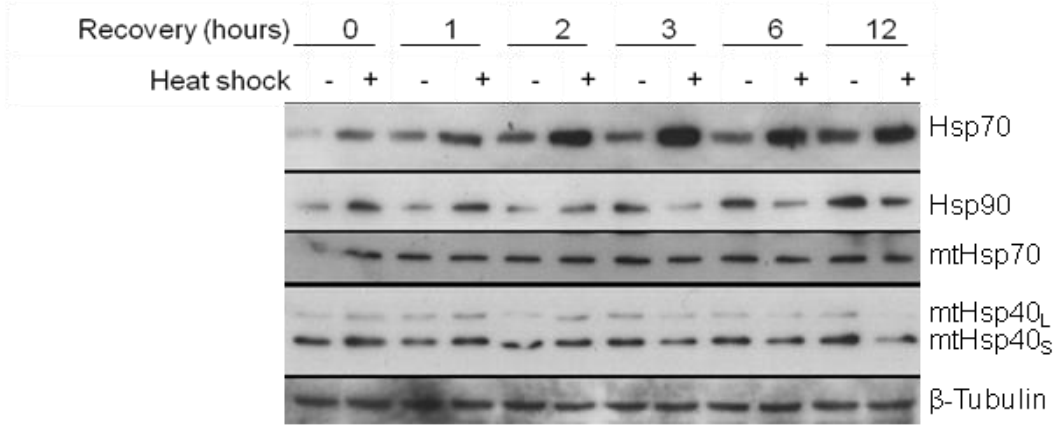
Recovery (hours)
0
1
2
3
6
12
Heat shock
- + - + - + - + - + - +
Hsp70
Hsp90
mtHsp70
mtHsp40L
mtHsp40S
β-Tubulin

29B

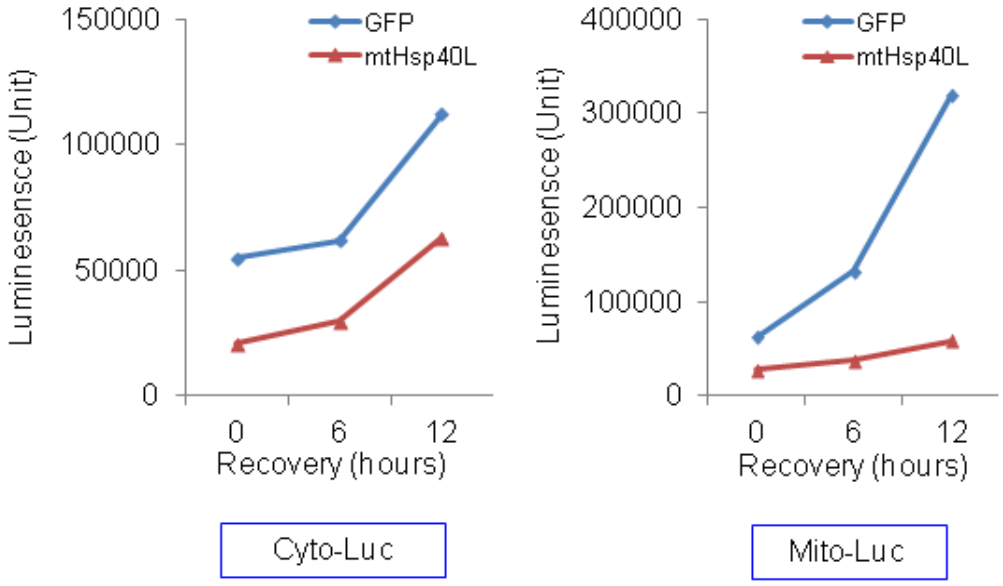
150000
100000
50000
0
Luminesensce (Unit)
GFP
mtHsp40L
0
6
12
Recovery (hours)
Cyto-Luc
400000
300000
200000
100000
0
Luminesensce (Unit)
GFP
mtHsp40L
0
6
12
Recovery (hours)
Mito-Luc

3.15 Discussion and Future Directions

From its discovery in 1998[37], human mtHsp40 has been classified as a tumor suppressor, and lines of report showed that mtHsp40 was associated with a number of cancer-related signaling pathways that lead to alterations in apoptosis, tumor metastasis, and senescence. Recently, our laboratory reported that mtHsp40 overexpression triggered TP53 translocation to mitochondria possibly in an mtHsp70-dependent manner, which enhances intrinsic apoptosis in the presence of proapoptotic stimuli[40]. It has been known that mtHsp70 interacts with TP53 in the cytosol, which abolishes TP53 import to the nucleus and ultimately inhibits its tumor suppressor activity, which is controversial with our previous reports[174]. We wish to elucidate the roles for mtHsp40 and mtHsp70 in apoptosis in this study.

To date, studies clearly showed that mitochondrial fragmentation is (in)directly associated with apoptosis; for example, mitochondria of apoptotic cells are highly fragmented[219]. Our initial finding showed that ectopic expression of mtHsp40 resulted in mitochondrial fragmentation independently of TP53. We thus proposed that mtHsp40 determines mitochondrial morphology independently of TP53, which may lead to apoptosis in cancer cells.

To test this proposal, we first investigated the effects of different levels of mtHsp40 on mitochondrial morphology and apoptosis. We found that ectopic expression of mtHsp40 in multiple cancer cell lines including breast cancer MCF7, glioma U87, neuroblastoma SK-N-SH, cervical cancer HeLa, and human skin fibroblast cells caused mitochondrial fragmentation, but did not affect cytochrome *c* release into the cytosol in the absence of proapoptotic chemicals such as desferroxamine mesylate and cisplatin. In addition, fragmented mitochondria caused by ectopic expression of mtHsp40 became more sensitive to those drugs and showed higher cytochrome *c* release, suggesting that mtHsp40 overexpression itself does not trigger apoptosis, but sensitizes cancer cells to apoptosis following mitochondrial fragmentation.

Following mtHsp40 overexpression, mitochondrial fragmentation occurred as a series of steps within three hours: tubular mitochondria were broken apart (1), shrank (2), and became perinuclear puncta (3). Using DOX-inducible mtHsp40 expressing HEK293 cells, we found that higher levels of mtHsp40 than thirty fold over control could induce mitochondrial fragmentation, indicating that levels of mtHsp40 determined mitochondrial morphology. As it was known that mitochondrial stress agents such as CCCP reversibly modulate mitochondrial morphology between tubular network and fragmented puncta, we tested whether mitochondrial morphology

change induced by ectopic expression of mtHsp40 is reversible with fluctuation of mtHsp40 protein levels. We found that mitochondrial morphology was reversible with mtHsp40 levels.

Our studies on the effects of mtHsp40 domains on mitochondrial morphology demonstrated that only the MTS and DnaJ domains are required for mitochondrial fragmentation. However, overexpression of another mitochondrial matrix DnaJ protein, DnaJC20, did not affect mitochondrial morphology, indicating that mitochondrial fragmentation is specific to the DnaJ domain of mtHsp40 and is associated with mtHsp70 function for certain reasons.

To test the above hypothesis, we first confirmed that mtHsp70 inhibition also resulted in mitochondrial fragmentation; however, ectopic expression of mtHsp70 did not affect mitochondrial morphology, which was also consistent with Burbulla's findings[215]. Using mtHsp70 domain deletion mutant constructs, we found that ectopic expression of a mutant $mtHsp70_{1\text{-}434}$ containing only the MTS and ATPase caused mitochondrial fragmentation, suggesting that binding of $mtHsp70_{1\text{-}434}$ to mtHsp40 may inhibit mtHsp40 activity leading to mitochondrial fragmentation, which was tested using mtHsp40 RNAi. As expected, the data showed that depletion of mtHsp40 resulted in mitochondrial fragmentation. Altogether, data suggest that imbalanced levels or activities of mtHsp40 and mtHsp70 result in mitochondrial fragmentation. To test this, we lastly examined the effects of combined expression of mtHsp40 with mtHsp70 on mitochondrial morphology. Data demonstrated that concomitant expression of mtHsp70 dampened the effects of mtHsp40 overexpression on mitochondrial morphology.

Collectively, we present a model describing the relevance of balance of expression levels or activities of mtHsp40 and mtHsp70 in mitochondrial morphology and apoptosis (Fig 30). Here, we propose that well-balanced ratio of mtHsp40 and mtHsp70 in the matrix plays certain important roles in the tubular network of mitochondria: excess mtHsp40 or DnaJ domain alone of mtHsp40 interacts with mtHsp70 through the interaction between DnaJ domain and ATPase domain, triggers ATP hydrolysis of mtHsp70 leading to LID domain closure, which in turn inhibits the activity of mtHsp70 folding or refolding, ultimately resulting in mitochondrial fragmentation independently of TP53, which sensitizes cells to apoptotic cell death. However, in this section, we still don't know how mitochondria are fragmented under imbalance of mtHsp40 and mtHsp70, and why fragmented mitochondria become sensitive to apoptosis. We will address these questions in next sections.

Figure 30. Proposed Model.

It was reported that mtHsp70 and mtHsp40 play opposing roles in apoptosis in the cytoplasm dependent on TP53. Our data in this study propose that ratio of levels or activities between mtHsp40 and mtHsp70 determines mitochondrial structure, and in turn apoptotic cell death or cell life. Imbalanced levels or activities between mtHsp40 and mtHsp70 disrupt functional mtHsp40:mtHsp70 chaperonic network, which perturbs mitochondrial morphology. Following mitochondrial morphology switch from tubular network to fragmented puncta in a certain mechanism, fragmented mitochondrial become sensitized to proapoptotic stimuli and highly release cytochrome *c* into the cytosol; however, the mechanism(s) how fragmented mitochondria elevates cytochrome *c* release are unknown.

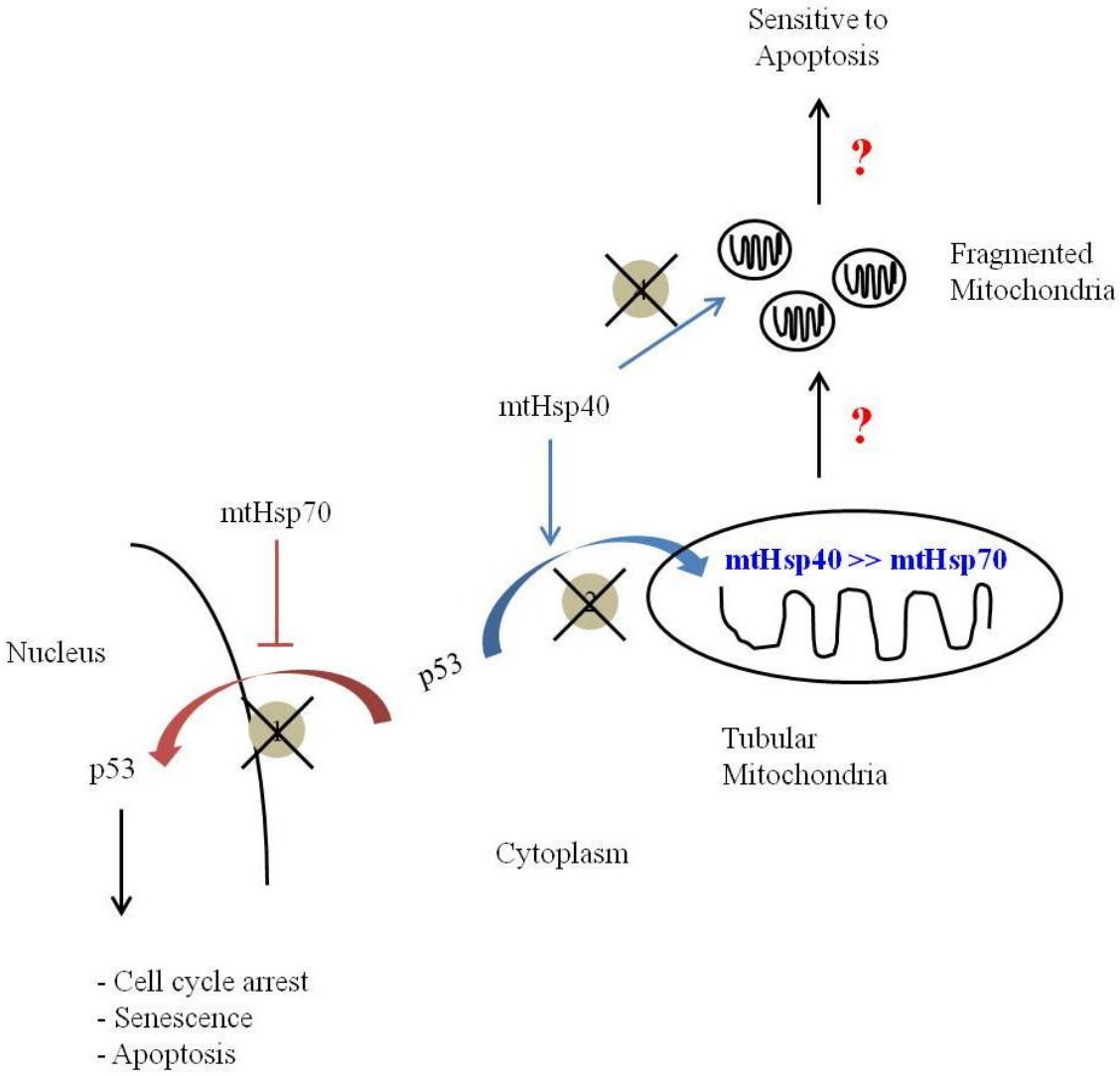
Sensitive to
Apoptosis
?
Fragmented
Mitochondria
mtHsp40
?
mtHsp70
mtHsp40 >> mtHsp70
Nucleus
p53
p53
Tubular
Mitochondria
Cytoplasm
- Cell cycle arrest
- Senescence
- Apoptosis

We could have observed clear difference in the mitochondrial morphology between tubular network and fragmented puncta with our eye-pieces. We did blind tests and excluded cells with mixed or unclear mitochondrial morphology to avoid biased errors. Other groups designed a specific algorithm to determine mitochondrial morphology based on the area of mitochondria, or measured mitochondrial morphology change based on the mitochondrial length. Even though those approaches have pros and cons, we should take these methods into consideration to increase the confidence of our data.

We propose in this study that ectopic expression of mtHsp40 or its DnaJ domain alone may bind the ATPase domain of mtHsp70, which stimulates ATP hydrolysis, LID closure and ultimately resulting in impaired protein folding/refolding. Thus, we could expect that ectopically expressed mtHsp70 may also result in mitochondrial fragmentation, but the result was different than our expectations. While the $mtHsp70_{1\text{-}434}$ mutant containing the MTS and ATPase domain caused mitochondrial fragmentation, full length mtHsp70 or ATPase-deletion mutant did not affect mitochondrial morphology. Possible explanations for these results are as follows: ATP-bound HSP70 is known to have relatively low affinity to substrate proteins compared with ADP-bound HSP70. Thus, it requires co-chaperones such as mtHsp40 for the efficient chaperonic cycle (Fig 5)[16]. Conversely, mtHsp40 has the high affinity to substrates. During the protein folding cycle, mtHsp40 first binds and transfers substrates to mtHsp70. Following ATP hydrolysis triggered by the DnaJ domain of mtHsp40, mtHsp40 is released and recycled rapidly[17]. In the case of mtHsp70 overexpression, excess mtHsp70 preferentially binds substrate-bound mtHsp40 to substrate-unbound mtHsp40 resulting in functional mtHsp40:mtHsp70 network and tubular mitochondrial morphology. As it is known that mtHsp40 is required for chaperonic activity at relatively low level compared with mtHsp70, this explanation is possible that levels of ectopically expressed mtHsp70 may not be sufficient to completely inhibit mtHsp40 activity. Consistently, it was hard to see mitochondrial fragmentation caused by depletion of mtHsp40 using shRNAs or siRNAs. At five days following mtHsp40 siRNA transfection, mitochondrial morphology came to an end to fragmented puncta. To address these problems, we therefore attempted to generate an mtHsp40 conditional knockout mouse model with the collaboration with University of Calgary Transgenic Services, and we expected MEF $mtHsp40^{-/-}$. Unfortunately, although we generated $mtHsp40^{flox/+}$, we failed in generating $mtHsp40^{flox/flox}$ mice, despite 6 months of genotyping of litters. We believe that $mtHsp40^{-/-}$ MEFs or mice can provide

us results clearly showing the effects of mtHsp40 deletion on mitochondrial morphology.

In this study, we showed that stoichiometric balance between mtHsp40 and mtHsp70 is required for the homeostasis of mitochondrial morphology; however, we lack evidence directly showing the stoichiometry between mtHsp40 and mtHsp70, and the relationship between their stoichiometry and chaperonic function. We thought that excess mtHsp40 or DnaJ domain alone physically interacts with the ATPase domain of mtHsp70 leading to inhibition of mtHsp70 activity. Although this interaction was well studied from bacterial DnaJ and dnaK[220] or yeast Mdj1 and Ssc1[221] and their crystal structures were released, data supporting the physical interaction between mtHsp40 mutants and mtHsp70 wild type, or mtHsp70 mutants and mtHsp40 wild type, or mtHsp40 mutants and mtHsp70 mutants are still required. As all mutants contain C-terminal Flag tags, we could perform Co-IP using anti-Flag antibodies, which can allow us its differential interaction with mtHsp70 from endogenous mtHsp40 interaction. In addition to interaction studies, experiments showing chaperonic activities of mtHsp70 are also required to provide the direct evidence proving whether fragmented mitochondria are defective in mitochondrial protein folding/refolding/ targeting resulting from the inhibition of mtHsp70 activity. To do this, we constructed the mitochondrial-targeted luciferase, but it did not appear to work for folding/refolding assay. As an alternative method, we first could suggest mass spectrometry (MS) following Co-IP using anti-Flag antibodies to screen and identify proteins interacting with mtHsp40 and mtHsp70. Those hits will be validated for Co-IP using primary antibodies, and target proteins showing differential interaction with mtHsp70 between in the absence and presence of mtHsp40 overexpression will be finally selected as final targets for further experiments. We expect these experiments can provide evidence directly showing that imbalance between mtHsp40 and mtHsp70 inhibits their interaction with substrate proteins, and also possible pathway(s) participated in mitochondrial fragmentation. In addition, to decide the stoichiometry between mtHsp40 and mtHsp70, MS analysis can be performed using mitochondrial fraction.

It has long been demonstrated that mtHsp70 plays dual roles in mitochondria: protein import and folding. As mtHsp40 interaction with mtHsp70 solely does not differentiate the roles of mtHsp70, it is possible to presume that mitochondrial fragmentation may result from inhibition of protein import mediated by mtHsp70. In other words, ectopic expression of mtHsp40 may inhibit the protein-import activity of mtHsp70 by masking the ATPase domain of

mtHsp70 integrated into the innermembrane of mitochondria. Thus, experiments to rule out the possibility that protein import is impaired in fragmented mitochondria caused by ectopic expression of mtHsp40 or mtHsp70 depletion are necessary.

In human mitochondria, there are several members of major chaperone families that play important roles in mitochondrial function[222]. Interestingly, it has been found that matrix chaperone system HSP60/HSP10 assists and facilitates protein folding activity of mtHsp40/mtHsp70[173]. Thus, it would be of interest to investigate whether another chaperone system such as HSP60 and Hsp10 in the mitochondrial matrix plays a certain role for mitochondrial morphology like mtHsp40:mtHsp70 network and the ratio between HSP60 and HSP10 is also important in their chaperonic activities.

In addition to mitochondrial fragmentation, ectopic expression of mtHsp40 resulted in perinuclear localization of mitochondria following mitochondrial fragmentation. Some studies showed that as a result of mitochondrial fragmentation in the presence of mitochondrial stresses like CCCP, damaged mitochondria were located around the nucleus and degraded by autophagy following Parkin translocation to mitochondria in a PINK1-dependent mechanism[223,224]. Thus, it would also be of interest to determine if the ectopic expression of mtHsp40 induces PINK1/Parkin-mediated mitophagy in certain cells other than HeLa cells, because HeLa cells are lacking Parkin.

Lastly, some groups were interested in the specific upregulation of mtHsp70 in numerous cancers, and are providing insights for new therapeutic approaches targeting mtHsp70 as a novel cancer therapy. They already reported some efficacy of inhibiting tumor growth or killing cancer cells by introducing adenovirus expressing shRNAs against mtHsp70[189] or small mtHsp70 inhibitors like MKT-077[184,225]. However, mtHsp70 knockdown and mtHsp70 inhibitors may affect its both functions, protein import and folding, which can be problematic to normal cells, because increasing evidence have shown that mtHsp70 dysfunction caused abnormalities in neurons or brain leading to neurodegeneratioin[215,216]. The strategies therefore need to be specific to the protein folding activity of mtHsp70, because inhibition of mtHsp70 chaperone functions may not have deleterious effect on normal cells. This study can provide those researchers with new insights into developing new approaches to retard cancer cell growth or stimulate cancer cell death by treating patients with small mitochondrial DnaJ domain of mtHsp40 (~15 kDa).

Overall, our findings evoke the idea that the stoichiometry between mtHsp40 and

mtHsp70 may determine the mitochondrial morphology resulting from the perturbations of mitochondrial proteostasis, which facilitates apoptotic cell death in a response to proapoptotic stimuli independently of TP53.

CHAPTER FOUR: MECHANISMS OF MITOCHONDRIAL FRGAGMENTATION CAUSED BY PERTURBATIONS OF MITHSP40:MTHSP70 NETWORK

4.1 Background

Mitochondrial morphology is tightly regulated through fission and fusion processes. Under normal condition, many origins of cells maintain the elongated tubular network of mitochondria via the balance between fusion and fission events, resulting in mitochondrial homeostasis of morphology. Several large GTPases mediate these fusion and fission events, and they are known to be expressed constitutively at the mitochondrial membranes or in the cytosol[41].

Mitofusin 1 (MFN1) and 2 (MFN2) are evolutionarily conserved in yeast and metazoans. They are MOM-bound GTPases, tether neighboring mitochondria by forming homodimers or heterodimers and mediate membrane fusion dependent on GTP hydrolysis. Following MOM fusion, another large GTPase integrated into the mitochondrial innermembrane (MIM), OPA1 mediates the MIM fusion. OPA1 has two alternative processing sites. Upon import into mitochondria, the MTS is cleaved off by MPP, and integrated into the MIM[50]. The MIM fusion mechanism is similar to the MOM fusion. Interestingly, OPA1 has a list of processing variants associated with several mitochondrial proteases including YME1L[52], AFG3L1/2[56] and OMA1[57], which results in five bands ranging in size from 85 kDa to 100 kDa on Western blot. It is also known that the long isoform is integrated into the MIM, and the short isoform is floating in the intermembrane space. Notably, its membrane fusion activity is dependent on the balance of $OPA1_L$:$OPA1_S$[53] Under normal condition, the concentration of the long isoform is expressed at an equimolar ratio with the small isoform resulting in the tubular network of mitochondria[53]

Mitochondrial fission events involve one major regulator, DRP1 and some partners such as MFF and hFIS1 recruiting DRP1 to mitochondria. DRP1 is known to be located mainly in the cytosol, but a small portion of them localize at mitochondria[48]. Whereas DRP1 constantly localizes at the MOM, following its activation with modifications such as phosphorylation and dephosphorylation, DRP1 is translocated by mediators and forms homo-oligomeric complexes at the MOM under certain conditions. Following GTP hydrolysis, DRP1 oligomeric structure constricts both outer- and inner-membrane leading to mitochondrial division[48].

4.2. Preliminary Findings and Rationales

Little is known regarding the relationship between mitochondrial fragmentation and mtHsp70 or mtHsp40 dysfunction. As ectopic expression of mtHsp40 and loss of mtHsp70 clearly resulted in mitochondrial fragmentation, we first were interested in the regulatory mechanisms of mitochondrial morphology. The known mechanisms inducing the overall mitochondrial fragmentation are as follow: first, ablation of MFN1 or MFN2 level on the MOM results in fragmented mitochondria. Several studies showed that mitochondrial membrane potential loss ($\Delta\psi_m$) caused MFN1/2 degradation depending on their ubiquitination; for example, PINK1-Parkin pathway[74,75,223,226]. In addition, OPA1 cleavage is also induced by $\Delta\psi_m$, which potentiates OPA1 cleavage as a sensor of mitochondrial dysfunction. Our data in this study clearly showed that fragmented mitochondria caused by ectopic expression of mtHsp40 were not apoptotic. We thus suggest that regulators such as MFN1/2 and OPA1 in the fragmented mitochondria caused by perturbations of mtHsp40:mtHsp70 balance are modulated independently of apoptotic factors BAX/BAK.

Thus, we would focus in this section on the possibility whether the impairment of mtHsp40:mtHsp70 stoichiometry modulates the activities of key mitochondrial dynamics regulators such as MFN1/2, OPA1 and DRP1 leading to mitochondrial fragmentation.

4.3 Expression Patterns of Key Regulators of Mitochondrial Dynamics in Fragmented Mitochondria

As it has been known that expression levels of key regulators of mitochondrial dynamics are tightly controlled to maintain the tubular network of mitochondria, we presumed that those regulators may be deregulated in fragmented mitochondria[227]. We thus analyzed protein lysates of $mtHsp40_L$-overexpressed and mtHsp40-suppressed cells by Western blots. Total protein levels of DRP1 or OPA1 were not affected with either overexpression or deletion of mtHsp40. As DRP1 has two splice variants, we could detect two isoforms, the long and short isoforms of DRP1, and the band pattern did not change. Of interest, OPA1 band patterns were altered: $OPA1_S$ accumulated, whereas $OPA1_L$ was reduced. The ratio between $OPA1_L$ and $OPA1_S$ of $mtHsp40_L$-expressed cells was ~ three times lower than that of control. Deletion of mtHsp40 reduced the ratio between $OPA1_L$ and $OPA1_S$ to ~ 3.5 times in a comparison with control (Fig 31A). However, the overall levels of OPA1 did not seem to be affected with either $mtHsp40_L$ overexpression or mtHsp40 deletion. Unfortunately, we could not perform MFN1/2 Western

blots due to the lack of anti-MFN1 or -MFN2 antibodies.

To test whether expression patterns of key regulators in HeLa cells were consistent among other cell lines, we included Hs68 and SK-N-SH cells. In Hs68 cells, endogenous mtHsp40 and mtHsp70 proteins were scarcely detected, but mtHsp40$_L$ was highly expressed. DRP1 levels and its splicing patterns were very similar to HeLa cells; there was no significant difference between control and mtHsp40$_L$-overexpressed cells (data not shown). Consistently, OPA1 cleavage was induced by mtHsp40$_L$-overexpression in Hs68 cells. The OPA1$_L$:OPA1$_S$ ratio dramatically decreased up to 18-fold compared with control. Interestingly, one new band was produced in between the long and short isoforms of OPA1 in mtHsp40$_L$-overexpressed cells. In addition, OPA1$_L$ accumulated more than OPA1$_S$ in Hs68 ells, which was different from both HeLa and SK-N-SH cancer cells. In SK-N-SH cells, expectedly, levels of OPA1 and DRP1 were similar between control and mtHsp40-expressed cells, whereas OPA1 was cleaved in mtHsp40-expressed cells. In particular, the OPA1$_L$:OPA1$_S$ ratio in mtHsp40$_L$-overexpressed cells was ~ eight times lower than control (Fig 31B). Taken together, these data suggest that mitochondrial fragmentation caused by ectopic expression and deletion of mtHsp40 may be associated with the induction of OPA1 cleavage.

4.4 DRP1 Involvement in Mitochondrial Fragmentation

Under some conditions like cytokinesis or Ca^{2+} overload, it is known that following its modifications such as phosphorylation or dephosphorylation, cytosolic DRP1 is recruited to the MOM by certain mediators including MFF and hFIS1. Thus, we could propose that ectopic expression of mtHsp40 or loss of mtHsp70 may induce DRP1 translocation leading to the overall fragmentation of mitochondria. To test this, we first investigated the effects of DRP1 depletion on mitochondrial morphology in the presence of ectopic expression of mtHsp40. Two days following transfection of DRP1 siRNAs, cells were infected with Ad-GFP (control) or Ad-mtHsp40$_L$, and one day following infection, proteins were analyzed by Western blots. Both DRP1 isoforms were suppressed to < 5 % of control. MtHsp40$_L$ was highly expressed in Ad-mtHsp40$_L$-infected cells. Irrespective of DRP1 levels, OPA1 cleavage was induced when mtHsp40$_L$ was highly expressed (Fig 32A). Simultaneously, mitochondrial morphology was analyzed by fluorescence microscopy. As both viral constructs carry an EGFP gene, we have focused on GFP-positive cells. Whereas Ad-GFP-infected cells (control) showed normal tubular

Figure 31. Levels and Patterns of Fusion and Fission Components in Fragmented Mitochondria Resulting from Ectopic Expression or Deletion of MtHsp40

(A) HeLa-mitoRFP cells were infected with Ad-GFP or Ad-mtHsp40$_L$ for two days, and were analyzed by Western blots using the indicated primary antibodies. HeLa-mitoRFP cells were transfected with siRNAs as indicated using Lipofectamine RNAiMAX for six days, and were analyzed by Western blots using the indicated primary antibodies. The ratio of OPA1$_L$:OPA1$_S$ was quantified using the Image J software. (B) Hs68 and SK-N-SH cells were infected with Ad-GFP or Ad-mtHsp40$_L$ for two days, and were analyzed by Western blots using the indicated primary antibodies. Up = unprocessed form.

31A

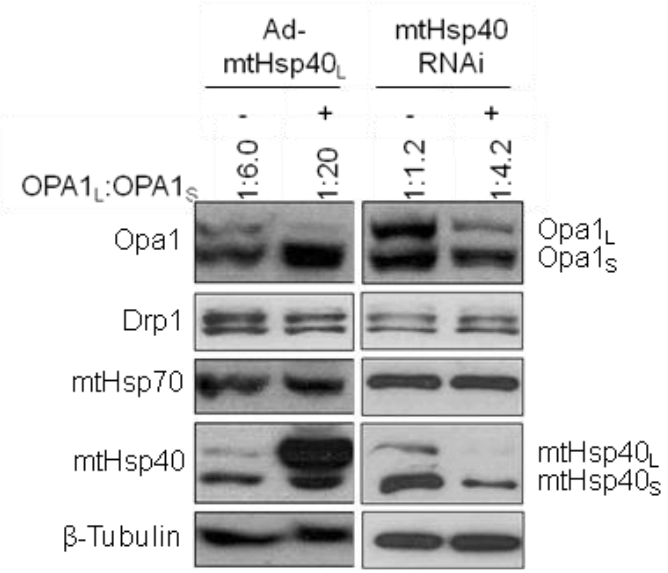
Ad-mtHsp40L
mtHsp40 RNAi
-
+
-
+
OPA1L:OPA1S
1:6.0
1:20
1:1.2
1:4.2
Opa1
Drp1
mtHsp70
mtHsp40
β-Tubulin
Opa1L
Opa1S
mtHsp40L
mtHsp40S

31B

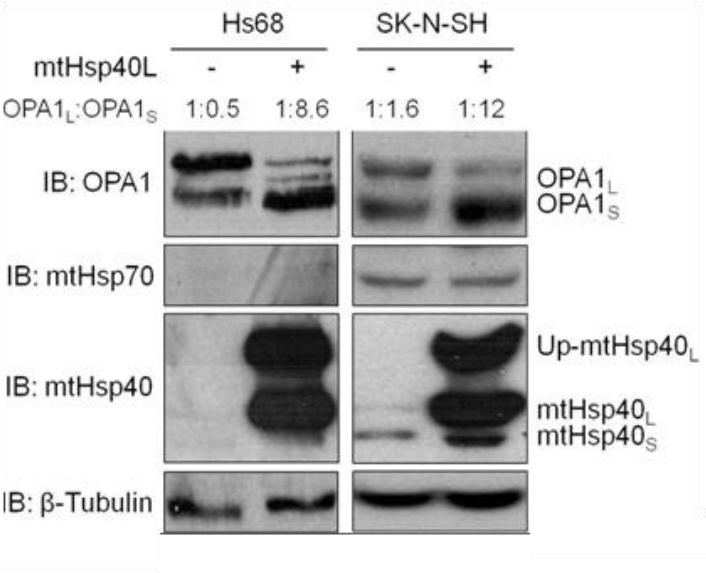
Hs68
SK-N-SH
mtHsp40L
-
+
-
+
OPA1L:OPA1S
1:0.5
1:8.6
1:1.6
1:12
IB: OPA1
IB: mtHsp70
IB: mtHsp40
IB: β-Tubulin
OPA1L
OPA1S
Up-mtHsp40L
mtHsp40L
mtHsp40S

network of mitochondria, Ad-mtHsp40$_L$-infected cells resulted in the typical fragmented mitochondria. DRP1 depletion alone rendered less branched, more intense, and elongated mitochondria. Interestingly, in the presence of ectopic expression of mtHsp40$_L$, DRP1 loss attenuated mitochondrial fragmentation, which produced short and condensed mitochondria (Fig 32B & 32C).

To test the effects of loss of DRP1 on mitochondrial morphology in the presence of mtHsp70 siRNAs, we transfected HeLa-mitoRFP cells with Scramble siRNA, Drp1 RNAi, mtHsp70 RNAi, or a combination of Drp1 and mtHsp70 RNAi. Two-days following transfection, protein samples were analyzed by Western blots and the mitochondrial morphology was visualized by fluorescence microscope. Both DRP1 and mtHsp70 were highly suppressed. Consistently with the ectopic expression of mtHsp40$_L$, loss of mtHsp70 also caused OPA1$_S$ accumulation compared with control, but DRP1 knockdown did not affect OPA1 cleavage. The effects of loss of DRP1on the protein levels of mtHsp70, mtHsp40 and OPA1 were not altered, similarly to mtHsp40$_L$ overexpression (Fig 33A). In the presence of mtHsp70 RNAi, mitochondria became completely fragmented. Of interest, a combination of DRP1 RNAi and mtHsp70 RNAi resulted in the condensed morphology of mitochondria. Mitochondria were not fragmented completely, but were not distributed evenly throughout the cells (Fig 33B). To quantify cells showing each type of mitochondrial morphology, we counted cells showing clear and homogenous morphology, but excluded cells with mixed morphology. Cells with condensed morphology of mitochondria were predominant up to 50 % of total cells under loss of both DRP1 and mtHsp70 (Fig 33C). These data suggest that DRP1 may play a certain role in the mitochondrial fragmentation resulting from ectopic expression of mtHsp40 or loss of mtHsp70.

In order to clarify DRP1 involvement in mitochondrial fragmentation with mtHsp40 overexpression, we tested DRP1 translocation to mitochondria. As Otera *et al* clearly showed that ectopic expression of MFF stimulated DRP1 translocation to mitochondria resulting in mitochondrial fragmentation[73], we included MFF-Flag as a positive control. We transfected HeLa-mitoRFP cells with a combination of HA-DRP1 and MFF-Flag or mtHsp40$_L$-Flag, and empty vector (control) and MFF-Flag or mtHsp40$_L$-Flag. One day following transfection, cells were subjected to immunofluorescence to determine HA-DRP1 location and mitochondrial morphology, and cell compartments were isolated for Western blots. MFF-Flag well co-localized with MitoRFP, and mitochondria were completely fragmented in most of Flag-positive cells,

Figure 32. Determination of Effects of DRP1 Depletion in Mitochondrial Fragmentation Caused by Ectopic Expression of MtHsp40

(A) HeLa-mitoRFP cells were transfected with Drp1 siRNA using Lipofectamine RNAiMAX for 2 days, and then infected with Ad-GFP or Ad-mtHsp40$_L$ for 24 hours. Cells were analyzed by Western blots using the indicated primary antibodies. Up = unprocessed form. (B) Cells were fixed using 4 % PFA, and MitoRFP was visualized as red (568 nm) and GFP as green (488 nm) by fluorescence microscopy. White bar indicates 10 μm. (C) Cells showing each mitochondrial morphology were quantified by counting more than 100 GFP-positive cells, and cells with unclear/mixed mitochondrial morphology were excluded. Bars mean + S.E.M., n = 3.

32A

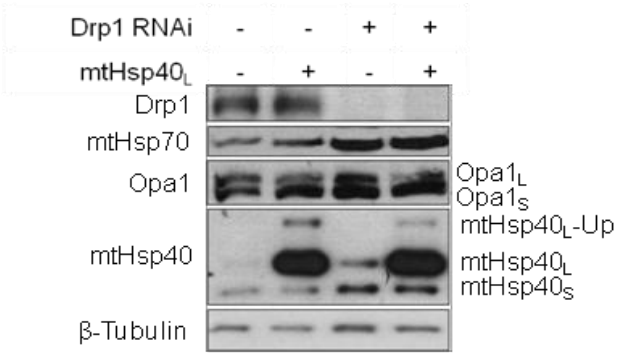
Drp1 RNAi - - + +
mtHsp40L - + - +
Drp1
mtHsp70
Opa1
mtHsp40
β-Tubulin
Opa1L
Opa1S
mtHsp40L-Up
mtHsp40L
mtHsp40S

32B

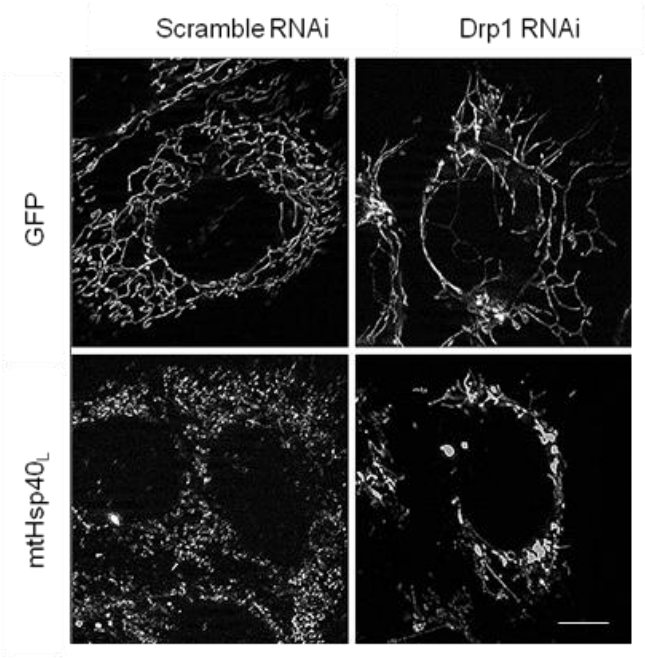
Scramble RNAi
Drp1 RNAi
GFP
mtHsp40L

32C

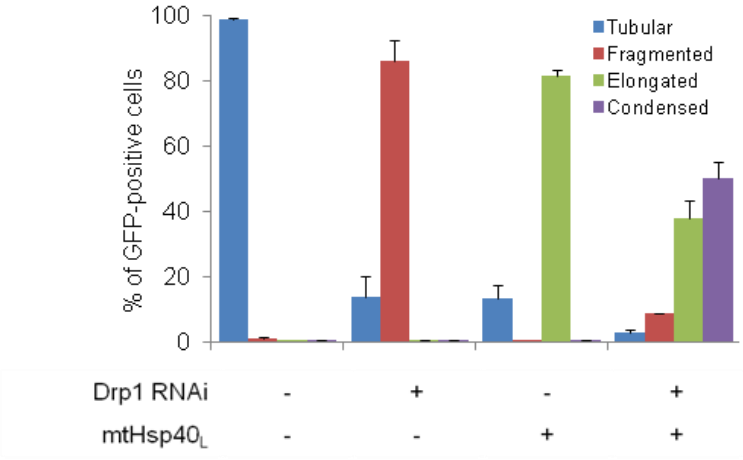
100
80
60
40
20
0
% of GFP-positive cells
Tubular
Fragmented
Elongated
Condensed
Drp1 RNAi - + - +
mtHsp40L - - + +

Figure 33. Determination of Effects of DRP1 Depletion on Mitochondrial Fragmentation Caused by MtHsp70 Loss

(A) HeLa-mitoRFP cells were co-transfected with Drp1 siRNA in a combination of Scramble or mtHsp70 RNAi using Lipofectamine RNAiMAX for 3 days, and cells were analyzed by Western blots using the indicated primary antibodies. (B) Cells were fixed using 4 % PFA, and stained by mtHsp70 / AF488 goat anti-mouse IgG. MitoRFP was visualized as red (568 nm) and mtHsp70 as green (488 nm) by fluorescence microscopy. White bar indicates 10 μm. (C) Cells showing each mitochondrial morphology were quantified by counting more than 100 cells, and cells with unclear/mixed mitochondrial morphology were excluded. Bars mean + S.E.M., n = 3.

33A

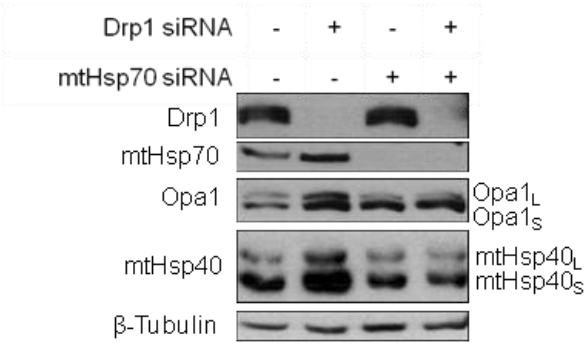
Drp1 siRNA - + - +
mtHsp70 siRNA - - + +
Drp1
mtHsp70
Opa1
Opa1L
Opa1S
mtHsp40
mtHsp40L
mtHsp40S
β-Tubulin

33B

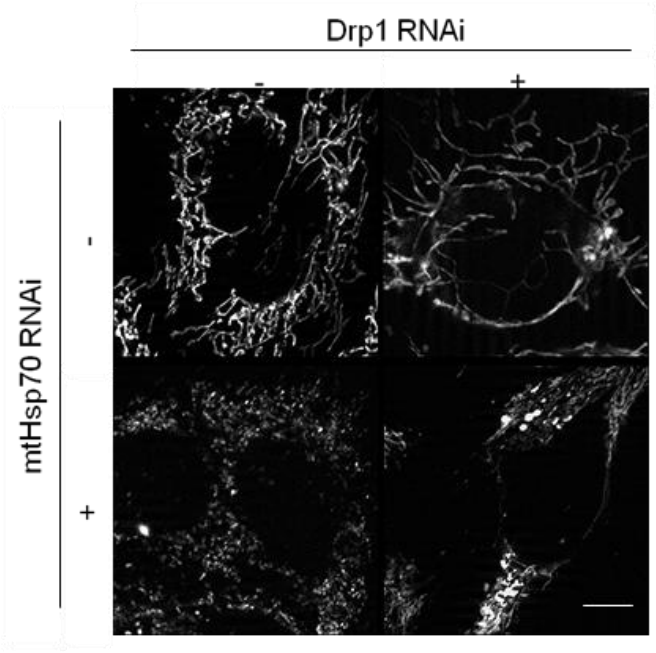
Drp1 RNAi
-
+
mtHsp70 RNAi
-
+

33C

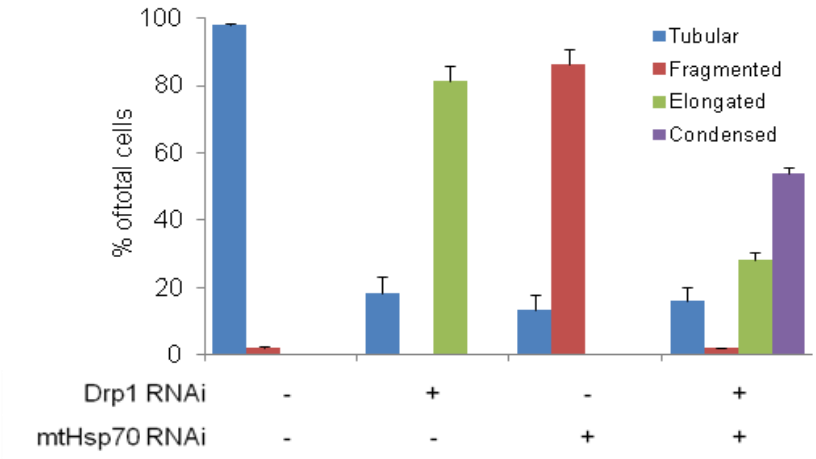
100
80
60
40
20
0
% oftotal cells
Tubular
Fragmented
Elongated
Condensed
Drp1 RNAi - + - +
mtHsp70 RNAi - - + +

which was similar to mtHsp40$_L$-Flag-overexpressed cells. Whereas HA-DRP1 was mainly cytosolic in control cells, it localized to fragmented mitochondria in MFF-Flag-overexpressed cells, which was consistent with Otera's findings. Conversely, mtHsp40$_L$-Flag-overexpressed cells showed mostly cytosolic HA-DRP1 in fragmented mitochondria (Fig 34A). Cellular compartment data confirmed the immunofluorescence results. We could not detect a significant difference in mitochondrial DRP1 levels between control and mtHsp40$_L$-Flag-overexpressed cells. Although we did not detect HA-DRP1 in mitochondria, we could also recognize no difference in the cytosolic HA-DRP1 between control and mtHsp40$_L$-Flag-overexpressed cells (Fig 34B). These data indicate that DRP1 is not translocated to the fragmented mitochondria under mtHsp40$_L$-Flag-overexpression. Together, data suggest ectopic expression and deletion of mtHsp40 cause OPA1 cleavage leading to mitochondrial fragmentation dependent on DRP1 located at mitochondria.

4.5 Effects of Ectopic Expression of MFN1/2 on Mitochondrial Fragmentation

Recently, accumulating data showed that MFN1 or MFN2 level is regulated by ubiquitin-mediated degradation pathways, and the PINK1-Parkin axis has been known to be deeply involved in this pathway[74,75]. Thus, we first attempted to determine the levels of MFN1 or MFN2 in fragmented mitochondria. Unfortunately, either anti-MFN1 or –MFN2 antibodies was not available in our laboratory. Alternatively, we investigated whether ectopic expression of MFN1/2 could rescue mitochondrial fragmentation caused by ectopic expression of mtHsp40 or loss of mtHsp70. To do this, we transfected HeLa-mitoRFP cells with a combination of control and MFN1-Myc/MFN2-Myc, or mtHsp40$_L$ and MFN1-Myc/MFN2-Myc. One day following transfection, proteins and mitochondrial morphology were analyzed. Ectopically expressed MFN1-Myc and MFN2-Myc well localized to mitochondria, but did not affect mitochondrial morphology. MtHsp40$_L$ overexpression resulted in the dramatic fragmentation of mitochondria, but was not rescued by ectopically expressing either MFN1-Myc or MFN2-Myc (Fig 35A). In addition, OPA1 cleavage was not rescued by ectopic expression of MFN1 or MFN2 (Fig 35B).

In addition, we determined PINK1 stabilization in fragmented mitochondria to investigate the levels of MFN1/MFN2 in fragmented mitochondria. PINK1 was not detectable in fragmented mitochondria in the presence of ectopic expression of mtHsp40$_L$ (Fig 36A & 36B). The data was consistent with loss of mtHsp70. Both mtHsp40$_L$ overexpression and mtHsp70

Figure 34. Determination of Drp1 Localization in Fragmented Mitochondria Caused by Ectopic Expression of MtHsp40

(A) HeLa-mitoRFP cells were co-transfected with HA-Drp1 in a combination of control, Mff-Flag or mtHsp40$_L$-Flag using Lipofectamine2000 for 24 hours. Cells were fixed using 4 % PFA, and stained by Flag / AF488 goat anti-mouse IgG or HA /AF488 goat anti-rat IgG. MitoRFP was visualized as red (568 nm) and Flag (or HA) as green (488 nm) by fluorescence microscopy. (B) From cells described in (A), cellular fractions were separated by biochemical fractionation (W = whole cell extracts; C = cytosolic fraction; M = mitochondrial fraction), followed by Western blots. Purity of the fractions was determined by Western blots with anti-mtHsp70 (mitochondrial) and anti-Tubulin antibodies (cytosolic).

34A

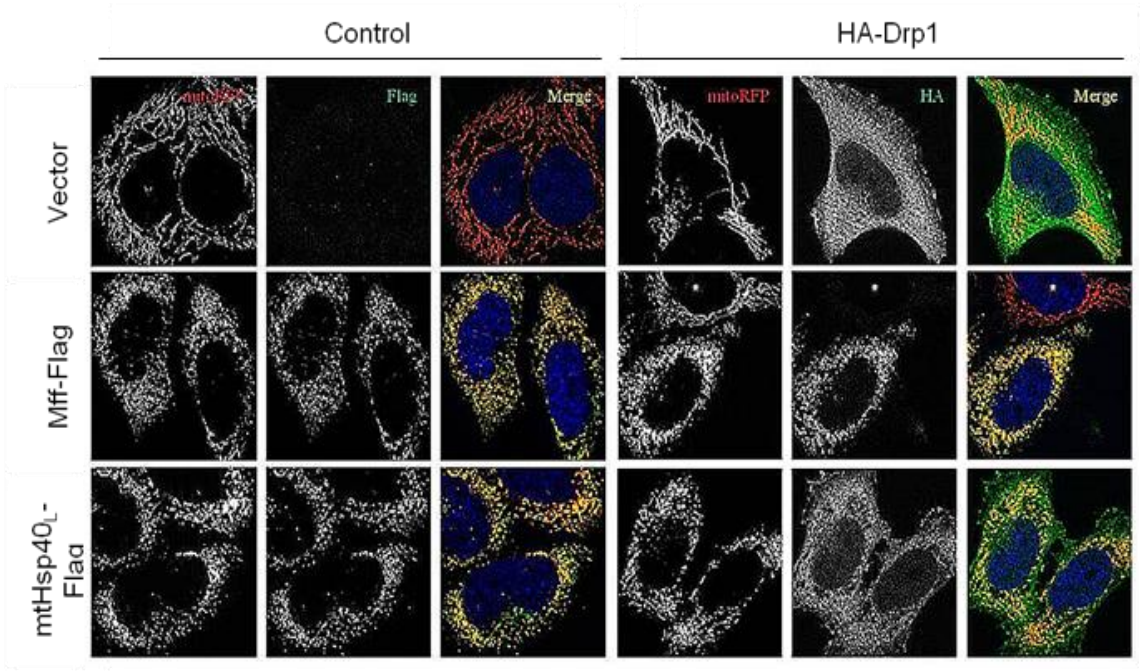
Control
HA-Drp1
Vector
Mff-Flag
mtHsp40L-Flag
mitoRFP
Flag
Merge
mitoRFP
HA
Merge

34B

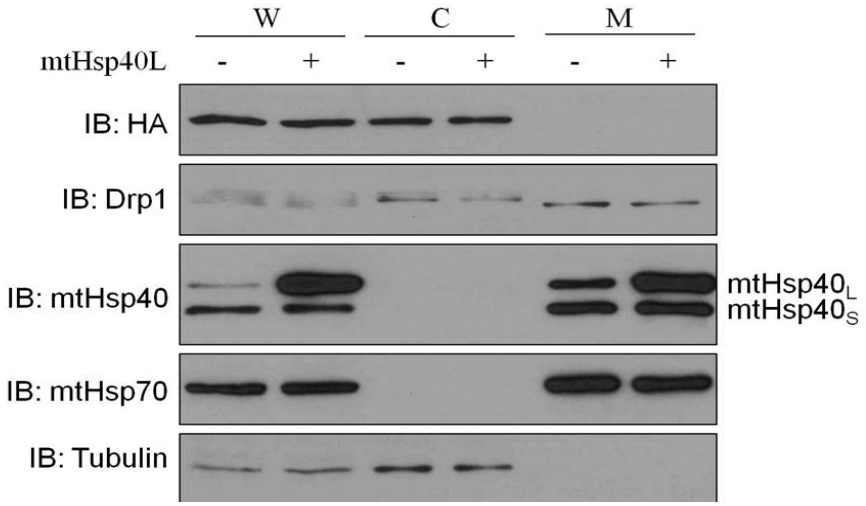
W
C
M
mtHsp40L
- + - + - +
IB: HA
IB: Drp1
IB: mtHsp40
IB: mtHsp70
IB: Tubulin
mtHsp40L
mtHsp40S

Figure 35. Effects of Upregulation of MFN1/2 on Mitochondrial Morphology under Ectopic Expression of MtHsp40

(A) HeLa-mitoRFP cells were co-transfected with pRK5 or pRK5-mtHsp40$_L$ in a combination of Mfn1-myc or Mfn2-myc for 24 hours. Cells were fixed using 4 % PFA, and stained by mtHsp40 / AF488 or Myc / AF488 goat anti-mouse IgG. MitoRFP was visualized as red (568 nm) and mtHsp40 or Myc as green (488 nm) by immunofluorescence microscopy. White bar means 10 μm. (B) Lysates were isolated from cells in (A), and analyzed by Western blots using the indicated primary antibodies. Up = unprocessed form.

35A

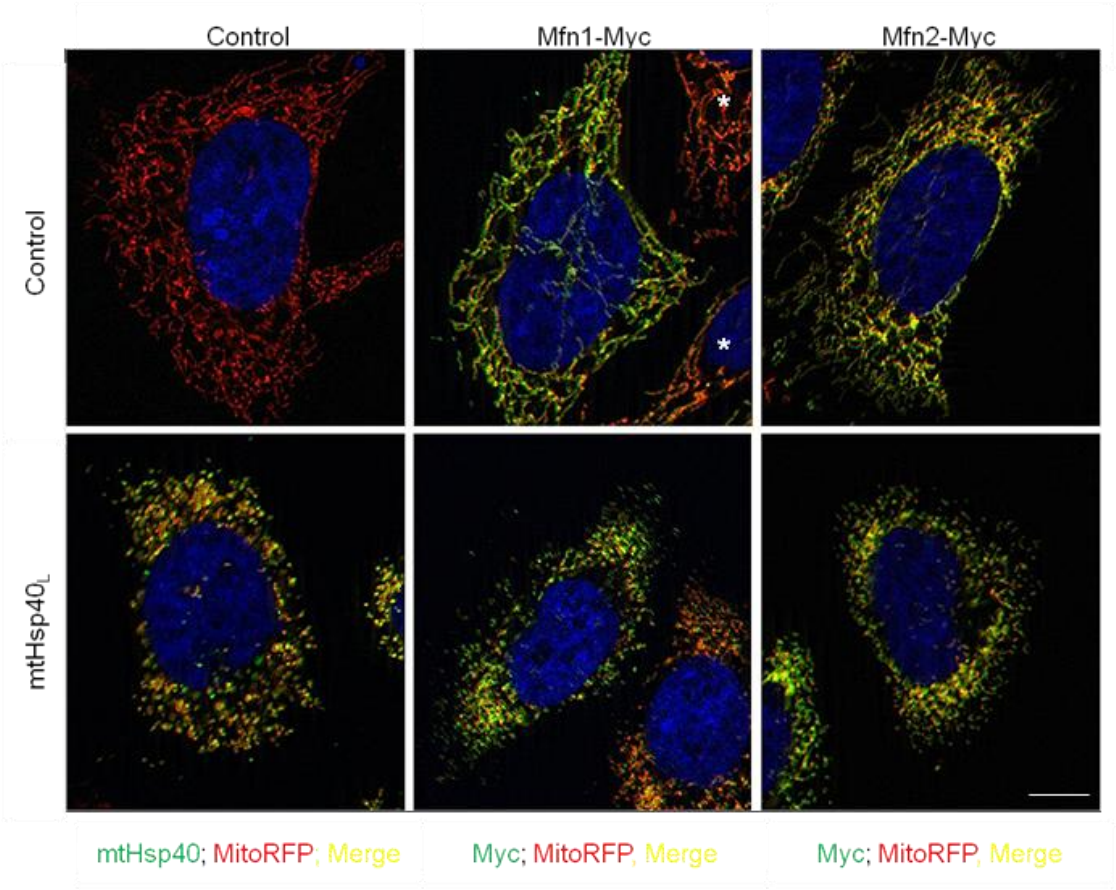
Control
Mfn1-Myc
Mfn2-Myc
Control
mtHsp40L
mtHsp40; MitoRFP; Merge
Myc; MitoRFP, Merge
Myc; MitoRFP, Merge

35B

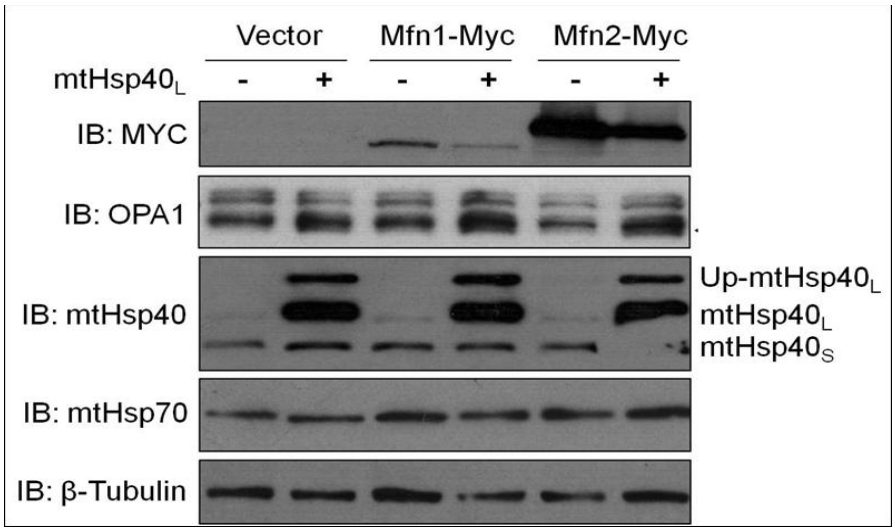
Vector
Mfn1-Myc
Mfn2-Myc
mtHsp40L
- + - + - +
IB: MYC
IB: OPA1
IB: mtHsp40
IB: mtHsp70
IB: β-Tubulin
Up-mtHsp40L
mtHsp40L
mtHsp40S

Figure 36. Determination of PINK1 Stabilization in Fragmented Mitochondria Caused by Ectopic Expression of MtHsp40 or Loss of MtHsp70

(A) HeLa-mitoRFP cells were infected by Ad-GFP or Ad-mtHsp40$_L$ for 24 hours, and grown in the absence or presence of CCCP, a mitochondrial membrane uncoupler (10 μM) for one hour. Cell lysates were analyzed by Western blots using the indicated primary antibodies. (B) HeLa-mitoRFP cells were transfected by pRK or pRK5-mtHsp40$_L$ using Lipofectamine2000 for 24 hours, or by Scramble or mtHsp70 RNAi using Lipofectamine RNAiMAX for two days. Cell lysates were analyzed by Western blots using the indicated primary antibodies.

36A

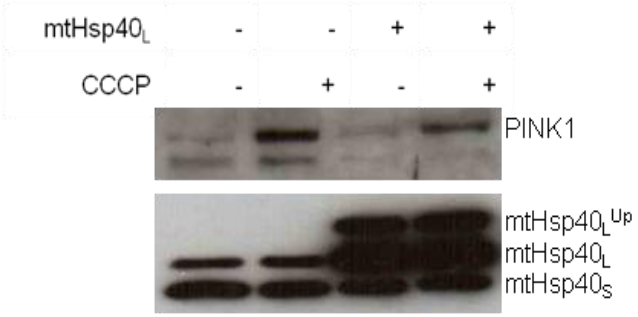
mtHsp40L - - + +
CCCP - + - +
PINK1
mtHsp40LUp
mtHsp40L
mtHsp40S

36B

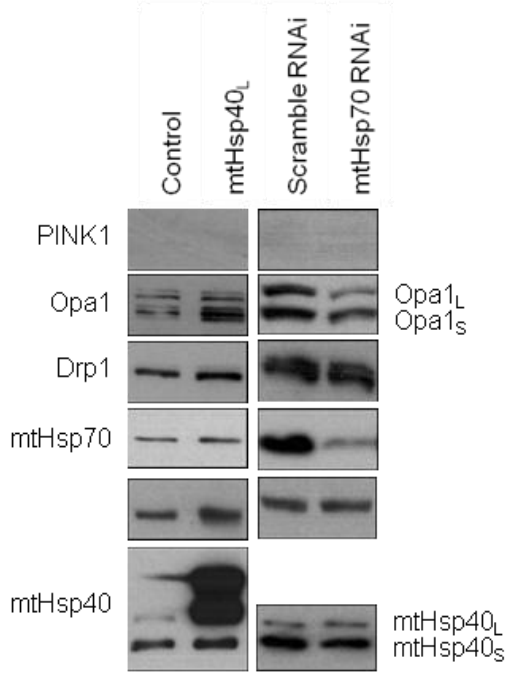
Control
mtHsp40L
Scramble RNAi
mtHsp70 RNAi
PINK1
Opa1
Drp1
mtHsp70
mtHsp40
Opa1L
Opa1S
mtHsp40L
mtHsp40S

knockdown resulted in OPA1 cleavage, but PINK1 was not stabilized. These data suggest that MFN1 or MFN2 may not be associated with mitochondrial fragmentation triggered by mtHsp40 overexpression and mtHsp70 loss.

4.6 Discussion and Future Directions

Our data here clearly showed that imbalance of protein levels or activities between mtHsp40 and mtHsp70 led to mitochondrial fragmentation possibly following inhibition of their chaperonic activities. In this section, we studied the mechanisms behind mitochondrial fragmentation caused by perturbing stoichiometric balance between mtHsp40 and mtHsp70.

Studies showed that mitochondria are fragmented under some cellular contexts to maintain cell life and mitochondrial homeostasis. For example, the overall mitochondrial network is completely disconnected during cytokinesis, and restores in the anaphase, which is dependent on DRP1 activation/deactivation[79]. Additionally, toxic chemicals such as CCCP and mitochondrial stresses such as Ca^{2+} overload also induce the complete fragmentation of mitochondria mainly by modulating mitochondrial fusion machinery including MFN1/2 and OPA1[82].

Thus, we first tested the effects of ectopic expression of mtHsp40 and the loss of mtHsp40 or mtHsp70 on expression and cellular localization of mitochondrial morphology regulators. We found that either ectopic expression of mtHsp40 or loss of mtHsp40 did not alter protein levels of DRP1, OPA1, and MFN1/2. Of interest, OPA1 cleavage was induced, resulting in $OPA1_S$ accumulation in all tested cell lines including HeLa, SK-N-SH, HEK293 and Hs68. The ratio of $OPA1_L$:$OPA1_S$ was various among cell lines. It has been widely known that cytosolic DRP1 is a major regulator of mitochondrial fission, and loss of DRP1 function inhibits fission process leading to mitochondrial elongation. Thus, we also tested the effects of loss of DRP1 on mitochondrial morphology and OPA1 cleavage in mtHsp40-overexpressed and mtHsp70-suppressed cells. Consistently, we found that loss of DRP1 elongated mitochondria in control cells, but it did not rescue OPA1 cleavage in fragmented mitochondria induced by both ectopic expression of mtHsp40 and mtHsp70 loss. Deletion of DRP1 mitigated mitochondrial fragmentation leading to condensed mitochondria. These findings suggest that ectopic expression of mtHsp40 and loss of mtHsp70 induces OPA1 cleavage leading to mitochondrial fragmentation, which is dependent on DRP1. We furthermore tested the effects of ectopic expression of

mtHsp40 and loss of mtHsp70 on the mitochondrial translocation of DRP1. DRP1 translocation to mitochondria was not detectable.

Lastly, we wanted to rule out the possible involvement of MFN1/2 in this mitochondrial fragmentation. Although MFN1 or MFN2 was expressed ectopically in fragmented mitochondria caused by mtHsp40 overexpression, fragmented mitochondria did not restore to tubular network. Additionally, we indirectly tested whether MFN1 or MFN2 level was downregulated in fragmented mitochondria by investigating PINK1 stabilization. We could not detect PINK1 in fragmented mitochondria. These data implicated that ectopic expression of mtHsp40 does not alter MFN1 or MFN2 level during mitochondrial fragmentation. Together, we propose that imbalance between mtHsp40 and mtHsp70 induces OPA1 cleavage leading to mitochondrial fragmentation, dependent on DRP1 and independent of MFN1/2 (Fig 37).

We found that OPA1 cleavage is a key regulating factor for mitochondrial fragmentation caused by perturbation of mtHsp40:mtHsp70 stoichiometry; however, we still need to confirm whether OPA1 cleavage plays a critical role in mitochondrial fragmentation with alternative methods, and we don't know the mechanism(s) linking OPA1 cleavage and mtHsp40:mtHsp70 network. To address the former question, we could investigate the effects of ectopic expression of wildtype and uncleavable OPA1 mutant on mitochondrial fragmentation. We expect that these experiments address whether OPA1 cleavage mainly triggers mitochondrial fragmentation, and OPA1 is inducibly cleaved by a certain peptidase or constitutively degraded. To address the latter question, both biased and unbiased approaches are possible: as OPA1 cleavage is likely to be modulated by several mitochondrial processing peptidases such as OMA1 and AFG3L1/2[56,57], it is possible that mtHsp40 or mtHsp70 physically binds these peptidases and modulates those activities, which ultimately induces OPA1 cleavage. Thus, it would be of worth to investigate whether OMA1 or AFG3L1/2 physically interacts with mtHsp40 or mtHsp70, and whether their interaction or levels of those peptidases is altered by ectopic expression of mtHsp40. Next, we could identify mtHsp70 interactome using mass spectrometry (MS) following Co-IP, which can provide us some potential target peptidases or pathways possibly linking OPAI cleavage and the mtHsp40:mtHsp70 machinery.

It is known that DRP1 is constantly translocated to mitochondria leading to mitochondrial fission. Ishihara *et al* found that mitochondria of $Drp1^{-/-}$ MEFs were highly elongated, and not fragmented by CCCP, claiming that DRP1 is a major mediator of

Figure 37. Proposed Model of Downstream Mechanism of Mitochondrial Fragmentation Caused by Impairing MtHsp40:MtHsp70 Stoichiometry

(A) Under normal conditions of maintained mtHsp40:mtHsp70 stoichiometry, mitochondria form a tubular network through the balance between DRP1-mediated fission and OPA1-mediated fusion. (B) Following the impairment of mtHsp40:mtHsp70 stoichiometry, $OPA1_L$ is cleaved by unknown peptidase(s) causing $OPA1_S$ to be released from the MIM and float in the intermembrane space, which triggers mitochondrial fragmentation in a DRP1-dependent manner. However, cytosolic DRP1 is not translocated to mitochondria, and MFN1/2 level is also not altered.

37A

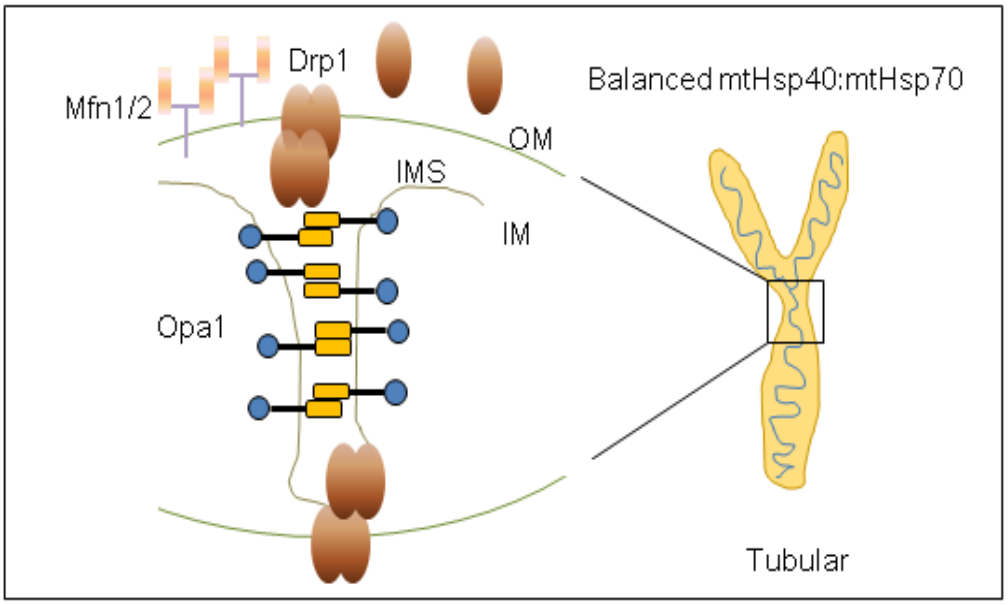
Drp1
Mfn1/2
OM
IMS
IM
Opa1
Balanced mtHsp40:mtHsp70
Tubular

37B

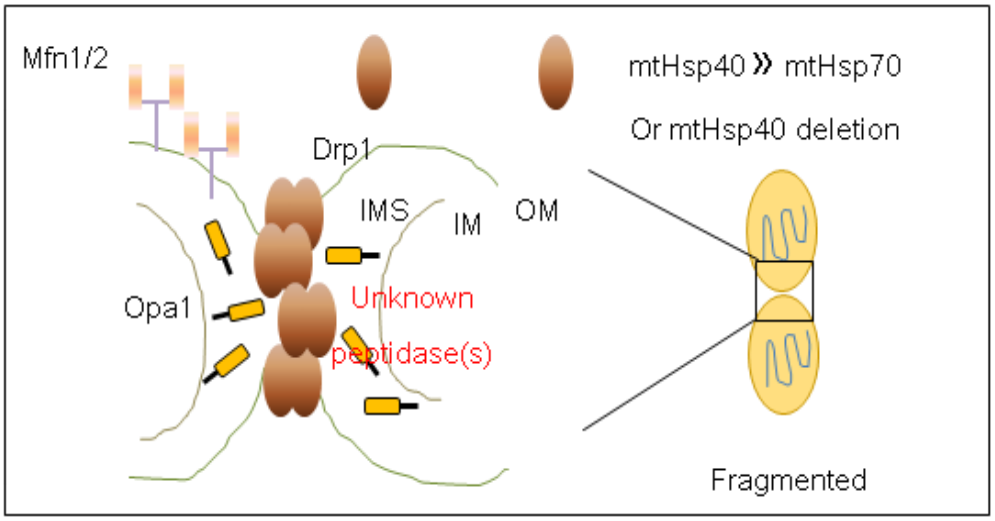
Mfn1/2
Drp1
IMS
IM
OM
Opa1
Unknown
peptidase(s)
mtHsp40 » mtHsp70
Or mtHsp40 deletion
Fragmented

mitochondrial fission[86]. We found that imbalance of mtHsp40:mtHsp70 caused mitochondrial fragmentation dependent on DRP1 following OPA1 cleavage, but DRP1 translocation was not detectable, which is consistent with numerous reports showing that OPA1 mutation and its cleavage induces mitochondrial fragmentation without DRP1 translocation; however, the roles for DRP1 during mitochondrial fragmentation caused by OPA1 cleavage still remain unclear. In addition, one question regarding cytosolic retention of DRP1 and mitochondrial fragmentation remains unanswered: how does OPA1 cleavage induce mitochondrial fragmentation without increase of DRP1 translocation to mitochondria? Here, we propose a new model that mitochondrial morphology depends on the activities of fusion and fission at the specific regions. Although DRP1 is constantly translocated to mitochondria, it does not always induce mitochondrial fission. For example, if DRP1 is located at certain regions of mitochondria where fusion proteins including MFN1/2 and active OPA1 are dominant, mitochondria then remain fused. Conversely, certain environments triggering DRP1 hyperactivation, MFN1/2 degradation, or OPA1 cleavage renders fission activity dominant, followed by mitochondrial fragmentation. It would be of interest to test this proposed model.

It is known that both isoforms of OPA1 are required for MIM fusion. Interestingly, we found a differential pattern of OPA1 isoforms between cancer cells and normal skin fibroblast. $OPA1_S$ is dominant to $OPA1_L$ in cancer cells including HeLa, SK-N-SH and HEK293, whereas Hs68 expresses $OPA1_L$ more than $OPA1_S$[16]. We do not know yet the relevance of this difference, but we propose that cancer cells may specifically modulate OPA1 processing resulting in $OPA1_S$ enrichment. Thus, it is necessary to test the correlation between OPA1 processing patterns and tumorigenesis, which, we expect, can provide us with another window by targeting OPA1 to develop a novel cancer therapeutics.

CHAPTER FIVE: EFFECTS OF MITOCHONDRIAL FRAGMENTATION CAUSED BY IMPAIRING THE BALANCE OF MTHSP40:MTHSP70 ON FUNCTIONAL HOMEOSTASIS OF MITOCHONDRIA

5.1 Background

Studies have shown the close link between mitochondrial functions and morphology. Genetic mutations causing abnormal mitochondrial dynamics result in mitochondrial dysfunction such as $\Delta\psi_m$ and ROS rise leading to a list of disorders[41]. Reversely, following mitochondrial dysfunction resulting from stresses or damages, mitochondrial dynamics is altered, which results in abnormal morphology[48].

To date, several genetic mutations related with mitochondrial dynamics have been found in numerous disorders: in particular, MFN2 in Charcot-Marie-Tooth type 2A[94], OPA1 in Optic Atrophy[95,96], and DRP1 in Huntington's Diesease[228,229] and Alzheimer' Disease[230]. Chan *et al* found that loss of MFN2 resulted in dysfunction of mitochondrial respiration, aberrant ultrastructure and distribution, and lack of mitochondrial DNA nucleoids leading to the ultimate degeneration of Purkinje cells[88,231]. Moreover, loss of MFNs resulted in severe mtDNA depletion in muscle cells and a high level of mtDNA mutations[231].

OPA1 deficiency produced similar mitochondrial dysfunction as the loss of MFN2 in the optic nerve. Chen *et al* found that loss of OPA1 led to suppression of antioxidant transcripts, disruption of mitochondrial organization, loss of crista structure, impaired mitochondrial respiration, depressed oxygen consumption, decrease in ATP level, mtDNA loss and increased ROS leading to late-onset cardiomyopathy[231,232]. These findings were reproduced in a Drosophila model, which reported that dOpa1 mutation in the eyes caused ROS rise and mitochondrial fragmentation leading to the loss of cone and pigment cells[233]. However, when we noticed that these studies employed animal models containing genetic mutations in MFN2/OPA1, we speculate that mitochondrial dysfunction and mtDNA loss may be established over long-time processes such as development following abnormal mitochondrial morphology. In addition, it has been known that membrane potential loss ($\Delta\psi_m$) resulting from mitochondrial dysfunction or stresses stimulates OPA1 cleavage leading to mitochondrial fragmentation[50-57]. Thus, OPA1 has been potentiated as a sensing molecule of mitochondrial function or health.

5.2 Rationale

As molecular chaperones are involved in numerous cellular events and pathways, we could expect with no doubt that impairment of mtHsp40 or mtHsp70 may cause abnormal phenotypes to mitochondria. Studies speculating the link between mitochondrial dynamics and functions as described above show that fragmented mitochondria become dysfunctional. In other words, mitochondria may become dysfunctional in fragmented mitochondria resulting from the impairment of mtHsp40:mtHsp70 stoichiometry. In this section, we thus would speculate the link between morphology and functions of mitochondria under impaired mtHsp40:mtHsp70 stoichiometry.

5.3 Crista Structure Remodeling in Fragmented Mitochondria

Studies have demonstrated that a profusion protein, OPA1 not only mediates crista formation, but also enhances crista integrity[51,234]. In addition, it is known that loss of OPA1 abrogates crista structure leading to mitochondrial fragmentation[49]. We wanted to confirm whether OPA1 cleavage in this study could also remodel crista structure of mitochondria during mitochondrial fragmentation. We visualized microstructure of mitochondria employing Transmission Electron Microscopy (TEM) at 4k and 10k magnification with the help of University of Calgary Microscopy and Imaging Facility. Whereas control cells showed long mitochondria with electron-dense and well-developed cristae, mtHsp40$_L$-overexpressed cells carried short fragmented mitochondria with remodeled cristae and scarce electron dense region. Of note, the morphology of fragmented mitochondria appeared to be swollen compared with tubular mitochondria (Fig 38A). More specifically, whereas it was hard to find crista structure in the mitochondria of HeLa cells, Hs68 cells showed mixed ultrastructure in the presence of mtHsp40$_L$ (Fig 38A & 38B). SK-N-SH cells clearly demonstrated that upon crista remodeling, mitochondria became swollen and fragmented (Fig 38B). HEK293 cells were affected relatively less in crista structure (Fig 38C). Loss of mtHsp40 or mtHsp70 also resulted in similar morphology of mitochondria and crista structure, but those effects were not as much as ectopic expression of mtHsp40 (Fig 38D). As far as our observations, other organelles including ER and ribosomes were not affected significantly. These data suggest that perturbation of mtHsp40:mtHsp70 network remodeled crista structure followed by mitochondria swelling and ultimate fragmentation, which is consistent with OPA1-deficient mitochondria.

Figure 38. Effects of Ectopic Expression or Deletion of MtHsp40 on Mitochondrial Microstructure

(A) HeLa-mitoRFP cells were infected by Ad-GFP (control) or Ad-mtHsp40$_L$ for 48 hours, or were transfected with Scramble or mtHsp40 RNAi for 6 days using RNAiMAX reagent. Cells were fixed using 2.5 % glutaraldehyde for one hour and processed for transmission electron microscopy (TEM). Images were magnified at 4,000 (4k) or 10,000 (10k) as indicated. Bars mean 500 nm. (B) Hs68 and SK-N-SH cells were infected by Ad-GFP (control) or Ad-mtHsp40$_L$ for 48 hours, and were imaged as described in (A). Bars mean 500 nm. (C) HEK293-MitoRFP-TetR-mtHsp40$_L$ cells were treated with DOX (100 ng/ml) for 24 hours. Following DOX-treatment, cells were washed with PBS and grown in the absence of DOX for three more days, fixed using 2.5 % glutaraldehyde, and further processed for TEM. Bars mean 500 nm, magnification = 10k. (D) HeLa-mitoRFP cells were transfected with mtHsp70 RNAi for two days, fixed using 2.5 % glutaraldehyde, and further processed for TEM. Bars mean 500 nm, magnification = 4k.

38A

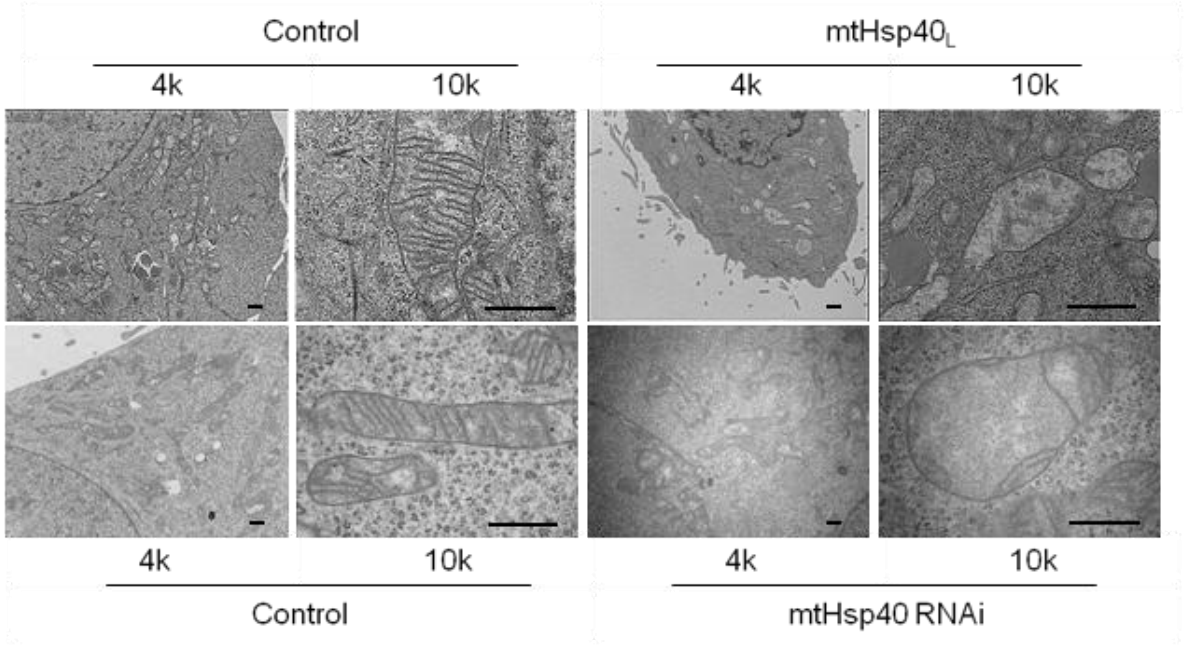
Control
mtHsp40L
4k
10k
4k
10k
4k
10k
4k
10k
Control
mtHsp40 RNAi

38B

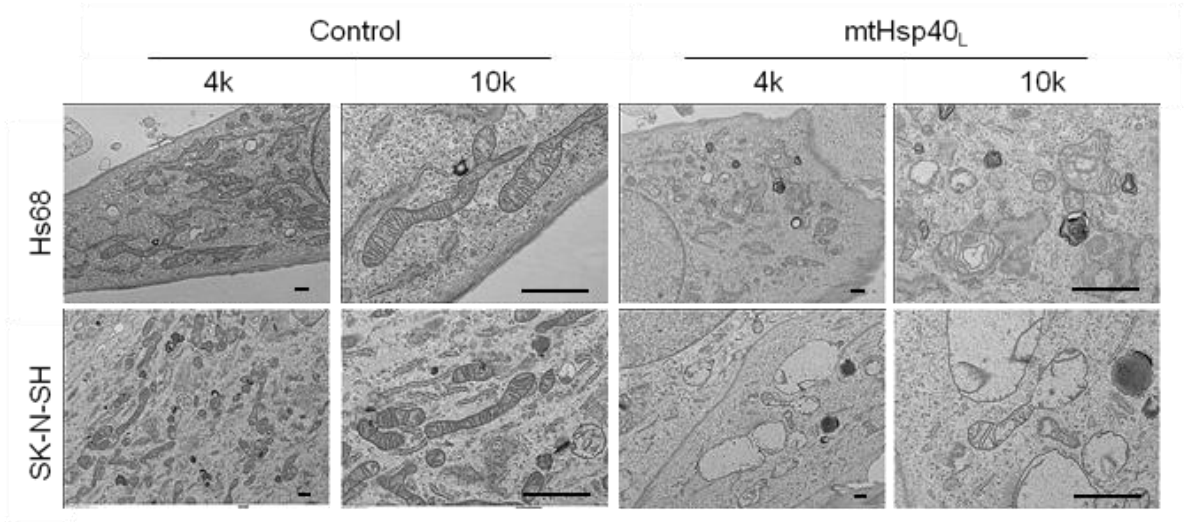
Control
mtHsp40L
4k
10k
4k
10k
Hs68
SK-N-SH

38C

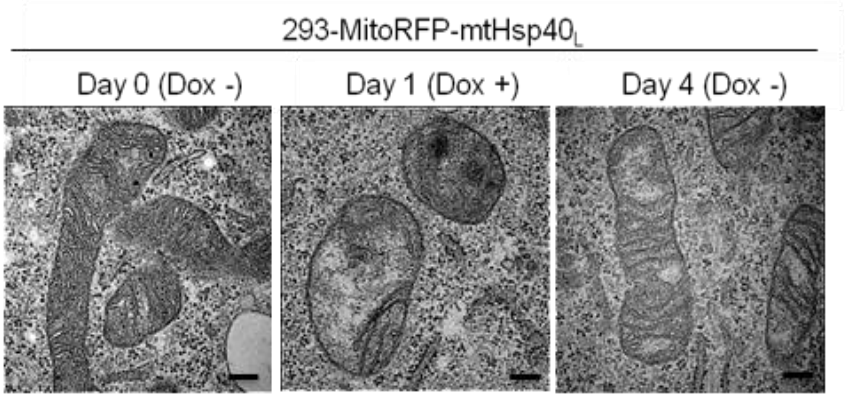

38D

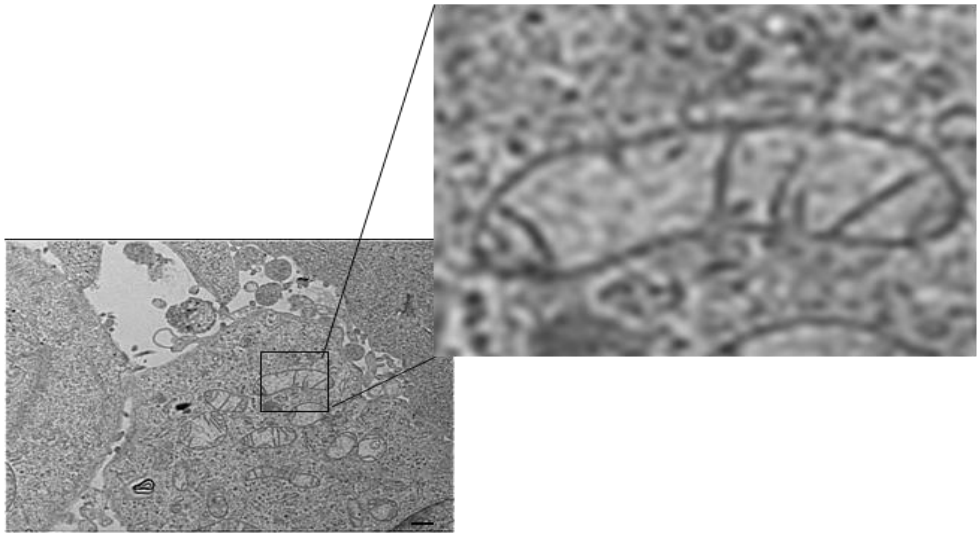

5.4 Attenuation of ATP Production in Fragmented Mitochondria

As two subunits of ATP synthase, ATP6 and ATP8, are encoded in the mitochondrial genome and assembled in the MIM following their mRNA translation in the matrix, molecular chaperones may be required for their proper assembly. It is also obvious that crista remodeling could reduce ATP production[235]. We thus measured ATP levels by using luciferase-based ATP assay kit, and not surprisingly, both ectopic expression and loss of mtHsp40$_L$ reduced ATP levels in fragmented mitochondria. Whereas ectopic expression of mtHsp40$_L$ decreased up to 40 % of control ATP level, loss of mtHsp40 produced ~ 80 % ATP of control cells (Fig 39). In order to examine indirectly ATPase activity, we tested the effects of an ATPase inhibitor, oligomycin, on ATP levels. Notably, ATP level was further decreased in the presence of oligomycin in mtHsp40$_L$-expressed cells, suggesting that ATPase was still functional. * This experiment was performed by Shin Kim.

5.5 Effects of Mitochondrial Fragmentation on Oxygen Consumption, Membrane Potential, and Reactive Oxygen Species Production

Among 13 polypeptides encoded in the mitochondrial genome, 11 proteins are components of mitochondrial oxidative phosphorylation complexes (OXPHOS); 7 subunits of NADH dehydrogenase, 3 subunits of cytochrome *c* oxidase and cytochrome *b*, and 2 proteins are subunits of ATP synthases. Recent studies have shown that mtHsp40 interacted with CRIF, a critical component of mitochondrial ribosomes, and mediated the integration of OXPHOS subunits into the MIM upon their synthesis in mitochondrial ribsomes[236], suggesting that mtHsp40 may play a certain role in OXPHOS assembly and functions. Therefore, we examined the effects of ectopic expression or loss of mtHsp40 on oxygen consumption rate (OCR), membrane potential and reactive oxygen species (ROS) production to study the OXPHOS in fragmented mitochondria. We first analyzed OCR using Seahorse XF24 cell culture microplates with sequential addition of antimycin A (respiratory chain Complex III inhibitor), FCCP (membrane uncoupler), and rotenone (respiratory chain Complex I inhibitor). Ectopic expression of mtHsp40 decreased OCR up to 40 % of control basal level (Fig 40A), and loss of mtHsp40 showed ~ 85 % OCR level of Scramble control (Fig 40B). Of note, the overall trend of OCR graphs was not different between control and mtHsp40-overexpressed or mtHsp40-depleted cells. In other words, fragmented mitochondria similarly responded to inhibitors, antimycin A and

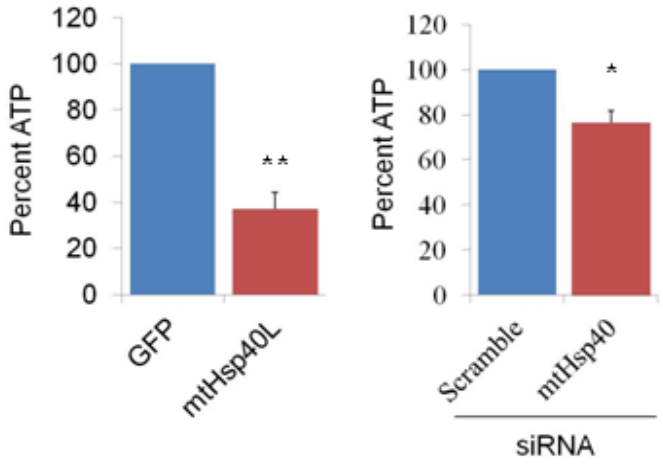

Figure 39. Effects of Ectopic Expression or Deletion of MtHsp40 on ATP Production

HeLa-mitoRFP cells were infected by Ad-GFP (control) or Ad-mtHsp40$_L$ for two days (A), or were transfected by Scramble or mtHsp40 RNAi for six days (B). ATP assay was performed using ATP luminescence assay kit. Bars mean + S.E.M., *$p < 0.05$ and **$p < 0.01$ denote significant difference than control, $n = 3$.

rotenone, with tubular mitochondria, suggesting that although the activity of respiratory chain complexes was reduced, each component of OXPHOS, complex I and III, were apparently functional (Fig 40C). *This experiment was performed by Yonghee Ahn.

Next, under normal condition, mitochondria are polarized to maintain homeostatic membrane potential in the MIS through a balance between proton pumping by CO I / CO III and proton intake by ATPases[237]. To analyze the overall activity of OXPHOS, we indirectly analyzed ψ_m by FACS following staining mitochondria with tetramethylrhodamine methyl and ethyl esters (TMRM), a rhodamine derivative accumulating in mitochondria driven by ψ_m. We could not detect any significant difference between control and mtHsp40$_L$-expressed Hs68 cells. Compared with control, ectopic expression of mtHsp40$_L$ in HeLa cells slightly decreased ψ_m, which was not statistically significant (Fig 41A). To confirm FACS results, we visualized TMRM-stained mitochondria. Both Hs68 and HeLa cells clearly showed that fragmented mitochondria were well stained with TMRM in the presence of ectopic expression of mtHsp40$_L$ (Fig 41B), but unfortunately, we could not quantify TMRM intensity due to a technical limitation with our fluorescence microscope. These data indicate that ectopic expression of mtHsp40 did not alter ψ_m at a significant level.

Lastly, we analyzed mitochondrial ROS level by staining cells with MitoSOX Red dye, a cationic derivative of dihydroethidum known as highly selective of superoxide in mitochondria. Results were variable among cell lines; while ectopic expression of mtHsp40 reduced ROS level in Hs68 cells, it elevated ROS levels in HeLa cells (Fig 42).

Taken together, the overall activity of OXPHOS was reduced, but it was functional in fragmented mitochondria caused by perturbations of mtHsp40:mtHsp70 network.

5.6 Lactate Production and Reducing Molecule Level

We wanted to look into glucose metabolism in fragmented mitochondria. As it was not feasible in our laboratory to analyze metabolites employing mass spectrometry (MS) and nuclear magnetic resonance (NMR) technologies, we alternatively chose assay methods to measure lactate and NADH/FADH$_2$ level. As most cancers activate lactate pathways to provide required ATP, lactate level or media acidification could be a relevant indicator of glycolysis. In addition, as NADH/FADH$_2$ is mainly produced during the TCA cycle from NAD^+/FAD^{2+} in mitochondria, NADH/FADH$_2$ level could indicate the TCA cycle activity. First, we thus measured lactate

Figure 40. Effects of Ectopic Expression or Deletion of MtHsp40 on OCR Levels

HeLa-mitoRFP cells were infected by Ad-GFP (control) or Ad-mtHsp40$_L$ for two days (A), or were transfected by Scramble or mtHsp40 RNAi for six days (B). OCR levels were measured using Seahorse XF24 analyzer. Oligo = oligomycin, an inhibitor of ATPase; FCCP = Trifluorocarbonylcyanide Phenylhydrazone, membrane uncoupler; Rot = rotenone, an inhibitor of complex I. Bars mean + S.E.M., *$p < 0.05$ denotes significant difference than control, $n = 4$. (B) A representative raw graph of OCR in (A) was shown. Inhibitors were treated as follows: A = oligomycin; B = FCCP; C = rotenone.

40A

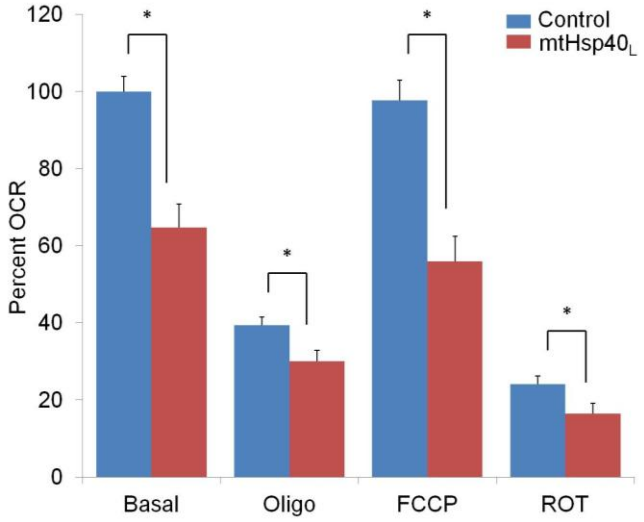
120
100
80
60
40
20
0
Percent OCR
*
*
*
*
Control
mtHsp40L
Basal
Oligo
FCCP
ROT

40B

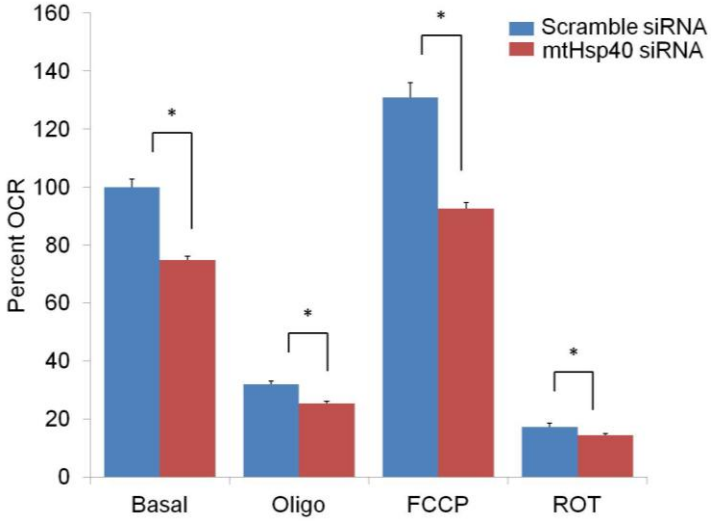
160
140
120
100
80
60
40
20
0
Percent OCR
*
*
*
*
Scramble siRNA
mtHsp40 siRNA
Basal
Oligo
FCCP
ROT

40C

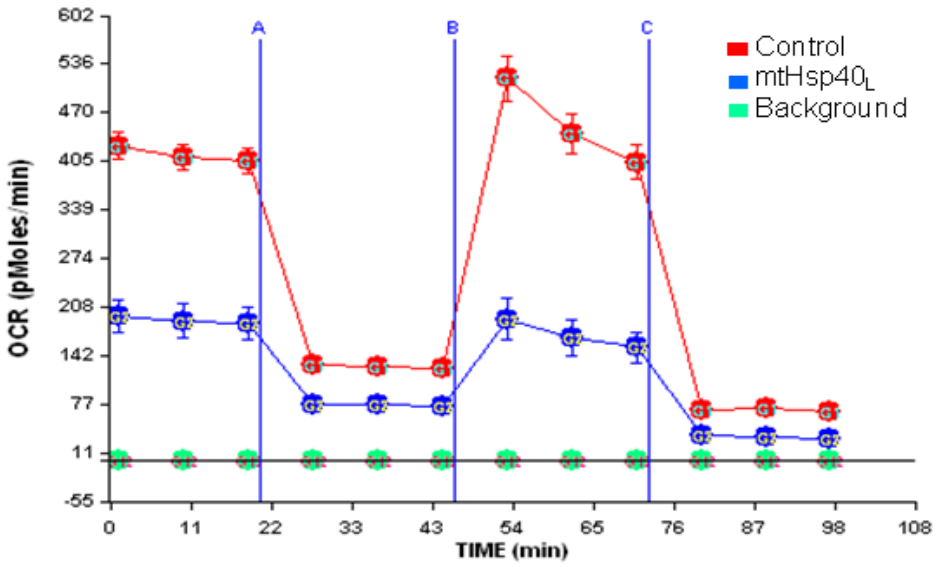
602
536
470
405
339
274
208
142
77
11
-55
OCR (pMoles/min)
A
B
C
Control
mtHsp40L
Background
0
11
22
33
43
54
65
76
87
98
108
TIME (min)

41A

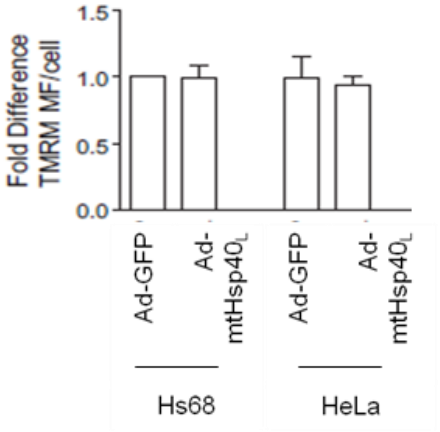

41B

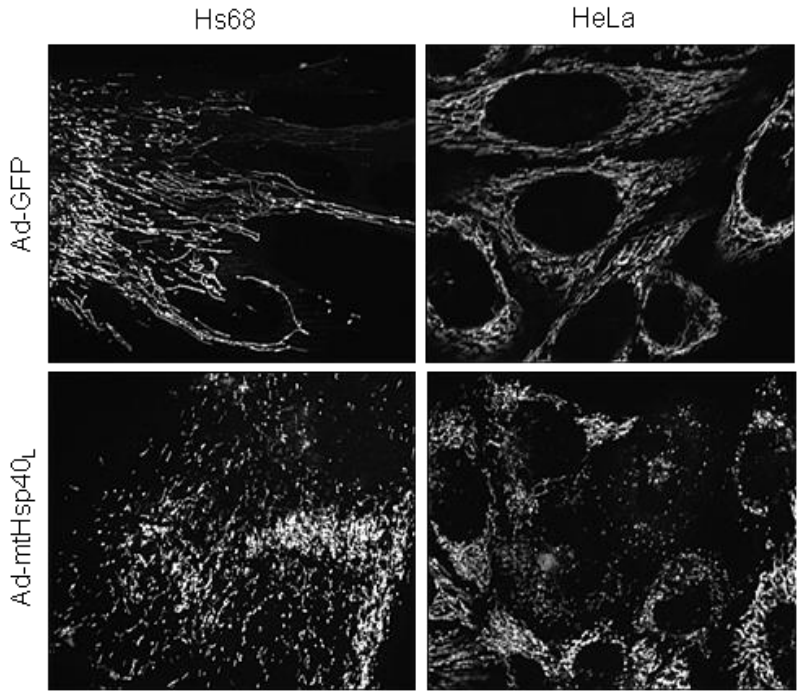

Figure 41. Effects of Ectopic Expression of MtHsp40 on Mitochondrial Membrane Potential Levels. (A) Hs68 and HeLa cells were infected with Ad-GFP or Ad-mtHsp40$_L$ as indicated for 48 hours, stained by TMRM, a dye specific to polarized mitochondria for 30 minutes, and analyzed by FACS. Bars mean + S.E.M., n = 4. (B) A representative image of TMRM-stained cells was shown. TMRM-stained cells in (A) were imaged by fluorescence microscopy at 568 nm.

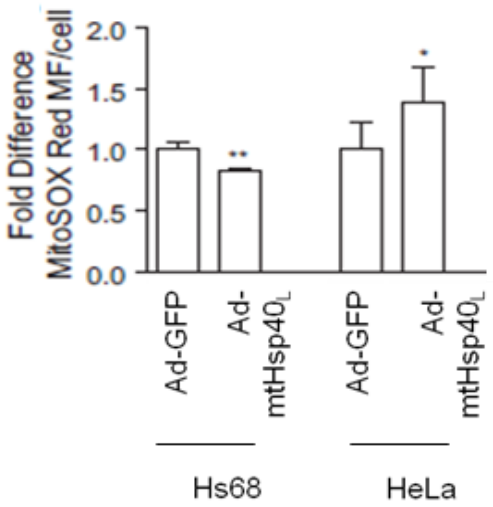

Figure 42. Effects of Ectopic Expression of MtHsp40 on ROS Levels. Hs68 and HeLa cells were infected with Ad-GFP or Ad-mtHsp40$_L$ as indicated for 48 hours, using MitoSOX Red dye specific to mitochondrial peroxide for 30 minutes, and were analyzed by FACS analysis. *$p < 0.05$ denotes a significant increase and **$p < 0.05$ denotes a significant decrease from control. Bars mean + S.E.M., n = 4.

concentration in media using HPLC in the collaboration with a Korean institute. We found that ectopic expression of mtHsp40 slightly decreased lactate level in media (Fig 43A). This experiment was performed once and thus needs to be repeated. Alternatively, we also analyzed the acidification in media using Seahorse XF24 cell culture microplates by collaborating with Dr Jong Rho's laboratory. Consistently with lactate level, ECAR level was slightly low in the presence of mtHsp40$_L$ or mtHsp40 RNAi (Fig 43B & 43C). *This experiment was performed by Yonghee Ahn.

Next, we measured NADH/$FADH_2$ level using AlamarBlue reagents. Basically, AlamarBlue^{Oxidized} reagent is converted to AlamarBlue^{Reduced} by $FMNH_2$, $FADH_2$, NADH, NADPH, and detected by fluorescence. We could not detect significant differences in AlamarBlue level between control- and mtHsp40$_L$-expressed cells, or scramble and mtHsp40-depleted cells (Fig 43D & 43E). These data indicate that glucose metabolism is not altered in fragmented mitochondria.

5.7 Mitochondrial DNA Amount and Mitochondrial Content

To date, *in vivo* studies clearly demonstrated that fragmented mitochondria in OPA1-deficient mice lack the mitochondrial genome[231]. As mtHsp40 interacts with mitochondrial DNA polymerase, DNA polymerase γ (Pol γ)[162], together led us propose that mitochondrial DNA may be decreased in fragmented mitochondria in the presence of mtHsp40$_L$ or mtHsp40 RNAi. To address this hypothesis, we performed quantitative PCR using 16S rRNA (genomic marker) and Cox 1 (cytochrome *c* oxidase subunit 1, mitochondrial marker). Unexpectedly, either ectopic expression or loss of mtHsp40 did not affect mtDNA amount (Fig 44).

As it is known that mitochondrial dynamics is coordinated with mitochondrial biogenesis[228], it would be possible that mitochondrial amount may be altered during mitochondrial fragmentation. Thus, to rule out this possibility, we measured mitochondrial amount using MitoTracker Green dye, known as a mitochondrial specific dye. We could not find any difference in mitochondrial amount between tubular and fragmented mitochondria (Fig 45), suggesting that mitochondrial DNA replication and mitochondrial biogenesis pathways are not altered in fragmented mitochondria.

Figure 43. Effects of Ectopic Expression of MtHsp40 on Lactate and NADH/$FADH_2$ Levels

(A) HeLa-mitoRFP cells were infected by Ad-GFP or Ad-mtHsp40_L as indicated for 48 hours, and lactate concentration in the media was measured using HPLC. Bars means + S.E.M., n = 1. HeLa-mitoRFP cells were infected by adenovirus as describe above for 48 hours (B), or were transfected with siRNAs as indicated using Lipofectamine RNAiMAX for six days (C). ECAR was analyzed using Seahorse XF24 analyzer. Bars mean + S.E.M., n = 4. HeLa-mitoRFP cells were infected by adenovirus as described in (A) for 48 hours (D), or were transfected with siRNAs as indicated using Lipofectamine RNAiMAX for six days (E). NADH/$FADH_2$ levels were analyzed using AlamarBlue reagent. Bars mean + S.E.M., n = 3.

43A

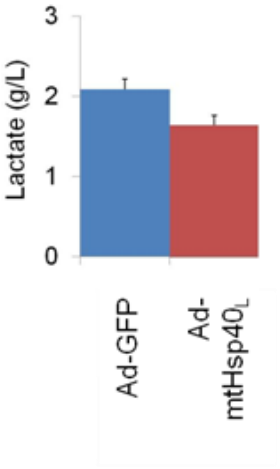

43B

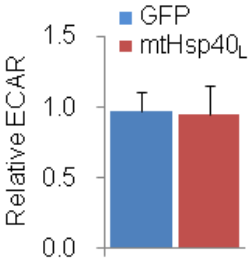

43C

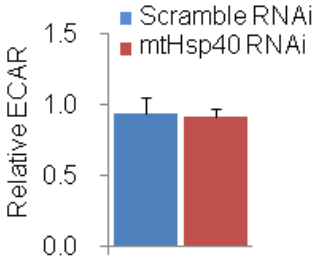

43D

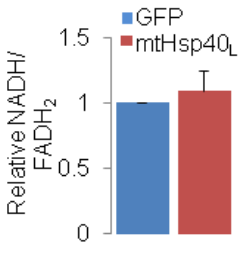

43E

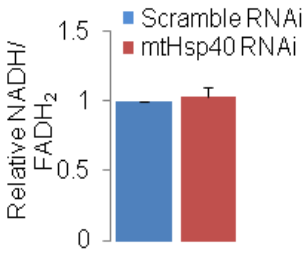

44A

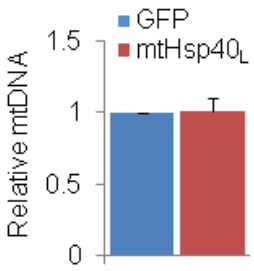

44B

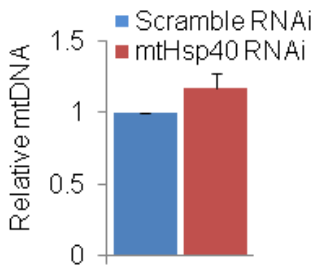

Figure 44. Effects of Ectopic Expression of MtHsp40 or Loss of MtHsp40 on MtDNA Amount. HeLa-mitoRFP cells were infected by Ad-GFP or Ad-mtHsp40$_L$ as indicated for 48 hours (A), or were transfected with siRNAs as indicated using Lipofectamine RNAiMAX for six days (B). Genomic DNA was isolated from cells above using Sigma GenElute DNA Isolation Kit, and quantitative PCR was performed using genomic DNAs with primers for 16S rRNA (nuclear) and cytochrome *c* oxidase I (mitochondrial). Bars mean + S.E.M., n = 2.

45A 45B

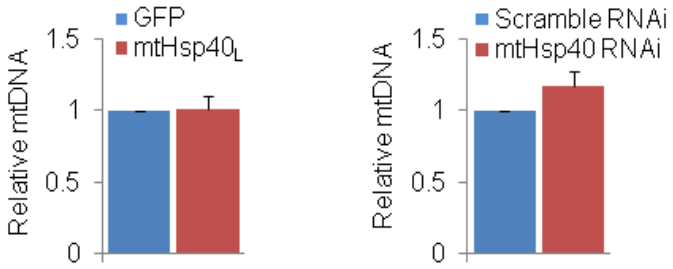

Figure 45. Effects of Ectopic Expression or Loss of MtHsp40 on Mitochondrial Contents. HeLa-mitoRFP cells were infected by Ad-GFP or Ad-mtHsp40$_L$ as indicated for 48 hours (A), or were transfected with siRNAs as indicated using Lipofectamine RNAiMAX for six days (B). Cells were stained by MitoTracker Green (1 μM) for 30 minutes and analyzed by FACS analysis. Bars mean + S.E.M., n = 2.

5.8 Cell Growth

Studies clearly showed that defects in fusion resulted in apoptotic cell death in neurons leading to neurodegeneration[88]. Our data in this study have clearly demonstrated that ectopic expression of mtHsp40 did not affect cell death in cancer cell lines, although it enhanced apoptosis with apoptotic stimuli such as Desferroxamine (DFX) and cisplatin[40,238]. We investigated the effects of mitochondrial fragmentation on cell growth instead. We grew HEK293-MitoRFP-TetR-mtHsp40$_L$ cells either in the absence or presence of DOX for one week, and counted cells every day following Tryphan Blue staining. We found the dramatic decrease of cell numbers from 2 days following DOX-treatment and up to 20 % of control at 5 days (Fig 46). However, we could not find significant difference in number of Tryphan Blue-positive cells between control and mtHsp40$_L$-overexpressed cells. Consistently with our data in Section 3.2 & 3.4, we could conclude that mitochondrial fragmentation in the presence of mtHsp40 negatively affects cell growth, but does not affect the apoptotic pathway.

5.9 Discussion and Future Directions

Of interest, mitochondrial dynamics has been known to play important roles as a mitochondrial quality control resulting in mitochondrial homeostasis. Mitochondria develop mitochondrial dynamics to actively repair damaged or sick mitochondria[41]. *In vivo* studies to date clearly show that loss of mitochondrial dynamics accumulates sick and mtDNA-depleted mitochondria, stimulating apoptotic cell death and ultimately leading to the degeneration of multiple tissues[231,232]. Therefore, under normal condition, mitochondria form a tubular network through the fusion process, enabling them to share functional contents including mtDNA and proteins with nonfunctional ones, which results in overall healthy mitochondrial network[41]. Conversely, a portion of mitochondria damaged too severely to repair need to be separated from the healthy network and ultimately deleted to protect whole network, which is mediated by the fission process[41]. Mitochondria appear to monitor the health of the whole network and divide damaged parts followed by removal through mitophagy[41]. Together, we could presume that the morphology of mitochondria may represent the health of mitochondria; fragmented mitochondria may be nonfunctional.

When it comes to the functions of molecular chaperones, we could presume that dysfunction or abnormal levels of mtHsp40 and mtHsp70 may affect numerous pathways or

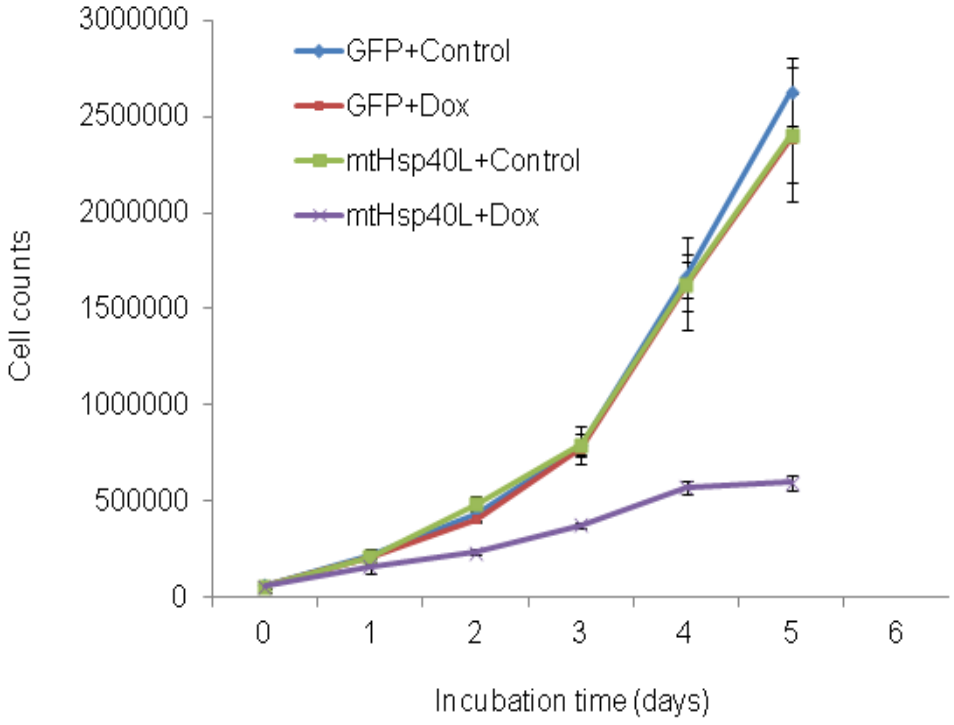

Figure 46. Growth Retardation by Mitochondrial Fragmentation Resulting From Ectopic Expression of MtHsp40. HEK293-MitoRFP-TetR-mtHsp40$_L$ cells were grown in the either absence or presence of DOX (100 ng/ml) for five days, and were counted using TryphanBlue reagent. Bars mean ± S.E.M., n = 3.

function of mitochondria. We thus tested the effects of ectopic expression and deletion of mtHsp40 on functions of fragmented mitochondria, but the result was different from our expectations: fragmented mitochondria were still functional in glucose metabolism, OXPHOS, mtDNA replication and mitochondrial biogenesis except crista structure.

Several studies showed that OPA1 depletion caused not only mitochondrial fragmentation but also crista remodeling[51,234]. Consistently, we found that both ectopic expression of mtHsp40 and loss of mtHsp40 resulted in crista remodeling in fragmented mitochondria, supporting that this mitochondrial fragmentation is followed by OPA1 cleavage. The crista number in cell lines was variable with Hs68 > SK-N-SH > HeLa, which was negatively correlated with the order of fragmentation efficiency and adenoviral infection efficiency, suggesting that the level of mtHsp40 expression may correlate its effects on mitochondrial fragmentation and crista remodeling. Whereas loss of mtHsp40 or mtHsp70 also caused crista remodeling, the number of cristae was not decreased as much as ectopic expression of mtHsp40. Of interest, SK-N-SH cells showed mixed crista structure, completely and partially remodeled cristae, suggesting that following ectopic expression of mtHsp40, OPA1 cleavage results in crista remodeling followed by mitochondria fragmentation.

A number of studies showed the correlation between crista number and ATP productivity, and the link between mitochondrial dysfunction and the decrease in ATP production[235]. It was thus of no surprise to find that both ectopic expression of and loss of mtHsp40 attenuated ATP levels; however, ATPase was responsive to its inhibitor, oligomycin, indicating that ATPases still function to produce ATP.

In order to investigate the effects of mitochondrial fragmentation on the activity of OXPHOS machinery, we indirectly measured its activity with OCR in fragmented mitochondria. Whereas basal OCR was significantly decreased in fragmented mitochondria, its responses to each drug such as antimycin A, FCCP and rotenone were not altered, indicating that both ectopic expression and loss of mtHsp40 decreased OCR, but did not affect the function of each component of OXPHOS. In addition, we tested the effects of ectopic expression and loss of mtHsp40 on mitochondrial membrane potential to confirm OCR results. We also found no difference in membrane potential between control and mtHsp40-overexpressed cells. In addition, mitochondrial ROS level was not significantly affected in fragmented mitochondria either, although it was slightly increased in HeLa cells. These data suggest that fragmented

mitochondria in this study are defective in crista structure, but contain functional OXPHOS.

As it is known that mtHsp40 and mtHsp70 are located mainly in mitochondrial matrix, we thus expected that deregulation of mtHsp40 and mtHsp70 may alter TCA cycle, which may in turn activate glycolysis. However, we found that lactate and ECAR level slightly decreased in fragmented mitochondria, and $NADH/FADH_2$ level was not significantly altered in fragmented mitochondria. Together, glucose metabolism was not altered in fragmented mitochondria. We confirmed that mitochondrial DNA and mitochondrial amount were not altered by ectopic expression and loss of mtHsp40. Lastly, growth rate was dramatically decreased by mitochondrial fragmentation, although cytochrome *c* release was not altered in fragmented mitochondria. Altogether, we propose that impaired mtHsp40:mtHsp70 stoichiometry causes OPA1 cleavage followed by crista remodeling, which results in decreases in ATP production and OCR leading to cell growth retardation (Fig 47).

Notably, the impacts of abnormal mitochondrial dynamics on mitochondrial functions and apoptosis were mostly investigated *in vivo* or in MEFs. However, in this study, we employed cancer cells to study the link between mitochondrial morphology and functions, which was a limitation to investigate the effects of long term expression or deletion of mtHsp40 on mitochondrial morphology, functions and apoptosis. To address this, we generated a Cre-inducible mtHsp40 mouse model using our construct as described in Fig 47. Following construction of iZEG-hmtHsp40$_L$, we confirmed Cre-induction of hmtHsp40$_L$ in HeLa cells (Fig 48), which was pronuclear-injected into C57BL/6 mice. Now, they are under mating (mtHsp40$_L$ $^{Tg/-}$ x Ca1mK.Cre $^{Tg/Tg}$) to generate mtHsp40L brain-specifically expressed mice (Fig 49). Using these mice, we would investigate the effects of ectopic expression of hmtHsp40$_L$ on mitochondrial proteostasis, dynamics, functions and cell death in mouse brain. We expect that these experiments could provide us with clear evidence coupling mitochondrial chaperonic network and mitochondrial homeostasis.

As all major regulators of mitochondrial fusion and fission processes, MFN1/2, OPA1 and DRP1, are large GTPases, cellular GTP level possibly regulates their activity, which in turn can determine mitochondrial morphology[48]. It thus would be of worth to investigate the effects of the GTP levels on mitochondrial morphology in fragmented mitochondria.

We found that crista remodeling following OPA1 cleavage in fragmented mitochondria in the presence of either ectopic expression or deletion of mtHsp40. DRP1 participates in

mitochondrial fragmentation, although it is not translocated to mitochondria. Thus, it is interesting to study the effects of OPA1 cleavage and DRP1 activity on crista structure in fragmented mitochondria in order to determine the roles for DRP1 in mitochondrial fragmentation caused by either ectopic expression or deletion of mtHsp40.

Figure 47. Proposed Model of Functional Alterations in Fragmented Mitochondria

(A) Under normal conditions where the mtHsp40:mtHsp70 stoichiometry is maintained, $Opa1_L$ normally mediates the MIM folding to form cristae structure, which enhances the activity of OXPHOS resulting in high OCR and ATP levels. (B) Aberrant ratio between mtHsp40 and mtHsp70 leads to $Opa1_L$ cleavage, which results in cristae remodeling, swollen mitochondria and decreases in ATP and OCR levels leading to the ultimate retardation of cell growth. However, overall glucose metabolism and activity of OXPHOS do not appear to be affected.

47A

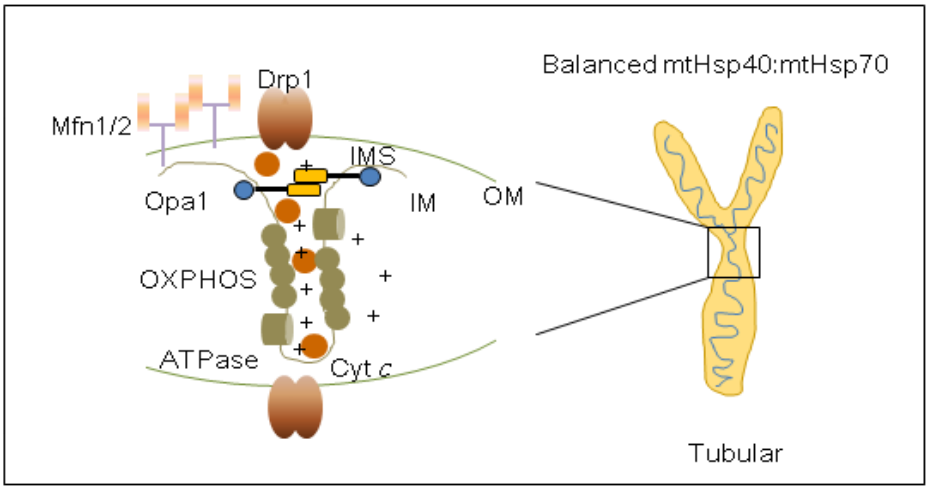
Balanced mtHsp40:mtHsp70
Drp1
Mfn1/2
IMS
Opa1
IM
OM
OXPHOS
ATPase
Cyt c
Tubular

47B

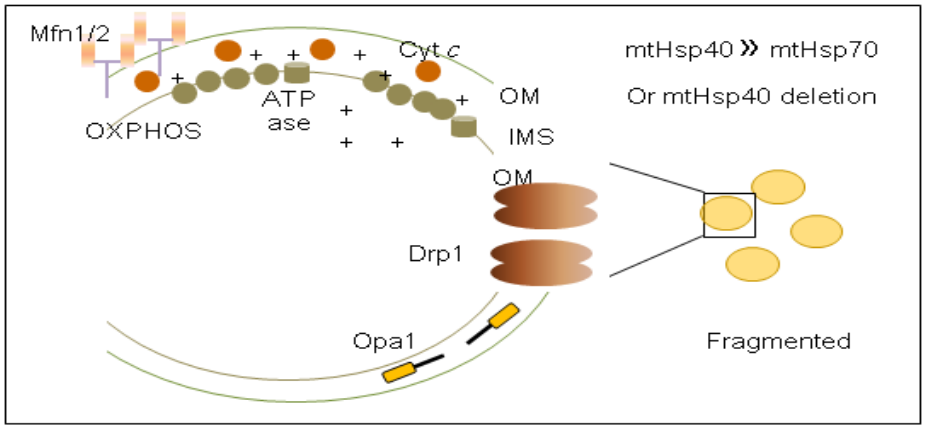
Mfn1/2
Cyt c
mtHsp40 » mtHsp70
Or mtHsp40 deletion
ATP
ase
OM
OXPHOS
IMS
OM
Drp1
Opa1
Fragmented

Figure 48. Generation of iZEG-human MtHsp40$_L$ Construct

(A) Map of iZEG plasmid. *XhoI* restriction enzyme site was employed to clone human mtHsp40$_L$ cDNA into iZEG plasmid. (B) A schematic diagram of iZEG-human mtHsp40$_L$ construct. Chicken β-actin promoter is located at 5' of lacZ gene fused with the neomycin resistance gene and next triple polyA sequences, which is flanked by two loxp sites. Next, human mtHsp40$_L$ cDNA was cloned and fused with the IRES:EGFP. Thus, lacZ is expressed but human mtHsp40$_L$ cDNA or EGFP is not in the absence of Cre recombinase. In the presence of Cre recombinase, lacZ:poly A region is deleted by Cre-recombinase at both loxp sites and then chicken β-actin promoter is fused with human mtHsp40$_L$ cDNA: IRES:EGFP, which enables human mtHsp40$_L$ and EGFP to be expressed.

48A

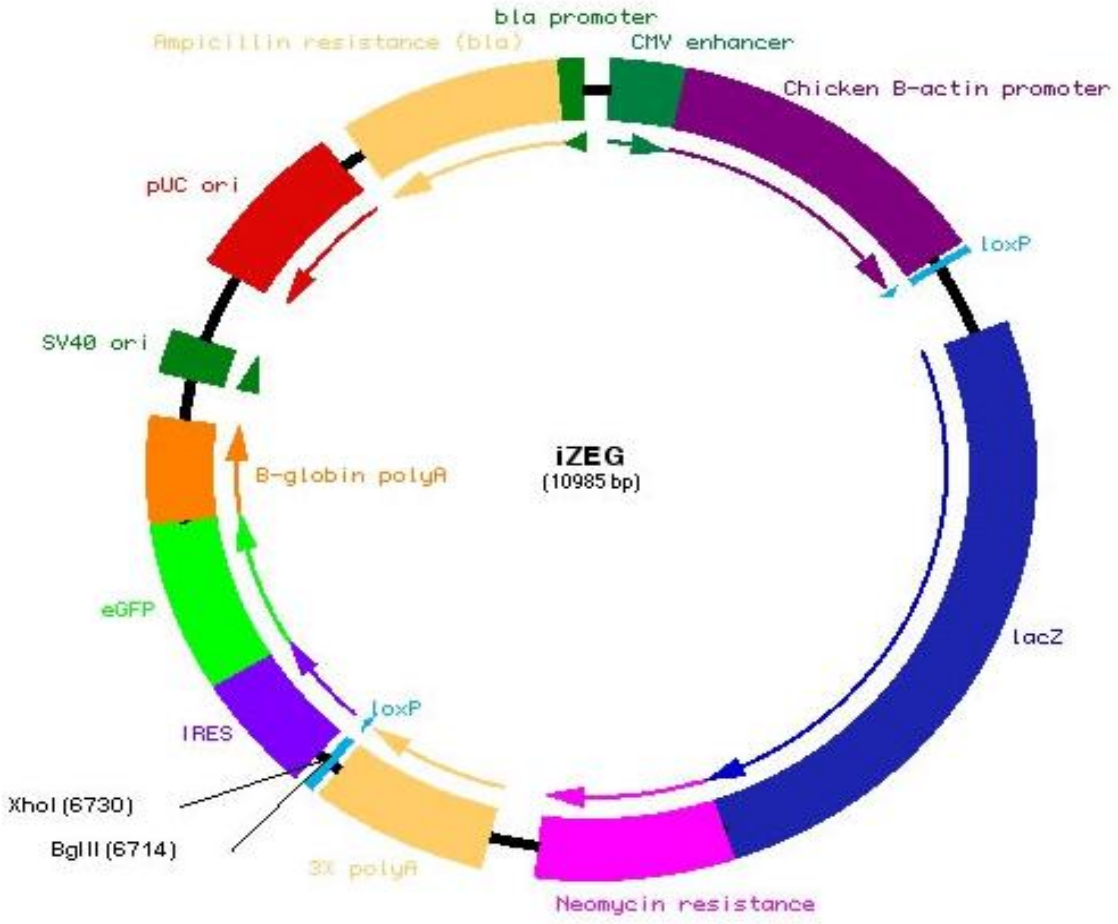
bla promoter
Ampicillin resistance (bla)
CMV enhancer
Chicken B-actin promoter
pUC ori
loxP
SV40 ori
iZEG
(10985 bp)
B-globin polyA
eGFP
lacZ
loxP
IRES
XhoI (6730)
BglII (6714)
3X polyA
Neomycin resistance

48B

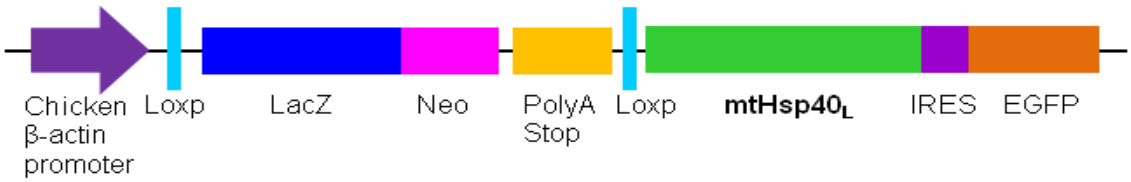
Chicken β-actin promoter
Loxp
LacZ
Neo
PolyA Stop
Loxp
mtHsp40L
IRES
EGFP

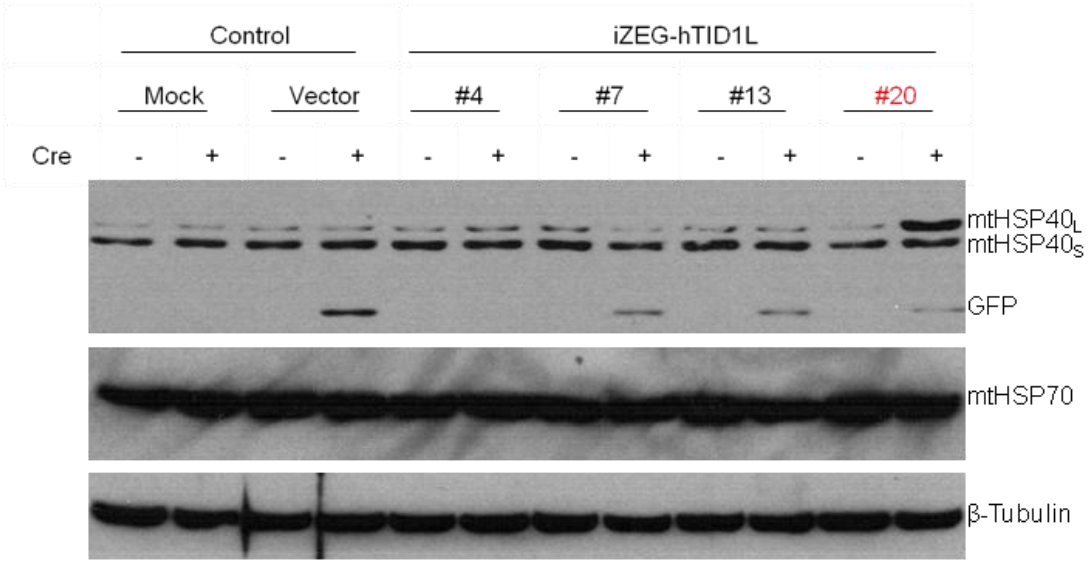

Figure 49. Confirmation of Cre-Induction of MtHsp40. HeLa-MitoRFP cells were transfected with iZEG-hmtHsp40$_L$ construct using Lipofectamine2000 for 24 hours, and then infected by Ad-Cre for further 24 hours, and were analyzed by Western blots using the indicated primary antibodies

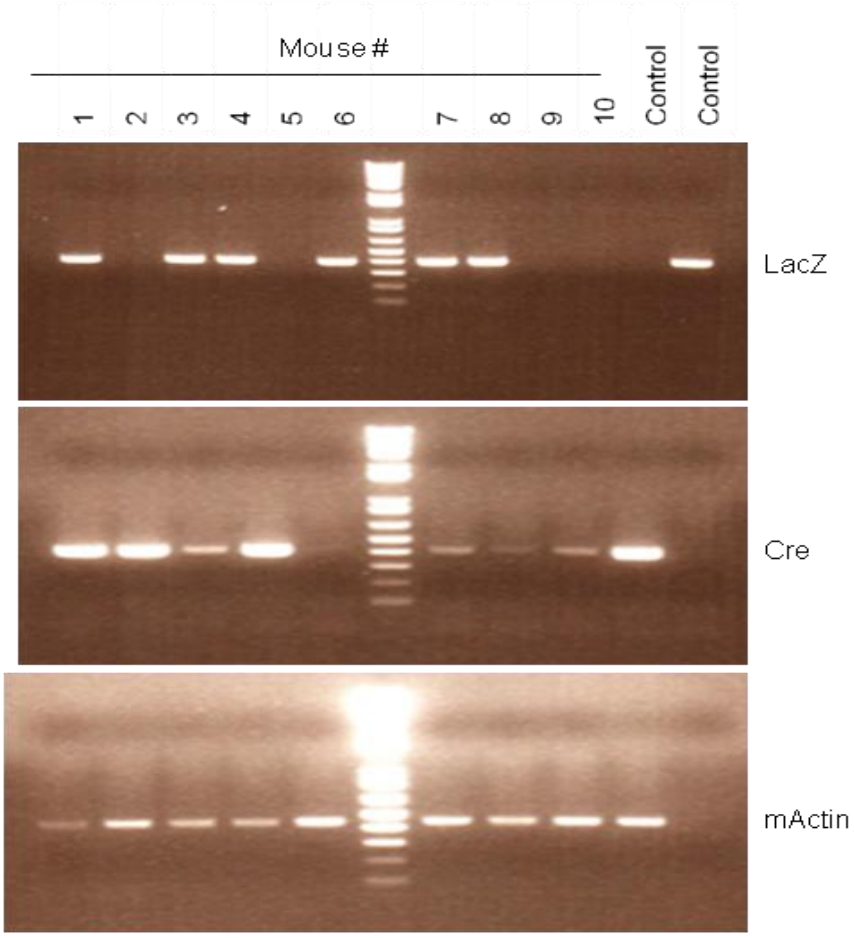

Figure 50. Genotyping PCR of Transgenic Mice ($MtHsp40_L^{Tg/wt}$, $CaMK.Cre^{Tg/wt}$)

Genomic DNAs isolated from ear samples were used for genotyping PCR using primers for lacZ, cre and mouse actin (Table 12). A representative result was shown. Three different genotypes of mice were isolated for further experiments as follows: $MtHsp40^{Tg/wt}$, $Cre^{wt/wt}$; $MtHsp40^{wt/wt}$, $Cre^{Tg/wt}$; $MtHsp40^{Tg/wt}$, $Cre^{Tg/wt}$

CHAPTER SIX: SUMMARY, DISCUSSION AND FUTURE DIRECTIONS

Molecular chaperones including HSP40 and HSP70 are ubiquitous and evolutionarily well-conserved proteins that mediate protein folding/refolding, subunit assembly, protein trafficking to target organelles and degradation of proteins, which indicates that molecular chaperons are critical for cellular proteostasis[29]. In humans, HSP40s have more than forty members that contain a distinct DnaJ domain, which binds DnaK domain (also called the ATPase domain) of HSP70 followed and stimulates ATP hydrolysis[30]. Whereas HSP40s vary in functions and structures, HSP70s have eleven members that share well-conserved domain structures: the ATPase domain, substrate binding domain, and Lid domain[30]. Studies on HSP40 and HSP70 propose a model showing the cooperative network between HSP40 and HSP70: HSP40 possesses the high binding affinity to substrates, but no ability to mediate protein folding. Conversely, ATP-bound HSP70 has low binding affinity to substrates, but following ATP hydrolysis, ADP-bound HSP70 tightly binds and mediates protein folding. Nucleotide exchange factors replace ADP of ADP-bound HSP70 by ATP[30]. This model implicates that intracellular levels of HSP40/HSP70/NEFs must be tightly regulated for the optimal function of their network. Increasing *in vitro* evidence clearly demonstrated that excess HSP40 has inhibitory effects on the folding/refolding or deaggregating activity of HSP70[143]. Notably, the existence of an *in vivo* stoichiometry between HSP40 and HSP70 for their functional network has been proposed by Kampinga *et al*[30].

Since mtHsp40 (also called Tid1) has been discovered and identified in Drosophila[36,37], studies have focused on its activities as a tumor suppressor modulating cancer cell invasion and metastasis, cell growth and proliferation, senescence and apoptosis[38-42]. Our laboratory found that mtHsp40 interacts with TP53, which facilitates apoptosis in the presence of proapoptotic stimuli; however, the mechanisms how mtHsp40 sensitizes cancer cells to apoptotic cell death remains unclear. Proteins interacting with mtHsp40 have been identified, and the majority of them were located in the cytosol (Table 6). MtHsp40 belongs to the DnaJA family that contains the DnaJ domain, G/F-rich domain, C-terminal domain I (CTD I) and II (CTD II), and dimerization domain (DD), and has the Mitochondrial Targeting Sequence (MTS) at the N-terminus[156]. Its interaction with mtHsp70 (also called Mortalin) is well known[40]; however, no evidence showing its roles in mitochondrial proteostasis and morphology has been made in

humans.

It is known that mtHsp70 interacts with TP53 causing TP53 retention in the cytosol, which inhibits the function of TP53 as a transcriptional activator and ultimately leads to cell survival and proliferation[179]. Studies on Ssc1, a yeast homolog of mtHsp70, have clearly demonstrated that mtHsp70 is constitutively expressed in mainly mitochondria, and plays a critical role in mitochondrial protein folding/refolding. Of note, it was also found that mtHsp70 interacts with TIM23, the mitochondrial protein import machinery, suggesting that mtHsp70 is also involved in protein import[212].

Mitochondrial morphology is tightly regulated by fusion and fission processes mediated by several large GTPases including MFN1/2 and OPA1 for fusion, and DRP1 for fission[48]. Specifically, MFN1 and MFN2 are constitutively expressed at the MOM mediating outermembrane fusion by forming homo- or hetero-dimers. Following outermembrane fusion, OPA1 forms homo-dimers to fuse the innermembrane[48]. Of note, OPA1 also plays an important role in crista development[49,54]. Studies to date show the regulatory mechanisms of fusion activity: degradation of MFN1/2 by PINK1/Parkin-activated ubiquitination[74] or OPA1 cleavage by certain peptidases reduces fusion activity, resulting in mitochondrial fragmentation[57].

Following its modifications in the cytosol, DRP1 is recruited to the mitochondria by mediators such as MFF, hFIS1, MiD49 and MiD51 triggering mitochondrial fragmentation[72,240]. The modification of DRP1 includes phosphorylation, dephosphorylation, ubiquitination, *etc*[82,239]. In addition, DRP1 abnormal interaction with aggregated proteins such as mutant Huntingtin, Tau, Aβ and α-synuclein also causes DRP1 hyperactivation leading to mitochondrial fragmentation[228-230]. Increasing evidence clearly showed a close link between mitochondrial fragmentation and apoptosis: for example, mitochondrial fragmentation is found in most apoptotic cells and attenuation of mitochondrial fission renders resistance to apoptotic cell death[219].

Lastly, studies clearly showed regulations of mitochondrial dynamics by mitochondrial dysfunction or cellular stresses: for example, during starvation, protein kinase A is activated and in turn phosphorylates DRP1, which causes DRP1 retention in the cytosol and ultimately leads to enhance mitochondrial fusion[239]. Conversely, mitochondrial membrane potential loss induces MFN1/2 degradation and OPA1 cleavage, resulting in mitochondrial fragmentation[241]. These data suggest that mitochondria regulate its morphology sensing cellular and mitochondrial health.

Recently, it is shown that dysfunction of mtHsp70 leads to mitochondrial fragmentation,

even though the link between mtHsp70 and mitochondrial dynamics still remains elusive. Besides recent findings regarding mtHsp70, our preliminary finding showed that ectopic expression of $mtHsp40_L$ and $mtHsp40_S$ apparently affects mitochondrial morphology in MCF-7 cells, suggesting a possible link between mitochondrial dynamics and mtHsp40-mtHsp70 network.

Taken altogether, data suggest that imbalance between mtHsp40 and mtHsp70 may disturb mitochondrial proteostasis, which results in mitochondrial fragmentation and apoptosis. Therefore, we set the goal of this study to understand the possible link between mtHsp40:mtHsp70 network and mitochondrial homeostasis of morphology, function and apoptosis.

We first tested the effects of ectopic expression and deletion of mtHsp40 on apoptosis and mitochondrial morphology, and we found that deletion of mtHsp40 and its expression over the threshold reversibly caused mitochondrial fragmentation within three hours. However, significant impact on apoptosis was not detected in fragmented mitochondria. Instead, we found that fragmented mitochondria became more sensitive to proapoptotic stimuli independently of TP53.

Next, we determined domains of mtHsp40 required for mitochondrial fragmentation in order to address why mitochondria are fragmented in the presence of either mtHsp40 expression or its deletion. Surprisingly, only mitochondrial-targeting sequence (MTS) and DnaJ domain of mtHsp40 were critical for mitochondrial fragmentation, suggesting that mtHsp70 play certain roles in this event. To test this, we first investigated the roles of mtHsp70 in mitochondrial fragmentation. As we expected, mtHsp70 inhibition and ablation of its protein level led to mitochondrial fragmentation. In addition, its truncated mutant lacking substrate binding domain and Lid domain also resulted in mitochondrial fragmentation. Altogether, our novel findings demonstrate that mtHsp40:mtHsp70 network, in particular the ratio between mtHsp40 and mtHsp70, determines mitochondrial morphology possibly through their central roles for mitochondrial proteostasis.

Furthermore, we identified downstream mechanisms of mitochondrial fragmentation. We first tested whether this event is dependent on or independent of known mitochondrial fusion/fission machinery such as DRP1, MFN1/2 and OPA1. We did not detect significant change of their protein levels or DRP1 translocation, whereas we found OPA1 cleavage in

fragmented mitochondria, led us conclude that perturbations of mtHsp40:mtHsp70 network induce OPA1 cleavage resulting in mitochondrial fragmentation, which is dependent on DRP1.

Lastly, as it is known that mitochondrial morphology is closely linked to its functions and structure, we investigated the effects of mitochondrial fragmentation on its function and microstructure. It was interesting that crista structure was remodeled and swollen in fragmented mitochondria. It was no surprise to see decreases in ATP production and oxygen consumption rate (OCR) in fragmented mitochondria with remodeled cristae. Other mitochondrial features including TCA cycle, mtDNA replication, and mitochondrial biogenesis were not altered in fragmented mitochondria.

Put altogether, we propose an overall model that perturbations of mtHsp40 and mtHsp70 network may disturb mitochondrial proteostasis resulting in remodeled cristae and fragmented mitochondria following OPA1 cleavage, which ultimately leads to slow growth rate and causes cells vulnerable to proapoptotic stimuli (Fig 51).

It is known that mtHsp40 and mtHsp70 interacting with TP53 in the cytosol have the opposing effects on cancer cell apoptosis; thus, mtHsp40 is known as a tumor suppressor and mtHsp70, an oncogene. In this study, we could not detect cytosolic mtHsp40 or mtHsp70 with either absence or presence of ectopic expression of mtHsp40 and mtHsp70. Additionally, ectopic expression or deletion of mtHsp40 or mtHsp70 did not affect apoptosis without proapoptotic reagents. It was not feasible to investigate the roles of cytosolic mtHsp40 or mtHsp70 in apoptosis and mitochondrial fragmentation. We therefore focused on the function of mtHsp40 and mtHsp70 in the mitochondrial matrix. Perturbations of mtHsp40:mtHsp70 network by expressing mtHsp40 or deleting mtHsp70 induce OPA1 cleavage and ablation of its innermembrane fusion activity followed by crista opening and cytochrome c disperse in IMS, leading to enhanced sensitivity to proapoptotic stimuli. These data present that mtHsp40:mtHsp70 network determines their function of tumor suppressor or oncogene by modulating MIM structure in the matrix. Interestingly, we also found that cancer cells show lower $OPA1_L$:$OPA1_S$ ratio than normal Hs68 cells. We thus expect that we could provide researchers with some insights into the potential of OPA1 as targets for developing novel anti-cancer therapeutics.

51A 51B

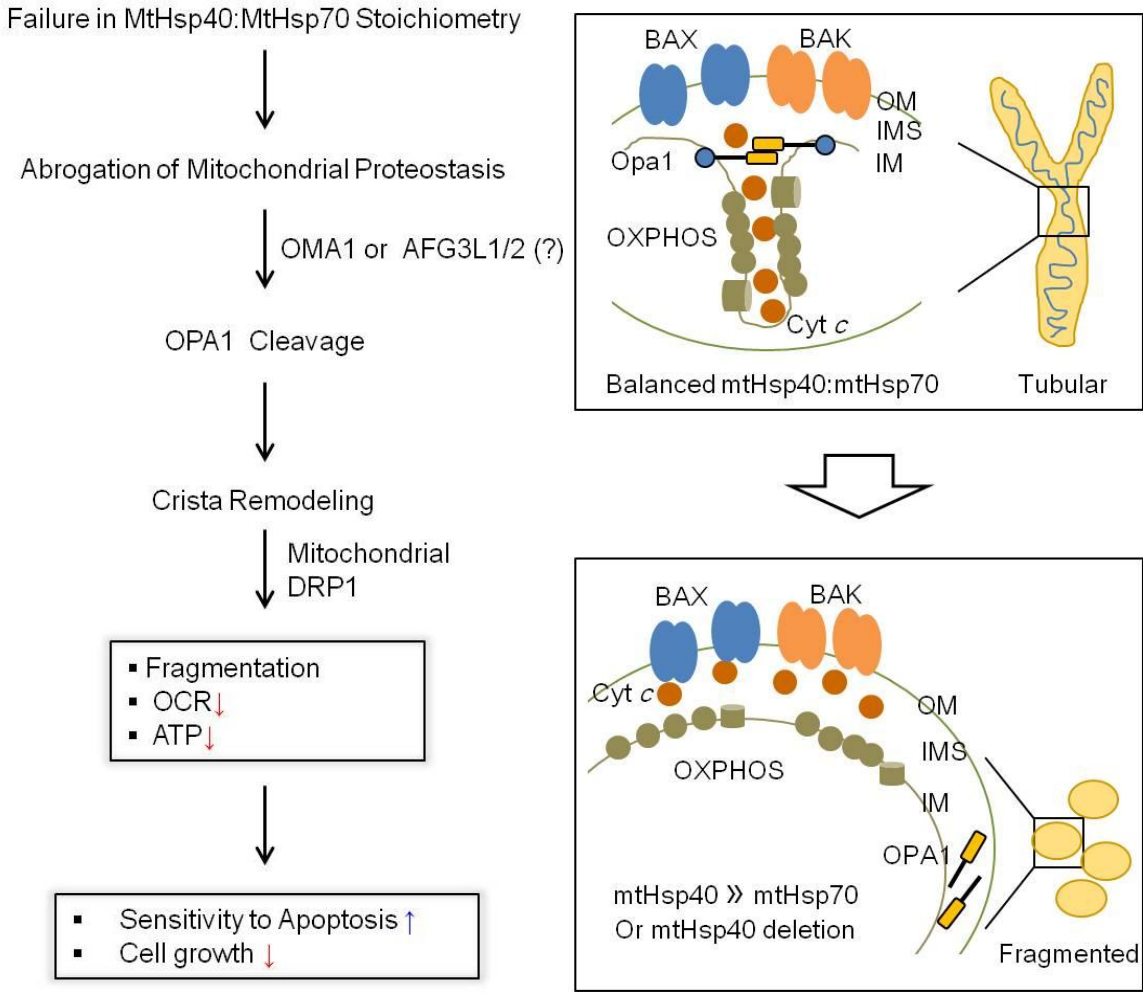

Figure 51. Overall Model.

(A) Mechanistic scheme of the effects of mtHsp40:mtHsp70 network on mitochondrial morphology, functions and apoptosis

(B) Microstructure of mitochondria undergoing apoptosis. Tubular mitochondria well develop crista structure and sequester cytochrome *c* in cristae. Fragmented mitochondria has cristae opened and swollen, which renders cytochrome *c* dispersed in the intermembrane space resulting in enhanced cytochrome *c* release through BAX and BAK responding apoptotic signals.

We found that OPA1 cleavage mainly induces mitochondrial fragmentation caused by imbalance between mtHsp40 and mtHsp70; however, we do not know how OPA1 is cleaved. It is possible that known peptidases such as OMA1 and AFG3L1/2 or unknown peptidases may participate in OPA1 cleavage. It would be of interest to investigate the mechanisms how mtHsp40:mtHsp70 network modulates OPA1 cleavage.

It has been known that mtHsp70 is a component of mitochondrial protein import complex TIM23 and participates in protein import. Thus, mtHsp70 loss possibly ablates not only protein import, but also protein (re)folding in mitochondria. To address this, we investigated the effects of longer expression of mtHsp40 or depletion of mtHsp70 on mitochondrial protein import and morphology. We first found that either ectopic expression of mtHsp40 or loss of mtHsp70 for two days did not affect protein import, suggesting that protein import was not altered during mitochondrial fragmentation (Fig 52A). Whereas ectopic expression of $mtHsp40_L$ for five days did not alter levels of mitochondrial proteins, following mtHsp70 RNAi transfection from for three days, mitochondrial proteins were dramatically decreased including mtHsp40 (matrix), OPA1 (innermembrane space) and BAK (outermembrane) (Fig 52A), indicating that depletion of mtHsp70 attenuates protein import, but ectopic expression of mtHsp40 does not. In addition to Western blot data, our fluorescence microscopy data also showed that mitochondrial proteins significantly decreased and mitochondrial-targeted GFP was located in the cytosol at five days post-transfection (Fig 52B). Of interest, mitochondria became highly fragmented and aggregated around the nuclei with five-day depletion of mtHsp70 (Fig 52B), and PINK1 was highly induced (Fig 52A), which indicates that mitochondria may undergo mitophagy-dependent degradation. Therefore, it would be of interest to investigate the effects of mtHsp70 depletion on protein import and mitophagy-dependent mitochondria quality control.

Studies demonstrated that defects in mitochondrial dynamics are closely linked in mitochondrial functions such as OXPHOS, mtDNA replication and mitochondrial distribution. Deletion of MFN1/2 or OPA1 in mouse brain results in mtDNA loss and defective OXPHOS in fragmented mitochondria and apoptotic neurons. Inconsistently, fragmented mitochondria following OPA1 cleavage in this study showed functional features of mitochondria such as glucose metabolism, mtDNA replication, OXPHOS, and biogenesis except crista remodeling. It is likely that crista remodeling attenuates OXPHOS activities such as ATP production and OCR.

Figure 52. Effects of Long-Term Expression of mtHsp40 or Loss of mtHsp70 on Mitochondrial Protein Import and PINK stabilization

HeLa-mitoGFP cells were infected by Ad-mtHsp40$_L$ or transfected with mtHsp70 RNAi using Lipofectamine RNAiMAX. Following infection or transfection, cells were grown for up to five days. Cells were analyzed by Western bots using the indicated primary antibodies (A). Yellow stars indicate PINK1 protein bands. Up = unprocessed form; MT = matrix; OM = outermembrane; IM = innermembrane. Cells above were fixed using 4 % PFA, and stained by anti-mtHsp40, -mtHsp70, Cytochrome *c*, or -Tom20 / AF568 as indicated (B). Images were taken with 568 nm (red; primary antibody) and 488 nm (green; mitoGFP) using fluorescence microscope. White stars indicate transfected cells.

52A

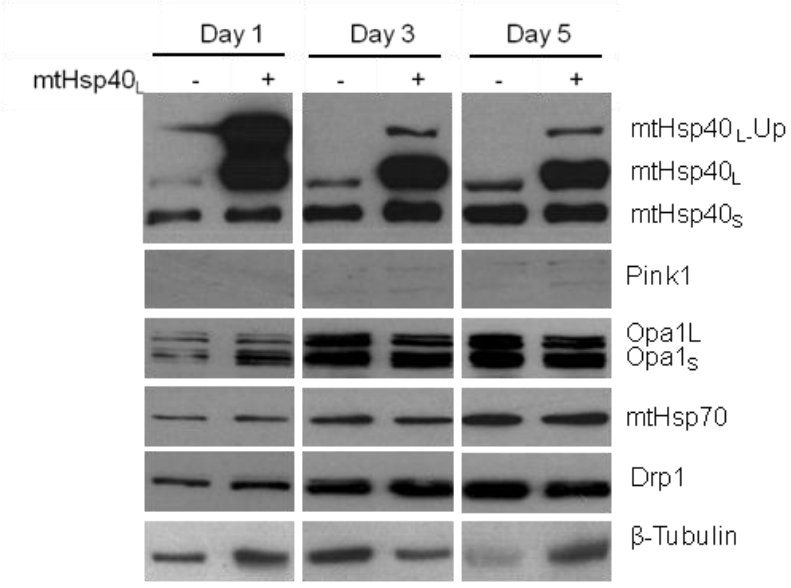
Day 1
Day 3
Day 5
mtHsp40L
-
+
-
+
-
+
mtHsp40L-Up
mtHsp40L
mtHsp40S
Pink1
Opa1L
Opa1S
mtHsp70
Drp1
β-Tubulin

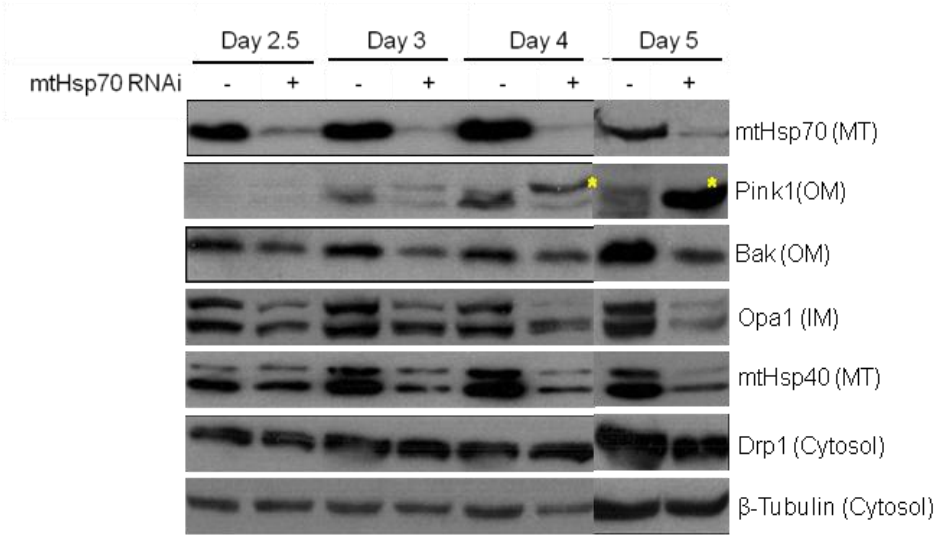
Day 2.5
Day 3
Day 4
Day 5
mtHsp70 RNAi
-
+
-
+
-
+
-
+
mtHsp70 (MT)
Pink1(OM)
Bak (OM)
Opa1 (IM)
mtHsp40 (MT)
Drp1 (Cytosol)
β-Tubulin (Cytosol)

52B

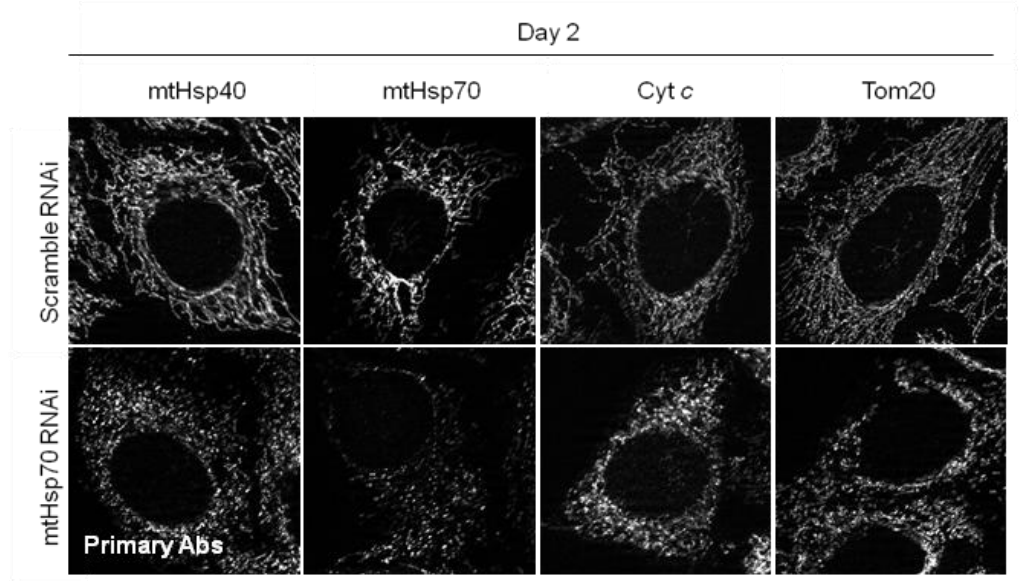
Day 2
mtHsp40
mtHsp70
Cyt c
Tom20
Scramble RNAi
mtHsp70 RNAi
Primary Abs

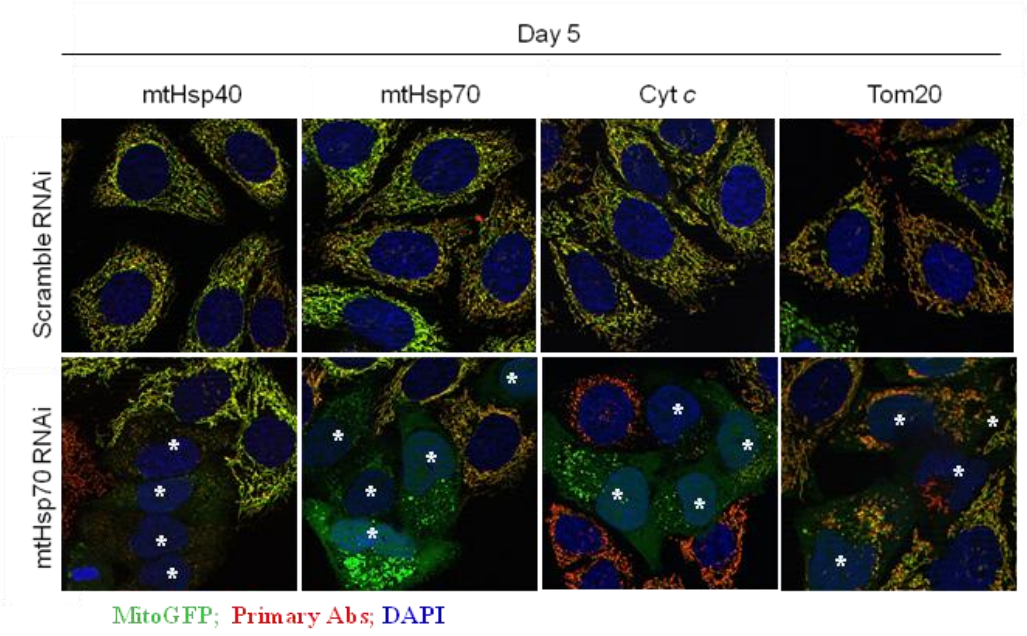
Day 5
mtHsp40
mtHsp70
Cyt c
Tom20
Scramble RNAi
mtHsp70 RNAi
MitoGFP; Primary Abs; DAPI

Overall, perturbations of mHsp40:mtHsp70 network disturb crista structure, but are not likely to alter mitochondrial functions in cancer cells. It is well known that cancers modulate mitochondrial functions during tumorigenesis, which enables cancers to proliferate in bulk and survive bulky growth. In addition, it is not feasible to reproduce *in vivo* contexts with transient expression or depletion. In order to address this limitation of *in vitro* experiments, we thus generated conditional mtHsp40$_L$ expression mouse model and will first investigate the effects of expression of mtHsp40$_L$ on mouse brain development and neuronal health/death, which, we expect, may provide us with insights into the functional link between mHsp40:mtHsp70 network and mitochondrial function, apoptosis, and proteostasis.

REFERENCES

1. Nunnari, J. and Suomalainen, A. Mitochondria: In sickness and in health. *Cell* **148**, 1145-1159 (2012)
2. Perkins, G. A. and Frey, T. G. Recent structural insight into mitochondria gained by microscopy. *Micron* **31**, 97–111 (2000)
3. Strauss, M. *et al.* Dimer ribbons of ATP synthase shape the inner mitochondrial membrane. *EMBO J*. **27**, 1154–1160 (2008)
4. Hakonen, A. H. *et al.* Mitochondrial DNA polymerase W748S mutation: a common cause of autosomal recessive ataxia with ancient European origin. *Am. J. Hum. Genet*. **77**, 430–441 (2005)
5. Holt, I. J. *et al.* A new mitochondrial disease associated with mitochondrial DNA heteroplasmy. *Am. J. Hum. Genet*. **46**, 428–433 (1990)
6. Chinnery, P. F. *et al.* MELAS and MERRF: the relationship between maternal mutation load and the frequency of clinically affected offspring. *Brain*, **121**, 1889-1894 (1998)
7. DeBerardinis, R. J. and Thompson, C. B. Cellular metabolism and disease: what do metabolic outliers teach us? *Cell* **148**, 1132-1144 (2012)
8. Ward, P. S. and Thompson, C. B. Metabolic reprogramming: a cancer hallmark even Warburg did not anticipate. *Cancer Cell* **21**, 297-308 (2012)
9. Dang, L. *et al.* Cancer-associated IDH1 mutations produce 2-hydroxyglutarate. *Nature* **462**, 739-744 (2009)
10. Zhao, H. *et al.* Targeting cellular metabolism to improve cancer therapeutics. *Cell Death and Disease* **4**, e532; doi:10.1038/cddis.2013.60 (2013)
11. Wallace, D. C. Mitochondria and cancer. *Nat Rev Cancer* **12**, 685-698 (2012)
12. Fulda, S. *et al.* Targeting mitochondria for cancer therapy. *Nature Reviews Drug Discovery* **9**, 447-464 (2010)
13. Taipale, M. *et al.* HSP90 at the hub of protein homeostasis: emerging mechanistic insights. *Nat Rev Mol Cell Biol* **11**, 515-528 (2010)
14. Ellis, R. J. *et al.* Protein aggregation in crowded environments. *Biol. Chem*. **387,** 485-497 (2006).
15. Dobson, C. M. *et al.* Protein folding — a perspective from theory and experiment. *Angew. Chem. Int. Edn Engl.* **37,** 868-893 (1998).
16. Kubelka, J. *et al.* The protein folding 'speed limit'. *Curr. Opin. Struct. Biol.* **14,** 76-88 (2004).
17. Herbst, R. S. *et al.* Equilibrium intermediates in the reversible unfolding of firefly (*Photinus pyralis*) luciferase. *J. Biol. Chem*. **272,** 7099-7105 (1997).
18. Young, J. C. *et al.* Molecular chaperones Hsp90 and Hsp70 deliver preproteins to the mitochondrial import receptor Tom70. *Cell* **112**, 41-50 (2003).
19. Fan, A. C. Y. *et al.* Hsp90 functions in the targeting and outer membrane translocation steps of Tom70-mediated mitochondrial import. *J. Biol. Chem*. **281**, 33313-33324 (2006).
20. Bhangoo, M. K. *et al.* Multiple 40-kDa heat shock protein chaperones function in Tom70-dependent mitochondrial import. *Mol. Biol. Cell* 18, 3414-3428 (2007).
21. Wolf, D. H. *et al.* The proteasome: a proteolytic nanomachine of cell regulation and waste disposal. *Biochim. Biophys. Acta* **1695,** 19-31 (2004).
22. Kopito, R. R. Aggresomes, inclusion bodies and protein aggregation. *Trends Cell Biol.* **10**, 524-530 (2000).

23. Tyedmers, J. *et al*. Cellular strategies for controlling protein aggregation. *Nat. Rev. Mol. Cell Biol.* **11**, 777-788 (2010).
24. Powers, E. T. *et al*. Biological and chemical approaches to diseases of proteostasis deficiency. *Annu. Rev. Biochem*. **78,** 959-991 (2009).
25. Macario, A. J. L. *et al*. Sick chaperones, cellular stress, and disease. *N. Engl. J. Med.* **353**, 1489-1501 (2005).
26. Slavotinek, A. M. *et al*. Unfolding the role of chaperones and chaperonins in human disease. *Trends Genet*. **17**, 528-535 (2001).
27. Young, J. C. *et al*. Pathways of chaperone-mediated protein folding in the cytosol. *Nat. Rev. Mol. Cell Biol.* **5**, 781-791 (2004).
28. McClellan, A. J. *et al*. Protein quality control: chaperones culling corrupt conformations. *Nat. Cell Biol.* **7**, 736-741 (2005).
29. Hartl, F. U. *et al*. Molecular chaperones in protein folding and proteostasis. *Nature* **475**, 324-332 (2011).
30. Kampinga, H. H. *et al*. The HSP70 chaperone machinery: J proteins as drivers of functional specificity. *Nat. Rev. Mol. Cell Biol.* **11**, 579-592 (2010).
31. Bukau, B. et al. Molecular chaperones and protein quality control. *Cell* **125**, 443-451 (2006)
32. Pearl, L. H. and Prodromou, C. Structure and mechanism of the Hsp90 molecular chaperone machinery. *Ann. Rev. Biochem*. **75**, 271-294 (2006)
33. Trepel, J. *et al*. Targeting the dynamic HSP90 complex in cancer. *Nat. Rev. Cancer* **10**, 537-549 (2010).
34. Macario, A. J. L. HSP60 expression, new locations, functions, and perspectives for cancer diagnosis and therapy. *Cancer Biology Therapy* **7**, 801-809 (2008)
35. Horwitz, J. Alpha-crystallin: the quest for a homogeneous quaternary structure. *Exp Eye Res*. **88**, 190–194 (2009)
36. Kurzik-Dumke, U. *et al.* Tumor suppressor in Drosophila is causally related to the function of the lethal(2) tumorous imaginal disc gene, a dnaJ homolog. *Dev. Genet*. **16**, 64-76 (1995).
37. Schilling, B. *et al*. A novel human DnaJ protein, hTid-1, a homolog of the Drosophila tumor suppressor protein Tid56, can interact with the human papillomavirus type 16 E7 oncoprotein. *Virology* **247**, 74-85 (1998).
38. Syken, J. *et al*. TID1, a human homolog of the Drosophila tumor suppressor l(2)tid, encodes two mitochondrial modulators of apoptosis with opposing functions. *Proc. Natl Acad. USA* **96**, 8499-8504 (1999).
39. Edwards, K. M. *et al*. Depletion of physiological levels of the human TID1 protein renders cancer cell lines resistant to apoptosis mediated by multiple exogenous stimuli. *Oncogene* **23**, 8419-8431 (2004).
40. Ahn, B. Y. *et al*. Tid1 is a new regulator of p53 mitochondrial translocation and apoptosis in cancer. *Oncogene* **29**, 1155-1166 (2010).
41. Westermann, B. *et al*. Mitochondrial fusion and fission in cell life and death. *Nat. Rev. Cancer* **11**, 872-884 (2010).
42. Bereiter-Hahn, J. Behavior of mitochondria in the living cell. *Int. Rev. Cytol.* **122,** 1-63 (1990).
43. Jahn, R. *et al*. SNAREs - engines for membrane fusion. *Nat. Rev. Mol. Cell Biol*. **7**, 631-643 (2006).
44. Hales, K. G. *et al*. Developmentally regulated mitochondrial fusion mediated by a conserved, novel, predicted GTPase. *Cell* **90**, 121-129 (1997).

45. Santel, A. *et al.* Control of mitochondrial morphology by a human mitofusin. *J. Cell Sci.* **114**, 867-874 (2001).
46. Fritz, S. *et al.* Connection of the mitochondrial outer and inner membranes by Fzo1 is critical for organellar fusion. *J. Cell Biol.* **152**, 683-692 (2001).
47. Rojo, M. *et al.* Membrane topology and mitochondrial targeting of mitofusins, ubiquitous mammalian homologs of the transmembrane GTPase Fzo. *J. Cell Sci.* **115**, 1663-1674 (2002).
48. Knott, A. B. *et al.* Mitochondrial fragmentation in neurodegeneration. *Nat. Rev. Neurosci.* **9**, 505-518 (2008).
49. Meeusen, S. *et al.* Mitochondrial inner-membrane fusion and cristae maintenance requires the dynamin-related GTPase Mgm1. *Cell* **127**, 383-395 (2006).
50. Duvezin-Caubet, S. *et al.* OPA1 processing reconstituted in yeast depends on the subunit composition of the m-AAA protease in mitochondria. *Mol. Biol. Cell* **18**, 3582-3590 (2007).
51. Cipolat, S. *et al.* OPA1 requires mitofusin 1 to promote mitochondrial fusion. *Proc. Natl Acad. Sci. USA* **101**, 15927-15932 (2004).
52. Song, Z. *et al.* OPA1 processing controls mitochondrial fusion and is regulated by mRNA splicing, membrane potential, and Yme1L. *J. Cell Biol.* **178**, 749-755 (2007).
53. Griparic, L. *et al.* Regulation of the mitochondrial dynamin-like protein Opa1 by proteolytic cleavage. *J. Cell Biol.* **178**, 757-764 (2007).
54. Cipolat, S. *et al.* Mitochondrial rhomboid PARL regulates cytochrome c release during apoptosis via OPA1-dependent cristae remodeling. *Cell* **126**, 163-175 (2006).
55. Ishihara, N. *et al.* Regulation of mitochondrial morphology through proteolytic cleavage of OPA1. *EMBO J.* **25**, 2966-2977 (2006).
56. Ehses, S. *et al.* Regulation of OPA1 processing and mitochondrial fusion by m-AAA protease isoenzymes and OMA1. *J. Cell Biol.* **187**, 1023-1036 (2009).
57. Head, B. *et al.* Inducible proteolytic inactivation of OPA1 mediated by the OMA1 protease in mammalian cells. *J. Cell Biol.* **187**, 959-966 (2009).
58. Koshiba, T. *et al.* Structural basis of mitochondrial tethering by mitofusin complexes. *Science* **305**, 858-862 (2004).
59. DeVay, R. M. *et al.* Coassembly of Mgm1 isoforms requires cardiolipin and mediates mitochondrial innermembrane fusion. *J. Cell Biol.* **186**, 793-803 (2009).
60. Malka, F. *et al.* Separate fusion of outer and inner mitochondrial membranes. *EMBO Rep.* **6**, 853-859 (2005).
61. Hoppins, S. *et al.* Mitochondrial outer and inner membrane fusion requires a modified carrier protein. *J. Cell Biol.* **184**, 569-581 (2009).
62. Ferguson, S. M. *et al.* Dynamin, a membrane-remodelling GTPase. *Nat. Rev. Mol. Cell Biol.* 13, 75-88 (2012).
63. Smirnova, E. *et al.* Dynamin-related protein Drp1 is required for mitochondrial division in mammalian cells. *Mol. Biol. Cell* **12**, 2245-2256 (2001).
64. Otsuga, D. *et al.* The dynamin-related GTPase, Dnm1p, controls mitochondrial morphology in yeast. *J. Cell Biol.* **143**, 333-349 (1998).
65. Labrousse, A. M. *et al.* C. elegans dynamin-related protein DRP-1 controls severing of the mitochondrial outer membrane. *Mol. Cell* **4**, 815-826 (1999).
66. Legesse-Miller, A. *et al.* Constriction and Dnm1p recruitment are distinct processes in mitochondrial fission. *Mol. Biol. Cell* **14**, 1953-1963 (2003).
67. Mozdy, A. *et al.* Dnm1p GTPase-mediated mitochondrial fusion is a multi-step process requiring the novel integral membrane component Fis1p. *J. Cell Biol.* **151**, 367-379 (2000).

68. Tieu, Q. & Nunnari, J. Mdv1p is a WD repeat protein that interacts with the dynamin-related GTPase, Dnm1p, to trigger mitochondrial division. *J. Cell Biol*. **151**, 353-365 (2000).
69. Tieu, Q. *et al*. The WD repeat protein, Mdv1p, functions as a molecular adaptor by interacting with Dnm1p and Fis1p during mitochondrial fission. *J. Cell Biol*. **158**, 445-452 (2002).
70. Ingerman, E. *et al*. Dnm1 forms spirals that are structurally tailored to fit mitochondria. *J. Cell Biol*. **170**, 1021-1027 (2005).
71. Gandre-Babbe, S. & Van der Bliek, A. M. The novel tail-anchored membrane protein Mff controls mitochondrial and peroxisomal fission in mammalian cells. *Mol. Biol. Cell* **19**, 2402-2412 (2008).
72. Otera, H. *et al*. Mff is an essential factor for mitochondrial recruitment of Drp1 during mitochondrial fission in mammalian cells. *J. Cell Biol*. **191**, 1141-1158 (2010).
73. Ishihara, N. *et al*. Regulation of mitochondrial morphology by membrane potential, and DRP1-dependent division and FZO1-dependent fusion reaction in mammalian cells. *Biochem. Biophys. Res. Commun*. **301**, 891-898 (2003).
74. Gegg, M. E. *et al*. Mitofusin 1 and mitofusin 2 are ubiquitinated in a PINK1/parkin-dependent manner upon induction of mitophagy. *Hum. Mol. Genet*. **19**, 4861-4870 (2010).
75. Rackovic, A. *et al*. Mutations in PINK1 and Parkin impair ubiquitination of mitofusins in human fibroblasts. *PLoS One* **6**, e16746 (2011).
76. Baricault, L. *et al*. OPA1 cleavage depends on decreased mitochondrial ATP level and bivalent metals. *Exp. Cell Res*. **313**, 3800-3808 (2007).
77. Karbowski, M. *et al*.The mitochondrial E3 ubiquitin ligase MARCH5 is required for Drp1 dependent mitochondrial division. *J. Cell Biol*. **178**, 71-84 (2007).
78. Braschi, E. *et al*. MAPL is a new mitochondrial SUMO E3 ligase that regulates mitochondrial fission. *EMBO Rep*. **10**, 748-754 (2009).
79. Taguchi, N. *et al*. Mitotic phosphorylation of dynamin-related GTPase Drp1 participates in mitochondrial fission. *J. Biol. Chem*. **282**, 11521-11529 (2007).
80. Cribbs, J. T. & Strack, S. Reversible phosphorylation of Drp1 by cyclic AMP-dependent protein kinase and calcineurin regulates mitochondrial fission and cell death. *EMBO Rep*. **8**, 939-944 (2007).
81. Han, X. J. *et al*. CaM kinase I α-induced phosphorylation of Drp1 regulates mitochondrial morphology. *J. Cell Biol*. **182,** 573-585 (2008).
82. Cereghetti, G. M. *et al*. Dephosphorylation by calcineurin regulates translocation of Drp1 to mitochondria. *Proc. Natl Acad. Sci. USA* **105**, 15803-15808 (2008).
83. Friedman, J. R. *et al*. ER tubules mark sites of mitochondrial division. *Science* **334**, 358-362 (2011).
84. Korobova, F. *et al*. An actin-dependent step in mitochondrial fission mediated by the ER-associated formin INF2. *Science* **339**, 464-467 (2013).
85. Taguchi, N. *et al*. Mitotic phosphorylation of dynamin-related GTPase Drp1 participates in mitochondrial fission. *J. Biol. Chem*. **282**, 11521-11529 (2007).
86. Ishihara, N. *et al*. Mitochondrial fission factor Drp1 is essential for embryonic development and synapse formation in mice. *Nat. Cell Biol*. **11**, 958-966 (2009).
87. Chen, H. *et al*. Disruption of fusion results in mitochondrial heterogeneity and dysfunction. *J. Biol. Chem*. **280**, 26185-26192 (2005).
88. Chen, H. *et al*. Mitochondrial fusion protects against neurodegeneration in the cerebellum. *Cell* **130**, 548-562 (2007).

89. Tait, S. W. G. and Green, D. R. Mitochondria and cell death: outer membrane permeabilization and beyond. *Nat. Rev. Mol. Cell. Biol.* **11**, 621-632 (2010)
90. Frank, S. *et al.* The role of dynamin-related protein 1, a mediator of mitochondrial fission, in apoptosis. *Dev. Cell* **1**, 515-525 (2001).
91. Thomas, K. J. and Jacobson, M. R. Defects in mitochondrial fission protein Dynamin-Related Protein 1 are linked to apoptotic resistance and autophagy in a lung cancer model. *PloS One* **7**, e45319 (2012)
92. Brooks, C. *et al.* Bak regulates mitochondrial morphology and pathology during apoptosis by interacting with mitofusins. *Proc. Natl Acad. Sci. USA* **104**, 11649-11654 (2007).
93. Wasiak, S. *et al.* Bax/Bak promote sumoylation of DRP1 and its stable association with mitochondria during apoptotic cell death. *J. Cell Biol.* **177**, 439-450 (2007).
94. Züchner, S. *et al.* Mutations in the mitochondrial GTPase mitofusin 2 cause Charcot-Marie-Tooth neuropathy type 2A. *Nat. Genet.* **36**, 449-451 (2004).
95. Alexander, C. *et al.* OPA1, encoding a dynamin-related GTPase, is mutated in autosomal dominant atrophy linked to chromosome 3q28. *Nat. Genet.* **26**, 211-215 (2000).
96. Delettre, C. *et al.* Nuclear gene OPA1, encoding a mitochondrial dynamin-related protein, is mutated in dominant optic atrophy. *Nat. Genet***. 26**, 207-210 (2000).
97. Craig, E. A. *et al.* The diverse roles of J-proteins, the obligate Hsp70 co-chaperone. *Rev. Physiol. Biochem. Pharmacol.* 1-20 (2006).
98. Hageman, J. *et al.* Computational analysis of the human HSPH/HSPA/DNAJ family and cloning of a human HSPH/HSPA/DNAJ expression library. *Cell Stress Chaperones* **14**, 1-21 (2009).
99. Cheetham, M. E. *et al.* Structure, function and evolution of DnaJ: conservation and adaptation of chaperone function. *Cell Stress Chaperones* **3**, 28-36 (1998).
100. Ohtsuka, K. *et al.* Mammalian HSP40/DNAJ homologs: cloning of novel cDNAs and a proposal for their classification and nomenclature. *Cell Stress Chaperones* **5**, 98-112 (2000).
101. Hennessy, F. *et al.* Analysis of the levels of conservation of the J domain among the various types of DnaJ-like proteins. *Cell Stress Chaperones* **5**, 347-358 (2000).
102. Tsai, J *et al.* A conserved HPD sequence of the J-domain is necessary for YDJ1 stimulation of Hsp70 ATPase activity at a site distinct from substrate binding. *J. Biol. Chem.* **271**, 9347-9354 (1996) .
103. Greene, M. K. *et al.* Role of the J-domain in the cooperation of Hsp40 with Hsp70. *Proc. Natl Acad. Sci. USA* **95**, 6108-6113 (1998).
104. Jiang, J. *et al.* Structural basis of J cochaperone binding and regulation of Hsp70. *Mol. Cell* **28**, 422-433 (2007).
105. Szyperski, T. *et al.* NMR structure determination of the Escherichia coli DnaJ molecular chaperone: secondary structure and backbone fold of the N-terminal region (residues 2-108) containing the highly conserved J domain. *Proc. Natl Acad. Sci. USA* **91**, 11343-11347 (1994).
106. Hennessy, F. *et al.* Analysis of the levels of conservation of the J domain among the various types of DnaJ-like proteins. *Cell Stress Chaperones* **5**, 347-358 (2000).
107. Hennessy, F. Characterisation of the J domain amino acid residues important for the interaction of DNAJ-like proteins with HSP70 chaperones. *PhD thesis, Rhodes Univ.* (2004).
108. D'Silva, P. D. *et al.* J protein cochaperone of the mitochondrial innermembrane required for protein import into the mitochondrial matrix. *Proc. Natl Acad. Sci. USA* **100**, 13839-13944 (2003).

109. Pellecchia, M *et al.* NMR structure of the J-domain and the Gly/Phe-rich region of the *Escherichia coli* DnaJ chaperone. *J Mol. Biol*. **260**, 236-250 (1996).
110. Karzai, A. W. et al. A Bipartite Signaling Mechanism Involved in DnaJ-mediated Activation of the *Escherichia coli* DnaK Protein. *J. Biol. Chem*. **271**, 11236-11246 (1996).
111. Goffin, L. *et al.* Genetic and biochemical characterization of mutations affecting the carboxyterminal domain of the *Escherichia coli* molecular chaperone DnaJ. *Mol. Microbiol.* **30**, 329-340 (1998).
112. Lu, Z. *et al.* The conserved carboxyl terminus and zinc finger-like domain of the co-chaperone Ydj1 assist Hsp70 in protein folding. *J. Biol. Chem*. **273**, 5970-5978 (1998).
113. Linke, K. *et al.* The roles of the two zinc binding sites in DnaJ. *J. Biol. Chem*. **278**, 44457-44466 (2003).
114. Li, J. *et al.* The crystal structure of the yeast Hsp40 Ydj1 complexed with its peptide substrate. *Structure* **11**, 1475-1483 (2003).
115. Kota, P. *et al.* Identification of a consensus motif in substrates bound by a Type I Hsp40. *Proc. Natl Acad. Sci. USA* **106**, 11073-11078 (2009).
116. Borges, J. C. *et al.* Identification of regions involved in substrate binding and dimer stabilization within the central domains of yeast Hsp40 Sis1. *PLoS One* **7**, e50927 (2012).
117. Wu, Y. *et al.* The crystal structure of the C-terminal fragment of yeast Hsp40 Ydj1 reveals novel dimerization motif for Hsp40. *J. Mol. Biol.* **346**, 1005-1011 (2005).
118. Sha, B. *et al.* The crystal structure of the peptide-binding fragment from the yeast Hsp40 protein Sis1. *Structure* **8**, 799-807 (2000).
119. Wu, Y. *et al.* The crystal structure of the C-terminal fragment of yeast Hsp40 Ydj1 reveals novel dimerization motif for Hsp40. *J. Mol. Biol.* **356**, 1005-1011 (2004).
120. Mayer, M. P. *et al.* Hsp70 chaperones: Cellular functions and molecular mechanism. *CMLS, Cell. Mol. Life Sci.* **62**, 670-684 (2005).
121. Mayer, M. P. Gymnastics of molecular chaperones. *Mol. Cell* **39,** 321-331 (2010).
122. Harrison, C. J. *et al.* Crystal Structure of the Nucleotide Exchange Factor GrpE Bound to the ATPase Domain of the Molecular Chaperone DnaK. *Science* **276**, 431-435 (1997).
123. Wisniewska, M. *et al.* Crystal structures of the ATPase domains of four human Hsp70 isoforms: HSPA1L/Hsp70-hom, HSPA2/Hsp70-2, HSPA6/Hsp70B', and HSPA5/BiP/GRP78. *PLoS One* **5**, e8625 (2011).
124. Liu, Y. *et al.* Role of Hsp70 ATPase domain intrinsic dynamics and sequence evolution in enabling its functional interactions with NEFs. *PLoS Comput. Biol.* e1000931 (2010)
125. Freeman, B. C. *et al.* Identification of a regulatory motif in Hsp7O that affects ATPase activity, substrate binding and interaction with HDJ-1. *EMBO J.* **14**, 2281-2292 (1995).
126. Craig, E. A. et al. The diverse roles of J-proteins, the obligate Hsp70 co-chaperone. *Rev. Physiol. Biochem. Pharmacol.* 1-21 (2006).
127. Zhu, X. *et al.* Structural analysis of substrate binding by the molecular chaperone DnaK. *Science* **272**, 1606-1614 (1996).
128. Zhu, X. *et al.* Structural analysis of substrate binding by the molecular chaperone DnaK. *Science* **272**, 1606-1614 (1996).
129. Rudiger, S. *et al.* Substrate specificity of the DnaK chaperone determined by screening cellulose-bound peptide libraries. *EMBO J.* **16**, 1501-1507 (1997).
130. Pellecchia, M. *et al.* Structural insights into substrate binding by the molecular chaperone DnaK. *Nat. Struct. Biol.* **7**, 298-303 (2000).

131. Laufen, T. *et al.* Mechanism of regulation of Hsp70 chaperones by DnaJ cochaperones. *Proc. Natl Acad. Sci. USA* **96**, 5452-5457 (1999).
132. Agashe, V. R. *et al.* Function of trigger factor andDnaK in multidomain protein folding: increase in yield at the expense of folding speed. *Cell* **117**, 199-209 (2004).
133. Johnson, J. L. *et al.* An essential role for the substrate-binding region of Hsp40s in *Saccharomyces cerevisiae*. *J. Cell Biol.* **152**, 851-856 (2001).
134. Sahi, C. *et al.* Network of general and specialty J protein chaperones of the yeast cytosol. *Proc. Natl Acad. Sci. USA* **104**, 7163-7168 (2007).
135. Swain, J. F. *et al.* Direct comparison of a stable isolated Hsp70 substrate binding domain in the empty and substrate-bound states. *J. Biol. Chem.* **281**, 1605-1611 (2006).
136. Swain, J. F. *et al.* Hsp70 chaperone ligands control domain association via an allosteric mechanism mediated by the interdomain linker. *Mol. Cell* **26**, 27-39 (2007).
137. Greene, M. K. *et al.* Role of the J-domain in the cooperation of Hsp40 with Hsp70. *Proc. Natl Acad. Sci. USA* **95**, 6108-6113 (1998).
138. Jiang, J. *et al.* Structural basis of J cochaperone binding and regulation of Hsp70. *Mol. Cell* **28**, 422-433 (2007).
139. Vogel, M. *et al.* Allosteric regulation of Hsp70 chaperones involves a conserved interdomain linker. *J. Biol. Chem.* **281**, 38705-38711 (2006).
140. Zhuravleva, A. *et al.* Allosteric signal transmission in the nucleotide-binding domain of 70-kDa heat shock protein (Hsp70) molecular chaperones. *Proc. Natl. Acad. Sci.* **108**, 6987-6992 (2011).
141. Schlecht, R. *et al.* Mechanics of Hsp70 chaperones enables differential interaction with client proteins. *Nat. Struct. Mol. Biol.* **18**, 145-151 (2011).
142. Diamant, S. *et al.* Temperature-controlled activity of DnaK-DnaJ-GrpE chaperones: protein folding arrest and recovery during and after heat shock depends on the substrate protein and the GrpE concentration. *Biochemistry* **37**, 9688-9694 (1998).
143. Iosefson, O. *et al.* Reactivation of protein aggregates by mortalin and Tid1-the human mitochondrial Hsp70 chaperone system. *Cell Stress Chaperones* **17**, 57-66 (2012).
144. Tokuriki, N. *et al.* Chaperonin overexpression promotes genetic variation and enzyme evolution. *Nature* **459**, 668-673 (2009).
145. Leu, J. I. J. *et al.* **A** small molecule inhibitor of inducible heat shock protein 70. *Mol. Cell* **36**, 15-27 (2009).
146. Whitesell, L. *et al.* HSP90 and chaperoning cancer. *Nat. Rev. Cancer* **5**, 761-772 (2005).
147. Trepel, J. *et al.* Targeting the dynamic HSP90 complex in cancer. *Nat. Rev. Cancer* **10**, 537-549 (2010).
148. Muchowski, P. J. Protein misfolding, amyloid formation, and neurodegeneration. *Neuron* **35**, 9-12 (2002).
149. Wacker, J. L. *et al.* Hsp70 and Hsp40 attenuate formation of spherical and annular polyglutamine oligomers by partitioning monomer. *Nat. Struct. Mol. Biol.* **11**, 1215-1222 (2004).
150. Muchowski, P. J. *et al.* Modulation of neurodegeneration by molecular chaperones. *Nat. Rev. Neurosci.* **6**, 11-22 (2005).
151. Kirkegaard, T. *et al.* Hsp70 stabilizes lysosomes and reverts Niemann-Pick disease-associated l ysosomal pathology. *Nature* **463**, 549-553 (2010).
152. Neef, D. W. *et al.* Heat shock transcription factor 1 as a therapeutic target in neurodegenerative diseases. *Nat. Rev. Drug Disc.* **10**, 930-944 (2011).

153. Trentin, G. A. *et al.* Identification of a hTid-1 mutation which sensitizes gliomas to apoptosis. *FEBS Lett*. **578**, 323-330 (2004).
154. Kim, S. W. *et al.* Tid1, the human homolog of a Drosophila tumor suppressor, reduces the malignant activity of ErbB-2 in carcinoma cells. *Cancer Res.* **64**, 7732-7739 (2004).
155. Chen, C. Y. *et al.* Tid1 functions as a tumour suppressor in head and neck squamous cell carcinoma. *J. Pathol.* **219**, 347-355 (2009).
156. Yin, X. *et al.* genomic organization and expression of the human timorous imaginal disc (TID1) gene. *Gene* **278**, 201-210 (2001).
157. Kurzik-Dumke, U. *et al.* HTid-1, the human homolog of the Drosophila melanogaster l(2)tid tumor suppressor, defines a novel physiological role of APC. *Cell Signal.* **19**, 1973-1985 (2007).
158. Lu, B. *et al.* Tid1 isoforms are mitochondrial DnaJ-like chaperones with unique carboxy termini that determine cytosolic fate. *J. Biol. Chem*. **281**, 13150-13158 (2006).
159. Trentin, G. A. *et al.* A mouse homolog of the Drosophila tumor suppressor l(2)tid gene defines a novel Ras GTPase-activating protein (RasGAP)-binding protein. *J. Biol. Chem*. **276**, 13087-13095 (2001).
160. Sohn, S. Y. *et al.* Negative regulation of hepatitis B virus replication by cellular Hsp40/DnaJ proteins through destabilization of viral core and X proteins, *J. Gen. Virol.* **87**, 1883-1891 (2006).
161. Liu, H. Y. *et al.* Human tumorous imaginal disc 1 (TID1) associates with Trk receptor tyrosine kinases and regulates neurite outgrowth in nnr5-TrkA cells. *J. Biol. Chem*. **280**, 19461-19471 (2005).
162. Hayashi, M. *et al.* A crucial role of mitochondrial Hsp40 in preventing dilated cardiomyopathy. *Nat. Med.* **12**, 128-132 (2006).
163. Lo, J. F. *et al.* Tid1, a cochaperone of the heat shock 70 protein and the mammalian counterpart of the *Drosophila* tumor suppressor l(2)tid, is critical for early embryonic development and cell survival. *Mol. Cell. Biol*. **24**, 2226-2236 (2004).
164. Kim, S. W. *et al.* Tid1 negatively regulates the migratory potential of cancer cells by inhibiting the production of interleukin-8. *Cancer Res.* **65**, 8784-8791 (2005).
165. Wakabayashi, Y. *et al.* Promotion of Hras-induced squamous carcinomas by a polymorphic variant of the Patched gene in FVB mice. *Nature* **445**, 761-765 (2007).
166. Jan, C. I. *et al.* Tid1, CHIP and ErbB2 interactions and their prognostic implications for breast cancer patients. *J. Pathol.* **225**,424-437 (2011).
167. Wadhwa, R. *et al.* Identification of a novel member of mouse hsp70 family. Its association with cellular mortal phenotype. *J. Biol. Chem*. **268**, 6615-6621 (1993).
168. Wadhwa, R. *et al.* Differential subcellular distribution of mortalin in mortal and immortal mouse and human fibroblasts. *Exp. Cell Res.* 207, 442-448 (1993).
169. Wadhwa, R. *et al.* Induction of cellular senescence by transfection of cytosolic mortalin cDNA in NIH 3T3 cells. *J. Biol. Chem*. **268**, 22239-22242 (1993).
170. Wadhwa, R. *et al.* Spontaneous immortalization of mouse fibroblasts involves structural changes in senescence inducing protein, mortalin. *Biochem. Biophys. Res. Commun*. **197**, 202-206 (1993).
171. Jin, J. *et al.* Proteomic identification of a stress protein, mortalin/mthsp70/GRP75: relevance to Parkinson disease. *Mol. Cell. Proteomics* **5**, 1193-1204 (2006).
172. Wadhwa, R. *et al.* Correlation between complementation group for immortality and the cellular distribution of mortalin. *Exp. Cell. Res*. **216,** 101-106 (1995).

173. Wadhwa, R. *et al.* Inactivation of tumor suppressor p53 by mot-2, a hsp70 family member. *J. Biol. Chem*. **273**, 29586-29591 (1998).
174. Wadhwa, R. *et al.* An Hsp70 family chaperone, mortalin/mthsp70/PBP74/Grp75: what, when, and where? *Cell Stress Chaperones* **7**, 309-316 (2002).
175. Massa, S. M. *et al.* Cloning of rat grp75, an hsp70-family member, and its expression in normal and ischemic brain. *J. Neurosci. Res*. **40**, 807-19 (1995).
176. Kaul, S. C. *et al.* Expression analysis of Mortalin, a unique member of the Hsp70 family of proteins, in rat tissues. *Exp. Cell Res.* **232**, 56-63 (1997).
177. Wadhwa, R. *et al.* Identification and characterization of molecular interactions between mortalin/mtHsp70 and HSP60. *Biochem. J*. **391**, 185-190 (2005).
178. Wadhwa, R. *et al.* Inactivation of tumor suppressor p53 by mot-2, a hsp70 family member. *J. Biol. Chem*. **273**, 29586-29591 (1998).
179. Gestl, E. E. *et al.* Cytoplasmic sequestration of the tumor suppressor p53 by a heat shock protein 70 family member, mortalin, in human colorectal adenocarcinoma cell lines. *Biochem. Biophys. Res. Commun.* **423**, 411-416 (2012).
180. Iosefson, O. & Azem, A. Reconstitution of the mitochondrial Hsp70 (mortalin)-p53 interaction using purified proteins--identification of additional interacting regions. *FEBS Lett*. **584**, 1080-1084 (2010).
181. Takano, S. *et al.* Elevated levels of mortalin expression in human brain tumors. *Exp. Cell. Res.* **237**, 38-45 (1997).
182. Dundas, S. R. *et al.* Mortalin is over-expressed by colorectal adenocarcinomas and correlates with poor survival. *J. Pathol.* **205**, 74-81 (2005).
183. Yi, X. *et al.* Association of mortalin (HSPA9) with liver cancer metastasis and prediction for early tumor recurrence. *Mol. Cell. Proteomics* **7**, 315-325 (2007).
184. Lu, W. J. *et al.* Induction of mutant p53-dependent apoptosis in human hepatocellular carcinoma by targeting stress protein mortalin. *Int. J. Cancer* **129**, 1806-1814 (2011).
185. Pilzer, D. *et al.* Mortalin inhibitors sensitize K562 leukemia cells to complement-dependent cytotoxicity. *Int. J. Cancer* 126, 1428-35 (2010).
186. Wadhwa, R. *et al.* Upregulation of mortalin/mthsp70/Grp75 contributes to human carcinogenesis. *Int. J. Cancer* **118**, 2973-80 (2006).
187. Rozenberg, P. *et al.* Elevated levels of mitochondrial mortalin and cytosolic HSP70 in blood as risk factors in colorectal cancer patients. *Int. J. Cancer***131**, (2013). In print.
188. Czarnecka, A. M. *et al.* Mitochondrial chaperones in cancer: from molecular biology to clinical diagnostics. *Cancer Biol. Ther.* **5**, 714-20 (2006).
189. Yoo, J. Y. *et al.* Tumor suppression by apoptotic and anti-angiogenic effects of mortalin-targeting adeno-oncolytic virus. *J. Gene Med*. 12, 586-595 (2010).
190. Lu, W. J. *et al.* Mortalin-p53 interaction in cancer cells is stress dependent and constitutes a selective target for cancer therapy. *Cell Death Differ*. **18**, 1046-1056 (2011).
191. Deocaris, C. C. *et al.* Druggability of mortalin for cancer and neuro-degenerative disorders. *Curr. Pharm. Des.* **19**, 418-429 (2013).
192. Moczko, M. *et al.* The mitochondrial ClpB homolog Hsp78 cooperates with matrix Hsp70 in maintenance of mitochondrial function. *J. Mol. Biol.* 254, 538-543 (1995).
193. Schilke, B. *et al.* The cold sensitivity of a mutant of *Saccharomyces cerevisiae* lacking a mitochondrial heat shock protein 70 is suppressed by loss of mitochondrial DNA. *J. Cell Biol.* **134**, 603-613 (1996).

194. Nwaka, S. *et al.* The heat shock factor and mitochondrial Hsp70 are necessary for survival of heat shock in Saccharomyces cerevisiae. *FEBS Lett*. **399**, 259-263 (1996).
195. Liu, Q. *et al.* Mitochondrial Hsp70 Ssc1: role in protein folding. *J. Biol. Chem*. **276**, 6112-6118 (2001).
196. Miao, B. *et al.* Mge1 functions as a nucleotide release factor for Ssc1, a mitochondrial Hsp70 of *Saccharomyces cerevisiae*. *J. Mol. Biol*. **265**, 541-552 (1997).
197. Sakuragi, S. *et al.* Interaction between the nucleotide exchange factor Mge1 and the mitochondrial Hsp70 Ssc1. *J. Biol. Chem*. **274**, 11275-11282 (1997).
198. Liu, Q. *et al.* Mitochondrial Hsp70 Ssc1: role in protein folding. *J. Biol. Chem*. **276**, 6112-6118 (2001).
199. Schmidt, S. *et al.* The two mitochondrial heat shock proteins 70, Ssc1 and Ssq1, compete for the cochaperone Mge1. *J. Mol. Biol*. **313**, 13-26 (2001).
200. Mapa, K. *et al.* The conformational dynamics of the mitochondrial Hsp70 chaperone. *Mol. Cell* **38**, 89-100 (2010).
201. Sichting, M. *et al.* Maintenance of structure and function of mitochondrial Hsp70 chaperones requires the chaperone Hep1. *EMBO J.* **24**, 1046-1056 (2005).
202. Goswami, A. V. *et al.* Understanding the functional interplay between mammalian mitochondrial Hsp70 chaperone machine components. *J. Biol. Chem*. **285**, 19472-19482 (2010).
203. Voos, W. *et al.* Differential requirement for the mitochondrial Hsp70-Tim44 complex in unfolding and translocation of preproteins. *EMBO J*. **15**, 2668-2677 (1996).
204. Voisine, C. *et al.* The protein import motor of mitochondria: unfolding and trapping of preproteins are distinct and separable functions of matrix Hsp70. *Cell* **97**, 565-574 (1999).
205. Geissler, A. *et al.* Mitochondrial import driving forces: enhanced trapping by matrix Hsp70 stimulates translocation and reduces the membrane potential dependence of loosely folded preproteins. *Mol. Cell. Biol*. **21**, 7097-7104 (2001).
206. Moro, F. *et al.* Mitochondrial protein import: molecular basis of the ATP-dependent interaction of MtHsp70 with Tim44. *J. Biol. Chem*. **277**, 6874-6880 (2002).
207. Strub, A. *et al.* The Hsp70 peptide-binding domain determines the interaction of the ATPase domain with Tim44 in mitochondria. *EMBO J.* **21**, 2626-2635 (2002).
208. D'Silva, P. D. *et al.* Regulated interactions of mtHsp70 with Tim44 at the translocon in the mitochondrial inner membrane. *Nat. Struct. Mol. Biol.* **11**, 1084-1091 (2004).
209. D'Silva, P. D. *et al.* J protein cochaperone of the mitochondrial inner membrane required for protein import into the mitochondrial matrix. *Proc. Natl Acad. Sci.* **100,** 13839-13844 (2003).
210. D'Silva, P. D. *et al.* Role of Pam16's degenerate J domain in protein import across the mitochondrial inner membrane. *Proc. Natl Acad Sci*. **102**, 12419-12424 (2005).
211. Schiller, D. *et al.* Residues of Tim44 involved in both association with the translocon of the inner mitochondrial membrane and regulation of mitochondrial Hsp70 tethering. *Mol. Cell. Biol.* **28**, 4424-4433 (2008).
212. Schmidt, O. *et al.* Mitochondrial protein import: from proteomics to functional mechanisms. *Nat. Rev. Mol. Cell Biol.* **11**, 655-667 (2010).
213. Jin, J. *et al.* Proteomic identification of a stress protein, mortalin/mthsp70/GRP75: relevance to Parkinson disease. *Mol. Cell. Proteomics* 5, 1193-1204 (2006).
214. Shi, M. *et al.* Mortalin: a protein associated with progression of Parkinson disease? *J. Neuropathol. Exp. Neurol.* **67**, 117-24 (2008).

215. Burbulla, L. F. *et al.* Dissecting the role of the mitochondrial chaperone mortalin in Parkinson's disease: functional impact of disease-related variants on mitochondrial homeostasis. *Hum. Mol. Genet*. **19**, 4437-4452 (2010).
216. Hui, Y. *et al.* Mitochondrial dysfunction induced by knockdown of mortalin is rescued by Parkin. *Biochem. Biophys. Res. Commun*. **410**, 114-120 (2011).
217. Goswami, A. V. *et al.* Enhanced J-protein interaction and compromised protein stability of mtHsp70 variants lead to mitochondrial dysfunction in Parkinson's disease. *Hum. Mol. Genet*. **21**, 3317-3332 (2012).
218. Frezza, C. *et al.* Organelle isolation: functional mitochondria from mouse liver, muscle and cultured filroblasts. *Nat. Protocol* **2**, 287-295 (2007).
219. Youle, R. J. and Karbowski, M. Mitochondrial fission in apoptosis. *Nat. Rev. Mol. Cell Biol*. **6**, 657-663 (2005).
220. Misselwitz, B. *et al.* J proteins catalytically activate Hsp70 molecules to trap a wide range of peptide sequences. *Mol. Cell* **2**, 593-603 (1998).
221. Ahmad, A. *et al.* Heat shock protein 70 kDa chaperone/DnaJ cochaperone complex employs an unusual dynamic interface. *Proc. Natl Acad. Sci. USA* **108**, 18966-18971 (2011).
222. Voos, W. *et al.* Molecular chaperones as essential mediators of mitochondrial biogenesis. *Biochim. Biophys. Acta*, 51- 62 (2002).
223. Shiba-Fukushima, K. *et al.* PINK1-mediated phosphorylation of the Parkin ubiquitin-like domain primes mitochondrial translocation of Parkin and regulates mitophagy. *Sci. Rep*. **2**, 1002 (2012).
224. Narendra, D. P. *et al.* PINK1 is selectively stabilized on impaired mitochondria to activate parkin. *PLoS Biol*. **8**, e1000298 (2010).
225. Wadhwa, R. *et al.* Rhodacyanine dye MKT-077 inhibits in vitro telomerase assay but has no detectable effects on telomerase activity in vivo. *Cancer Res.* **62**, 4433-4438 (2002).
226. Leboucher, G. P. *et al.* Stress-induced phosphorylation and proteasomal degradation of Mitofusin 2 facilitates mitochondrial fragmentation and apoptosis. *Mol. Cell* **47**, 547-557 (2012).
227. Detmer, S. A. and Chan, D. C. Functions and dysfunctions of mitochondrial dynamics. *Nat. Rev. Mol. Cell Biol*. **8**, 870-879 (2007).
228. Shirendeb, U. P. *et al.* Mutant huntingtin's interaction with mitochondrial protein Drp1 impairs mitochondrial biogenesis and causes defective axonal transport and synaptic degeneration in Huntington's disease. *Hum. Mol. Genet*. **21**, 406-520 (2012).
229. Song, W. *et al.* Mutant huntingtin binds the mitochondrial fission GTPase dynamin-related protein-1 and increases its enzymatic activity. *Nat. Med*. **17**, 377–382 (2011).
230. Manczak, M. *et al.* Abnormal interaction between the mitochondrial fission protein Drp1 and hyperphosphorylated tau in Alzheimer's disease neurons: implications for mitochondrial dysfunction and neuronal damage. *Hum. Mol. Genet*. **21**, 2538-47 (2012).
231. Chen, H. *et al.* Mitochondrial fusion is required for mtDNA stability in skeletal muscle and tolerance of mtDNA mutations. *Cell* **141**, 280–289 (2010).
232. Chen, L. *et al.* OPA1 mutation and late-onset cardiomyopathy: mitochondrial dysfunction and mtDNA nstability. *J. Am. Heart Assoc*. **1**, e003012 (2012).
233. Yarosh, W. *et al.* The molecular mechanisms of OPA1-mediated optic atrophy in Drosophila model and prospects for antioxidant treatment. *PLoS Genet*. **4**, e6 (2008).
234. Frezza, C. *et al.* OPA1 controls apoptotic cristae remodeling independently from mitochondrial fusion. *Cell* **126**, 177-189 (2006).

235. Yarosh, W. *et al.* The molecular mechanisms of OPA1-mediated optic atrophy in Drosophila model and prospects for antioxidant treatment. *PLoS Genet*. **4**, e6 (2008).
236. Kim, S. J. *et al.* CRIF1 is essential for the synthesis and insertion of oxidative phosphorylation polypeptides in the mammalian mitochondrial membrane. *Cell Meta*. **16**, 274-283 (2012).
237. Durieux, J. *et al.* The cell-non-autonomous nature of electron transport chain-mediated longevity. *Cell* **144**, 79–91 (2011).
238. Trinh, D. L. *et al.* Direct interaction between p53 and Tid1 proteins affects p53 mitochondrial localization and apoptosis. *Oncotarget*. **1**, 396-404 9 (2010).
239. Gomes, L. C. *et al.* During autophagy mitochondria elongate, are spared from degradation and sustain cell viability. *Nat*. *Cell Biol*. **13**, 589-598 (2011).
240. Loson, O. C. *et al.* Fis1, Mff, MiD49 and MiD51 mediate Drp1 recruitment in mitochondrial fission. *Mol. Biol. Cell* (2013) [Epub ahead of print].
241. Quiros, P. M. *et al.* Loss of mitochondrial protease OMA1 alters processing of the GTPase OPA1 and causes obesity and defective thermogenesis in mice. *EMBO J* **31**, 2117- 2133 (2012).
242. Sarraf, S. A. *et al.* Landscape of the PARKIN-dependent ubiquitylome in response to mitochondrial depolarization. *Nature* **496**. 372-377 (2013).
243. Moisoi, N. *et al.* Mitochondrial dysfunction triggered by loss of HtrA2 results in the activation of brain-specific transcriptional stress response. *Cell Death Diff*. **16**, 449-464 (2009).